Optimization radio frequency components of cryogenic nuclear magnetic resonance spectroscopy system.

Kolar, Petar

University of Zagreb

FACULTY OF ELECTRICAL ENGINEERING AND COMPUTING

Petar Kolar

OPTIMIZATION OF RADIO FREQUENCY COMPONENTS OF CRYOGENIC NUCLEAR MAGNETIC RESONANCE SPECTROSCOPY SYSTEM

DOCTORAL THESIS

Zagreb, 2020

University of Zagreb

FACULTY OF ELECTRICAL ENGINEERING AND COMPUTING

Petar Kolar

OPTIMIZATION OF RADIO FREQUENCY COMPONENTS OF CRYOGENIC NUCLEAR MAGNETIC RESONANCE SPECTROSCOPY SYSTEM

DOCTORAL THESIS

Supervisors: Professor Silvio Hrabar, PhD
Assistant Professor Mihael S. Grbić, PhD

Zagreb, 2020

Sveučilište u Zagrebu

FAKULTET ELEKTROTEHNIKE I RAČUNARSTVA

Petar Kolar

OPTIMIZACIJA RADIOFREKVENCIJSKIH KOMPONENTI SUSTAVA KRIOGENE SPEKTROSKOPIJE NUKLEARNE MAGNETSKE REZONANCIJE

DOKTORSKI RAD

Mentori: prof. dr. sc. Silvio Hrabar
doc. dr. sc. Mihael S. Grbić

Zagreb, 2020.

This doctoral thesis was made at University of Zagreb, Faculty of Electrical Engineering and Computing, Department of Wireless Communications, and University of Zagreb, Faculty of Science, Department of Physics.

Supervisors: Professor Silvio Hrabar, PhD, and Assistant Professor Mihael S. Grbić, PhD

Number of pages: 151

Doctoral thesis No.: _____

About the Supervisors

Silvio Hrabar was born in Trogir, Croatia in 1962. He received Dipl. Ing. and M.S. degrees from University of Zagreb, Croatia and a Ph.D degree from Brunel University of West London, United Kingdom, in 1986, 1991 and 1999, respectively, all in electrical engineering.

Until 1988, he worked at Institute of Radio Industry Zagreb, Croatia, as R&D Engineer, involved in the development of UHF transceivers and antenna systems. From 1988 to 1995 he was at Faculty of Electrical Engineering and Computing (FER), University of Zagreb, working in applied electromagnetics, microwave electronics and microwave measurements. In 1995, he joined Electronic Systems Research Group at Brunel University of West London, where he was involved in various projects concerning electromagnetic compatibility, computational electromagnetics and electrostatics. At the same time, he was working as a consultant for several microwave companies in United Kingdom. From 1999, he has been affiliated again with FER, where now he holds a position as Full Professor of Applied Electromagnetics.

His research interests include applied electromagnetics, nanoelectromagentics, microwave electronics, radiofrequency and microwave measurements, antenna technology, and metamaterials. He was leading several international scientific projects that involved different partners from universities and governmental and industrial labs in Europe, Asia, and United States. He made a couple of important contributions in the field of metamaterials: theoretical explanation and experimental verification of subwavelength propagation in metamaterial waveguide as well as the first experimental demonstrations of a subwavelength resonator and broadband non-Foster active metamaterial in the world.

He is author and co-author of many journal papers, book chapters, conference contributions and studies and serves as a reviewer for dozen of scientific journals. In 2012, prof. Hrabar received an award from University of Zagreb, FER for "Outstanding achievement in research and innovations".

Mihael Grbić was born on January 13^{th} 1982 in Sisak, Croatia. He enrolled the elementary school in 1988 in Lekenik and completed it in Zagreb. In 1996 he enrolled the gymnasium Ivan Supek in Zagreb. From years 2000 to 2005 he studies physics at the Department of Physics, Faculty of Science, University of Zagreb. He graduates with a master thesis titled "*Studying the vortex dynamics in thin films of niobium*" under the mentorship of prof. Miroslav Požek. In 2004 he was awarded with a Rectors award for the research that was later the core of the master thesis. He attended his postgraduate studies from 2006 to 2011, when he defended his PhD thesis "*Investigation of superconducting fluctuations and pseudogap in high temperature superconductors by microwave technique*". During the postgraduate studies he was a co-worker on an EU funded project SOLeNeMaR (PI: prof. Miroslav Požek) at the Department of Physics that founded the first nuclear magnetic resonance (NMR) laboratory for solid state physics in Croatia, and within the scope of the project he spent 7 months at Laboratoire National des Champs Magnétiques Intenses (LNCMI) in Grenoble (France) for training in NMR technique. After defending his PhD thesis in 2011 he was promoted to the position of higher assistant at the Department of Physics Faculty of Science and on the same year received recognition from the dean of the Faculty as the best junior researcher of the year.

In the period from March 2011 to the end of August 2012, Mihael Grbić spent 16 months at LNCMI as a postdoctoral researcher, in the group of dr. Mladen Horvatić. During that time he began studying quantum magnetism by NMR, in collaboration with the newly founded laboratory at the Department of Physics and published 3 papers in Physical Review Letters (impact factor 7.435). By now, the papers accumulated more than 50 citations in CC journals. Within this period Mihael Grbić acquired the experience of applying and conducting the experiments in high magnetic fields (up to 34 T), and performing NMR experiments in a dilution refrigerator.

From October 2012 to April 2014 Mihael Grbić spent his second postdoctoral training at the Institute for Solid State Physics (ISSP), University of Tokyo (Japan) in the group of prof. Masashi Takigawa, where he studied intermetallic compounds of heavy fermions by NMR; expanding his area of research.

Since May 2014 Mihael Grbić works as an assistant professor at the Department of Physics, Faculty of Science. By now he published 19 research papers in international journals, with 210 citations and an h-index 7.

O mentorima

Silvio Hrabar rođen je u Trogiru, R. Hrvatska 1962. Godine. Diplomirao je i magistrirao na Elektrotehničkom fakultetu Sveučilišta u Zagrebu, a doktorirao na Brunel University of West London, Velika Britanija, sve u polju elektrotehnike, 1986., 1991., odnosno 1999. godine.

Do 1988. radio je u Institutu Radio Industrije Zagreb, Hrvatska, kao inženjer za istraživanje i razvoj i sudjelovao u razvoju UHF primopredajnika i antenskih sustava. Od 1988. do 1995. bio je zaposlen na Fakultetu elektrotehnike i računarstva (FER) Sveučilišta u Zagrebu, sudjelujući u nastavi i istraživanjima u primijenjenom elektromagnetizmu, mikrovalnoj elektronici i mikrovalnim mjerenjima. Godine 1995. otišao je na Brunel University of West London, Electronic Systems Research Group, gdje je bio uključen u projekte vezane uz elektromagnetsku kompatibilnost, numerički elektromagentizam i elektrostatiku. Istodobno je radio kao konzultant za nekoliko mikrovalnih tvrtki u Ujedinjenom Kraljevstvu. Od 1999. godine ponovno je zaposlen na FERu, gdje je trenutno redoviti profesor iz primijenjenog elektromagnetizma.

Autor je i koautor mnogih radova u znanstvenim časopisima, poglavlja u knjigama, konferencijskih priopćenja i tehničkih studija i recenzent je desetak znanstvenih časopisa. U 2012. godini prof. Hrabar je dobio nagradu Sveučilišta u Zagrebu, FER, za „Iznimna postignuća u istraživačkom radu i inovacijama“.

Mihael Grbić rođen je 13.01.1982. u Sisku, Republika Hrvatska. Osnovnu školu upisuje 1988. u Lekeniku, a završava je u Zagrebu. 1996. upisuje se u Gimnaziju Ivan Supek u Zagrebu. U periodu 2000.-2005. godine studira fiziku na Fizičkom odsjeku Prirodoslovno-matematičkog fakulteta (PMF) Sveučilišta u Zagrebu, gdje izrađuje i svoj diplomski rad „*Proučavanje dinamike virova u tankim filmovima niobija*“ pod mentorstvom prof. dr. sc. Miroslava Požeka. 2004. godine dodijeljena mu je Rektorova nagrada za istraživanje koje je kasnije produbljeno u diplomski rad. Doktorski studij upisuje 2006. godine, te 2011. godine brani svoju doktorsku dizertaciju s temom „*Proučavanje supravodljivih fluktuacija i pseudoprocjepa u visokotemperaturnim supravodičima mikrovalnom metodom*“. Tijekom poslijediplomskog studija uključuje se u aktivnosti europskog projekta SOLeNeMaR (voditelj: prof. dr. sc. Miroslav Požek) na Fizičkom odsjeku koji osniva prvi NMR laboratorij za fiziku čvrstog stanja u Hrvatskoj i u sklopu projekta boravi 7 mjeseci na stručnom usavršavanju na Laboratoire National des Champs Magnétiques Intenses (LNCMI) u Grenoblu (Francuska). Obranom doktorata 2011. godine stječe uvjete za izbor u višeg asistenta na Fizičkom odsjeku PMF-a, te iste godine prima priznanje dekana PMF-a za najboljeg znanstvenog novaka.

U periodu od ožujka 2011. godine do kraja kolovoza 2012. godine boravi 16 mjeseci na poslijedoktorskom usavršavanju na LNCMI-u u grupi dr. Mladena Horvatića. Pritom se sasvim orijentira na proučavanje kvantnog magnetizma metodom nuklearne magnetske rezonancije (NMR), u suradnji s novoosnovanim laboratorijem za NMR čvrstog stanja na Fizičkom odsjeku i objavljuje 3 rada u časopisu Physical Review Letters (faktor utjecaja 7.435). Radovi su dosad prikupili preko 50 citata u CC časopisima. U ovom periodu stekao je iskustvo prijave i provođenja mjerenja u visokim magnetskim poljima (do 34 T), te je naučio provoditi mjerenja u dilucijskom hladnjaku.

Od listopada 2012. godine do kraja travnja 2014. godine boravi na drugom poslijedoktorskom usavršavanju na Institute for Solid State Physics (ISSP), University of Tokyo (Japan) u grupi prof. dr. sc. Masashija Takigawe, gdje tehnikom NMR-a proučava intermetalične spojeve sustava teških fermiona, te time dalje proširuje područje istraživanja.

Od svibnja 2014. godine radi kao docent na Fizičkom odsjeku PMF-a. Trenutno je naveden kao autor 19 znanstvenih radova u časopisima s međunarodnom recenzijom, od kojih je na njih 13 prvi ili glavni autor. Radovi su dosad ukupno prikupili oko 210 citata i h-indeks 7.

"You've got to stick to what you believe in, just carry on and don't change because you think that's what people want. That's how something new comes up. Doing what everybody else is doing is the easy way out, you've got to do your own thing."

Tony Iommi,
the guitarist of *Black Sabbath* and the father of heavy metal

Zahvale

Povuci, potegni, iščupati ne mogu! Kao što ni djed nije mogao sam iščupati repu, tako niti moj doktorat ne bi ugledao svjetlo dana da nije bilo dobrih ljudi koji su mi pomogli da uspješno „iščupam“ svoju doktorsku titulu iz mraka. Prije nego li u ovoj disertaciji opišem svoje doktorsko istraživanje, najprije bih se želio zahvaliti tim ljudima.

Zahvaljujem se svojim mentorima, prof. dr. sc. Silviju Hrabaru i doc. dr. sc. Mihaelu Srđanu Grbiću, što su mi dali priliku da doktoriram, radim na zanimljivome projektu, proširim svoje horizonte (što direktno, što indirektno vezano za moj doktorat), putujem po Europi, i na kraju krajeva – uspješno i doktoriram. Gospodo, beskrajno sam Vam zahvalan!

Zahvaljujem se izv. prof. dr. sc. Dubravku Babiću. Literatura koju mi je posudio i pitanja koja mi je postavio riješila su ključan dio mojeg doktorskog istraživanja. Bez njegove pomoći, dobar dio ovog doktorata vrlo vjerojatno ne bi postojao.

Zahvaljujem se prof. dr. sc. Miroslavu Požeku, koji mi je, uz Mihaela, puno pomogao da se brzo i dobro uklopim i na Fizički odsjek, ali i u naš labos. Nisam često k njemu išao po pomoć, ali kada bih došao, uvijek bi mi pomogao – bilo da je u pitanju odgovor na neko znanstveno pitanje, nabavka (skupe) znanstvene literature, ili „povlačenje“ pravih osoba „za rukav“.

Zahvaljujem se Josipu Žilaku i Željku Osrečkom za sve elektroničarske *know-how* savjete i za čelične živce kada sam ih gnjavio s beskonačnim mjerenjima faktora šuma raznih sklopova koje sam koristio u svojem istraživanju. Također, zahvaljujem se i Damiru Altusu, koji mi je isto tako dao „brdo“ praktičnih elektroničarskih savjeta, i koji je rekao da će me zadaviti ako mu se ne zahvalim na početku svoje disertacije! Nadam se da sam ovim činom kupio njegovo milosrđe i da ću živjeti još koju godinu i možda, samo možda, doživjeti i duboku starost.

Zahvaljujem se doc. dr. sc. Daliboru Paaru i doc. dr. sc. Emilu Tafri, koji su imali povjerenja u mene i omogućili mi da se okušam i kao predavač na njihovim predmetima. Držanje predavanja i rad sa studentima često je na mene djelovalo rehabilitacijski i razbijalo mi je monotoniju, pogotovo kada sam znao „zaglaviti“ sa svojim doktorskim istraživanjem. Nadam se da sam opravdao njihovo povjerenje.

Zahvaljujem se svojim roditeljima na podršci, ljubavi i razumijevanju (ili barem pokušaju istog!) kroz sve ove godine. Tata, hvala ti što si prepoznao da me zanima „struja“ i što si me znao u ključnim trenucima „pogurnuti“ u pravome smjeru. Hvala ti i što si me naučio „masu“ praktičnih stvari, i to ne samo vezano uz moju struku. Mama, hvala ti za sva fina jela (pogotovo ona na žlicu!) i kolače, za sav oprani i ispeglani veš, i najvažnije, za sve naše intimne razgovore. Onda kada sam to najviše trebao, ti si uvijek znala što treba reći. I naravno – mama, tata, hvala vam što ste me napravili ovako pametnog i ovoliko prokleto neodoljivog!

Zahvaljujem se svojoj maloj sestri Klari (koja više i nije tako mala) što mi je bila psiholog, prijatelj, najbolji cimer, hrid i – redovita mušterija za slušanje svih mojih glupih fora, priča i

viceva. Svi oni koji misle da su neke moje fore ili priče čuli puno puta: niste ih čuli ni približno onoliko puta koliko ih je čula ona!
Zahvaljujem se svojoj ekipi: Miceku, Žuki, Nevenu, Živcu i Danču, uz koje su mi studentski dani, od prvog do posljednjeg, bili lakši, ugodniji i zabavniji. Također, kao „dotepencu“, činjenica da sam pronašao ovako dobru ekipu uvelike mi je olakšala prilagodbu na novu sredinu. Dečki, hvala vam za sva „taksiranja“, „prespavance“, druženja, kartanja, *hard reset*-ove i *soft reset*-ove! Ako ništa drugo, barem imamo jedni druge!
Zahvaljujem se svojemu pajdašu Lovri Blažoku – jednoj od rijetkih osoba iz mojeg kraja s kojom sam se družio, a s kojom sam si i dalje blizak. Vrijeme koje smo proveli kao cimeri jedno mi je od ljepših razdoblja otkako živim u Zagrebu. A i danas, s obzirom na to da smo obojica u Zagrebu, puno mi znači to što mogu s nekime otići na kavu, pivu ili gemišt i „pomenjiti se po domaći“.
Zahvaljujem se Branimiru Mihaljeviću, čije mi je društvo omogućilo da se od svojeg šestog radnog dana (jer je prvih pet bio na godišnjem odmoru – oporavljao se od svoje svadbe!) na Fizičkome odsjeku osjećam kao doma. Nadam se da sam mu barem djelomično vratio uslugu kada sam ga dočekao u Ericssonu. Brane, već sam ti to rekao, i opet ću ti reći: ti si najdobroćudnija osoba koju sam ikad upoznao. Uz tvoju pozitivnost, teško je (p)ostati tužan ili ljut. Molim te, nemoj se nikad promijeniti!
Zahvaljujem se Davoru Zaluškom, „dežurnome krivcu“ na ZRK-u, kako je on sam to govorio. On je dežurni krivac i za to što sam uopće počeo razmišljati o doktoratu, za to da sam na kraju i upisao doktorat, ali i za to da nisam odustao od doktorata (a bio sam u nekoliko navrata blizu tome). „Navukao“ me je na šah i pomoću šaha naučio me je da uvijek nastojim planirati barem dva-tri koraka unaprijed. Često me je znao izvesti na ručak na interesantna mjesta s još interesantnijom „špajz kartom“ i naučio me je da, kako i jelo, tako i život, uvijek mora imati dinamike da bi bilo dobro. I najvažnije, imao je beskonačno strpljenje za moju kuknjavu u vezi doktorata i uvijek me je saslušao jer je znao da ću se poslije osjećati bolje.
Zahvaljujem se Dariju Bojanjcu. Njemu mi je najteže zahvaliti se jer ne znam odakle bih počeo. Svojim maltretiranjem naučio me je poniznosti i kontroli mojeg često nezgodnog temperamenta (ovo, doduše, još uvijek savladavam!). Svojim savjetima naučio me je da čvrsto stojim na zemlji: da budem svjestan svojih prednosti, ali i svojih nedostataka, da prednosti čuvam i jačam, a nedostatke popravljam. Našim čestim odlascima na kavu i sladoled podsjetio me je da se čovjek treba radovati malim stvarima. Odlascima na Dinamove tekme i razna događanja sličnog štiha pomogao mi je da u sebi probudim pomalo usnulu dinamovštinu i da se sjetim zašto sam uopće zavolio Dinamo. I ono najvažnije, pomogao mi je da shvatim da je najbitnija stvar u životu dobro se za*ebavati! Zbog svega što su me naučili, Darija i Davora smatram svojom starijom braćom.
I za kraj, ovu disertaciju posvećujem svojoj baki Kati.

Abstract

Nuclear magnetic resonance (NMR) is a physical phenomenon used to study materials by recording the interaction of radiofrequency (RF) electromagnetic radiations with the nuclei placed in a strong magnetic field. The spectroscopic technique, used to observe local magnetic fields around atomic nuclei, is called NMR spectroscopy. Modern NMR spectroscopy measurements, especially in condensed matter physics, have a trend of continuous decrease of magnitude of receiving signals, which is a problem because, as response signal levels decrease, the background noise of the used NMR spectroscopy systems gradually becomes a bigger problem. Indeed, the assurance of high measuring sensitivity is one of the most challenging issues for any NMR spectroscopy system today. In this thesis, an accurate noise model of the entire probe-to-spectrometer receiving chain for condensed matter physics is proposed. It is based on the concept of noise figure. The model predicts both the signal and noise levels in every component of the NMR spectroscopy receiving chain. Furthermore, it enables identification of the "weakest" component and, therefore, the optimization of the whole system. The most important property of the proposed model is the possibility to find system parameters that reduce the measurement time by an *a priori* calculation, rather than an *a posteriori* approach. The model was tested experimentally by NMR measurements on several different samples. It was found that the measurement time can still be significantly shortened, down to at least one half of the measurement time, starting from optimized conditions with commercially available components. Thus, the proposed model can be used as a tool for both quantitative analysis of the noise properties and a sensitivity prediction of practical NMR systems in physics and material science. A Python-written program, which calculates noise figure and predicts input and output signal-to-noise ratios (SNRs) of the NMR receiving chain, based on the described noise model of the receiving chain, has been created and made available online. Additionally, an electromagnetic model of the NMR probe, which predicts SNR level at its output, has been developed and presented in this thesis. This model has been compared to the proposed noise model of the receiving chain, and the comparison results showed to be satisfactory. Finally, two possible upgrades of NMR preamplifiers: one in terms of power gain level enhancement with the addition of a second stage amplifier, and the other in terms of a new proposed scheme, PCB layout and proper electronic components selection for the NMR preamplifier, have been proposed in order to further improve noise properties of the NMR spectroscopy system receiving chain.

Keywords: NMR, noise, noise figure, preamplifier, measurement time decrease, sensitivity enhancement

Prošireni sažetak

Optimizacija radiofrekvencijskih komponenti sustava kriogene spektroskopije nuklearne magnetske rezonancije

Ovaj doktorski rad opisuje rezultate istraživanja u području niskošumnih radiofrekvencijskih (RF) prijemnika za primjenu u sustavima kriogene spektroskopije nuklearne magnetske rezonancije (NMR spektroskopije). Najveći problem u konstrukciji RF prijemnika sustava kriogene NMR spektroskopije jest mali odnos signal-šum koji ograničava osjetljivost sustava. Taj se problem u komercijalnim NMR sustavima u fizici kondenzirane tvari obično rješava korištenjem kriogeničke antene-sonde i usrednjavanjem rezultata mjerenja. Iako je usrednjavanje signala efikasno, ono uzrokuje vrlo dugo vrijeme mjerenja, koje ponekad prelazi i 10 sati. U ovoj disertaciji predlaže se metoda skraćenja vremena mjerenja zasnovana na optimizaciji šumnih svojstava sklopovlja cjelokupnog prijemnog lanca kriogene NMR spektroskopije. Postignuti teorijski i eksperimentalni rezultati pokazuju da je optimizacijom komponenti i njihovog položaja u mjernom lancu moguće skratiti ukupno vrijeme mjerenja na manje od 50% početne vrijednosti. U ovome radu primjenjuje se znanje mikrovalne i RF elektronike na sustavima NMR spektroskopije korištenih u fizici kondenzirane tvari s ciljem teorijskog i numeričkog opisa navedenih sustava sa stajališta šuma. Na ovaj način moguće je odrediti usko grlo sustava NMR spektroskopije i njegova ograničenja te predložiti potencijalna unapređenja uskog grla, kao i cjelokupnog sustava, s ciljem maksimalnog povećanja mjerne osjetljivosti. Ideja rada je da razvijene metode budu razumljive i fizičarima čvrstog stanja, kao i RF inženjerima. Prvi dio rada opisuje princip NMR-a, metodu NMR spektroskopije i sustave NMR spektroskopije koji se koriste u fizici kondenzirane tvari. Na taj način RF inženjeri imaju kratak uvod u vrstu sustava koji će biti analiziran i poboljšavan. S druge strane, ovdje se pripadnici fizičarske zajednice mogu ili podsjetiti, ili mogu učvrstiti svoje znanje o NMR-u. U drugome dijelu rada prelazi se sa pogleda na sustave NMR spektroskopije sa stajališta fizičara čvrstog stanja na pogled sa strane RF inženjera, gdje se navedeni sustavi analiziraju koristeći koncept faktora šuma. Nadalje, određena su uska grla sustava NMR spektroskopije, te su predložena odgovarajuća poboljšanja. Nadalje, dana je osnovna definicija šuma i njegovih glavnih svojstava, kao i konkretan opis šuma u sustavima NMR spektroskopije, s ciljem da fizičari čvrstog stanja utvrde njegove mehanizme nastajanja, njegova svojstva i ograničenja sustava koja diktira šum. Između ostaloga, ovaj dio rada služi i kako bi se RF inženjerima prikazalo korištenje njihovih alata na sustavu NMR spektroskopije. S druge strane, fizičari čvrstog stanja mogu utvrditi razloge kako i zašto implementirana poboljšanja sustava NMR spektroskopije rade, njihova ograničenja, te moguće dodatne nadogradnje koje znatno mogu povećati mjernu osjetljivost sustava.

U 1. poglavlju ("*Introduction*" – „Uvod") dana je motivacija koja se krije iza samog istraživanja u ovome radu. Navode se osnovna ograničenja postojeće NMR tehnologije, s posebnim naglaskom na problematiku osjetljivosti prijemnog sustava, i daje pregled tradicionalnih rješenja u sustavima kriogene NMR spektroskopije u fizici kondenzirane tvari. Ističe se nužnost interdisciplinarnog pristupa zbog potrebe za znanjima iz RF inženjerstva, elektronike i fizike.

U 2. poglavlju ("*Nuclear magnetic resonance*" – „Nuklearna magnetska rezonancija") daje se pregled fizikalnih osnova, počevši od kvantnih veličina nuklearnoga spina i gradijenta električnog polja, preko mjerenja izmjeničnoga odziva jezgre, pa sve do uspostavljanja njezine spektralne karakteristike. Opisani su principi NMR-a i nuklearne kvadrupolne rezonancije (NQR-a) te metoda NMR spektroskopije. Opisana su dva osnovna tipa mjerenja: tzv. *free induction decay* (FID) mjerenje i tzv. *spin-echo* mjerenje, te su dani primjeri tri osnovna mjerenja: tzv. longitudinalnog relaksacijskog vremena (T_1), tzv. transverzalnog relaksacijskog vremena (T_2) i frekvencijskog spektra odzivnog signala. Navode se inženjerski parametri NMR sustava i naglašava potreba optimizacije u cilju skraćenja vremena mjerenja. Daju se fizikalne informacije koje se mogu dobiti pravilnom interpretacijom NMR mjerenja. Na kraju poglavlja navedene su osnovne primjene sustava NMR spektroskopije.

U 3. poglavlju ("*The system of nuclear magnetic resonance spectroscopy*" – „Sustav spektroskopije nuklearne magnetske rezonancije") dan je opis općenitog načina rada sustava NMR spektroskopije koji se koriste u fizici kondenzirane tvari. Opisuje se eksperimentalni sustav kriogene NMR spektroskopije za primjenu u fizici kondenzirane tvari kao RF odašiljački lanac koji preko male magnetske antene pobuđuje mjerni uzorak, dok se elektromagnetski (EM) odziv uzorka, uzrokovan Larmorovom precesijom, obrađuje u prijemnom lancu. Također, dan je detaljan pregled najvažnijih dijelova sustava (a to su spektrometar, duplekser, sonda i predpojačalo) i njihovih funkcija – kao dio sustava, ali i kao zasebnih elemenata. Na kraju poglavlja daju se osnovni teorijski principi, kao i inženjerski parametri sustava s primjerima raspoloživih tehnoloških rješenja.

U 4. poglavlju ("*Noise in nuclear magnetic resonance spectroscopy system*" – „Šum u sustavu spektroskopije nuklearne magnetske rezonancije") predstavljen je koncept šuma. Osnovni tipovi šuma (termički šum, $1/f$ šum i šum sačme) koji se javljaju u svim RF prijemničkim sustavima, pa tako i u prijemničkom sustavu NMR spektroskopije, opisani su u ovome poglavlju, a najvažniji elementi sustava NMR spektroskopije raspoređeni su prema tipu šuma koji je u njima dominantan. Također, uvedena je mjera koja uspoređuje razinu željenog signala s razinom neželjenog pozadinskog šuma (tzv. odnos signal-šum), kao i mjera koja opisuje degradaciju odnosa signal-šum kroz sustav (tzv. faktor šuma). Na kraju poglavlja daje se pregled metoda analize lanca šumnih četveropola.

U 5. poglavlju ("*Electromagnetic model of the probe*" – „Elektromagnetski model sonde") opisan je razvijeni elektromagnetski model NMR sonde koji služi za procjenu odnosa signal-

šum na izlaznim krajevima sonde. Pokazuje se da se sonda sustava NMR spektroskopije može modelirati kao mala antena-petlja (magnetski dipol) koja radi u bliskome polju. Izvedeni su aproksimativni izrazi za inducirani prijemni signal i odnos signal-šum, uzevši u obzir temperaturni gradijent okoline.

U 6. poglavlju ("*Noise model of the receiving chain*" – „Šumni model prijemničkog lanca") opisan je razvijeni model najosjetljivijeg dijela sustava NMR spektroskopije sa stajališta šuma – njegovog prijemnog lanca. Predloženi model omogućuje predikciju i optimizaciju osjetljivosti sustava. Izvedeni izraz koji opisuje šumna svojstva prijemnog lanca dan je u ovome poglavlju, kao i opis njegova izvoda, te zaključke koji se mogu izvući iz navedenog izraza. Predloženi model zasnovan je na faktoru šuma kaskade četveropola koji se nalaze na različitim temperaturama. Uvodi se efektivni odnos signal-šum koji uzima u obzir sklopovske i programske postavke spektrometra, uključujući i usrednjavanja signala.

U 7. poglavlju ("*Experimental verification of the developed models*" – „Eksperimentalna verifikacija razvijenih modela") prikazana je eksperimentalna verifikacija modela prezentiranih u prethodna dva poglavlja. Također, navedeni modeli uspoređeni su međusobno, čime je njihova točnost analizirana, testirana i verificirana. Opisana su mjerenja nekoliko različitih uzoraka s različitom sklopovskom organizacijom sustava i različitim programskim postavkama. Rezultati potvrđuju ispravnost razvijenog modela i pokazuju da je optimizacijom parametara sustava, u slučaju mjerenja uzoraka sa slabim odzivom, moguće skratiti vrijeme mjerenja na manje od 50% početne vrijednosti. Na kraju, potencijalna poboljšanja sustava NMR spektroskopije su analizirana, komentirana i predložena.

U 8. poglavlju ("*Design and optimization of high-gain and low-noise NMR preamplifiers*" – „Projektiranje i optimizacija niskošumnih NMR predpojačala visokog pojačanja") dan je teorijski prikaz općenitog procesa dizajna i optimizacije mikrovalnih niskošumnih pojačala. Daje se pregled standardnih metoda projektiranja jednostupanjskih i dvostupanjskih predpojačala s naglašavanjem specifičnosti dizajna za NMR sustave. Nadalje, prikazan je praktični primjer optimizacije komercijalnog kriogenog niskošumnog NMR predpojačala dodavanjem drugog stupnja pojačanja. Konačno, prikazan je praktični primjer analize, dizajniranja i konstrukcije niskošumnog NMR predpojačala visokog pojačanja. Projektirano je i konstruirano NMR predpojačalo s HEMT-ovima kao aktivnim elementima, izmjereni su njegovi parametri i uspoređeni su s komercijalnim NMR predpojačalima.

U Zaključku ("*Conclusion*" – „Zaključak") predstavljen je *summa summarum* zaključaka cijelog istraživanja. Pokazano je da je pravilnim odabirom ključnih komponenata sustava NMR spektroskopije moguće skratiti trajanje NMR mjerenja na jednu polovinu početnog trajanja. Također, pokazano je da su potencijalne nadogradnje sustava NMR spektroskopije daleko od svojih gornjih granica, što znači da postoji i više nego dovoljno prostora za relativno lako postizanje povećanja mjerne osjetljivosti u ovakvim sustavima. Dakle, sažeti su svi postignuti

rezultati istraživanja, ukratko je objašnjena njihova izvornost i dane su preporuke za buduća istraživanja.

Konačno, u dodatku na kraju rada ("*Appendix A. Receiving chain noise figure calculator*" – „Dodatak A. Kalkulator faktora šuma prijemničkog lanca") nalazi se programski kôd, napisan u programskom jeziku *Python*, a koji služi za izračun faktora šuma prijemnog lanca sustava NMR spektroskopije, kao i za procjenu odnosa signal-šum na ulazu, odnosno izlazu, navedenog lanca. Ovaj programski kôd temelji se na šumnome modelu prijemnog lanca NMR spektroskopije opisanome u 6. poglavlju. Navedeni program dostupan je *online* korištenjem *GitHub*-a ili *Dropbox*-a, a poveznice na program dostupne su u popisu literature ovog doktorskog rada.

U rezultatima istraživanja opisanoga u ovoj disertaciji ostvareni su sljedeći izvorni znanstveni doprinosi:

- Model šumnih svojstava antene-sonde i prijemnog lanca sustava kriogene NMR spektroskopije
- Poboljšanje mjerne osjetljivosti prijemnog lanca sustava kriogene NMR spektroskopije s ciljem smanjenja vremena mjerenja
- Optimizacija parametara radiofrekvencijskog predpojačala kriogene NMR spektroskopije s ciljem poboljšanja odnosa signal-šum i eksperimentalna verifikacija

Zaključak istraživanja opisanoga u ovoj disertaciji je sljedeći: Najveći problem kod današnjih mjerenja NMR spektroskopijom, posebno u fizici kondenzirane tvari, jest kontinuirani trend smanjenja razina odzivnih signala. Kako se razine odzivnih signala smanjuju, pozadinski šum korištenih sustava NMR spektroskopije postepeno postaje sve veći problem. Usrednjavanje rezultata više mjerenja, koje se u zadnjih tridesetak godina pokazalo kao moćan alat prilikom raznih mjerenja signala niskih razina, počinje konzumirati znatne količine vremena: neka današnja NMR mjerenja mogu potrajati i preko 10 sati. Primijenjene nadogradnje, poput procesa kriogeničkog hlađenja NMR sonde i, u novije vrijeme, NMR predpojačala, pokazuju vidljiva poboljšanja sustava NMR spektroskopije, ali te su nadogradnje utvrđene empirijski, bez dubljeg razumijevanja njihovih načina rada ili njihovih gornjih granica. Znanstveno istraživanje, opisano u ovoj disertaciji, izrodilo je teorijski opis najosjetljivijeg dijela sustava NMR spektroskopije sa stajališta šuma, što je njegov prijemni lanac, a točnost ovog teorijskog opisa potvrđena je i eksperimentalno i numerički. Nadalje, izveden je elektromagnetski model sonde koji omogućuje predikciju odnosa signal-šum na njenom izlazu, a taj model uspoređen je sa razvijenim modelom prijemnog lanca sustava NMR spektroskopije. Rezultati usporedbe potvrdili su točnost oba razvijena modela. Ne samo da razvijeni teorijski opis prijemnog lanca sustava NMR spektroskopije objašnjava kako i zašto primijenjene nadogradnje sustava rade, nego su i jasno vidljiva potencijalna buduća poboljšanja sustava. Pokazano je da je pažljivim

odabirom ključnih elemenata sustava NMR spektroskopije moguće skratiti vremena mjerenja na manje od polovice početne vrijednosti. Također je pokazano da su primijenjene nadogradnje sustava daleko od svojih gornjih granica, što znači da postoji dovoljno mjesta da se i već primijenjene nadogradnje znatno poboljšaju na relativno jednostavne načine. Na kraju, predložena su dva potencijalna poboljšanja NMR predpojačala: prvo je povećanje razine pojačanja dodavanjem drugog stupnja pojačanja, a drugo je nova predložena shema, dizajn tiskane pločice i pravilni odabir elektroničkih komponenti za NMR predpojačalo, oboje s ciljem dodatnog poboljšanja šumnih svojstava prijemnog lanca sustava NMR spektroskopije.

Ključne riječi: NMR, šum, faktor šuma, predpojačalo, skraćenje vremena mjerenja, povećanje mjerne osjetljivosti

Contents

List of abbreviations

NMR … nuclear magnetic resonance
NQR … nuclear quadrupolar resonance
MRI … magnetic resonance imaging
FID … free induction decay
VOCS … variable offset cumulative spectra
SNR … signal-to-noise ratio
VSNR … voltage signal-to-noise ratio
SWR … standing wave ratio
FWHM … full width at half maximum
RMS … root mean square
SSB … single sideband
CW … continuous wave
FT … Fourier transformation
RF … radiofrequency
S … scattering
Tx … transmit(ter)
Rx … receive(r)
T/R … transmit/receive
TL … transmission line
A/D … analog to digital
AGC … automatic gain control
DSP … digital signal processor
PC … personal computer
CAD … computer aided design
VNA … vector network analyzer
PCB … printed circuit board
SMD … surface–mount device
SMA … SubMiniature version A
SOT … small outline transistor
LNA … low–noise amplifier
HEMT … high-electron-mobility transistor
CMOS … complementary metal-oxide semiconductor
FET … field effect transistor
MESFET … metal-semiconductor field effect transistor
BJT … bipolar junction transistor
Op Amp … operational amplifier
AC … alternating current
DC … direct current
SOA … state-of-the-art
2STA … two–stage preamplifier
M290 … MITEQ AU-1114-SMA
T77 … THAMWAY N141-206AA(D)
MC290 … Mini-Circuits HELA -10D+
NCP … new–constructed preamplifier

Chapter 1

Introduction

In the 20^{th} century, among many revolutionary events and discoveries, the two processes that, in the author's opinion, laid the foundation for the technological advance we have nowadays are the electrification and the long distance wired communication. What these two processes have in common is the fact that their main "product" gets transmitted from the provider to the end-user by some kind of a conductor: electricity is transmitted from the power plants to the consumers by the power lines, while the information was firstly transmitted from the sender to the receiver via the telegraph lines, later via the telephone wires, and nowadays via the copper pairs or even optical fibers. Of course, wireless transmission is nowadays also very popular, but even in this kind of systems, there are conductors between the transmitter and the transmitting antenna on one end, and between the receiving antenna and the receiver on the other end. The point is, in order to transmit electricity or communication from one place to another, one needs to use conductive materials.

Because of our human nature of craving to make everything bigger, better, faster and stronger, exhausting efforts are being made on a daily basis in order to be able to send more electricity, and more information, to more people, with higher quality, and in less time. One of the first remarks in the history of improving these systems surely has to be that not every material has the same transmission capacity. Nowadays, even the children in the elementary schools learn that it is not the same if one makes an electric cable out of copper, gold, wood, paper or plastic. In high schools or during the academic education, it is taught that the cause of this is the fact that not every material has the same atomic or crystal structure, and that not every structure conducts electricity equally well. We learn that there is a group of materials that always conduct electricity very well, a group of materials that conduct electricity well under certain conditions, and a group of materials that are very poor conductors, we learn that they are called conductors, semiconductors and isolators, respectively, and we learn their crystal structures in order to be able to distinguish them.

One of the techniques that is being used in the analysis of local properties of different

materials is called nuclear magnetic resonance (NMR) spectroscopy. The application of this technique is rising in the last 60 years, as the use of common conducting materials is reaching its upper limit, so there is an increasing need for the new conducting materials, whose capacities can surpass the capacities of common conductors. These new conducting materials are known under the name of superconductors.

However, a very serious issue with superconductors is that, as years pass by and more exotic materials get discovered and measured, their NMR measurements have a negative trend of the response signal levels. This started becoming an immense problem because, as response signal levels gradually decrease, the background noise levels of the used NMR spectroscopy systems gradually become of the same, or even higher, order of magnitude, compared to the response signal levels. Therefore, the measuring sensitivity of modern NMR samples is sometimes very poor, compared to, for example, the sensitivity of modern radio receivers. The averaging of multiple measurements showed to be a mighty tool in the NMR measurements, however, nowadays it starts consuming exhausting amounts of time, as some modern NMR measurements can last up to ten hours for a single point. Some improvements, like the introduction of the cryogenic cooling process, to the NMR spectroscopy systems, proved to be very efficient, but these improvements have been determined empirically, without the deeper understanding of their upper limit or the reason why and how these improvements work.

Of course, the latter fact leaves a lot of unanswered questions hanging in the air: How exactly do the implemented improvements work? What is their upper limit? What else can be improved in order to notably enhance NMR measurements' sensitivity? What is the shortest achievable measurement time with the equipment available in our NMR laboratory? What could be the shortest achievable measurement time if we replaced some of the components in our NMR laboratory with better ones, and which components would be the best to replace? Which component is the bottleneck in the NMR spectroscopy system? And so on...

In order to answer the aforementioned questions, a collaboration between the Laboratory for Solid State NMR and High Frequency Measurement from the Department of Physics, Faculty of Science, and the Department of Wireless Communications from the Faculty of Electrical Engineering and Computing, both from the University of Zagreb, Croatia, has been made, and its end result is a scientific research presented in this thesis. The idea was to make a crossover from the solid state physicist's point of view on the NMR spectroscopy systems to the one of a radiofrequency (RF) and antenna engineer, and to combine the knowledge of solid state, condensed matter and material physics, with the knowledge of antennas, RF and microwave engineering, in order to describe these systems both theoretically and numerically, and then determine their bottlenecks and the upper limits of their possible enhancements.

The author tried to present his research in this thesis in a way so that both solid state physicists and microwave engineers can find it interesting to read. The first half of the thesis describes

the principle of NMR, the method of NMR spectroscopy and the NMR spectroscopy systems used in condensed matter physics in order for the microwave engineers to have an introduction and a short tutorial to the type of systems that is going to be analysed and improved. On the other hand, the physicists can either refresh their memory or strengthen the knowledge of NMR here. In the second half of the thesis, a crossover to the RF engineering point of view on the NMR spectroscopy systems occurs, where these systems are analysed and described from the aspect of noise, mainly with the use of noise figure. Furthermore, potential bottlenecks of the NMR spectroscopy systems have been determined, and their potential solutions have been proposed. A fundamental definition of noise and its main properties has also been given here, as well as a specifical description of noise in the NMR spectroscopy systems, in order for the solid state physicists to understand its generation mechanisms, its properties and its boundaries. This part of the thesis serves for the RF engineers to examine the use of "their tools" on a system that is very rarely used in their branch, while the solid state physicists can learn the reason why all the implemented improvements in the NMR spectroscopy systems work, their upper limits, and possible additional upgrades that can drastically enhance NMR measurements' sensitivity.

Nevertheless, in the end, the success rates of both the above-mentioned colaboration and the intent of the author to make this thesis interesting and useful is up for the reader to decide.

Chapter 2

Nuclear magnetic resonance

In this chapter, an overview of the phenomenon of nuclear magnetic resonance (NMR) will be given, as well as overviews of the method of NMR spectroscopy, its basic measurements and different types of acquisition of the basic measurements, respectively.

2.1 The concept of nuclear spin

Any time a question appears to describe something (e.g. an object, a phenomenon, some material...), a natural human reaction is to try to explain the object that needs description by "dissecting" it to its more basic parts. This way, one explains smaller and simpler parts of an object in order to try to understand its whole picture more easily than in the case of explaining the whole object at once. So, for example, the simplest description of a human body would be that it is a structure comprised of arms, legs, a trunk and a head. A bit more detailed description of a human body may be that it is comprised of arms, hands, legs, feet, thorax, abdomen, a neck and a head. The next step would be to count internal organs of a trunk, the step after may be to describe which materials are the organs made of, and so on, until one gets to the point where every matter (so human body obviously counts, too) is dissected to the same structure – the atomic structure.

The atomic and subatomic levels are very often used to easily explain something complex that is going on at macroscopic level by explaining simpler processes occuring at microscopic level. This is the case with NMR, where various materials are being analysed by manipulation of and interaction with some of its subatomic properties. So, from the subatomic point of view, there are three important physical properties of atomic nuclei that define all matter: *mass*, *electric charge* and *nuclear spin* [1]. The *mass* of bulk matter is a physical property that is the easiest to understand and to grasp because it is pretty straightforward: the mass of this doctoral thesis is equal to the sum of masses of all the atoms this thesis is comprised of. This property, therefore, is easy to imagine at both microscopic and macroscopic level. The *electric charge*

is a physical property where atoms and molecules are bound together by strong electrostatic interactions between the positively charged nuclei and the negatively charged electrons. This property is one of the properties that define magnetic properties of matter on a macroscopic level. Although this property is not always visible at macroscopic level, it is possible, by performing simple experiments, to separate some of the charges and achieve obvious macroscopic effects, such as sticking a balloon to the ceiling by rubbing it on a woolly jumper. The *nuclear spin* (represented in condensed matter physics by I) is a physical property that defines magnetic properties of the nucleus. There are some materials that have visible magnetic properties at macroscopic level, which are called magnets, but generally, nuclear spin is a physical property that cannot be seen at macroscopic level for the most of matter.

The physical property of nuclear spin is an intrinsic property of the atomic nuclei. Atomic nuclei simply *have* spin. A visualization of the nuclear spin can be seen in Figure 2.1.

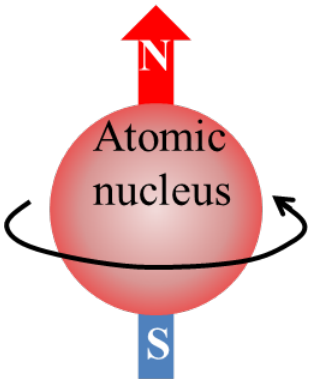

Figure 2.1: Visualization of nuclear spin

When observed at macroscopic level, nuclear spins of all the nuclei of some matter cancel each other out, so that the overall nuclear spin of the matter is equal to zero. However, it is possible to "mess around" with this overall angular momentum and make some conclusions about the observed matter due to the matter's response. This means that the atomic property of nuclear spin provides scientists with a powerful tool for the analysis of microscopic properties and internal structure of matter without disturbing it (e.g. NMR), so these properties have an important role in modern physics.

2.2 The principle of nuclear magnetic resonance

Nuclear magnetic resonance (NMR) is a physical phenomenon used to study materials by recording the interaction of radiofrequency (RF) electromagnetic radiations with the nuclei placed in a strong magnetic field. The consequences of this interaction are created by an effect similar to the effect of stimulated emission in laser physics: when in thermal equilibrium and zero magnetic field, spin energy levels of the nuclei are equal to E_0. However, if the nuclei are placed in a magnetic field, its energy levels split to $2I+1$ states, where $I \in \{\frac{1}{2}, 1, \frac{3}{2}, 2, \cdots\}$. For simplicity, we will look at $I = \frac{1}{2}$, where levels split to two independent states. Here, the energy difference, ΔE, between the two energy states increases with increasing value of the applied external magnetic field, B_0 [2]:

$$\Delta E = \hbar \cdot \gamma \cdot B_0, \tag{2.1}$$

where $\hbar$ stands for reduced Planck's constant, while γ represents the magnetic property of the observed nuclei called *gyromagnetic ratio*. This energy splitting is known as the *Zeeman effect* (Figure 2.2).

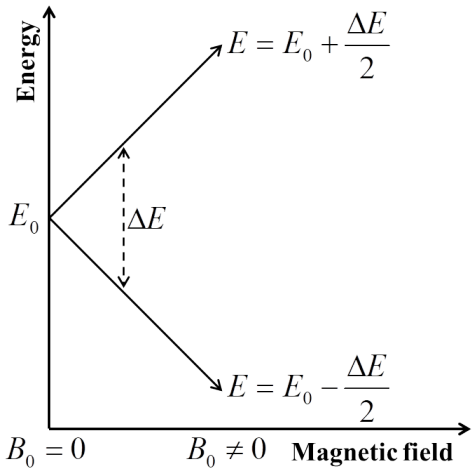

Figure 2.2: The Zeeman effect

After the split of the energy states, the lower energy level is more populated by the nuclear spins than the higher one. Now, if one applies RF electromagnetic radiation to the observed nuclei, whose energy equals ΔE, population inversion of the spins is going to occur. And just as the excited electrons in the laser return to the lower available energy state by emitting light (or more precise, photons), excited nuclear spins also return to the lower available energy state by emitting electromagnetic radiation. This principle of causing transitions of nuclei spins between the Zeeman energy levels is in fact the *principle of nuclear magnetic resonance* [2, 3].

2.3 The method of nuclear magnetic resonance spectroscopy

In section 2.2, NMR has been explained by the analysis of spin energy levels of the observed nuclei. Here, the phenomenon of NMR is going to be explained in time domain.

The overall magnetic moment, when the nuclei are in thermal equilibrium, is equal to zero. This is because, in the absence of the external magnetic field, observed nuclear spins are oriented in different directions when compared to each other, and in such a way that their overall contribution is equal to zero. On the other hand, when placed in a strong external direct magnetic field, these spins orientations change so that the orientation of the overall magnetic moment is equal to the orientation of the external magnetic field. This effect can be compared to the motion of a compass needle in a magnetic field (Figure 2.3).

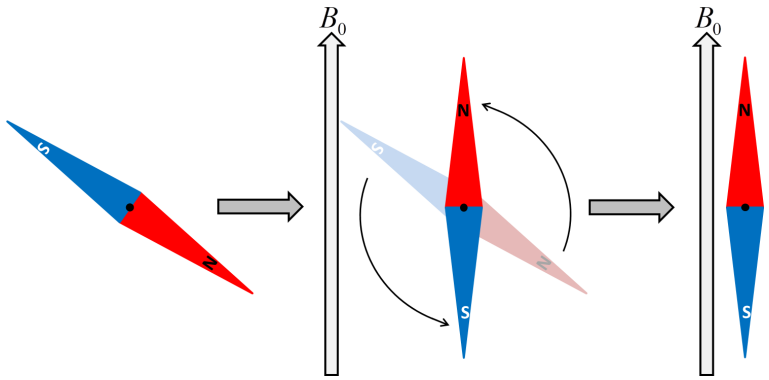

Figure 2.3: Motion of a compass needle in a magnetic field

However, it is necessary to mention that the analogy with a compass needle is not completely accurate: the orientation of the overall magnetic moment, just as the orientation of the compass needle, really is equal to the orientation of the external magnetic field, but not all the orientations of the nuclear spins are equal to the orientation of the external magnetic field. Most of nuclear spins actually move *around* the field in a motion called *precession* (Fig 2.4).

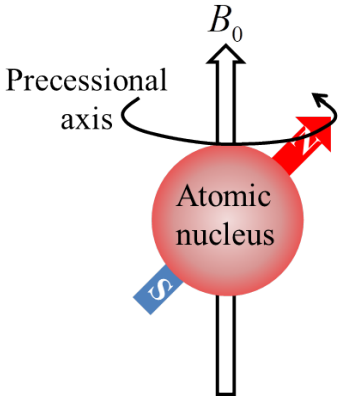

Figure 2.4: Nuclear spin precession

To better understand the concept of precession, one can consider the motion of a child's

spinning top [1]: if the top is set spinning with its spinning axis exactly vertical with respect to the gravitational force, it has a stable motion. However, if the top is spinned in a sloppy way, so that the spinning axis is slightly skew, then the gravitational pull on the top and the reaction of the ground on the top's tip combined produce a torque that tries to pull the top to the ground. If the top is spinning fast enough. it does not fall over immediately, but instead, the spinning axis executes a precessional motion, going around in a circle. This kind of motion happens to the nuclear spin placed in an external magnetic field, where the angle of precession depends on the initial orientation of the nuclear spin itself.

Of course, just as it is possible to determine the frequency of the spinning top's precession motion, it is also possible to determine the frequency of the precession of nuclear spins. This precession frequency of nuclear spins is called *Larmor frequency*, and it can be shown that it depends on the level of the external strong direct magnetic field, B_0, and gyromagnetic ratio, γ [1]:

$$\omega_L = \gamma \cdot B_0. \tag{2.2}$$

As it was already mentioned, when placed in a strong external direct magnetic field, the orientation of the overall magnetic moment is in equilibrium equal to the orientation of the magnetic field (Figure 2.5):

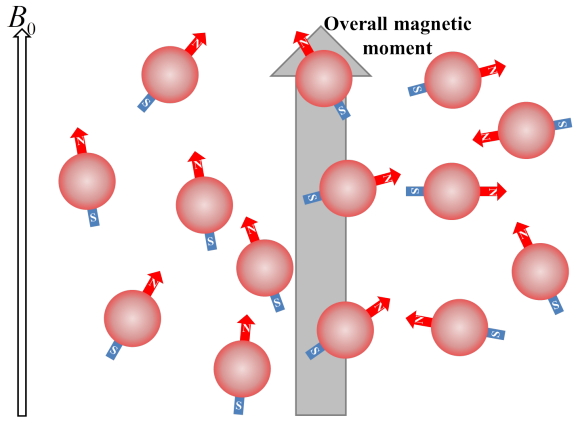

Figure 2.5: Orientation of overall magnetic moment in equilibrium

However, if one applies additional alternating magnetic field, with its frequency equal to Larmor frequency, the orientation of the overall magnetic moment changes and the described system gets thrown out of balance. If this additional alternating magnetic field is applied for a short time (i.e. as a pulse), just enough to unbalance the system, the orientation of the magnetic moment is no longer equal to the orientation of the external strong direct magnetic field. But after the end of the pulse, the orientation of the overall magnetic moment gradually changes until it gets equal again to the orientation of the external strong direct magnetic field. The amount of time needed for the disbalanced orientation of the magnetic moment to become equal again to the orientation of the external strong direct magnetic field is not always equal. It depends on

magnetic properties of the observed nuclei, and also on the orientation of the additional applied alternating magnetic field. Not only can this amount of time be observed in time domain (e. g. see Figure 2.11a), but can also be transformed into frequency domain by Fourier transformation (e. g. Figure 2.11b), and then, one can observe its frequency spectrum [4]. Obviously, different amounts of time needed for the disbalanced orientation of the magnetic moment to become equal again to the orientation of the external strong direct magnetic field will also have different spectra. And because of these different spectra, one can analyse different materials and draw some conclusion about their structures and properties on a microscopic level. This method of exploration of materials' properties on a microscopic level is, in principle, the *method of nuclear magnetic resonance spectroscopy* [5].

2.4 The principle of nuclear quadrupolar resonance

In sections 2.2 and 2.3, the principle of NMR and its method of spectroscopy have been described, respectively. In its essence, NMR is a phenomenon that occurs due to the interaction of nuclei with the external magnetic field. However, there is also an interaction between the nuclei due to the gradient of the local electric field. This phenomenon is called *nuclear quadrupolar resonance* (NQR) [6] and it occurs when nuclei with spin order higher than $\frac{1}{2}$ are being observed. The shapes of the observed nuclei become flattened, which means that their structure is not spherically symmetrical. This leads to the splitting of the distances between neighbouring Zeeman's energy levels, thus enabling more possible energy transitions at different frequencies. The effect of quadrupolar splitting on the Zeeman effect for the nuclei with spin order of $\pm\frac{3}{2}$ is shown in Figure 2.6.

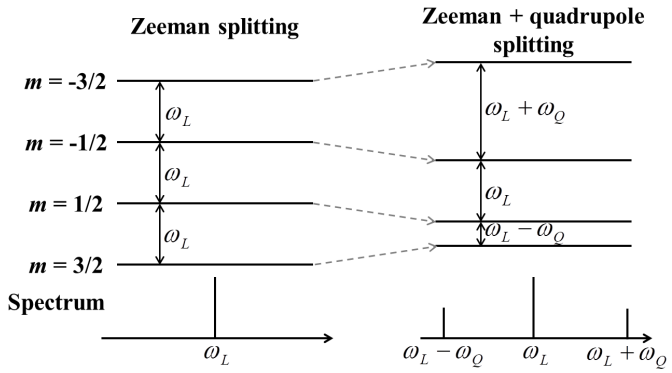

Figure 2.6: Zeeman effect without (left) and with quadrupolar splitting (right)

It can be seen that the distance between the lowest energy level ($\pm\frac{1}{2}$) and the higher level ($\pm\frac{3}{2}$) is shortened on one side, while it is lengthened on the other side, thus enabling two more energy transitions at frequencies that are equal to the difference and the sum of Larmor frequency and the frequency of the NQR effect. The result of the effect of NQR can be seen in

the spectrum of the obtained NMR signal, where two new components appear symmetrically around the basic component at Larmor frequency. The frequencies of these components are exactly equal to the difference and the sum of Larmor frequency and the frequency of the NQR effect, respectively. One more thing that can be seen here is that the value of spin order dictates the number of spectral lines in the observed spectrum. So, if the spin order is equal to 3/2, there will be three spectral lines in the spectrum; if the spin order is equal to 7/2 (like in the case of the ^{133}Cs measurement, whose obtained spectrum is shown in Figure 7.1a), there will be seven spectral lines in the spectrum. Therefore, there will be n spectral lines in the observed spectrum of the nuclei whose spin order is equal to $n/2$. Furthermore, it is also worth mentioning that, due to the fact that NQR happens because of the electric, and not the magnetic field, the effect of NQR can not only be measured as the unwanted effect on the NMR signal, but also separately, as the sole effect itself. The measurements of this effect are performed without the strong external magnetic field, which makes these measurements similar (but not the same!) to the so–called zero–field NMR, where NMR measurements are performed with the use of the Earth's magnetic field, or an internal magnetic field, if magnetic materials (i. e. magnets) are being measured.

2.5 Measurement techniques in NMR spectroscopy

To sum sections 2.2 and 2.3 up, certain nuclei possess a spin angular momentum and hence a corresponding magnetic moment. When such nuclei are placed in a strong direct magnetic field, they can adopt multiple, but discrete, number of quantized orientations. Each of these orientations corresponds to a certain energy level. In the lowest energy orientation, the magnetic moment of the nucleus is most closely alligned with the external direct magnetic field. Transitions from the lower energy level to the higher energy level can occur by the absorption of RF radiation of the correct frequency (the so-called Larmor frequency).

When placed in the external direct magnetic field, the nucleus exhibits a precessional motion. If an additional alternating magnetic field is applied at Larmor frequency, absorption of energy will occur and the nucleus will suddenly flip from its lower energy orientation (in which its magnetic moment was precessing in a direction alligned with the external direct magnetic field) to the higher energy orientation (in which it is alligned in some other direction). The process of transition from the higher energy orientation of the nucleus back to the lower one (and thus achieving equilibrium again) is called *relaxation*. The detected signals of a relaxation process have a form of a decaying pattern, where the value of a decaying constant depends on the type of measured nucleus. There are two basic measurement techniques of detected NMR signals, and they will be described in this section.

2.5.1 Free Induction Decay (FID)

Free Induction Decay (FID) is a name for the detected signals with a form of a decaying pattern, described at the beginning of this section. This name is derived so that it indicates the fact that the signal is *free* of the influence of the external RF field *, that it is *induced* in the coils, and that it *decays* to a zero value [1]. As said before, the decay constant of the FID signal depends on the nucleus under measurement and its environment. Of course, the overall acquisition time of the observed measurement then depends on the decay constant of the FID signal. The idea of this measurement is to somehow unbalance the overall magnetic moment, so that its orientation becomes perpendicular, or anti–parallel in some cases, to the orientation of the external direct magnetic field, and then measure the time needed for the orientation of the overall nuclear magnetic moment to return to its thermal equilibrium (Figure 2.7a). The process of unbalancing (Figure 2.7b) is done with the use of the additional external alternating magnetic field, which is sent as a pulse with its length long enough so that the pulse energy is high enough to rotate the overall magnetic moment for 90 degrees (or 180 degrees in some cases). The frequency of the package inside the pulse is equal to Larmor frequency of the observed nuclei. After the overall magnetic moment gets rotated for 90 (or 180) degrees, the relaxation process starts: the disbalanced magnetic moment starts precessing around the external direct magnetic field (Figure 2.7c) until its orientation gets equal again to the orientation of the magnetic field around which it precesses (Figure 2.7d).

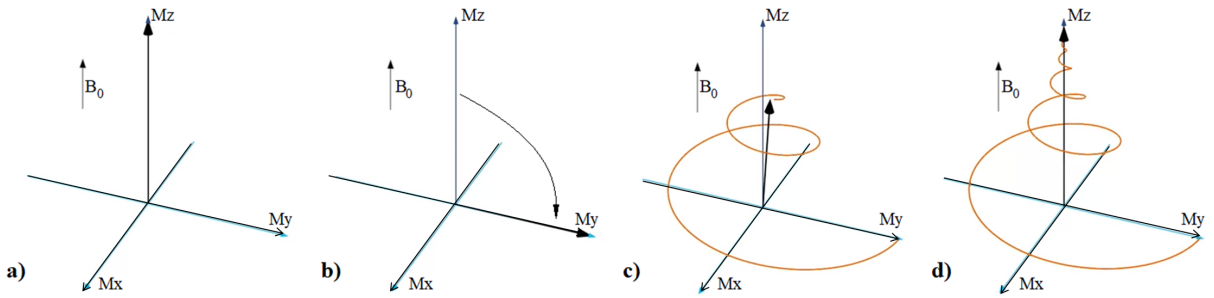

Figure 2.7: Overall magnetic moment of the observed nuclei during the FID measurement:
a) Thermal equilibrium; b) Rotation by the alternating magnetic field;
c) During the precession; d) The end of the precession

It is necessary to mention here that, before the start of the actual FID measurement, the length of the pulse, which unbalances the orientation of the overall magnetic moment, needs to be optimized. Namely, if this pulse does not have a proper length, some wrong conclusions can be drawn about the nuclei under measurement. So, to ascertain the right conclusions about the measurment, the pulse length needs to be set so that the rebalanced magnetization vector attains its maximum value. This is achieved by the multiple measurements with different excitation

*In a sense that there is no additional RF field during detection that would combine with the detected signal and thus influence its detected form.

pulse lengths, where the proper pulse length is *a posteriori* determined to be the smallest time value with the maximum rebalanced magnetization vector magnitude [7]. An example of the described optimization can be seen in Figure 2.8.

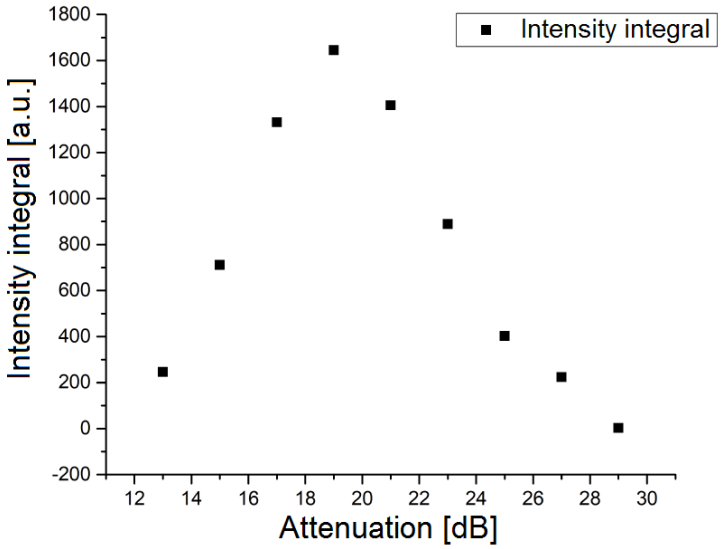

Figure 2.8: Optimization of the excitation pulse length

2.5.2 Spin–echo

The relaxation process, described in this section, is a process whose measurement usually yields a signal with a very fast decay. This means that the disbalanced orientation of the overall magnetic moment returns back to its equilibrium state orientation in a very short amount of time. Practically speaking, there might be a problem due to the limitations of the measuring system, or more precisely, the limitations of the detector. Every detector has its minimum time span in which it can measure. Anything shorter than that, unfortunately, can not be detected. So, to avoid the relaxation time span being shorter than the minimum detection time span, the idea is to somehow "rewind and repeat" the relaxation process. This way, the detector would be able to measure the relaxation process, after all. This kind of detected signal, or better yet, sequence, is called the *spin–echo* [7], and its form is shown in Figure 2.9. To obtain the spin–echo signal, one needs to use one additional step, when compared to the FID measurement. The beginning of the spin–echo measurement is the same as the beginning of the FID measurement: a pulse that rotates the thermal equilibrium orientation of the overall magnetic moment (Figure 2.10a) for 90 degrees is applied (Figure 2.10b). After that, the magnetic moment starts precessing, and its components, that are in the plane perpendicular to the orientation of the external direct magnetic field, start losing their coherence (Figure 2.10c) due to different precession speeds of different magnetic moments. Now, here is the additional step in this measurement that does the trick: a new pulse is now applied to the observed nuclei, but the length of this pulse is such

that it changes the phase of every perpendicular component of the overall magnetic moment for 180 degrees. This way, slower changing perpendicular components "outpace" the quicker ones, and after some time, the quicker components "catch up" with the slower ones (Figure 2.10d), causing the coherence of the perpendicular components again (Figure 2.10e). Now it is possible to obtain the spin–echo signal [7].

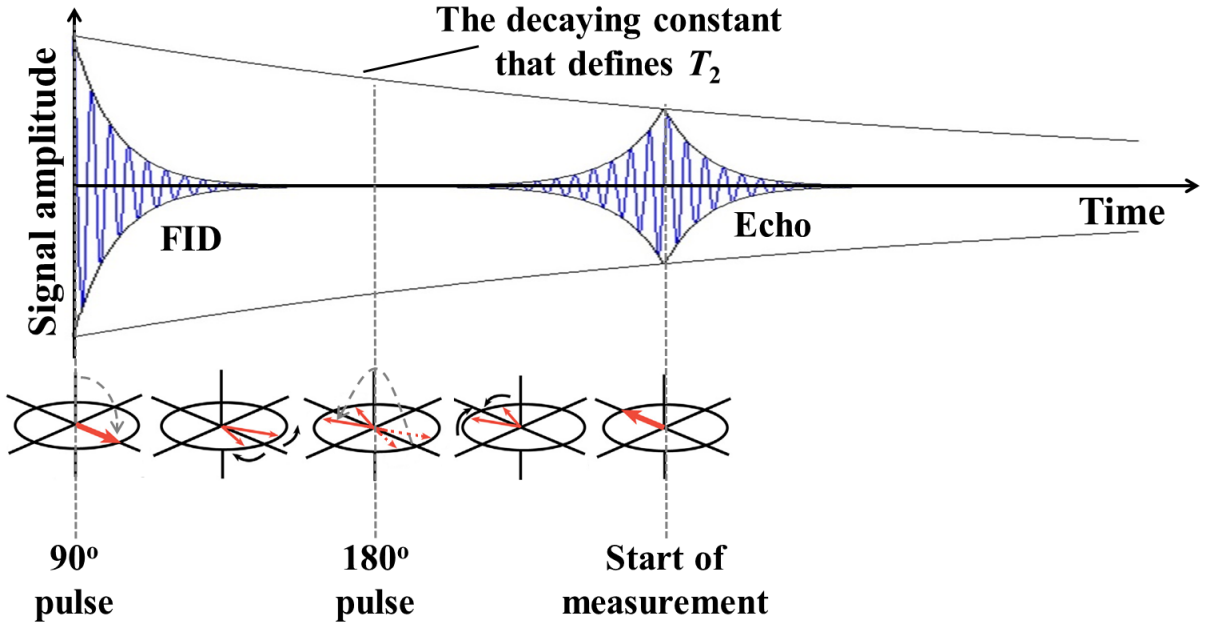

Figure 2.9: Spin–echo signal and its pulse sequence

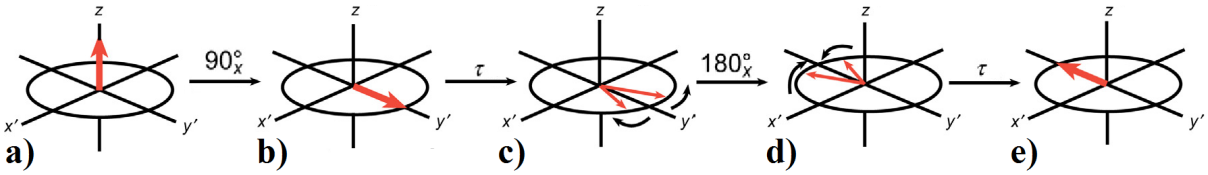

Figure 2.10: Overall magnetic moment of the observed nuclei during the spin–echo measurement [5]:
a) Thermal equilibrium;
b) Rotation by the alternating magnetic field for 90 degrees;
c) Loss of magnetization in the plane perpendicular to the direct magnetic field;
d) Rotation by the alternating magnetic field for 180 degrees;
e) Magnetization in the plane perpendicular to the direct magnetic field is re-obtained

2.6 Measurable values in NMR spectroscopy

In the last section, two basic NMR measurement techniques have been described. So now is a good idea to present the values that can be obtained with the use of the described NMR measurement types.

2.6.1 Spectrum

If the energy levels of the measured nuclei (see the description of the Zeeman effect in Section 2.4) are defined very clearly, as a result, the spectral line of the obtained NMR signal is going to be narrow. In fact, it is going to be notably narrower than the frequency bandwidth of the excitation pulse. If this is the case, the spectrum of the measured nuclei can be obtained very easily. Making a Fourier transformation (FT) of the obtained signal (Figure 2.11a), regardless of the measurement type, will lead to the spectrum of the measured nuclei (Figure 2.11b) [4].

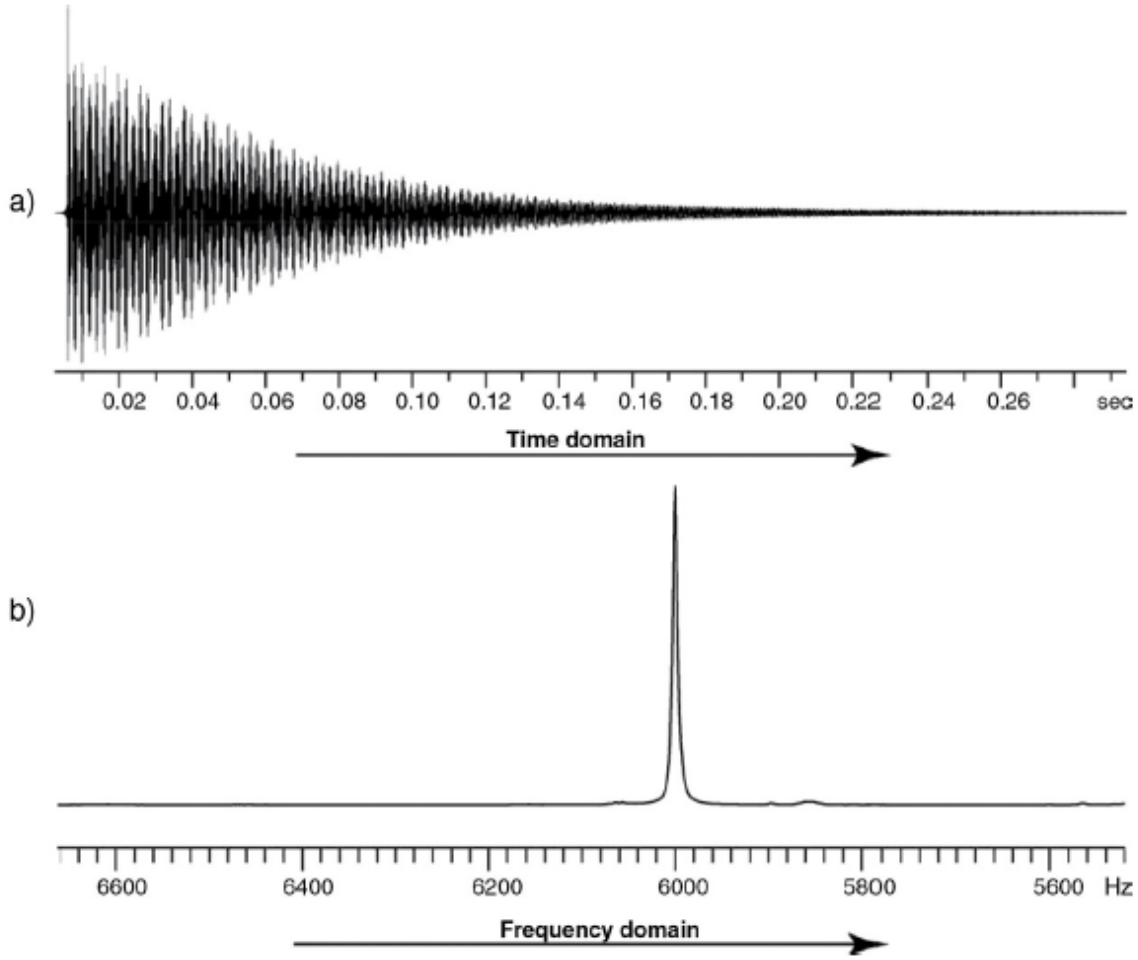

Figure 2.11: a) Obtained NMR signal in time domain [5]
b) Fourier transformation of the time domain signal [5]

However, if the energy levels of the measured nuclei are not clearly defined, but are "smeared" instead, then the effect of dispersion is going to occur, causing the spectral line's magnitude to decrease and its frequency bandwidth to increase. If the dispersion is large enough, so that the spectral line's bandwidth becomes broader than the frequency bandwidth of the excitation pulse, making an FT of the obtained signal will not be enough. Fortunately, it was shown [8] that it is possible to "sweep" through the entire spectrum piece by piece, using the aforementioned method, and then "glue" all the pieces together. This method is called *Variable Offset Cumula-*

tive Spectra (VOCS) [8], and an example of the spectrum obtained with the use of VOCS can be seen in Figure 2.12.

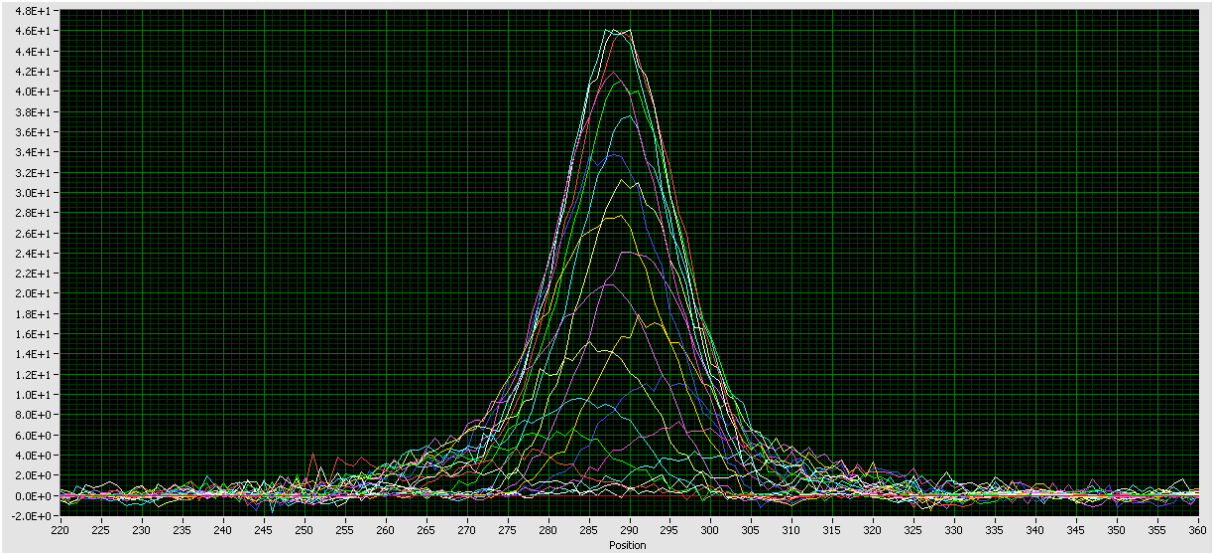

Figure 2.12: An example of the VOCS–obtained spectrum: all the coloured spectra combined together form an overall, white, spectrum

Nevertheless, if VOCS is used to obtain the wanted spectrum, it is necessary to be careful about frequency step size selection. Namely, if the step size is too big, than the spectrum gets obtained with low precision, causing the deformation of the overall spectrum. It was shown empirically that the maximum step size is equal to $\Delta\omega = \frac{0.63}{\Delta t}$, where Δt represents the length of the excitation pulse [8]. On the other hand, if the step size is too narrow, than the process of obtaining overall spectrum consumes too much time and computer memory. So, the idea is to find an optimum step size, where the precision of the spectrum obtainment is high enough, while at the same time, this process itself does not consume an exhausting amount of time and data.

2.6.2 Spin–spin relaxation time (T_2)

The spin–spin (or transverse) relaxation time, T_2, is the decay constant for the component of the observed disbalanced nuclear magnetic moment orientation that is perpendicular to the orientation of the external direct magnetic field [5]. It represents the time needed for the observed disbalanced nuclear magnetic moment orientation to become minimum (or, in other words, zero) in the direction perpendicular to the direction of the external direct magnetic field. This is because different magnetic moments of different observed nuclei lose coherence with different speeds, causing the complete loss of magnetization in the plane perpendicular to the orientation of the external direct magnetic field. T_2 is easily measured with the use of spin–echo measurement. Namely, multiple measurements, with different time delay between the 90 degree pulse and the 180 degree pulse, are made, and the echo magnitudes of the obtained measurements

get analysed. Then, from the dependency of the echo magnitude on the time delay between the two pulses, the value of T_2 is derived. Actually, it can be seen in Figure 2.9 that T_2 actually represents the decaying constant of the obtained spin–echo signal.

2.6.3 Spin–lattice relaxation time (T_1)

The spin–lattice (or longitudinal) relaxation time, T_1, is the decay constant for the recovery of the observed disbalanced nuclear magnetic moment orientation towards its thermal equilibrium orientation [5]. Unlike T_2, which represents the time needed for the observed disbalanced nuclear magnetic moment orientation to become minimum in the direction perpendicular to the direction of the external direct magnetic field, T_1 represents the time needed for the nuclei to return to thermal equilibrium. T_1 can, for instance, be measured with the use of FID measurement, described in subsection 2.5.1: a 180 degree excitation pulse is sent, and the orientation of the observed nuclear magnetic moment rotates for 180 degrees. After the excitation, the observed orientation starts getting back to its initial state. After a time t, the value of $M_z(t)$ gets checked. By the variation of the time t, it is possible to obtain a chart shown in Figure 2.13, and deduce the amount of time needed for the value of $M_z(t)$ to become maximum. This amount of time then matches the value of T_1 [7]. It is also worth mentioning that T_1 can also be measured with the use of spin–echo measurement. However, more complicated pulse sequences than the one described in subsection 2.5.2 need to be used here [7].

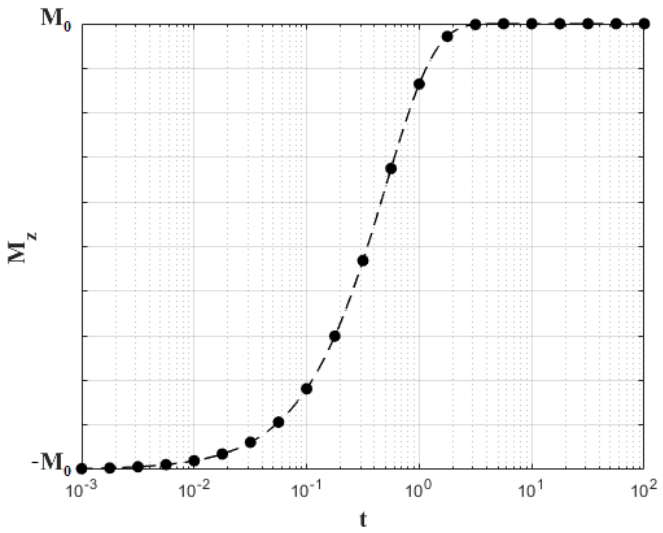

Figure 2.13: The result of the T_1 FID measurement

2.6.4 Visualization of T_1 and T_2

To better understand the connection between the times T_1 and T_2, a good idea is to analyse their visual representations, shown in Figure 2.14.

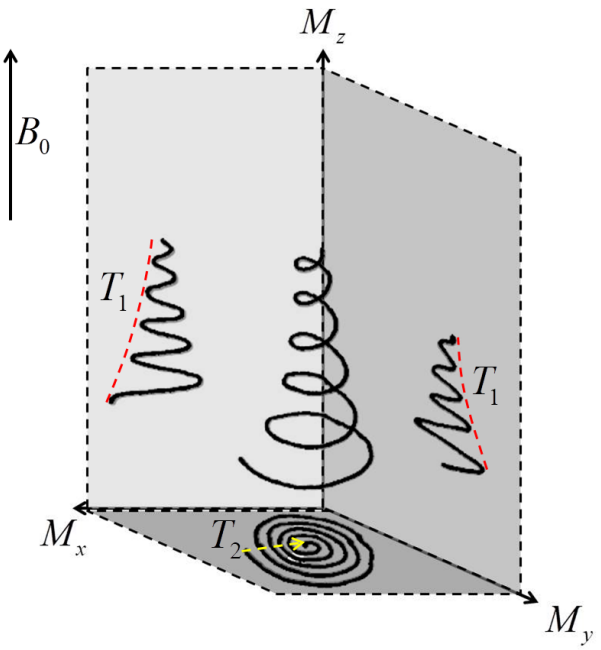

Figure 2.14: Visualization of T_1 and T_2 relaxation times

As it can be seen in Figures 2.7 and 2.10, the precession of the disbalanced overall magnetic moment is a process which takes place in three spatial dimensions and one temporal dimension. Three–dimensional projections to a two–dimensional plane (which is the instrument screen or a sheet of paper, on which the measurement results can be shown) are difficult to interpret more often than not, especially if the arrangements of these "three–dimensional points" change in time. So, the idea is to break the three–dimensional relaxation process to three two–dimensional projections that show the time dependence of every spatial dimension separately. This way, it is much easier to track the measurement results. Accordingly, as it can be seen in Figure 2.14, the planes that are parallel to the external direct magnetic field, B_0, can be used for T_1 measurements (so, front view and side view can be used here), and the plane that is perpendicular to the same magnetic field can be used for T_2 measurements (top view).

2.6.5 NMR measurable values classification

To sum up, in the NMR community, there are three main values that can be measured: the T_1 time, the T_2 time and the spectrum of the measured nuclei. These values can be measured with the use of two different techniques: the free induction decay (FID) and the spin–echo. The classification of the three mentioned NMR measurable values in accordance with the two available measurement techniques is shown in Table 2.1.

Table 2.1: NMR measurable values classification in accordance with available measurement techniques

Measured value	Measurement technique	
	FID	Spin–echo
Spectrum	$\surd$	$\surd$
T_1 time	$\times$	$\surd$
T_2 time	$\surd$	$\surd$

FID is described in section 2.5.1, while the spin–echo is described in section 2.5.2. Furthermore, as the main emphasis of this thesis will soon prove to be put on the analysis and the description of the NMR spectroscopy system from the RF engineer's point of view, and this chapter's purpose is for the RF community to get the general idea of the measurements the described system performs, only a few measurements from Table 2.1 have been described in this chapter. The T_1 measurement is described in subsection 2.6.3, while the T_2 measurement is described in subsection 2.6.2. Additionally, the spectrum measurement is described in subsection 2.6.1.

2.7 Applications of nuclear magnetic resonance spectroscopy

The application of NMR is very popular in solid state physics. For example, the analysis of some "exotic" properties of different materials, like superconductivity, is done with the use of NMR spectroscopy. This analysis is also done in our laboratory, which is the Laboratory for solid state NMR and high frequency measurement at the Department of Physics of Faculty of Science, University of Zagreb [9, 10, 11, 12].

The most well–known application of NMR spectroscopy is definitely magnetic resonance imaging, or MRI. MRI is the popular application of NMR spectroscopy nowadays to analyse protons of hydrogen in molecules of water that are situated inside human body. Using two-dimensional NMR spectroscopy, it is possible to "make a map" of the surface of human body by the excitation of molecules of water inside it. Also, using different frequencies for the excitation signal, thus changing the penetration depth of the signal, it is possible to "make a map" of multiple layers of human body. Combining all the created maps of human body layers, it is possible to create a three–dimensional map of human body. This described process is, in principle, the process used in MRI [13].

Chapter 3

The system of nuclear magnetic resonance spectroscopy

In this chapter, general mode of operation of the NMR spectroscopy system will be given. Detailed overview of the system's most important elements, and their function, both in the system and as the sole element, can be found here.

3.1 General mode of operation

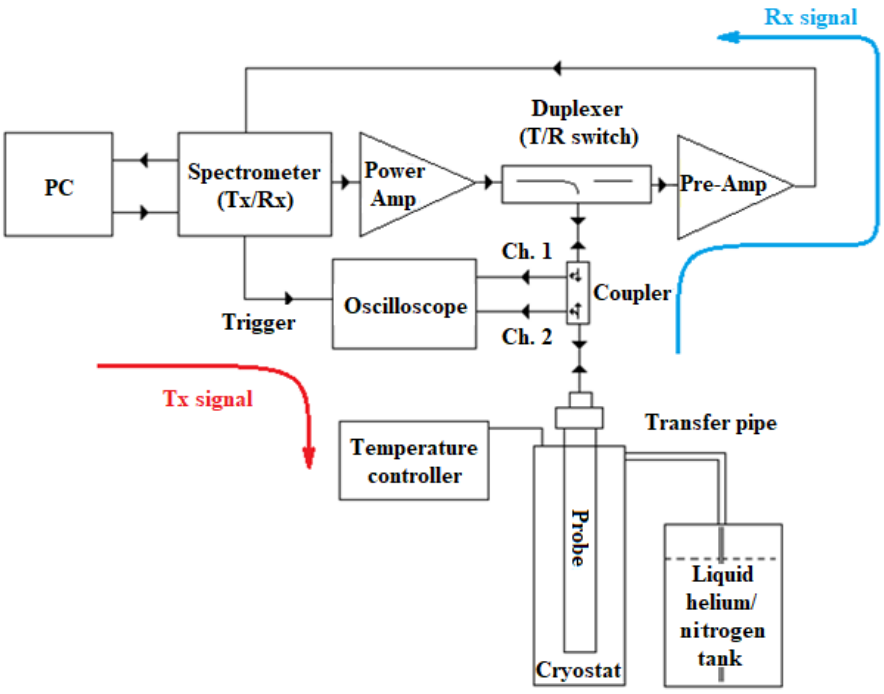

Figure 3.1: NMR spectroscopy system – basic diagram

The block diagram of NMR spectroscopy system is shown in Figure 3.1. In principle, the NMR spectrometer, as well as the rest of the system, operates in two modes: the transmitting

(Tx) mode and the receiving (Rx) mode [7]. During the Tx mode, pulses, which are used for excitation of the nuclei of the sample under measurement, are first generated by the spectrometer's oscillator (or, in more advanced version, a synthesizer with a waveform generator). The pulses are then amplified up to the order of a kW by a power amplifier, and transmitted, via the duplexer, to the coil of the probe. During the Rx mode, these high–power pulses generate the magnetic field within a coil that excites the nuclei of the embedded sample. The sample's response has a very low magnitude (down to the order of a fW), and it needs to be amplified before further processing in the spectrometer's receiver. The amplification of the receiving signal is achieved by a low–noise preamplifier, where response signal is sent via the duplexer. In the spectrometer, the received signal is down–converted to the intermediate frequency and further amplified by variable–gain amplifier that serves as amplitude optimization before the analog–to–digital (A/D) conversion. After detection and A/D conversion, the signal is digitally post–processed using different methods, such as time averaging of multiple measurements and digital filtering. In the end, this processed signal is shown on the spectrometer screen.

The elements that are shown in Figure 3.1, but are not mentioned in the last paragraph, are used either as different types of sensors, but they do not change its mode of operation. So, a personal computer (PC) is used to control the spectrometer, and also to analyse and process measurement results received from the spectrometer. Oscilloscope is used to observe both excitation and response signals in real–time in order to detect eventual errors (e.g. wrong power level, length or frequency of excitation pulses) or unwanted effects (e.g. ringing of the probe's coil). Directional coupler is just used here as a tool that forwards samples of excitation and response signals to the oscilloscope. Furthermore, if NMR measurements are done at very low (cryogenic) temperatures, the probe's coil is not only placed in a strong magnet, but also in a cryostat, filled with liquid nitrogen or liquid helium, in order to enhance sensitivity of the measurements. Temperature controller is obviously used here to maintain constant temperature inside the cryostat.

It is necessary to mention that the NMR spectroscopy systems, described in this section, are the ones that are used in condensed matter physics. This kind of systems is very bulky and very rugged since all the elements of the system are independent of each other and can be replaced easily. Obviously, this is an open type of systems in a sense that all the elements are easily accessible, as the systems are not closed in one enclosure and then used as a "black box". Also, cryostats and very strong magnets are typical for condensed matter physics NMR spectroscopy, especially in the last years, with the need for higher magnetic fields and lower background noise, as measured samples mostly tend to have have lower and lower response signal levels. Such kind of NMR spectroscopy systems is opposed to the ones used in chemistry, where commercialy available instruments that perform NMR spectroscopy measurements are used. This is a closed type of systems, as all its elements are placed in one enclosure, and are

used as one instrument, or one "black box". NMR spectroscopy systems used in chemistry usually measure elements with high–level response signals (e. g. hydrogen), so this type of systems does not need strong magnets and cryostats. Actually, the NMR spectroscopy systems, used in chemistry, that measure hydrogen response signals are actually analogous to the MRI systems, used in hospitals, as these systems map human body by 2D measurements of hydrogen inside the water molecules that the body is comprised of. Anyhow, the scientific research presented in this thesis is based on the NMR spectroscopy systems used in condensed matter physics, so the reader needs to bear this fact in mind while reading the scientific research presented in this thesis.

Finally, as it can be seen in this section, general mode of operation of the NMR spectroscopy system used in condensed matter physics is described here very superficially, and the rest of the chapter is going to serve as more detailed description of the most important elements of the system, as well as the processes these elements execute. Also, the start of transition from the physicist's point of view on this system to the one of the RF and microwave engineer occurs from here to the end of this chapter.

3.2 Spectrometer

As it can be seen in Figure 3.1, spectrometer is "the heart" of NMR spectroscopy system. Its operation is very important in both the Tx mode (when it generates excitation pulses of necessary length, frequency and power level) and the Rx mode (when it processes response signals and presents measurement results).

Technically speaking, there are two main types of spectrometers: *continuous wave* (CW) and *pulsed Fourier transform* (FT) *spectrometers* [5]. CW spectrometers are the older type and they operate in a way that they scan the sample by sweeping through the frequency spectrum that needs to be measured one frequency at a time. Here, only nuclei with Larmor frequencies equal to the current frequency in the sweep are being excited. So, as the entire frequency range is scanned, all NMR–active nuclei are gradually excited, and a plot of signal intensity versus frequency is generated [7, 14]. This means that NMR measurements, done with a CW spectrometer, are actually measurements of absorption of the nuclei, and these measurements are done directly in frequency domain [5]. FT spectrometers, on the other hand, operate in a way that they excite the sample with a pulse in time domain. This way, by the manipulation of the pulse length and its package frequency, it is possible to create spectrum of the pulse such that it contains entire spectrum of the sample's NMR–active nuclei. In other words, it is possible to excite much larger number of NMR–active nuclei *at once* (compared to the CW spectroscopy) [7, 14]. However, NMR measurements, done with an FT spectrometer, are done in time domain. This means that, in order to obtain NMR spectrum, the signal needs to be transformed to frequency domain using Fourier transform (this is, obviously, how this type of spectrometer got its name). Also, since pulses have finite length, meaning that the sample is not measured all the time, but only his response signal is what is measured, it can be said that NMR measurements, done with an FT spectrometer, are measurements of emission of the NMR–active nuclei in time domain [5].

Since a great number of the observed NMR–active nuclei can be excited at once with the use of FT spectrometer, compared to the sweep through the entire nuclei frequency spectrum, but only one frequency at a time, with the use of CW spectrometer, it is obvious that NMR measurements are notably faster in the first case. It turns out that the time difference of these two measurements is equal to almost two orders of magnitude of time: if the CW measurement lasts 5 minutes (which is equal to 300 seconds), the FT measurement lasts 5 seconds [7, 14]. So, if one does NMR measurements that demand a period of time of a few hours (e.g. up to ten hours [15]), the difference between consumed times for both types of measurements is even bigger. This is why, nowadays, CW spectrometers are almost extinct in NMR laboratories all around the world. Our laboratory, of course, is no different. We too use an FT spectrometer, whose basic block diagram is shown in Figure 3.2.

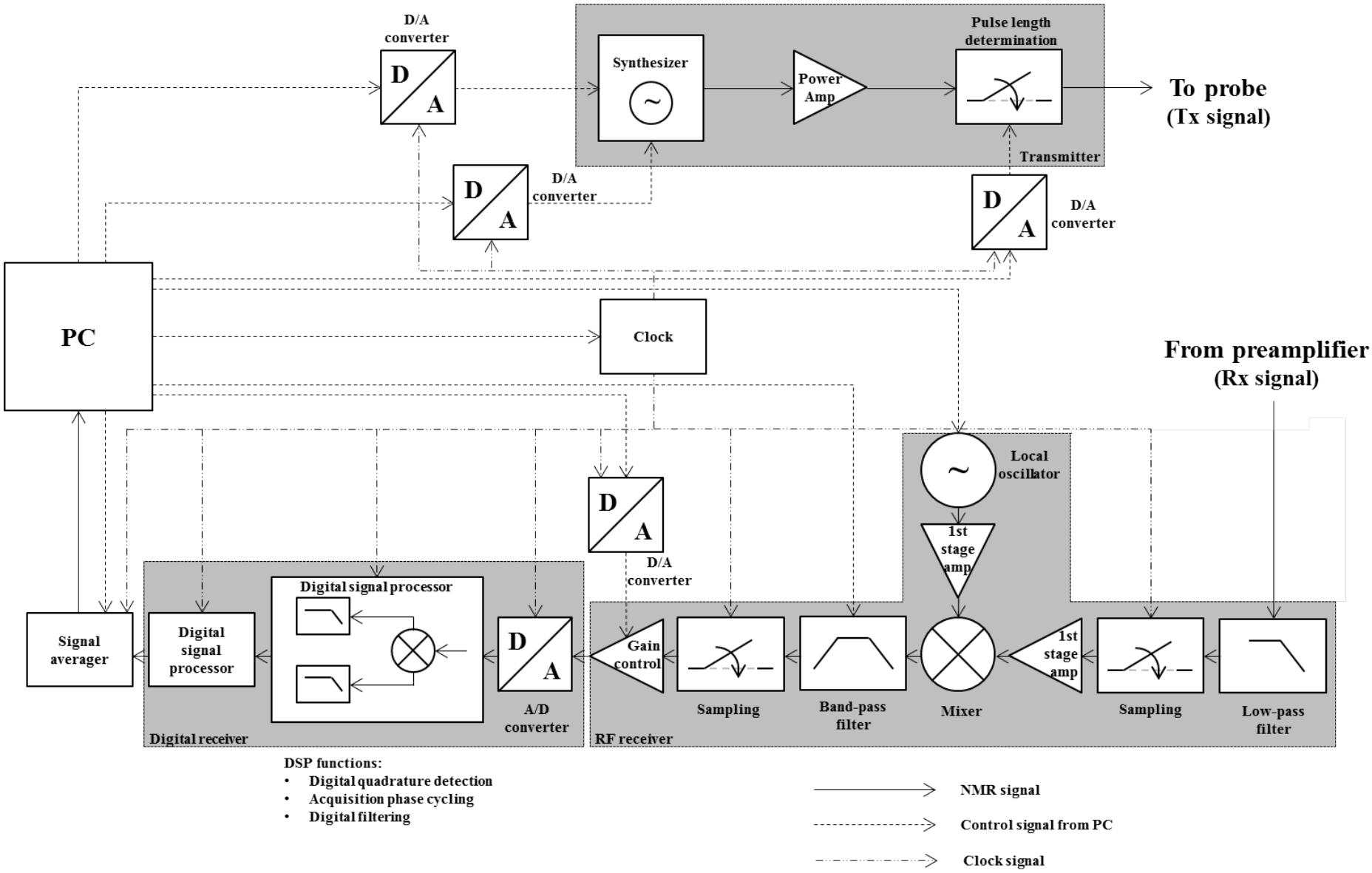

Figure 3.2: Basic block diagram of a pulsed Fourier transform spectrometer

The Tx part of the spectrometer is shown in the upper part of Figure 3.2 and the signal flows from left to right, while the Rx part is shown in the lower part of the same figure, where the signal flows from right to left. It can be seen that PC is "the brain" of the spectrometer, since it controls most of processes in the instrument, and it also synchronises all the processes, since it controls the clock signal.

During the Tx mode, PC sends the control signal, which contains data about the setup package frequency of the pulse, to the synthesizer, which then generates sine signal of the setup frequency. Then, PC sends the control signal, which contains data about the setup output power level of the pulse, to high-power amplifier, which amplifies the sine signal from the synthesizer. After the adjustment of power level and package frequency of the pulse, PC sends the control signal, which contains data about the setup length of the pulse, to the switch, which turns itself on and off, and thus creates pulses of the proper length. In the end, these generated pulses are sent outside of the spectrometer, to the probe.

After excitation of the sample, and after its response signal arrived to the input of the spectrometer, the Rx mode, shown in the lower part of Figure 3.2, starts. Here, the signal first passes through the RF receiver, whose task is to filter the signal (so that there is as little unwanted signal around the response signal as possible), down–convert it to intermediate frequency (so that only one, universal, hardware can be used to measure all NMR frequencies), and amplify or weaken the signal in order for its amplitude to reach optimum value at the input of the A/D converter (this is called *automatic gain control*, or AGC [16]). Then, the signal passes through the digital receiver, whose task is to convert the signal from analog to digital domain (because computers only work with binary data), filter it digitally (because there are some powerful filtering techniques that can not be done in analog domain, but can be done in digital domain) and do additional processing (like phase cycling), if necessary. Before it goes to PC, the signal passes through the signal averager, whose task is to average results of multiple measurements (in order to increase overall sensitivity of the system [17]). The final step of NMR measurement with the use of FT spectrometer is, of course, Fourier transformation of the signal [4]. It is done by PC, and the final measurement result is shown on the PC screen.

3.3 Duplexer

Duplexer is the element whose purpose is to switch the rest of the system between Tx and Rx modes (since spectrometer does that for itself). This is why duplexer is also called transmit/receive (T/R) switch. Generally, duplexers are built either with the use of lumped electronic components (Figure 3.3), where the best transition of signal gets tuned to wanted frequency by resonant LC circuits [18], or with the use of microstrip lines and two quadrature hybrid–based couplers (Figure 3.4), where its physical dimensions determine the frequency of the best

transmission [19]. However, the main parts of both types of duplexers, that do the trick of T/R switching, are antiparallel diode connections. As it is well known from the electronics fundamentals, diode is an electronic element that serves as a ramp for the electric current flow. Until voltage drop across the diode is lower than its threshold voltage, U_γ, the electric current does not flow through the diode. When the voltage drop rises above the threshold voltage, the ramp goes up and current starts to flow through the diode. So, it can be said that the diode is actually a voltage limiter for the direct current, while two antiparallel diodes are a voltage limiter for the alternating current. The same applies to power, as power is proportional to square value of voltage. Practically speaking, two antiparallel diodes, connected to the circuit in series, form a power limiter that allows only high–power signals to pass through the circuit. On the other hand, these diodes, connected to the circuit in parallel, form a power limiter that allows only low–power signals to pass through the circuit. So, for the example of lumped circuit–based duplexer (Figure 3.3a), the high–power signal from the spectrometer transmitter passes through diodes D_1 and D_2, then one part of the signal flows through L_1, the other part flows through C_1, R_1 and D_3, and the last part flows directly to D_4. Since diodes D_4 are connected in parallel, they form the power limiter that allows only low–power signal to pass through to the spectrometer receiver. For that, the input signal reflects and goes to the probe either directly or through inductor L_1. After this signal excites the nuclei of the sample inside the probe, the low–level response signal goes back to the duplexer. Since diodes D_1, D_2 and D_3 are connected in series, thus forming the power limiter that allows only high–power signals to pass through, the low–power response signal can only pass through L_1 and progress to C_2 and, ultimately, the spectrometer receiver. The same applies to quadrature hybrid–based duplexer (Figure 3.4a), where power limiters are connected in a proper way so that the signal reaches its destinations during the entire process of NMR measurement. In the last few years, new, cryogenic, duplexers have been made [20] in order to further increase both its sensitivity and the sensitivity of the entire NMR spectroscopy system, but the mode of operation of such duplexer is the same as the described mode of operation of room temperature duplexers.

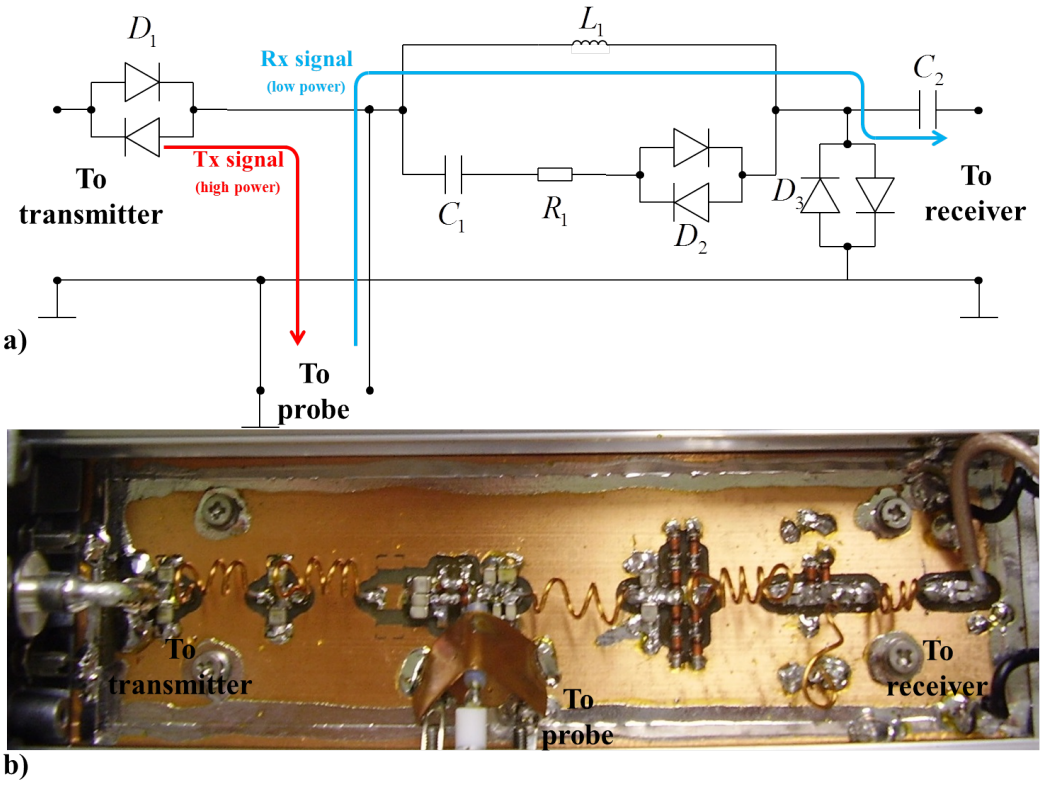

Figure 3.3: Lumped circuit–based duplexer;
a) Basic diagram; b) Implementation

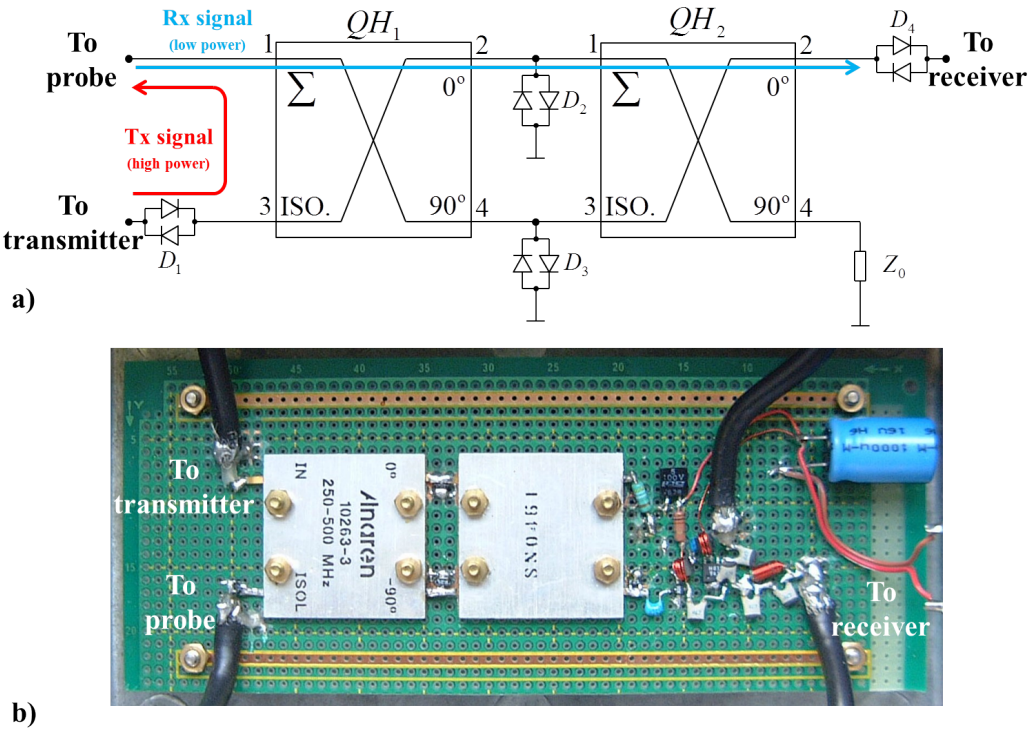

Figure 3.4: Quadrature hybrid–based duplexer;
a) Basic diagram; b) Implementation

3.4 Probe

Probe is the element of NMR spectroscopy that is directly in touch with sample under measurement. As it can be seen from its schematic diagram (Figure 3.7a), NMR probe is comprised of a coil (whose inductance is represented by L_{coil}, while its ohmic resistance is represented by R_{coil}), two capacitors – the matching capacitor, C_M, and the tuning capacitor, C_T, and a transmission line – usually a coaxial cable that connects the coil and the tuning/matching network to the input/output of the probe.

The coil is the most important part of the probe since its tasks are both to excite the sample placed inside it and to detect the response signal from the sample, and also to define resonant frequency and characteristic impedance of the entire probe in combinations with the two capacitors, C_M and C_T. As it was mentioned in sections 2.2 and 2.3, the measured sample needs to be excited by an alternating magnetic field in order to perform NMR measurements. This is done by the flow of an alternating electric current through the coil, which, according to the Faraday's law of induction, induces alternating magnetic field in the direction of coil's axis that is perpendicular to the current flow direction [21]:

$$\nabla \times \mathbf{E} = -\frac{\partial \mathbf{B}}{\partial t}. \tag{3.1}$$

On the other hand, when the sample responds to the exciting magnetic field, this change of the magnetic field, caused by the response signal, induces electric current in the coil according to the Ampère's law [21]:

$$\nabla \times \mathbf{B} = \mu_0 \mathbf{J}. \tag{3.2}$$

Such induced signal is in fact sample's response signal. After a mathematical manipulation of equations (3.1) and (3.2), shown in [2], the expression that predicts the voltage value of the induced response signal at the coil's terminals is derived:

$$U_{ind} = \frac{1}{24\pi^2} N \frac{\omega_L^2 h^2 \gamma \mu_0^2 I(I+1) r_{coil}^2 n_{coil}^2}{k_B T_{sample} V_{sample}}, \tag{3.3}$$

where N is the number of nuclei in the sample, γ is the nuclear gyromagnetic constant, ω_L is the Larmor frequency, I is the nuclear spin size, r_{coil} is the coil radius, n_{coil} is the number of turns of the coil, T_{sample} is the sample temperature, and V_{sample} is the sample volume. Additionally, h, k_B and μ_0 are the Planck constant, Boltzmann constant, and vacuum permeability, respectively. Here, it can be seen that the voltage value of the induced response signal depends on the square value of the operating frequency, ω_L. This means that low frequency signals are difficult to measure due to this square dependence. Although this constatation might seem like a digression, after the next chapter (especially the subsection 4.2.2), one will understand the motivation for

the research presented in this thesis even more, but more about that in chapters 4, 5, 6 and 7. Now, back to the induced response signal. In order for the response signal to be created in the first place, and then to be successfully transferred to the preamplifier, the probe network first needs to be adjusted. First of all, resonant frequency of the probe needs to be adjusted to Larmor frequency of the sample. This is achieved by the combination of probe coil's inductance, L_{coil}, and tunable capacitor C_T. By changing C_T's value, it is possible to tune the probe's resonant frequency to sample's Larmor frequency. Also, the probe's characteristic impedance needs to be matched to characteristic impedance of the rest of the system, which is usually equal to 50 Ω, in order to avoid unwanted signal loss due to the reflection caused by the impedance mismatch between the probe and the rest of the system. This is achieved by the combination of probe coil's inductance, L_{coil}, and tunable matching capacitor, C_M. By changing C_M's value, it is possible to tune the probe's characteristic impedance to the one of the rest of the system.

From the antenna engineer's point of view, the probe's coil is practically a small loop antenna, which is actually an elementary magnetic dipole antenna [22]. Because its dimensions (a few milimeters in diameter and in length) are much smaller than the wavelengths of NMR measurements frequencies (between 300 meters for a 1 MHz signal and 60 centimeters for a 500 MHz signal), its radiation resistance is very small (compared to $Z_0 = 50\ \Omega$). This means that, not only are these antennas inefficient, but there is also a non–negligible reflection between the antenna itself and the rest of the system, causing even lower level of already weak NMR response signal. So, in order to avoid these reflections, the antenna's resistance needs to be matched to the characteristic impedance of the rest of the system, which is Z_0. This is done with the matching capacitor, C_M. Furthermore, this impedance matching needs to be done at the frequency that exactly matches the desired frequency of the NMR measurement. Obviously, the antenna needs to be tuned to this frequency by the tuning capacitor, C_T. Radiation pattern of a small loop antenna is shown in Figure 3.5

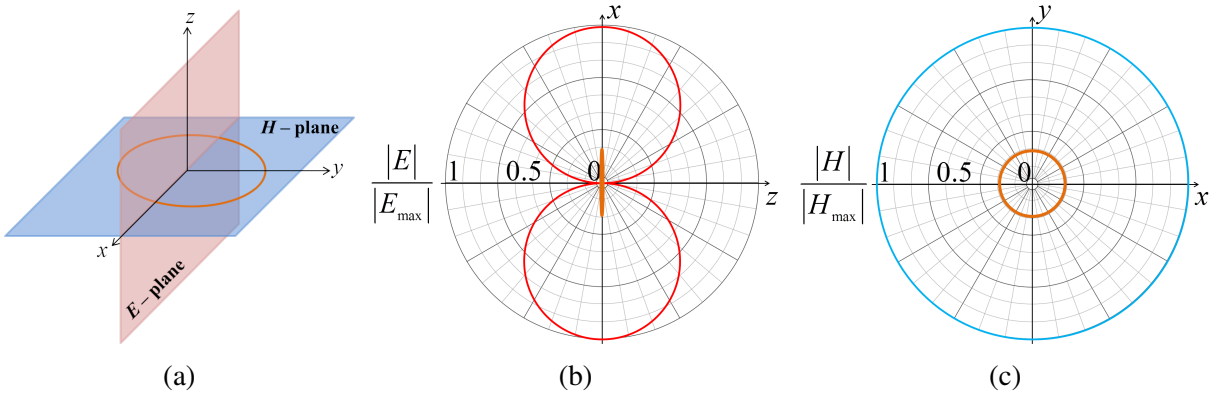

Figure 3.5: Loop antenna: a) Orientation; b) Radiation pattern: E–plane; c) Radiation pattern: H–plane

As it was also mentioned in sections 2.2 and 2.3, the sample might need to be placed in a strong direct magnetic field during NMR measurements. Lately, with the development of cryogenic NMR, these enclosures are additionally filled with liquid nitrogen or liquid helium in order to be able to analyse and measure NMR samples at extremely low temperatures, and to be able to generate stronger magnetic fields inside coils, compared to the magnetic fields at room temperature. As a consequence, this effect of cryogenic cooling also additionally improves sensitivity of NMR measurements [23]. Obviously, the coil and the sample placed inside it, along with the tuning/matching network, somehow have to be lowered down to the environment of strong magnetic field and cryogenic temperature. This is usually done by the use of a rigid coaxial cable placed in the middle of a metal construction (Figure 3.7f). The probe's coil, along with the tuning/matching capacitors, are shown in Figure 3.7c, the capacitors' tuners, placed at the input/output of the probe, are shown in Figure 3.7b, while two examples of samples, just to get a feeling for their dimensions, are shown in Figures 3.7d and 3.7e. The cross–section of a magnet and its enclosure is shown in Figure 3.6.

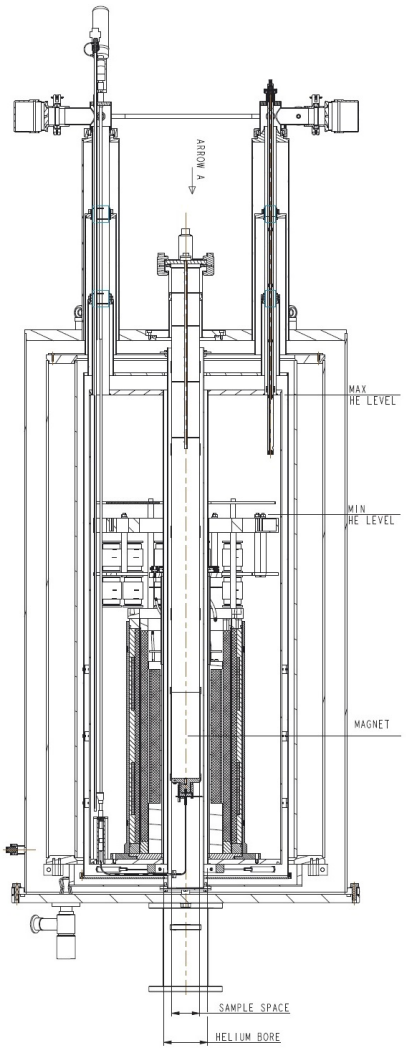

Figure 3.6: Cross–section of NMR magnet and its enclosure

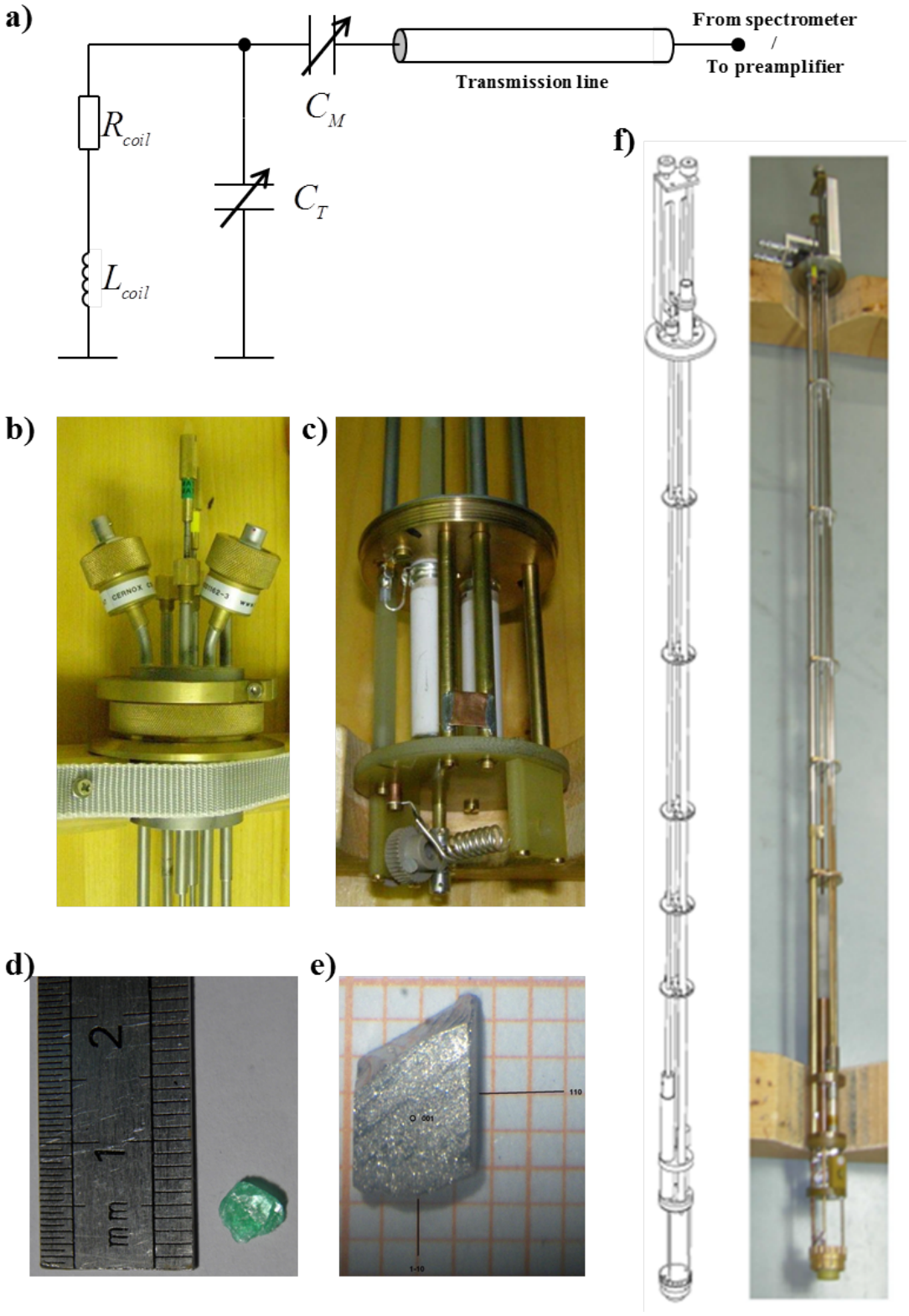

Figure 3.7: a) Schematic diagram of NMR probe;
b) Top part of the probe: input/output connector and tuners for C_M and C_T;
c) Bottom part of the probe: capacitors C_M and C_T and coil L_{coil};
d) Sample of $SeCuO_3$ next to milimeter grid ruler;
e) Sample of $Cs_2Cu_3SnF_{12}$ on milimeter grid paper;
f) Construction of NMR probe [24]

3.5 Preamplifier

One of the biggest problems in NMR measurements is that some materials have very low response signals. As it was mentioned in section 3.1, power levels of response signals can be as low as an order of a fW. This is a problem because such a low level signal would probably weaken so much that it would be impossible for the spectrometer receiver to detect it. Furthermore, signals with such a low power level are comparable to noise power of the system. If the response signal weakens so much that its power level falls under the noise level, it is very hard or even impossible to detect it on the spectrometer screen, especially without the use of additional signal processing techniques (e.g. averaging). This is why it is necessary to preamplify the response signal before passing it to the spectrometer receiver.

There are five main criteria for choosing the ideal NMR preamplifier:

1. The preamplifier should have its power gain as high as possible.
2. The preamplifier should have its noise figure as low as possible.
3. The preamplifier's characteristic impedances should be matched to the one of the system.
4. The preamplifier needs to be linear.
5. The preamplifier needs to be stable.

The first criterion comes from the fact that the preamplifier's gain annihilates noise that spectrometers injects into the system: the higher the preamplifier's gain, the more annihilated spectrometer's injected noise gets (more on this subject in section 6.2).
The second criterion comes from the fact that the preamplifier itself also injects some amount of noise into the system. Obviously, the lower the preamplifier's injected noise, the better the NMR spectroscopy system is (more on this subject in section 4.4).
The third criterion comes from the fact that there is a reflection in the system if there is an impedance mismatch. Of course, reflection is unwanted because signal loss happens as its consequence (a concept of return loss). Therefore, the better preamplifier's input and output characteristic impedances are matched to the characteristic impedance of the rest of the system, the smaller the reflection, and hence, higher the signal level and better the measurement results (more on this subject in section 6.2).
The fourth criterion comes from the fact that the preamplifier needs to be able to produce signals at its output that are accurate copies of the input, meaning that the output signal must not be distorted. Also, it must not generate any output signal if there is no input signal present.
The fifth criterion comes from the fact that the preamplifier must not be prone to generating unwanted oscillations at its output. At least, it would be a shame if a preamplifier's oscillation got declared as a revolutionary NMR result, just to become a bitter disappointment in the end.

Unfortunately, it is impossible to achieve all the criteria at the same time. The user has to make a compromise between the criteria and determine an optimum point based on the existing setup and the type of NMR measurement. This usually means finding a criterion that is the least harmful to "sacrifice" on behalf of the rest of the criteria in order to achieve the best performance of the NMR preamplifier as the integral part of the NMR spectroscopy system.

There are different designs and techniques available for the amplifier construction. Based on frequency bandwidth of NMR measurements, which is the area between 10 MHz and 500 MHz, classification of available techniques, from the aspect of noise properties, has been made according to [25], [26], [27], [28] and [29], their ranking from best to worst has been presented in Table 3.1, and the explanation of the ranking, from the aspect of noise properties, has been described below.

Table 3.1: Classification of available techniques for NMR preamplifier; ranked from best to worst from the aspect of noise properties

No.	Design
1	HEMT–based
2	CMOS–based
3	FET–based
4	BJT–based
5	Op Amp–based

Bipolar junction transistors (BJTs), are, among field–efect transistors (FETs), the basic transistor types. Colloquially speaking, BJTs are current controlled devices. This is said so because of the fact that the BJTs input current levels exceed the ones of the FETs for a few orders of magnitude. Because of a relatively high current levels that flow through this type of transistors, BJTs thermal noise levels are much higher on average than the ones of the other available amplifier techniques mentioned in Table 3.1 (except operational amplifiers). Therefore, BJTs are generally not used for the construction of NMR low–noise amplifiers (LNAs).
Operational amplifier (Op Amp) technology is a very popular technology in a modern consumer electronics due to its versatility and usage simplicity. However, Op Amps are usually comprised of multiple number of different BJTs, where every BJT injects its own noise in the system. Obviously, multiple BJTs on average have higher noise levels than a single BJT, making this technique even more unfavourable for the LNA construction that the aforementioned BJT technology, at least from the aspect of noise, which is the most important aspect in the NMR LNA design and construction.

FETs, because of their low input current levels (compared to BJTs), are colloquially known as voltage controlled devices. Because of the low current levels that flow through this type of transistors, FETs thermal noise levels are notably lower than the ones of BJTs, making them more suitable for the construction of LNAs.
CMOS (or complementary metal–oxide–semiconductor) is a complementary and symmetrical structure of one of the types of FETs, called metal–oxide–semiconductor FETs (or MOSFETs). From the aspect of noise, CMOS is a technology that further improved noise properties of FETs (meaning that the overall noise levels of CMOS are lower than the ones of FETs). This is achieved by the use of two complementary MOSFET types: p–MOS and n–MOS; where p–MOS are the MOSFETs that only use holes as charge carriers in their operation, while n–MOS are the MOSFETs that only use electrons as charge carriers in their operation. So, practically speaking, complementary properties of n–MOS and p–MOS transistors "cancel out" each others imperfections, even from the noise properties point of view, making CMOS technology even better technology to use for the construction of LNAs, compared to FETs.
High–electron–mobility transistors (HEMTs), also known as heterostructure FETs, is one of the newer FET types, where the current levels flowing through the transistors are even more lowered, compared to the ordinary FETs, causing even lower noise levels. Furthermore, current variations are much lower in HEMTs, compared to the ordinary FETs, which not only stabilizes the characteristics of these transistors, but it also additionally decreases their external noise levels. That is why this technology is the most appropriate technology for the NMR LNA design and construction, from the aspect of noise.

Finally, it is necessary to point out once more that this classification has been made from the aspect of noise properties and for the design and construction of LNAs for the specific use in NMR spectroscopy. Namely, the highest priority in this classification has been given to achieving the lowest possible noise figure, while the operational frequency bandwidth has been set roughly to the bandwidth between 0 and 500 MHz. The technology ranking, shown in Table 3.1 would certainly have been much different if some other property (like, for example, the power gain level) would have been given the highest priority, and this would most definitely be true if a notably higher frequency bandwidth would have been observed. In the end, the author feels that the the ranking presented in Table 3.1 is the best suited one for the design of low noise preamplifiers, used in NMR spectroscopy, with the operational frequency bandwidth roughly being between 0 and 500 MHz.

Chapter 4

Noise in nuclear magnetic resonance spectroscopy system

In this chapter, the concept of noise will be introduced. Fundamental types of noise present in electronic systems will be described, and elements of NMR spectroscopy system will be classified by the type of noise they generate. Additionally, the measure that compares desired signal level to the one of the background noise, called signal–to–noise ratio, will be introduced, as well as the measure of degradation of the signal–to–noise ratio, called noise figure.

4.1 Noise definition and its properties

Broadly speaking, noise can be defined as any unwanted disturbance, regardless of whether it comes from the communication channel itself or from outside of the channel, that interferes with the desired signal. The disturbances that come from the sources external to the observed system (e. g. electrostatic or electromagnetic coupling between the circuit and power lines, radio transmitters or fluorescent lights, hum from power supplies etc.) are usually not stochastic. All these disturbances are caused by radiation from electrical equipment. On the other hand, the disturbances, which are an intrinsic property of the communication channel, form a stochastic signal. In electronics, the word "noise" represents spontaneous fluctuations that result from the physics of the devices and materials that make up the electrical system [26]. The first papers that defined noise in electronics defined it as *the electromotive force due to thermal agitation in conductors* [30, 31].

Noise is important because it defines the limit of resolution of sensors and the dynamic range of various systems. Although the highest signal level that can be processed in a system is defined by the characteristics of elements that make the system, the lowest detectable signal level is set by noise. Generally, the reason why noise is such a problem in electronic systems lies within a fact that it is a totally random signal. Its spectrum consists of multiple frequency

components whose amplitudes and phases are completely stochastic. This means that it is impossible to predict the amplitude nor the phase of noise in any given moment in time.

When speaking specifically about NMR spectroscopy systems, noise is the biggest problem during the Rx mode of NMR measurements. Namely, as it was mentioned in section 3.1, levels of response signals of the measured samples are usually very low – they can go down even to the order of a fW. Such low signal levels are comparable to or even lower than the noise of NMR spectroscopy system, which makes it difficult to detect these signals.

Fortunately, although it is impossible to predict the exact value of noise, it is possible to predict its randomness. It turns out that noise has a Gaussian distribution of its amplitude in time [26]. The curve of common Gaussian distribution, along with the example of noise signal is shown in Figure 4.1.

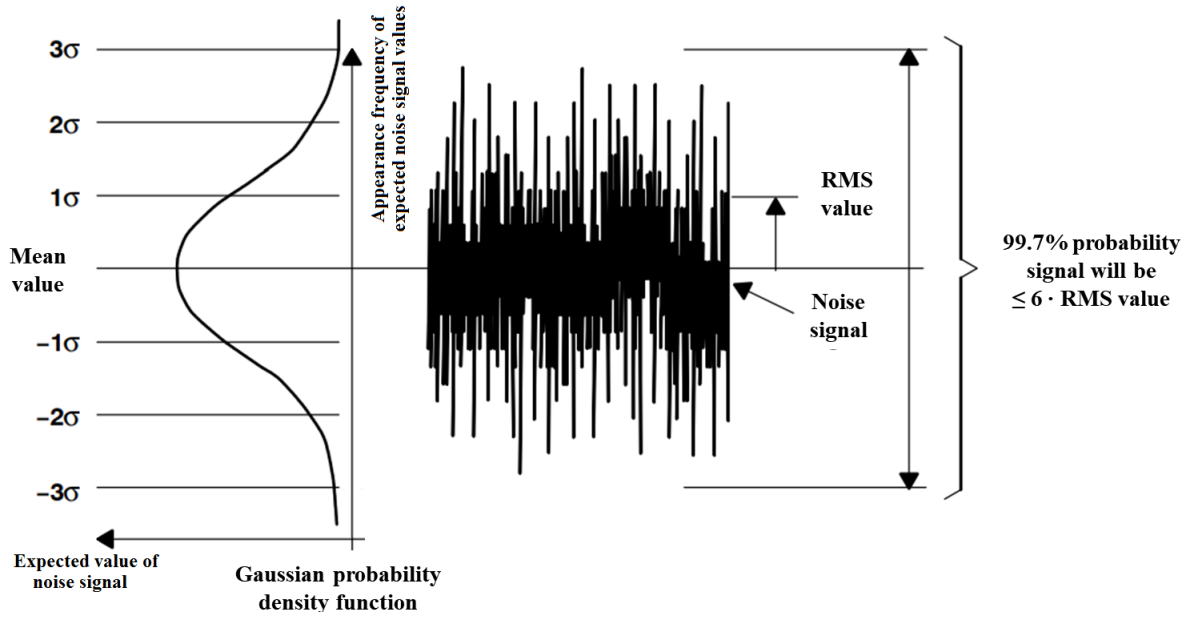

Figure 4.1: Noise waveform and Gaussian probability density function of noise amplitude [32]

This Gaussian distribution arises when noise voltage level gets measured with a great number of data points and then occurences with the same amplitude get summed up. Mathematically, this distribution can be expressed as:

$$f(x) = \frac{1}{\sigma\sqrt{2\pi}} e^{-\frac{(x-\mu)^2}{2\sigma^2}}, \tag{4.1}$$

where μ is the average value, while σ is the standard deviation or root mean square (RMS) value of the variable x [26]. A good engineering approximation is that common electrical noise lies within $\pm 3\sigma$ of the average value, μ. This means that, for 99.7% of the time, the peak–to–peak value of the noise is less than six times its RMS value [26].

Fortunately, the noise mostly has its mean value equal to zero, while its RMS value is relatively easy to measure or predict. Since the RMS definition is based on the equivalent

heating effect, the RMS value, U_{RMS}, of the time–dependent voltage, $u(t)$, can be determined with the use of expression (4.2):

$$U_{RMS} = \sqrt{\frac{1}{T_{meas}} \int_0^{T_{meas}} u^2(t)dt}, \tag{4.2}$$

where T_{meas} represents time duration of the noise measurement [26]. Because they can be relatively easily measured and determined, noise RMS values are the ones used in noise analysis in electronic systems.

4.2 Fundamental types of noise

There are three main types of fundamental noise mechanisms: *thermal noise*, *low–frequency* $(1/f)$ *noise* and *shot noise*. Effects of every type of noise occur in different types of electronic components and devices and are evident in different forms. And although noise, unfortunately, cannot be completely removed from electronic systems, it can be controlled, manipulated and even damped, if handled properly. *If you know the enemy and know yourself*, as Sun Tzu states, *you need not fear the result of a hundred battles*. So, let us learn to know the enemy!

4.2.1 Thermal noise

Thermal noise is a type of noise that is encountered the most, so it is considered first. It has first been observed by J. B. Johnson in 1927 [30] and H. Nyquist in 1928 [31], so this type of noise is also called *Johnson noise* or *Nyquist noise*. Thermal noise is caused by the random thermally excited vibration of the charge carriers in a conductor [26].

Namely, in every conductor at a temperature above absolute zero, which equals 0 K, its charge carriers, which are the electrons and the holes, are in random motion, which is dependent on temperature of the conductor. Since carriers carry a charge equal to $1.602 \cdot 10^{-19}$ C, and since there are miniature changes of charge, $dq(t)$, through the cross section of the conductor, that occur in very short periods of time, dt, a low–level, random–direction and time dependent electric current, $i(t)$, exists in the conductor [33]:

$$i(t) = \frac{dq(t)}{dt}. \tag{4.3}$$

Since every realistic conductor is resistive, R, the current from the expression (4.3) causes rise of a voltage, $u(t)$, across the terminals of the conductor [33]:

$$u(t) = i(t) \cdot R. \tag{4.4}$$

It can be shown that the RMS thermal noise voltage, E_t, depends on temperature of the conductor, T, in kelvins, conductor's resistance or real part of its impedance, R, and noise bandwidth of the measuring system, Δf, in Hz [26]:

$$E_t = \sqrt{4kTR\Delta f}, \tag{4.5}$$

where k represents Boltzmann's constant, which equals $1.38 \cdot 10^{-23}$ J/K. Available thermal noise power in a conductor, N_t, therefore equals [26]:

$$N_t = kT\Delta f. \tag{4.6}$$

Obviously, available thermal noise power is dependent only on the temperature of the conductor and the frequency bandwidth of the measuring system. The most important thing to notice in expression (4.6) is that, since noise power is proportional to the noise bandwidth, there is equal noise power in each hertz of bandwidth. For example, noise power between 1 Hz and 2 Hz is equal to the one between 1000 Hz and 1001 Hz. This is why thermal noise is also being called *white noise*: because, just as white color is comprised equally of all the colors, the spectrum of thermal noise is comprised equally of all the frequencies.

As it can be seen from the expressions (4.5), and (4.6), thermal noise is present in all passive resistive elements. So, in NMR spectroscopy systems, this type of noise is dominant in NMR probes, duplexers, directional couplers and cables that are connected between the elements of the system.

4.2.2 Low–frequency $(1/f)$ noise

In subsection 4.2.1 it has been shown that thermal noise is a consequence of random electron vibrations in a conductor at a temperature above absolute zero. This means that a conductor can generate voltage at its terminals even without being connected to an external voltage or current source. However, if the conductor is connected to some kind of external source, currents created by the source and by conductor's thermal noise are not the only currents that flow through the conductor. There is one more additional current, created by the inhomogeneity and the discontinuity of the conductor.

Because an external source is connected to the conductor's terminals, it creates a voltage drop across the conductor, which means that the current flows through the conductor. Let us assume that the external source generates direct current (DC) through the conductor. This means that the current flows constantly in the same direction. Because the conductor is discontinuous and inhomogeneous, its cross-section does not always have the same value nor the shape, and also, there are some parts inside the conductor (e. g. impurities) where electrons simply cannot

pass through. As a consequence, the electrons do not flow through the conductor in parallel straight lines; they change their transversal directions and they collide into each other. Imagine a crowded multi lane, high–speed motorway that suddenly shrinks to only one lane, then suddenly extends to three lanes, then there's a barricade that blocks the middle lane, then the motorway extends again to four lanes, etc., and all that without any prior warning or a traffic sign. It sounds like a motorway where frequent nasty collisions and accidents are a part of an everyday life! But that is exactly what happens in the conductor; except electrons do not have a brake, so they keep going in spite of all the collisions. These "lane switches" and collisions of electrons generate additional noise that adds to thermal noise. This is why $1/f$ noise is also known in literature as *excess noise* [26].

The effects of this type of noise are more visible with the decrease of frequency – that is why it is called $1/f$ noise in the first place. The reason for this lies in a fact that any frequency and its period are inversely proportional. Or in other words, signals of a lower frequency switch the direction of the current flow less times in a certain time gap than the ones of a higher frequency. This means that, at lower frequencies, electrons' "mileage" will be larger than the one at higher frequencies. Because of this, the amount of electron collisions and "lane switches" will be higher at lower frequencies because there is a greater "road length" to pass, and therefore, a greater chance of the electrons colliding . To better understand this statement, one should imagine electron flow at infinite frequency. In this case, direction switches are so fast that the electron simply does not manage to react to the switch, causing it to stand still in one place. Since all electrons stand still in one place, it is obvious that they cannot collide with each other, so there would obviously be no effects caused by $1/f$ noise.

Since $1/f$ noise is inversely proportional to frequency, it is possible to determine its available power, $N_{1/f}$, by integration over the range of frequencies in which our interest lies:

$$N_{1/f} = K_1 \int_{f_l}^{f_h} \frac{df}{f} = K_1 \ln \frac{f_h}{f_l}, \tag{4.7}$$

where f_l and f_h stand for the lowest and the highest frequency in the bandwidth of interest, respectively, while K_1 is the conductor's dimension constant, usually given in the device's datasheet [26]. The most important thing to notice in expression (4.7) is that, unlike thermal noise, whose available noise power is equal for every hertz of the bandwidth of interest, available $1/f$ noise power is equal for every decade of frequency. So, as the available thermal noise power between 1 Hz and 2 Hz is equal to the one between 1000 Hz and 1001 Hz, the available $1/f$ noise power between 0.1 Hz and 1 Hz is equal to the one between 1000 Hz and 10000 Hz.

As it is explained at the beginning of this subsection, in order for the $1/f$ noise to exist, electric current has to flow through the conductor or device. If this electric current is a low–frequency or a DC one, then the effects of $1/f$ noise are visible. Obviously, this type of noise

is dominant in active devices – the devices that need a DC power supply in order to operate properly. In NMR spectroscopy systems, the active devices are spectrometers and preamplifiers, so this type of noise is dominant in these two types of elements.

4.2.3 Shot noise

Shot noise is a type of noise that occurs in electronic elements with a potential barrier (e. g. diodes and transistors). To understand this type of noise, one should consider the case of an ordinary forward–biased silicon diode, where electrons and holes are crossing the potential barrier. When, for example, an electron enters the diode's *p*–type semiconductor via its anode, it starts accelerating and moving towards the *n*–type semiconductor with increasing speed. Before it enters the *n*–type semiconductor and exits the diode via its cathode, the electron smashes into the potential barrier, causing an impulse of electric current. The overall pulsing current flow caused by all the electrons and holes inside the diode is a granulated effect and it resembles a shotgun penetration. That is why such current variations are called shot noise.

The RMS value of the shot noise current, I_{sh}, is given by:

$$I_{sh} = \sqrt{2qI_{DC}\Delta f}, \tag{4.8}$$

where q represents absolute value of the charge of an electron ($1.602 \cdot 10^{-19}$ C), I_{DC} is the direct current, while Δf is the noise bandwidth [26]. To envisage the effect of shot noise, a great example to observe is a heavy rain on a tin roof. Here, raindrops correspond to charge carriers, precipitation rate corresponds to the current I_{DC}, the roof itself represents the potential barrier, and the area of the roof relates to the noise bandwidth, Δf [26].

Since shot noise is associated with current flow across a potential barrier, and due to the fact that such a barrier exists in the *pn* junctions in semiconductor devices, this type of noise is present in diodes, in bipolar transistors' (BJT) emitter–base junctions and field effect transistors' (FET) gate–source junctions. In NMR spectroscopy systems, devices that comprise such elements are duplexers, preamplifiers and spectrometers.

4.3 Signal–to–noise ratio

Sometimes, when a signal is being measured, its power or amplitude or any information that regards just the signal itself is not enough. It is necessary to know the origin of the noise that surrounds the signal. Measurements in NMR spectroscopy are a great example, since their amplitudes are comparable or even lower than the surrounding noise, so it is a good idea to know something about the dynamics between the signal and its surrounding noise. As it was mentioned in the second paragraph of section 4.1, noise defines the lowest detectable signal

level, so, if nothing else, it would be good to know the level of noise in NMR spectroscopy system in order to know how much weak signals can the system detect.

One of the most often used measures that describes the dynamics between the desired signal and its background noise is called *signal–to–noise ratio* (SNR), and it is defined as the ratio of the average power of the signal and the one of its background noise:

$$SNR = \frac{P_S}{P_N}, \tag{4.9}$$

where P_S and P_N stand for average power levels of signal and noise, respectively [27]. An example of SNR determination of a signal can be seen in Figure 4.2. SNR can also be expressed via RMS voltage level of the signal, U_S, and the one of the noise, U_N, in which case the described measure is called *voltage signal–to–noise ratio* (VSNR) [27]:

$$VSNR = \frac{U_S}{U_N}. \tag{4.10}$$

Both SNR and VSNR are very often expressed in decibels (dB). In this case, their values are the same and can be calculated as follows:

$$SNR[\text{dB}] = 10 \cdot \log(SNR[\text{lin.}]) = 20 \cdot \log(VSNR[\text{lin.}]). \tag{4.11}$$

This is necessary to mention because different communities, and even different journals of the same community, define and abbreviate these two ratios differently, so this way, the level of misunderstanding should be much lower.

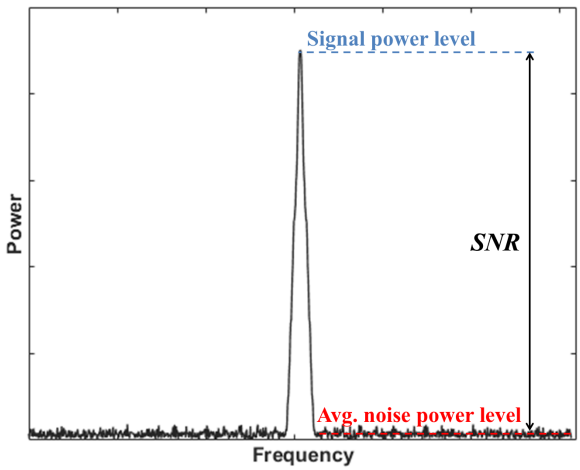

Figure 4.2: An example of SNR determination

4.4 Noise figure

To sum this chapter up, noise is a problem in electronic system because it is ever–present and because it is stochastic, so it is impossible to predict its value, and therefore, impossible to get rid of it. When a signal flows through electronic devices, not only does it have a certain amount of noise straight away after its "birth", but every electronic device the signal flows through also gives it an additional amount of noise. But how exactly does this concern the dynamics between the signal and its background noise? An example of a realistic active element (e. g. an amplifier) is going to serve well to explain this (Figure 4.3).

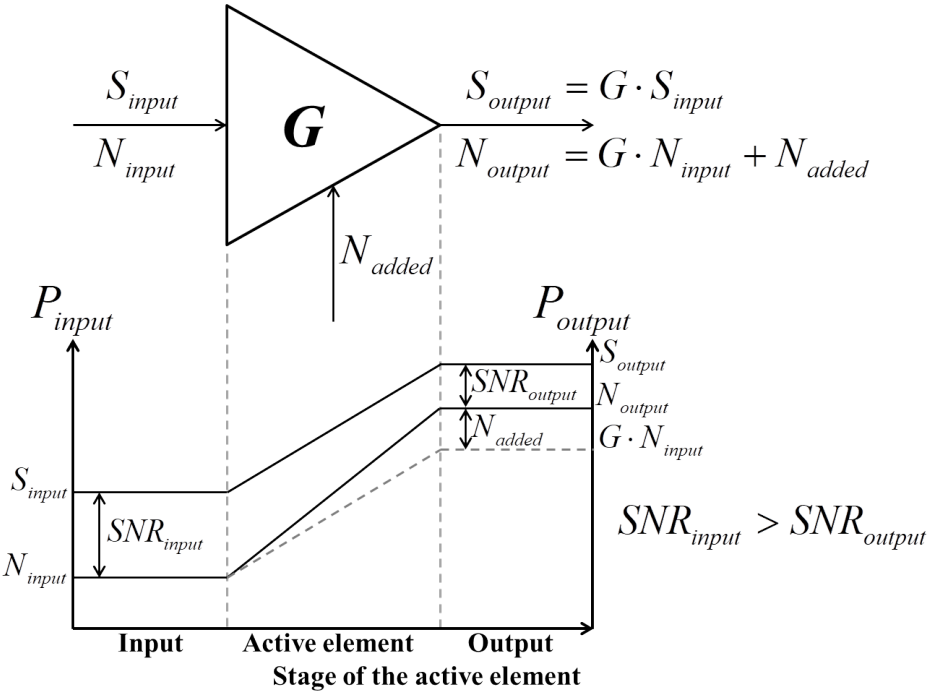

Figure 4.3: Dependence of SNR on the signal position in an electronic device

Let there be a signal with a power level S_{input} and the power level of its background noise N_{input} at the input of the active element, with its power gain G. The signal's SNR at the input of the active element is then equal to:

$$SNR_{input} = \frac{S_{input}}{N_{input}}. \tag{4.12}$$

After the signal passes through the active element, it gets amplified for the amount of G, but so does its background noise. That being said, one would expect that SNR at the output of the active element would then be equal to:

$$SNR_{output} = \frac{S_{output}}{N_{output}} = \frac{G \cdot S_{input}}{G \cdot N_{input}} = \frac{S_{input}}{N_{input}} = SNR_{input}. \tag{4.13}$$

But that, unfortunately, is not correct. The problem is that the active element itself creates a certain amount of noise that adds up to the input noise. So, SNR at the output of the active element is really equal to:

$$SNR_{output} = \frac{S_{output}}{N_{output}} = \frac{G \cdot S_{input}}{G \cdot N_{input} + N_{added}} = \frac{S_{input}}{N_{input} + \frac{N_{added}}{G}} < SNR_{input}. \tag{4.14}$$

It can be seen that the output SNR from the expression (4.14) is smaller than the one from the expression (4.13). This means that SNR of a signal *deteriorates* when it passes through electronic devices; and not just the active ones, but also the pasive ones!

This is why a figure–of–merit that describes the deterioration of a signal's SNR through electronic elements has been introduced. This figure–of–merit is called *noise figure* (F), and noise figure of an electronic element is equal to the ratio of the SNR at the input of the element, SNR_{input}, and the one at the output of the element, SNR_{output}, respectively [26]:

$$F = \frac{SNR_{input}}{SNR_{output}}. \tag{4.15}$$

Noise figure is very often expressed in decibels:

$$F[\text{dB}] = 10 \cdot \log(F[\text{lin.}]). \tag{4.16}$$

If the observed element is noise–free, it can be seen from expressions (4.15) and (4.16) that its noise figure is then equal to 1 in linear scale, or 0 dB in logarithmic scale, respectively. But as it was described by now, such an element, unfortunately, exists only on paper.

One great thing about noise figure is that, not only can it describe SNR deterioration through only one electronic element, but it can also describe SNR deterioration through the entire system! It can be shown that, if there is a system, built as a cascade network (Figure 4.4) of n elements, all mutually matched to the same impedance (e. g. to $Z_0 = 50\Omega$), it is possible to describe noise figure of the entire system as:

$$F_{cascade} = F_1 + \frac{F_2 - 1}{G_1} + \cdots + \frac{F_n - 1}{\prod_{i=1}^{n-1} G_n}, \tag{4.17}$$

where G_n and F_n stand for power gain and noise figure of the n–th element, respectively [26]. When noise figure of a cascade is determined with the use of expression (4.17), input and output SNRs of the cascade are, similar to the expression (4.15), connected as:

$$F_{cascade} = \frac{SNR_{input}}{SNR_{output}}. \tag{4.18}$$

The expression (4.17) is going to be used to describe the most sensitive part of the NMR spectroscopy system from the aspect of noise, but more on this is going to be written in Chapter 6.

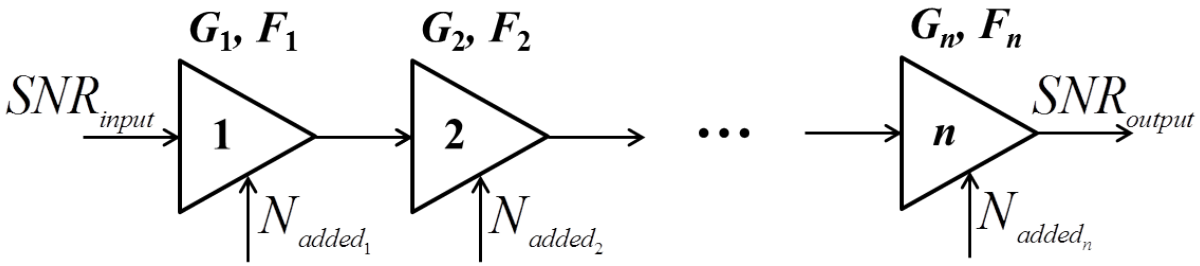

Figure 4.4: Cascade of *n* electronic devices

Chapter 5

Electromagnetic model of the probe

In this chapter, available expression for induced voltage on the coil [2], as well as its modernized version [34], and knowledge about noise, described in Chapter 4, are going to be used to create an expression that describes signal–to–noise ratio at the output of the probe.

5.1 Motivation

Schematic diagram of NMR probe, along with temperature environments of different parts of the probe, are shown in Figure 5.1.

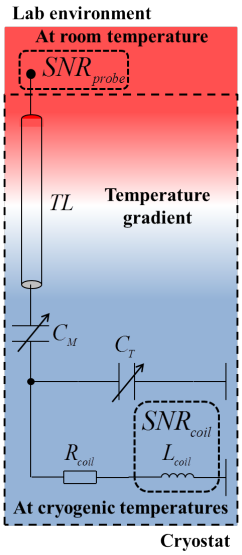

Figure 5.1: Schematic diagram of NMR probe and temperature environments of its different parts

There are expressions available in the literature that describe induced voltage on the coil and noise level around the coil [2, 34]. Combining these expressions, it is possible to calculate SNR at the coil's terminals (SNR_{coil} in Figure 5.1). However, such an expression neglects some of the effects described in Chapter 2. It also neglects the fact that the response signal passes through

the transmission line with inherent losses, and whose temperature also gradually changes from cryogenic temperatures to room temperature. These two efects cause additional noise that gets summed up to the response signal's background noise, thus causing a degradation of the response signal's SNR. So, the idea is to take all these neglected effects and derive an expression that describes SNR of the response signal, but at the output of the probe, that is situated in the environment of room temperature (SNR_{probe} in Figure 5.1). This expression should serve as a more precise electromagnetic model of the NMR probe than the one already available in the literature, and it will also be used as a comparison to another created electromagnetic model that will be described in Chapter 6.

5.2 Induced signal at the coil's terminals

It is shown that the voltage level of the sample's response signal, induced at the terminals of the NMR probe's coil, U_{ind}, depends on Larmor frequency of the sample, ω_L, overall magnetization of the sample, M, cross section's area of the coil, A_{coil}, and number of turns of the coil, n_{coil} [2]:

$$U_{ind} = \mu_0 \omega_L M A_{coil} n_{coil}, \tag{5.1}$$

where μ_0 represents vacuum permeability ($4\pi \cdot 10^{-7}$ H/m). In this expression, all the variables (except for the constant, μ_0) first need to be calculated. So, the idea is to manipulate the expression (5.1) until all the parameters are either constants or are immediately easy to determine. The first step that can be done is to express Larmor frequency with its basic expression:

$$\omega_L = 2\pi\gamma B_0, \tag{5.2}$$

where γ stands for the gyromagnetic ratio of the sample, while B_0 represents direct magnetic field in whose environment the sample is placed. After the insertion of (5.2) into (5.3), U_{ind} is now expressed as:

$$U_{ind} = 2\pi\gamma B_0 \mu_0 M A_{coil} n_{coil}. \tag{5.3}$$

In order to simplify the expression (5.3), an assumption will be made is that the coil's cross section has a circular shape. Now it is possible to express the cross section area by the mean radius of a coil's turn, r_{coil} as:

$$A_{coil} = r_{coil}^2 \pi. \tag{5.4}$$

After the insertion of (5.4) into (5.3), U_{ind} is expressed as:

$$U_{ind} = 2\pi^2 \gamma B_0 \mu_0 M r_{coil}^2 n_{coil}. \tag{5.5}$$

Overall sample magnetization, M, can be expressed as:

$$M = \frac{N\gamma^2\hbar^2 I(I+1)B_0}{3kT_{coil}V_{sample}}, \tag{5.6}$$

where N stands for the amount of substance (in this case, the amount of the observed nuclei in the observed sample), $\hbar$ stands for reduced Planck constant ($1.055 \cdot 10^{-34}$ Js), I stands for the spin of the observed nuclei, k represents Boltzmann constant ($1.38 \cdot 10^{-23}$ J/K), V_{sample} represents the volume of the sample, while T_{coil} represents temperature, expressed in kelvins, in which environment the sample is placed in. After the insertion of (5.6) into (5.5), U_{ind} is now equal to:

$$U_{ind} = \frac{2\pi^2}{3}\frac{\gamma^3\hbar^2 B_0^2\mu_0 I(I+1)Nr_{coil}^2 n_{coil}}{kT_{coil}V_{sample}}. \tag{5.7}$$

In order to get rid of π^2, one can express reduced Planck constant via the non–reduced one, h ($6.63 \cdot 10^{-34}$ Js):

$$\hbar = \frac{h}{2\pi} \Rightarrow \hbar^2 = \frac{h^2}{4\pi^2}. \tag{5.8}$$

U_{ind} is now expressed as:

$$U_{ind} = \frac{1}{6}\frac{\gamma^3 h^2 B_0^2\mu_0 I(I+1)Nr_{coil}^2 n_{coil}}{kT_{coil}V_{sample}}. \tag{5.9}$$

One last substitution that will be done is the one of the amount of substance, N, via the mass, m, and molar mass, M, of the sample:

$$N = \frac{m}{M}N_A, \tag{5.10}$$

where N_A represents Avogardro constant ($6.022 \cdot 10^{23}$ mol^{-1}). Finally, U_{ind} can be expressed as:

$$U_{ind} = \frac{1}{6}\frac{m}{M}N_A\frac{\gamma^3 h^2 B_0^2\mu_0 I(I+1)r_{coil}^2 n_{coil}}{kT_{coil}V_{sample}}. \tag{5.11}$$

This expression represents voltage level of the induced response signal at the coil's terminals. Before the "translation" to the probe's terminals, a good idea is to first discuss a few occuring, potentially problematic, effects. The first effect is reflection of the signal due to the impedance mismatch. However, since one part of the probe is the tuning/matching network, the coil is almost perfectly matched to characteristic impedance of the transmission line, which is equal to 50 Ω, at the frequency that is exactly equal to the sample's Larmor frequency. Therefore, this effect can in this case be neglected. The second effect is signal loss due to the series distributed resistance and shunt distributed conductance of the transmission line. However, ultra–low–loss coaxial cables are frequently used as transmission lines in NMR probes, so this effect can

also be neglected. There are also a few effects that are caused by the phenomena described in Chapter 2, but more about these effects will be discussed in section 5.4.

5.3 Background noise of the response signal

In order to desribe and express background noise of the response signal, first it is necessary to identify the correct type of noise that needs to be taken into consideration. To do that, a good idea is to observe the coil and its environment first. It can be seen in Figure 5.1 that the probe is comprised of only passive elements. This means that there are no power supplies needed to connect to the probe for it to work, so there are no DC currents flowing through the probe. Therefore, $1/f$ noise can be neglected. Also, since there are no active elements in the probe, there are obviously no transistors, that possess a *pn* junction, in the probe. There are also no diodes in the probe, so shot noise can also be neglected. On the other hand, thermal noise is ever–present, regardless of the type of the electronic element, and since the effects of both shot noise and $1/f$ noise can be neglected, thermal noise is the dominant type of noise in NMR probes.

Now that the dominant type of noise is determined, the next step is to detect all noise sources in the probe. As it is explained in subsection 4.2.1, electronic elements with ohmic resistance are the ones that generate thermal noise. It can be seen in Figure 5.1 that the only two elements of the probe with ohmic losses are the real part of the coil's impedance and the transmission line's input impedance (which is calculated under the assumption that the transmission line is terminated with Z_0 at its output; in our case this assumption is correct). So, in order to express overall background noise of the response signal, caused by the effect of thermal noise, it is first necessary to express background noises of both aforementioned elements separately, and then somehow observe its overall effect.

As it can be seen in expression (4.5), voltage level of the background noise depends mostly on the ohmic resistance value of the element that generates noise, and on the temperature in which environment the resistor is placed in. So, in order to express background noise voltage level caused by the coil's ohmic resistance, $U_{noise_{coil}}$, it is necessary to determine this resistance, R_{coil}, and the temperature of the coil's environment,T_{coil}, also needs to be known:

$$U_{noise_{coil}} = \sqrt{4kT_{coil}R_{coil}\Delta f}, \tag{5.12}$$

where k represents Boltzmann constant, while Δf stands for the observed frequency bandwidth. The resistance of the coil can be expressed as:

$$R_{coil} = \rho_{wire}\frac{l_{wire}}{S_{wire}}, \tag{5.13}$$

where l_{wire} represents the length of the wire the coil is made of, S_{wire} represents the cross-section of the wire the coil is made of, while ρ_{wire} represents resistivity of a material the wire is made of [35]. The length of the wire, l_{wire} can be calculated as:

$$l_{wire} = n_{coil} 2 r_{coil} \pi, \tag{5.14}$$

where n_{coil} represents number of turns of the coil, while r_coil represents mean radius of the coil's cross section. The wire's cross-section, S_{wire}, can be expressed as:

$$S_{wire} = r_{wire}^2 \pi - (r_{wire} - d)^2 \pi = (2 r_{wire} - d) d \pi, \tag{5.15}$$

where r_{wire} represents the diameter of the wire the coil is made of, while d represents the depth of the skin effect. The skin effect can be expressed as:

$$d = \sqrt{\frac{2\rho_{wire}}{\omega_L \mu_{wire}}}, \tag{5.16}$$

where ω_L represents the Larmor frequency, while μ_{wire} represents the magnetic permeability of the wire, which is equal to μ_0. Taking expressions (5.14), (5.15) and (5.16) into consideration, the coil's resistance can now be expressed as:

$$R_{coil} = \rho_{wire} \frac{2 n_{coil} r_{coil}}{(2 r_{wire} - d) d}. \tag{5.17}$$

On the other hand, the input impedance of the transmission line, R_{TL}, can be determined as [35]:

$$R_{TL} = \frac{Z_0 l_{TL} \alpha_{coax}[\text{dB/m}]}{4.343}, \tag{5.18}$$

where Z_0 and α_{coax} represent characteristic impedance (usually 50 Ω) and losses per length (given in the cable's datasheet) of the coaxial cable the transmission line is made of, respectively, while l_{TL} represents the length in meters of the same coaxial cable [35] Again, this input impedance is determined under the assumption that the transmission line is terminated with Z_0 at its output, which is true in the described case.

However, the determination of the transmission line's temperature is not so straightforward. The problem is that one side of the transmission line is situated in the environment of cryogenic temperature (just as the probe's coil and the tuning/matching network), while the other side is situated in the environment of room temperature, so it is obvious that none of the temperatures can be used as the temperature in whose environment the transmission line is placed in. However, since there is a temperature gradient along the transmission line from one side to another, a good approximation is to use the arithmetic mean value of the two temperatures. So, the

temperature in whose environment the transmission line is placed in, T_{TL}, can be expressed as:

$$T_{TL} = \frac{T_{coil} + T_0}{2}, \tag{5.19}$$

where T_0 represents the so–called standard temperature that is equal to 290 K (this temperature is used as a room temperature). Now, background noise voltage level caused by the transmission line's input impedance, $U_{therm.noise_{TL}}$, can be expressed as:

$$U_{therm.noise_{TL}} = \sqrt{4kT_{TL}R_{TL}\Delta f}. \tag{5.20}$$

Now the two background noise voltages need to be combined in order to determine the overall background noise voltage level. It is shown that uncorrelated voltage sources (which noise sources definitely are), can be combined by the summation of their RMS values, thus getting the overall background noise RMS voltage level [26]. So, the overall background noise RMS voltage level, $U_{noise_{overall}}$, expressed via noise RMS voltage levels caused by the coil, $U_{noise_{coil}}$, and the transmission line, $U_{thermalnoise_{TL}}$, is equal to:

$$U_{noise_{overall}} = \sqrt{U^2_{noise_{coil}} + U^2_{therm.noise_{TL}}}. \tag{5.21}$$

After insertion of (5.12) and (5.20) into (5.21), the expression for $U_{noise_{overall}}$ now stands as:

$$U_{noise_{overall}} = \sqrt{4kT_{coil}R_{coil}\Delta f + 4kT_{TL}R_{TL}\Delta f} = 2\sqrt{k(T_{coil}R_{coil} + T_{TL}R_{TL})\Delta f}. \tag{5.22}$$

This is the expression of background noise that will be used in the derived expression for the SNR at the probe terminals.

5.4 Signal–to–noise ratio at the probe's terminals

In order to derive the expression for VSNR at the probe's terminals, one simply needs to combine expressions (5.11) for the voltage level of the induced response signal, and (5.22) for the overall background noise voltage RMS level:

$$VSNR_{probe} = \frac{1}{12}\frac{m}{M}N_A \frac{\gamma^3 h^2 B_0^2 \mu_0 I(I+1) r^2_{coil} n_{coil}}{T_{coil}V_{sample}\sqrt{k^3(T_{coil}R_{coil} + T_{TL}R_{TL})\Delta f}}, \tag{5.23}$$

where R_{coil}, R_{TL} and T_{TL} can be determined by the use of (5.17), (5.18) and (5.19), respectively. In order to make this expression more precise, a few more effects (whose description is available at the end of subsection 7.2) have been taken into consideration: signal reduction due to short T_2 time, K_{T_2}, due to spectral linewidth broadening, K_{LW}, due to NQR spectral lines splitting,

K_{LS}, and due to number of crystallographic sites, K_{CS}, as well as the abundance of the observed isotope, $n_{isotopes}$, which makes the final expression for VSNR at the probe's terminals to be equal to:

$$VSNR_{probe} = \frac{1}{12}\frac{m}{M}N_A\frac{\gamma^3 h^2 B_0^2 \mu_0 I(I+1) r_{coil}^2 n_{coil}}{T_{coil}V_{sample}\sqrt{k^3(T_{coil}R_{coil}+T_{TL}R_{TL})\Delta f}}K_{T_2}K_{LW}K_{LS}K_{CS}n_{isotopes}. \quad (5.24)$$

Equivalent SNR at the probe's terminals is then equal to:

$$SNR_{probe} = \left(\frac{1}{12}\frac{m}{M}N_A\frac{\gamma^3 h^2 B_0^2 \mu_0 I(I+1) r_{coil}^2 n_{coil}}{T_{coil}V_{sample}\sqrt{k^3(T_{coil}R_{coil}+T_{TL}R_{TL})\Delta f}}K_{T_2}K_{LW}K_{LS}K_{CS}n_{isotopes}\right)^2. \quad (5.25)$$

Equations (5.24) and (5.25) can also be expressed in decibels, where $VSNR_{probe}$ can be expressed as:

$$VSNR_{probe}[\text{dB}] = 20\cdot\log(VSNR_{probe}[\text{lin.}]) =$$

$$= 20\cdot\log\left(\frac{1}{12}\frac{m}{M}N_A\frac{\gamma^3 h^2 B_0^2 \mu_0 I(I+1) r_{coil}^2 n_{coil}}{T_{coil}V_{sample}\sqrt{k^3(T_{coil}R_{coil}+T_{TL}R_{TL})\Delta f}}K_{T_2}K_{LW}K_{LS}K_{CS}n_{isotopes}\right), \quad (5.26)$$

while SNR_{probe} can be expressed as:

$$SNR_{probe}[\text{dB}] = 10\cdot\log(SNR_{probe}[\text{lin.}]) =$$

$$= 10\cdot\log\left[\left(\frac{1}{12}\frac{m}{M}N_A\frac{\gamma^3 h^2 B_0^2 \mu_0 I(I+1) r_{coil}^2 n_{coil}}{T_{coil}V_{sample}\sqrt{k^3(T_{coil}R_{coil}+T_{TL}R_{TL})\Delta f}}K_{T_2}K_{LW}K_{LS}K_{CS}n_{isotopes}\right)^2\right]. \quad (5.27)$$

Chapter 6

Noise model of the receiving chain

In this chapter, the development of the noise model of NMR spectroscopy Rx chain is explained. The derived expression for the Rx chain's noise figure is given here, as well as its development and the conclusions this expression offers.

6.1 Motivation

One of the biggest problems in today's NMR measurements is that in the case of very low response signals of specific samples the averaging of a high number of acquisitions has to be used, which results in very long measurement times [11]. Depending on sample properties, these measurements can last up to a few tens of hours [15] for a single dataset. This is because it can easily happen that the signal arriving from the coil is lower than the noise level. The enhancements, such as cryogenic NMR spectroscopy [36, 37], proved to be effective in the improvement of the noise properties. However, if the goal is to study the temperature properties of a particular system, they are set by measurement conditions and can hardly be used arbitrarily to further improve the signal characteristics. Thus, it is necessary to quantitatively analyse every segment of the NMR's receiving chain, find its weak links and look for the solutions of improvement there. This way, it is possible to examine the feasibility of further improvement of the existing setup, and also to determine new potential ways of enhancing the sensitivity of the NMR measurements, which could lead to a significant additional shortening of the measurement time.

6.2 Development of the receiving chain's noise model

6.2.1 Basic noise model of the receiving chain

As it was already mentioned in section 3.1, the response signal is much weaker than the exciting one (an order of a fW compared to an order of a kW). Due to very low levels of the response signal, close to or even smaller than the background noise level [26], the sensitivity of the NMR system operating in Rx mode is very limited. That is why the receiving chain is the most sensitive part of the NMR spectroscopy system and also why it is necessary to quantitatively define this part of the system.

The block diagram of the receiving chain is shown in Figure 6.2. Here, L_1, L_2 and L_4 stand for the linear values of power losses of the input cable, the duplexer and the output cable, respectively, while G_3 and F_3 stand for the linear values of power gain and noise figure of the preamplifier, respectively. F_5 stands for the linear equivalent value of noise figure of the entire spectrometer (its RF receiver, A/D converter and digital signal processor – DSP). The explanation on how the value of F_5 was determined can be found in section 6.3. Inserting above definitions for various chain parameters into 4.17, one gets the expression for the overall noise figure of the NMR receiving chain:

$$F_{NMR_{Rx}} = F_1 + \frac{F_2 - 1}{G_1} + \frac{F_3 - 1}{G_1 G_2} + \frac{F_4 - 1}{G_1 G_2 G_3} + \frac{F_5 - 1}{G_1 G_2 G_3 G_4}. \tag{6.1}$$

However, (6.1) is correct only if the noise temperature at the chain input is equal to T_0, and if the impedances of all the elements are matched to the system impedance, Z_0. Since this might not be the case in practical NMR receiving chain, some corrections of the expression (6.1) need to be made. The corrections will be described and explained step-by-step, until the final expression is created.

6.2.2 Corrections due to lossy elements of the receiving chain

In Figure 6.2, it is shown that the receiving chain is comprised of the input cable, the duplexer, the preamplifier, the output cable and the spectrometer. Clearly, the input cable, the duplexer and the output cable are all passive lossy devices. They are always manufactured in a way that their input/output impedance is matched to the system impedance Z_0. Even if the associated impedance is not identical to Z_0, inevitable losses "improve" matching (but, at the same time, deteriorate the noise figure). Hence, the corrections regarding the impedance mismatch in (6.1) is not necessary. Furthermore, it is well-known [35] that the gain and the noise figure of a

matched lossy two–port network are related by very simple expressions:

$$G_i = \frac{1}{L_i}; \quad F_i = L_i, \tag{6.2}$$

where L_i stand for power loss, and G_i and F_i as previously defined power gain and noise figure, of the i–th element of the chain, respectively. By insertion of (6.2) into (6.1), the receiving chain (Figure 6.2) noise figure can be expressed as:

$$F_{NMR_{Rx}} = L_1 + L_1(L_2 - 1) + L_1L_2(F_3 - 1) + \frac{L_1L_2(L_4 - 1)}{G_3} + \frac{L_1L_2L_4(F_5 - 1)}{G_3}. \tag{6.3}$$

This way, all the elements' losses and gains can be measured using a vector network analyzer (VNA), which is often found in NMR laboratories, by measuring S_{21} scattering parameter of every element, and then using (6.4) if the element is passive, or (6.5) if the element is active [38]:

$$L_i[\text{lin.}] = 10^{-\frac{|S_{21_i}|[\text{dB}]}{10}}; \tag{6.4}$$

$$G_i[\text{lin.}] = 10^{\frac{|S_{21_i}|[\text{dB}]}{10}}. \tag{6.5}$$

Noise figures of any element can also be measured by a noise figure meter [39]. This is a standard instrument widely used in RF engineering, but it is not often found in an average NMR laboratory. A special problem, which is the determination of the spectrometer's equivalent noise figure value by a simple approximate method that uses just a signal generator, is given in section 6.3. An alternative route in determining it is to use the values found in associate datasheets.

From Figure 6.2, it is clear that the first element in the NMR receiving chain is the cable that connects the output of the probe to the input of the duplexer. Its noise properties limit minimal value of the overall noise figure of the chain (6.3) There is no hardware nor software improvements that can decrease overall noise figure below the value of cable losses (the first element in 6.3). Therefore, to achieve a lower overall noise figure of the NMR receiving chain (and, therefore, to increase sensitivity), it is necessary to shorten or completely remove the input cable, if it is possible. If not, the recommendation is to use a cable with as low losses as possible.

6.2.3 Correction due to impedance mismatch of the preamplifier

Coaxial RF components (including those in the NMR system) are usually designed to be matched to a system characteristic impedance of $Z_0 = 50\ \Omega$. If some of the chain elements have different input/output impedance, reflections of the signal are going to occur, causing an effective

deterioration of noise figure of both the element itself and the entire RF system. In the NMR receiving chain (Figure 6.2), there are two active elements that may cause impedance mismatch: the preamplifier and the spectrometer. Spectrometer is basically a special RF receiver that is constructed very carefully and great efforts were put in obtaining its good matching. Thus, it is assumed that the spectrometer input is perfectly matched to Z_0 and possible small mismatch is neglected in our analysis. The preamplifier, however, is not always matched to Z_0. As it was already mentioned in section 3.5, during the construction of an NMR preamplifier, there are three conditions that need to be met: i) the preamplifier needs to have its power gain as high as possible, ii) its noise figure as low as possible, and iii) it has to be matched to Z_0. In addition, the amplifier should be stable (i.e. not prone to unwanted self-oscillations) and to have a high dynamic range. Unfortunately, it is impossible to meet all the conditions above at the same time and some trade-off is necessary. To take this into account, a situation where both the elements connected to the input and the output of the preamplifier are well matched to Z_0, while the preamplifier is only mismatched at its input, will be considered. This is a rather realistic assumption. In such a case, the element connected to the preamplifier's output is well-matched to Z_0, and the signal is not going to reflect back from it. In this scenario, the preamplifier gain and noise figure are given by [26]:

$$G_{corr.} = G(1-|S_{11}|^2) \tag{6.6}$$

$$F_{corr.} = 1 + \frac{F-1}{1-|S_{11}|^2} \tag{6.7}$$

where G and F stand for the measured power gain and the determined noise figure of an element that needs to be corrected due to an impedance mismatch, respectively [35]. S_{11} effectively stands for the linear value of the input reflection coefficient of the same element. The S_{11} parameter can also be measured by a VNA [38], and its linear value can be determined as:

$$S_{11}[\text{lin.}] = 10^{\frac{|S_{11}|[\text{dB}]}{20}}. \tag{6.8}$$

Taking all of the above into consideration, the NMR receiving chain noise figure is now expressed as:

$$F_{NMR_{Rx}} = L_1 + L_1(L_2-1) + \frac{L_1L_2(F_3-1)}{1-|S_{11_3}|^2} + \frac{L_1L_2(L_4-1)}{G_3(1-|S_{11_3}|^2)} + \frac{L_1L_2L_4(F_5-1)}{G_3(1-|S_{11_3}|^2)}. \tag{6.9}$$

6.2.4 Introduction of the non–standard temperature of the probe

When using the expression (6.9) to determine the NMR receiving chain noise figure, it is implicitly assumed that the noise temperature at the input of the chain is set to the standard tem-

perature, T_0, which is equal to 290 K. This is sometimes, and even often, not really the case in modern NMR measurements of materials, where the vast majority of measurements has been made with both the probe and the sample placed in the environment of very low temperatures, sometimes even as low as the order of 100 mK. Obviously, these temperatures differ significantly from T_0, used in noise figure definition (4.15). Considering the fact that, on standard available cryogenic temperatures and magnetic fields, the noise power changes linearly with temperature [26], it is clear that a temperature correction of expression (6.9) needs to be made. It can be shown that the non-standard noise figure of some RF element or chain (where by 'non-standard' the input noise temperature T of that element or chain, with $T \neq T_0$, is regarded) can be expressed via the standard noise figure of the same element or chain as [40]:

$$F = 1 + \frac{T_0}{T}(F_0 - 1). \tag{6.10}$$

Here, F and F_0 stand for non-standard and standard noise figure of an element of the chain under correction, respectively. Before this correction is introduced to the expression (6.9), first it is necessary to determine the temperature T. The temperature of both the coil and the sample is equal to T_{coil}, while the temperature at the output of the NMR probe is T_0. The temperature of the coaxial cable will therefore have a gradient along its length from T_0 at its output connector to T_{coil} at the other end. Since the coaxial cables are usually made from standard metallic materials that are good heat conductors, and the temperature T_{coil} does not vary significantly during the measurement, there will be a temperature gradient from one end of the cable to another. This can be approximated by a linear gradient, enabling definition of the average temperature of the probe:

$$T_{probe} = \frac{T_{coil} + T_0}{2} \tag{6.11}$$

Now it is possible to write the expression (6.9) as:

$$F_{NMR_{Rx}} = 1 + \frac{2 \cdot T_0}{T_{coil} + T_0}\left[L_1 + L_1(L_2 - 1) + \frac{L_1 L_2 (F_3 - 1)}{1 - |S_{11_3}|^2} + \frac{L_1 L_2 (L_4 - 1)}{G_3(1 - |S_{11_3}|^2)} + \frac{L_1 L_2 L_4 (F_5 - 1)}{G_3(1 - |S_{11_3}|^2)} - 1\right]. \tag{6.12}$$

6.2.4.1 Why cryogenic preamplifier noise figure is not corrected?

One of the most recent notable advances in NMR spectroscopy is the use of cryogenic preamplifiers [36]. The idea is to construct the preamplifier that can withstand cryogenic temperatures, which can go down even to an order of 100 mK. This way, the preamplifier's thermal noise level decreases significantly, causing a large decrease of its overall noise figure. And because this kind of preamplifier does not operate in the environment of temperatures similar or equal to T_0, it might seem logical that the preamplifier's noise figure also needs temperature correction. However, this, in fact, is not the case. As it was described in the former section, 6.2.4, standard

noise figure measurements are performed in such a way that the input signal of the device under measurement is placed in the environment of T_0. If this is not the case, temperature correction of noise figure of the device, described in (6.10), is performed. This is so because noise figure of a device represents a measure that describes how much noise the device injects into the system, and the standard measurement is *set* to be made with the input signal at T_0. So, standard temperature is in fact a norm created so that all the noise figure measurements of different devices would be done in universal conditions, and therefore, would be comparable to each other.

Therefore, even when the preamplifier is cooled down to cryogenic temperatures, the temperature environment of the preamplifier itself is changed, but the environment of its input signal remains unaltered. Noise figures of the same preamplifier, when it is measured in the environment of T_0 and in the cryogenic environment, would be different because thermal noise levels would be different, but both noise figures would be considered standard because the environment of the input signal was the same for both measurements. This means that, if a certain preamplifier can be used both in the environment of T_0 and cryogenic environment, one needs to consider noise figure value that was measured in the proper temperature environment, and this value can be inserted into the expression (6.12) without the correction described in (6.10).

6.2.5 Introducing the signal averaging

As it is already known in the NMR community, the averaging of multiple measurements can improve effective SNR drastically. It is important to stress out that this improvement presumes that the physical properties of the NMR system do not vary during the averaging. A well-known fact is that the effective output voltage SNR increases by a square root of the number of averaged measurements due to its stochastic nature [17]. Since power is proportional to the square value of voltage, the power SNR increases linearly by the number of averaged measurements [41]:

$$SNR_{avg} = n_{meas} \cdot SNR_{single} \tag{6.13}$$

where SNR_{single} and SNR_{avg} stand for the SNR of the single and averaged measurement, respectively, while n_{meas} stands for the number of averaged measurements. To illustrate the correctness of this approach, multiple measurements of the ^{63}Cu response signal in the NMR sample $SeCuO_3$ were performed. During all the measurements, the only parameter that was changed was the number of averaged measurements. The rest of the parameters were fixed to the values described in Table 7.2. The measurement results of the ^{63}Cu in $SeCuO_3$ can be seen in Figure 6.1. As it can be seen, SNR really does increase linearly with the linear increase of the averaged measurements number. Furthermore, since the fundamental definition of noise figure of an element or a chain (4.15) is expressed as the ratio of its input and output SNRs, respectively, it is clear that the output SNR is enhanced linearly with the number of averaged

measurements. This means that noise figure *decreases* linearly with the number of averaged measurements:

$$F_{avg} = \frac{SNR_{in}}{SNR_{out_{avg}}} = \frac{SNR_{in}}{SNR_{out_{single}} \cdot n_{meas}} = \frac{F_{single}}{n_{meas}} \tag{6.14}$$

where F_{single} and F_{avg} stand for the noise figure of the single and averaged measurement, respectively. Finally, the NMR receiving chain noise figure can now be expressed, and it can be seen under Figure 6.2, as expression (6.15).

The expression (6.15) is the final model of the NMR receiving chain using a single-stage preamplifier (Figure 6.2). Here, L_1, L_2 and L_4 stand for linear values of power losses of the input cable, the duplexer and the output cable, respectively, F_3, G_3 and S_{11_3} stand for linear values of noise figure, power gain and input reflection coefficient of the preamplifier respectively, F_5 stands for the linear value of noise figure of the entire spectrometer, T_0 and T_{coil} stand for standard temperature of 290 K and the temperature of the environment which the coil and the sample are placed in, respectively, and n_{meas} stands for the number of averaged measurements.

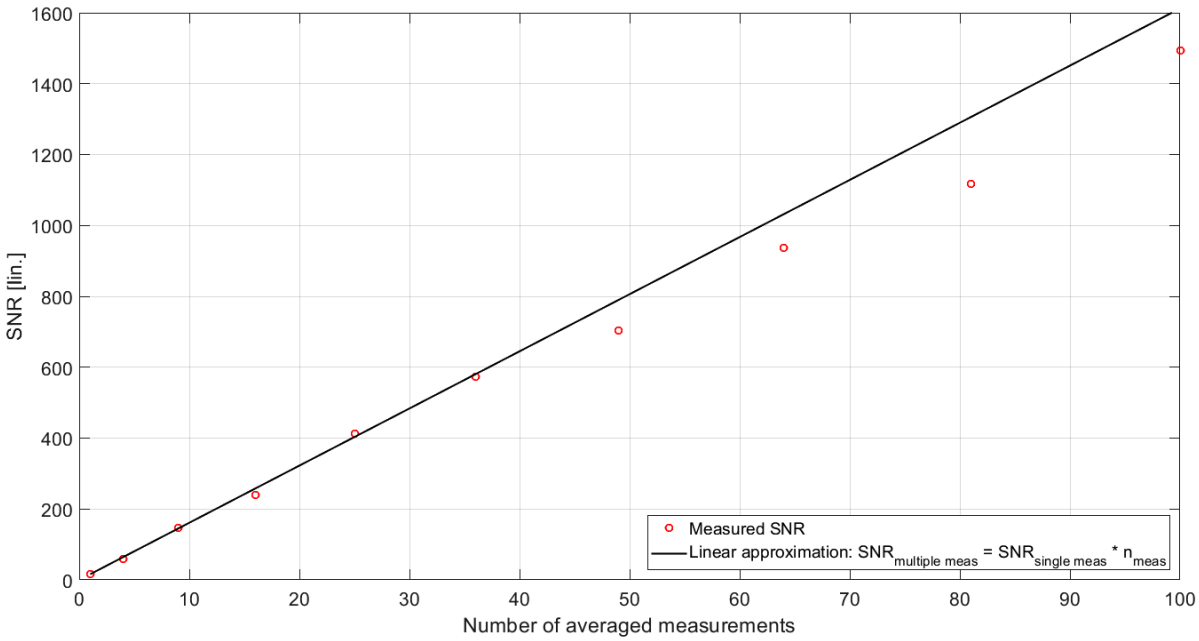

Figure 6.1: Dependence of the measured SNR level on the number of averaged measurements (measured signal: ^{63}Cu in $SeCuO_3$)

6.2.6 The case of a two–stage preamplifier

The case of a two-stage preamplifier (Figure 6.3) is also being considered here. The expression (6.15) can be extended to (6.16), where the indices are the same as in (6.15), except now the index '3*b*' refers to the second stage of the two-stage preamplifier. The expression for the case of a two–stage preamplifier can be seen under Figure 6.3, as expression (6.16).

The main idea behind the addition of the second stage amplifier is to improve the preamplifier so that its parameters, such as its gain (G_3), its noise figure (F_3) and its input reflection coefficient (S_{11_3}), come closer to its optimal values, described in section 3.5, depending on the rest of the NMR spectroscopy system. The validity check of this well-known approach will be described in Chapter 7.

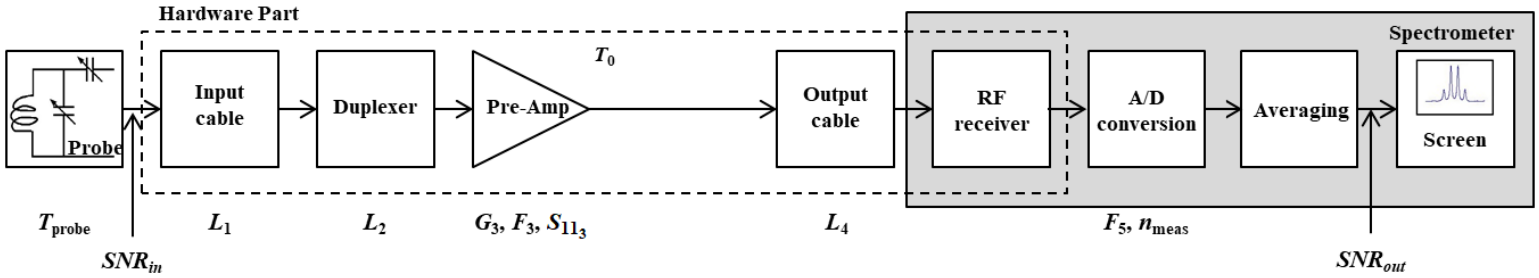

Figure 6.2: Block diagram of the NMR spectroscopy receiving chain with a single–stage preamplifier (up) and its noise figure expression (down)

$$F_{NMR_{Rx}} = \frac{1 + \frac{2T_0}{T_{coil}+T_0}\left[L_1 + L_1(L_2-1) + \frac{L_1L_2(F_3-1)}{1-|S_{11_3}|^2} + \frac{L_1L_2(L_4-1)}{G_3(1-|S_{11_3}|^2)} + \frac{L_1L_2L_4(F_5-1)}{G_3(1-|S_{11_3}|^2)} - 1\right]}{n_{meas}} \tag{6.15}$$

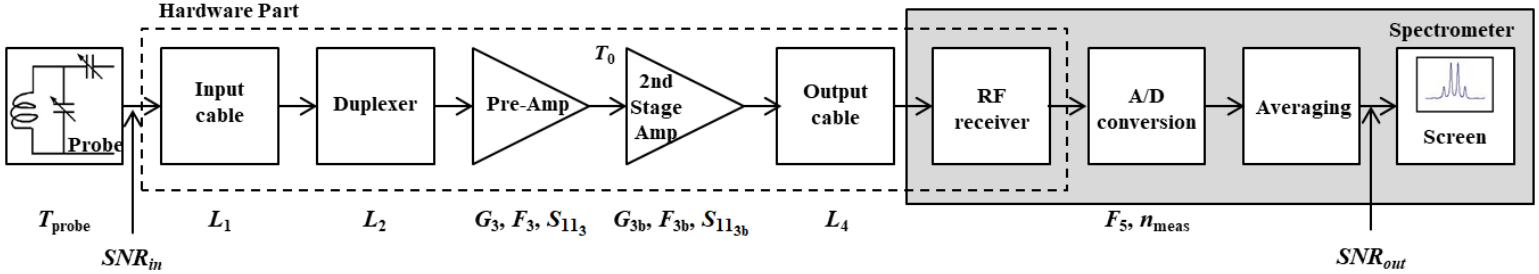

Figure 6.3: Block diagram of the NMR spectroscopy receiving chain with a two–stage preamplifier (up) and its noise figure expression (down)

$$F_{NMR_{Rx}} = \frac{1 + \frac{2T_0}{T_{coil}+T_0}\left[L_1 + L_1(L_2-1) + \frac{L_1L_2(F_3-1)}{1-|S_{11_3}|^2} + \frac{L_1L_2(F_{3b}-1)}{G_3(1-|S_{11_3}|^2)(1-|S_{11_{3b}}|^2)} + \frac{L_1L_2(L_4-1)}{G_3(1-|S_{11_3}|^2)G_{3b}(1-|S_{11_{3b}}|^2)} + \frac{L_1L_2L_4(F_5-1)}{G_3(1-|S_{11_3}|^2)G_{3b}(1-|S_{11_{3b}}|^2)} - 1\right]}{n_{meas}} \tag{6.16}$$

6.3 Spectrometer noise figure determination

The spectrometer is one of the most important and most expensive parts of the NMR spectroscopy system. It is an RF receiver that does rather complex processing of the NMR measurement signal before the results could be properly shown on the spectrometer screen. The typical processing blocks of the spectrometer include analog filtering, pre-amplification, down-converting to intermediate frequency, gain control, analog-to-digital conversion, digital quadrature detection, digital filtering, Fast Fourier Transformation and averaging. Each of the aforementioned processes is done within an electronic device that injects its own excess noise into the NMR spectroscopy system, causing deterioration of the overall noise properties. So, to calculate the noise properties of the spectrometer, one would need to know a detailed noise model of each of its building elements. In practice, this information is never available to the NMR user. Fortunately, it is possible to describe the spectrometer as a "black box" with its own effective noise figure. This enables a simple measurement of the spectrometer noise figure.

6.3.1 Noise figure measurement using the Twice Power Method

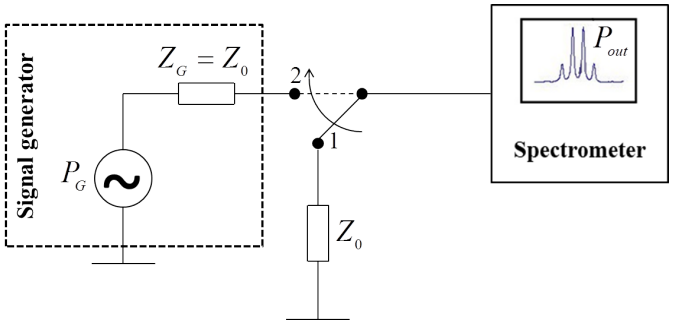

Figure 6.4: Noise figure measurement of the entire spectrometer: the block diagram

The block diagram of the noise figure measurement of the entire spectrometer is shown in Figure 6.4. In order to determine the noise figure of the entire spectrometer, one needs to use the so-called Twice Power Method [42]. This method is used when both output signal and noise levels cannot be determined directly, as it is the case with the spectrometer's noise figure measurement, where the output signal is expressed in arbitrary units representing the measured voltage signal. Therefore, the idea is to perform two measurements: the first measurement is the output signal measurement where the input is terminated with the load Z_0, while the second measurement is the one with the sine wave signal generator connected to the input of the spectrometer; and the relative ratio of the two measurements is then used to determine the spectrometer's noise figure. So, the first measurement is used in order to determine the output noise power, P_1. Then, the signal generator is connected to the input of the spectrometer instead of the termination, Z_0, and the input signal power level is tuned in so that the output power of

the second measurement, P_2, becomes twice the level of the first measurement, P_1:

$$P_2 = 2P_1. \tag{6.17}$$

As the signal generator also contains the termination Z_0, which generates noise power level equal to the one of the first measurement, the expression (6.17) actually states that in this case, the output signal power level is exactly equal to the noise power level of the first measurement. So, with the use of the second measurement, the output noise power level from the first measurement is indirectly determined. After this, the spectrometer's noise figure is determined as follows:

$$F_{SM} = \frac{P_G}{kT_0\Delta f}, \tag{6.18}$$

where P_G represents the signal generator's input power level, while Δf represents the filter bandwidth of the spectrometer. Obviously, the Twice Power Method is actually an indirectly performed Direct Noise Measurement Method. However, as the spectrometer's output signals have a dimension of voltage, the expression (6.17) needs to be modified so that the Twice Power Method can be used by measuring output voltage signals instead of output power signals. As power is proportional to the squared value of voltage, (6.17) can be rewritten as:

$$U_2^2 = 2U_1^2, \tag{6.19}$$

where U_2 represents the effective value of the output voltage sine signal of the second measurement, while U_1 represents the root mean square value of the output voltage noise signal of the first measurement. But since it is more straightforward to determine the magnitude of the sine signal, instead of its effective value, U_2 can be expressed by its magnitude, A_2:

$$U_2 = \frac{A_2}{\sqrt{2}}. \tag{6.20}$$

Consequently, (6.19) can now be rewritten as:

$$\frac{A_2^2}{2} = 2U_1^2. \tag{6.21}$$

Finally, after calculating a square root of (6.21), one gets the expression:

$$A_2 = 2U_1. \tag{6.22}$$

To sum up, in order to perform the Twice Power Method, but with the use of voltage output signals, instead of the power ones, one needs to tune the signal generator's input power level in such a way that the magnitude of the second measurement gets equal to twice the value of the

root mean square value of the first measurement's voltage signal:

$$F_{SM} = \frac{P_G|_{A_2=2U_1}}{kT_0\Delta f}. \tag{6.23}$$

In the end, it is also necessary to mention that this method is effective only when used under the condition that the measured component possesses noise figure values higher than 20 dB. This is a condition that the spectrometer will soon prove to accomplish (Figure 6.5).

6.3.2 Important notes about the spectrometer noise figure determination

It is necessary to mention here that the value of the overall noise figure of the entire spectrometer depends on the values of the spectrometer's parameters, such as its power gain, frequency bandwidth of its filter and number of acquisition points of current measurement, and on the value of measurement frequency, which is the frequency of the generated sine wave at the spectrometer input. This means that the value of the overall noise figure of the entire spectrometer, calculated with the help of expression (6.23), is true for the current set of parameters of the spectrometer, but will change if some of the aforementioned parameters change. It is also very difficult to predict its value because there are multiple elements in the spectrometer whose parameters can be altered. This is especially true for its gain control, as it is comprised of multiple variable–gain amplifier stages (see Figure 3.2), and it is hard to predict how exactly the gain level of every amplifier stage changes with the change of gain control's power gain level. The problem is that the receiver of the spectrometer is comprised of multiple elements, connected in a cascade, whose parameters (like, for example, the power gain levels of the amplifiers) can be altered. As the power gain levels of the amplifiers that form the spectrometer's receiver change, the overall noise figure of the spectrometer changes, too. However, since the spectrometer's processing unit, whose operating program code is not available to the end user, is responsible for the control of the amplifiers' power gain levels, the end user cannot tell how exactly did the aforementioned parameters change. Therefore, it is almost impossible to predict the exact value of the spectrometer's noise figure *a priori* without the measurements described in this section. Furthermore, in order to predict the value of the spectrometer's noise figure, the end user should also be familiar with all the devices that form the spectrometer, and their complete mode of operation, which is, again, very hard to find out, as the companies that construct the spectrometers do not reveal the entire schematics and the list of the used devices and elements to the public. This is why the measurement of the spectrometer's noise figure, described in this section, is proposed. One should regard the proposed method as a bypass method so that it is not necessary to be familiar with the exact construction of the entire spectrometer. Without further ado, the dependence of spectrometer's noise figure on gain control's power gain level, set in the NMR measurements' software, is shown in Figure 6.5. As it can be seen, the values of the

spectrometer's noise figure are very high. At first glance, these values might come as a surprise, as even the low-quality RF receivers do not have noise figure levels this high. Therefore, now is a good time to recall the schematic diagram of the entire spectrometer (Figure 3.2) again. Here, it can be seen that not only the spectrometer's RF receiver contributes its overall noise figure values. There are more processes after the signal reception, like A/D conversion, I/Q modulation, digital filtering and phase cycling, that contribute greatly to the overall value of the spectrometer's noise figure. Furthermore, the variable-gain amplifiers inside the spectrometer's gain control are actually fixed gain amplifiers with variable attenuators at their inputs. So, in order to achieve low power gain levels, attenuators' attenuation levels need to be set high. In this case, not only is the output signal's power level lower than in the case of maximum power gain level, but also, its noise level is higher due to the higher attenuation levels (because passive components with higher losses have higher noise figures – see (6.4)). A very similar situation occurs when the input attenuation level of a spectrum analyzer is set to the values higher than 0 dB, which effectively increases the analyzer's noise figure. This is a problem for the output SNR determination, as the noisy output sine signal gets dissected to the noiseless sine signal and the noise, and then the former is used to calculate A_2 from the expression (6.22). Namely, as the gain control's power gain level decreases, output signal's power level also decreases, while in the same time, output noise level increases, making it harder to dissect the output signal. Therefore, spectrometer's noise figure estimation errors are higher for low gain control's power gain levels. This is actually why the levels below 100 are very rarely used in the NMR measurements, as only noise figures for higher power gain levels can be suppressed successfully with the use of higher-gain NMR preamplifier. As a matter of fact, NMR measurements described in the next chapter are obtained with gain control's power gain levels equal to 200 and 300.

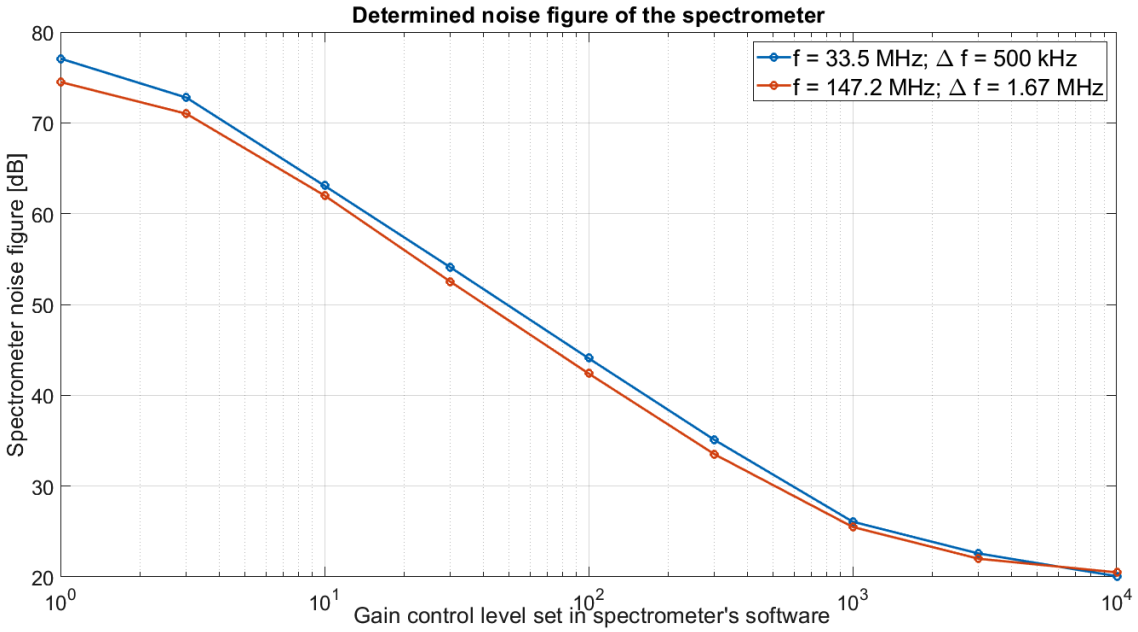

Figure 6.5: Spectrometer's noise figure in dependence on the set level of gain control's power gain

Another reason why one needs to bear in mind the exact level selection of the gain control's gain level is the VSNR saturation effect. Namely, as noise levels are usually lower than the signal levels, noise levels switch A/D converter's quantization levels slower than signal levels with the increase of the gain. Here, the intrinsic noise of the spectrometer is the dominant type of noise. However, once noise levels reach high enough levels, they start switching quantization levels with the same speed as signal levels, causing the VSNR levels to stop increasing [16, 43]. Here, the gain level where VSNR levels stop increasing can be called as the saturation point, and NMR signal's background noise becomes the dominant type of noise. Although this saturation effect seems to be an unwanted effect during the determination of the spectrometer's noise figure value, it is actually the area where the spectrometer's operating point needs to be placed. Namely, as some useful information can be hidden in the background noise of the NMR response signal (e. g. higher order spectral lines shown in Figure 7.1a), if the level of this noise is lower than the level of the spectrometer's intrinsic noise, it is very difficult to salvage this useful information afterwards. Therefore, the AGC's gain level needs to be set in such a way that the NMR response signal's background noise level surpasses the intrinsic noise of the spectrometer. The area where this condition is met is the saturated part of the curves shown in Figures 6.6a and 6.6b. If the condition is not met, the caused error can lead to huge measurement errors here, and, ultimately, to the wrong Rx chain SNR and noise figure estimation. Of course, on the other hand, the gain level must not be set too high in order to avoid the clipping effect of the output signal [7]. In order to show the effect of VSNR saturation, multiple NMR measurements of ^{63}Cu signal in $SeCuO_3$ were performed with various gain control's gain levels and various numbers of averaged measurements. Voltage signal's behaviour for different gain control's voltage gain levels can be seen in Figure 6.6a, noise voltage value's behaviour for the same levels can be seen in Figure 6.6b, while the VSNR saturation effect can be seen in Figure 6.7. Figure 6.7 can also be used to once more confirm the method of multiple measurements averaging, described in subsection 6.2.5. If VSNR increases with the square root of the number of averaged measurements, then it is possible to say the reverse: if VSNRs, acquired by the use of averaging, get divided by the square root of their belonging number of averaged measurements, all the VSNR values should be the same. To prove this, all the measurements from Figure 6.7 have been divided by the square root of their number of averaged measurements, and, as it can be seen in Figure 6.8, they are all laying on top of each other, so the effect of multiple measurements averaging has been confirmed once more.

To sum this subsection up, in order to get the correct value of the spectrometer's noise figure, one needs to measure the noise figure of the entire spectrometer for the exact set of spectrometer's parameters one intends to use in the current NMR measurement, and also be very careful with the selection of gain control's gain level in order to avoid the unoptimized operation mode, and therefore, the loss of the useful information of the measurement.

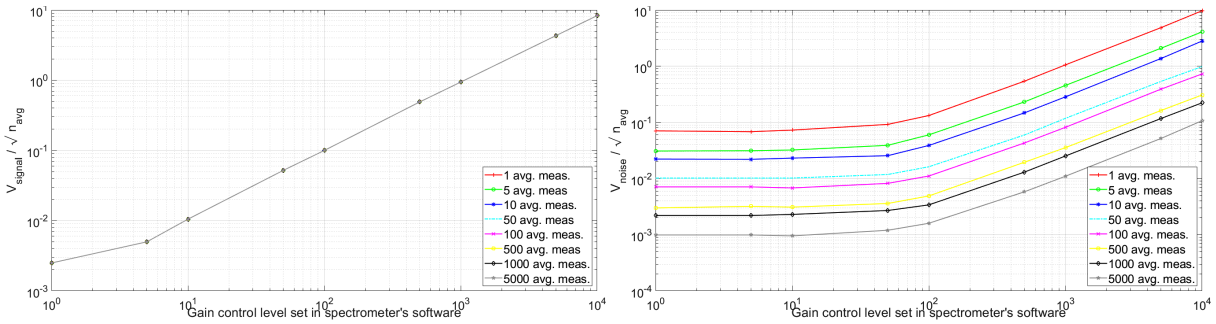

(a) Voltage signal's behaviour (b) Noise voltage value's behaviour

Figure 6.6: Behaviour of different voltage signals for different gain control's voltage gain levels and for different number of averaged measurements

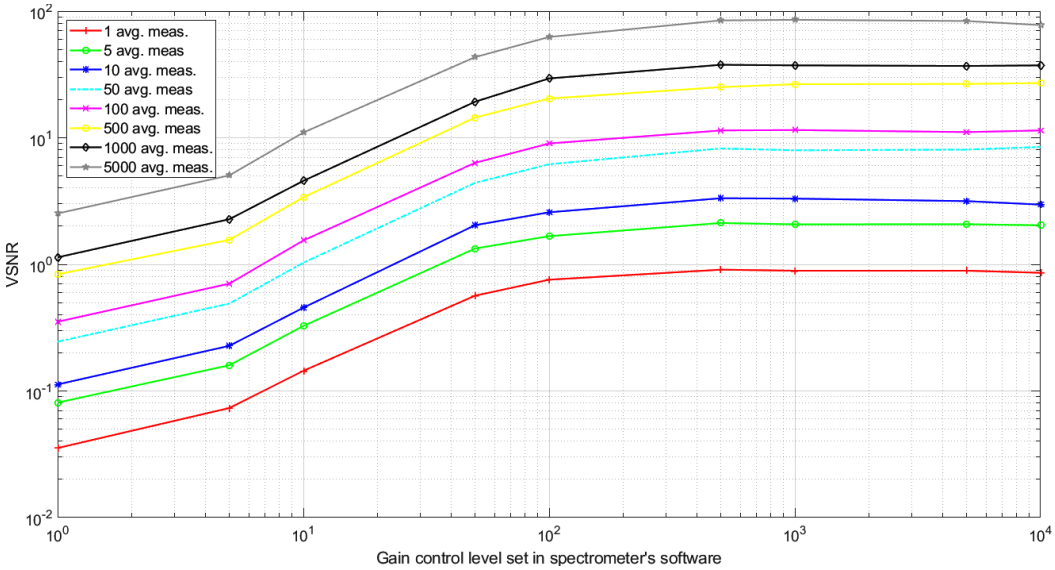

Figure 6.7: VSNR saturation effect

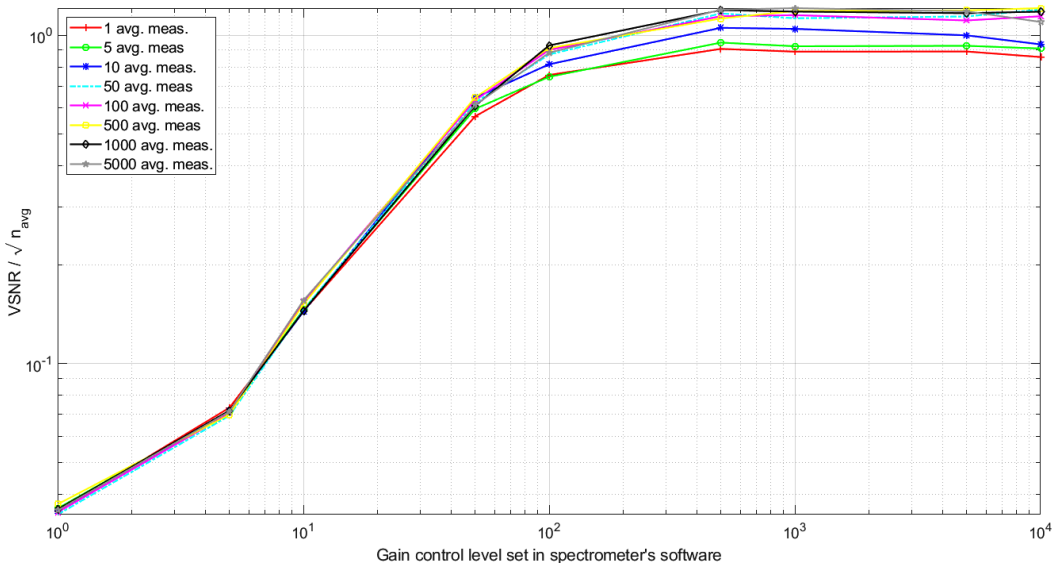

Figure 6.8: Normalized VSNR saturation effect

Chapter 7

Experimental verification of the developed models

In this chapter, derived electromagnetic models, described in chapters 5 and 6, are compared and their correctness is analysed, tested and verified. In addition, potential improvements of the NMR spectroscopy system have been analysed, commented and suggested.

7.1 General approach

To make an experimental verification of the derived expression for the NMR receiving chain noise figure, multiple measurements have been performed on two different samples with a modified measurement setup. Using the expressions (6.15) and (6.16) and by measuring the characteristics of individual elements of the chains, it is possible to check whether the right hand side equals the left hand side of the expression. Following from expression (4.15) a set of measurements performed on one sample should always result with the same input SNR since only one or two elements have been switched or replaced in the receiving chain. This will show the inner consistency of the aforementioned analysis. Also, the value of the calculated input SNR has to be comparable to the value expected from (5.25), which will prove the absolute validity of this approach.

7.2 Measurements description

To verify the derived expression for the NMR receiving chain noise figure, two sets of measurements on two different nuclei in two samples were performed . The first one was the measurement of ^{63}Cu signal in $SeCuO_3$ (two sets of measurements) [12], while the second one was the signal of ^{133}Cs in $Cs_2Cu_3SnF_{12}$ (three sets of measurements) [44]. NMR properties of the measured nuclei are available in Table 7.1, while the full description of measurements' setups is

available in Table 7.2. The spectrometer used for the aforementioned measurements is Tecmag Apollo (now called Tecmag Redstone [45]). The full measurement setup from the Laboratory for solid state NMR and high frequency measurement at the Department of Physics of Faculty of Science, University of Zagreb, used for these measurements, is shown in Figure 7.7.

Table 7.1: NMR properties of the nuclei used in experiments.

Compound	Nucleus	γ (MHz/T)	Spin	Abundance (%)	Quadrupole splitting
$SeCuO_3$	^{63}Cu	11.285	3/2	69.1	48.05 MHz
$Cs_2Cu_3SnF_{12}$	^{133}Cs	5.5844	7/2	100	9.54 kHz

The main focus is set on the effects of different preamplifiers in the measurement setup because there is a vast number of commercially available types, and also because it is the only active element (besides the spectrometer). While making selection of the preamplifier one should bear in mind that its characteristics have a significant impact on the overall noise figure (because $G > 1$). It can be seen in (6.15 and 6.16) that the preamplifier gain (G) may decrease the contribution of losses accumulated up to the observed point (preamplifier output). This, in turn, may drastically affect the overall noise properties of the receiving chain. A non-negligible improvement when a higher quality coaxial cable connecting the NMR probe and the duplexer was used, as was already shown in subsection 6.2.2. The parameters of used amplifiers are given in Table 7.2.

The two preamplifiers used in ^{63}Cu measurements were MITEQ AU-1114-SMA [46] (abbreviated as M290) and THAMWAY N141-206AA(D) [47] (abbreviated as T77). The first preamplifier operates in the environment of the standard temperature, T_0, while the second one is cooled to the temperature of liquid nitrogen (77 K). Both were used as single-stage preamplifiers. On the other hand, for the ^{133}Cs measurements, these two units were used as single-stage preamplifiers, but T77 was also used as the first stage of a two-stage preamplifier, where Mini-Circuits HELA -10D+ [48] (abbreviated as MC290) was used as the second stage. MC290 was operating at the standard temperature, T_0.

Table 7.2: Electric parameters of receiving chain elements used in both sets of measurements

Compound		$SeCuO_3$	$Cs_2Cu_3SnF_{12}$
Parameter	Symbol	Values	
Measurement frequency (MHz)	-	147.20	33.50
Coil and sample temperature (K)	T_{coil}	20	30
DC magnetic field (T)	B_0	11.90	6
Input cable loss (dB)	L_1	0.28	0.10
Duplexer loss (dB)	L_2	0.27	0.43
M290 gain (dB)	G_3	36.13	36.52
M290 noise figure (dB)	F_3	1.11	1.14
M290 reflection coefficient (dB)	S_{11_3}	-16.43	-13.50
T77 gain (dB)	G_3, G_{3a}	28.54	27.89
T77 noise figure (dB)	F_3, F_{3a}	0.32	1.07
T77 reflection coefficient (dB)	S_{11_3}, $S_{11_{3a}}$	-7.57	-8.05
MC290 gain (dB)	G_{3b}	-	10.75
MC290 noise figure (dB)	F_{3b}	-	4.22
MC290 reflection coefficient (dB)	$S_{11_{3b}}$	-	-27.58
Output cable loss (dB)	L_4	0.46	0.62
Spectrometer noise figure (dB)	F_5	33.50	38.40
Number of measurements	n_{meas}	200	400
Input impedance M290 (Ω)	Z_{in}	51.20	72.80
Output impedance M290 (Ω)	Z_{out}	54.50	45.60
Input impedance T77 (Ω)	Z_{in}	45.77	34.70
Output impedance T77 (Ω)	Z_{out}	101.46	38.20
Input impedance MC290 (Ω)	Z_{in}	50	50
Output impedance MC290 (Ω)	Z_{out}	50	50

Before the presentation of the data, it is first necessary to describe several properties of NMR signals that will help understand its behaviour and role in signal intensity. They have already been mentioned before in this thesis (e. g. see subsection 5.4): quadrupolar splitting, linewidth, spin–spin relaxation time and isotope abundance. The latter is perhaps the easiest to explain - in nature, every element can be found in several isotopes. These have different nuclear properties, such as the gyromagnetic constant γ which defines the measurement frequency. Thay can also be found in different relative abundance, such as ^{63}Cu and ^{65}Cu, whose abundance ratio equals 0.691:0.309. So, by recording an NMR signal of ^{63}Cu, signal intensity will be only $\approx$69% of all the copper nuclei in the sample. Hence, the ratio of the isotopes needs to be kept in mind when calculating the expected signal level.

Linewidth is, as the name says, the width of the NMR line. It is defined by local homogeneity of the crystal in the vicinity of the measured nuclei, and by the homogeneity of the external magnetic field. If these were perfectly homogeneous, the NMR signal could be described by a Dirac's delta function $\delta(\omega - \omega_0)$ of infinitesimal width. In reality, neither the samples nor the magnetic field are ever ideally homogeneous. This will manifest so that the NMR frequency will be defined by a Lorentzian (or Gaussian) function of finite width. As the spectral width is preserved, signal amplitude will proportionally drop to compensate it.

Quadrupolar splitting (as mentioned in subsection 2.4) appears with the nuclei of spin $I > 1/2$, in which case the observed nucleus is sensitive to the direction of local electrostatic gradients. Unless it is located at a very symmetrical position, the NMR signal will split into $2 \cdot I$ lines of well defined intensities [2, 7] since it will sense the local distribution of electric potential. A textbook example is shown in Figure 7.1a where ^{133}Cs signal splits into seven lines. Again, as the spectral weight is preserved, the split signal amplitude will drop from the "unsplit case". The size of quadrupolar splitting can vary from a few kHz (as for the ^{133}Cs signal) to several tens of MHz (as for the ^{63} Cu signal).

Briefly, the spin–spin relaxation time (T_2) is just a measure of how rapidly in time the NMR signal drops from the moment the nucleus is excited to the moment the NMR signal is recorded (as mentioned in subsection 2.6.2). Normally it follows an exponential $e^{-\frac{t}{T_2}}$ dependence, and is determined by the properties of the sample. The time of measurement of the signal, t, is set by the dead-time of electrical discharge of the coil after the pulse.

7.3 Results

The results of the experimental verification are shown in Table 7.3, and the measured data are shown in Figures 7.1a and 7.1b.

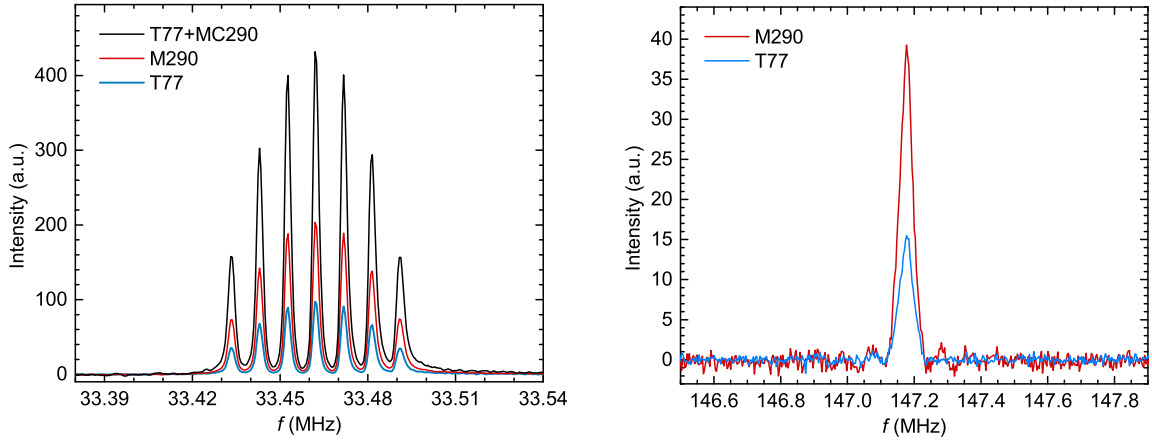

Figure 7.1: NMR spectra measured to check the validity of the NMR receiving chain's noise figure calculation: a) ^{133}Cs in $Cs_2Cu_3SnF_{12}$, b) central line of ^{63}Cu in $SeCuO_3$ (the quadrupolar satellites are too far apart to be excited by a single pulse).

To be able to follow the comparison of the results more easily, NMR properties of the measured nuclei have also been listed in Table 7.1. From the two measurements of ^{63}Cu in $SeCuO_3$, i.e. the associated SNRs at the spectrometer, it follows that the values of the NMR receiving chain input SNRs are 12.17 dB and 12.14 dB, for M290 and T77 preamplifier, respectively. The difference between the predicted values is around 0.03 dB, which is comparable to the measurement uncertainty. The evaluated value of the same SNR from (5.25) equals 17.23 dB. Here, it has also been taken into account that the amplitude of the signal is reduced due to the short T_2 time (to 75% of value), broadened linewidth, NQR splitting of the spectral lines (to 33% of value), number of crystallographic sites (to 50% of value) and the abundance of ^{63}Cu isotope (69%). Out of these, the most ambiguous parameter is the line broadening because it cannot be estimated correctly. However, even if it is (conservatively) estimated that the spectral weight is reduced to 10 % of its value, the input SNR estimation, using (5.25), is of acceptable order of magnitude. To keep this estimate simple, the dependence of intensity on the orientation of the sample, i.e. the quadrupolar principle value with respect to the external field, or the NMR coil, has not been discussed here, but it is worth mentioning that these effects can also only *reduce* the signal intensity and thus make the result match even better.

The calculated values of the NMR receiving chain input SNRs for the measurements of ^{133}Cs in $Cs_2Cu_3SnF_{12}$, shown in Figure 7.1a, where M290 and T77 preamplifiers were also used, are equal to 37.54 dB and 37.55 dB, respectively, again showing a good consistency of the results. The evaluated value of the NMR receiving chain input SNR, from (5.25), in this

case equals 35.31 dB, which is now adjusted only for NQR splitting of the spectral lines (to 25% of value) since the linewidth is only ∼5kHz (FWHM). In this system there is only one crystallographic site, the abundance of ^{133}Cs isotope is 100% and the T_2 time does not show any considerable effect. Therefore, the validity of the derived expression is confirmed in this case as well.

Table 7.3: Results of experimental verification of the derived expression for NMR spectroscopy receiving chain

Compound	$SeCuO_3$	$Cs_2Cu_3SnF_{12}$
Frequency (MHz)	147.20	33.50
M290		
Measured SNR_{out} (dB)	30.11	56.00
Determined $F_{NMR_{Rx}}$ (dB)	-17.95	-18.46
Calculated SNR_{in} via (6.15) and (4.15) (dB)	12.17	37.54
T77		
Measured SNR_{out} (dB)	24.97	48.32
Determined $F_{NMR_{Rx}}$ (dB)	-12.83	-10.77
Calculated SNR_{in} via (6.15) and (4.15) (dB)	12.14	37.55
T77 with MC290		
Measured SNR_{out}	-	55.65
Determined $F_{NMR_{Rx}}$ (dB)	-	-19.41
Calculated SNR_{in} via (6.16) and (4.15) (dB)	-	36.24
Calculated SNR_{in} via (5.25) (dB)	15.20	35.31

Now it is possible to discuss the effect of temperature of the coaxial cable in the NMR probe (6.11). If it is conservatively taken that the temperature of the cable is T_{coil} then all of the calculated results in Table 7.3 should be *decreased* by 0.6 - 1.0 dB. In the other conservative limit, if the temperature of the cable is taken as T_0 then all of the calculated results should be *increased* by the same amount. Therefore, the uncertainty of the average temperature concept is well within accuracy of both the analysis and the comparison to the estimated results using (5.25).

From the measured values presented in Table 7.3 it can be seen that in both cases the output SNRs are higher in the case of M290 preamplifier, regardless that the T77 has a lower noise factor at 77 K. This is because the amplifier does not reduce the overall noise factor as much as it does the gain. The improvement would have occured if the gain value of T77 had also been $\sim$36 dB. To analyse this situation in more detail, the idea was to see the effect of increasing the gain of T77 unit artificially – by adding a second amplifier in a cascade after the T77, and thus creating a two-stage amplifier module.

This was done using the MC290 preamplifer mentioned earlier. The overall gain of such a created two–stage preamplifier is equal to 37.89 dB, while its noise figure is equal to 1.25 dB. Compared to the same parameters of T77 from Table 7.2, it can be seen that the gain of the created two–stage preamplifier is much higher than the one of T77, but the price paid is its noise figure being slightly worse than the one of T77. From Figure 7.1a it can be seen that it resulted in a signal amplitude that is indeed larger than in the case of M290, but did not result with a better output SNR. In this case, the predicted value of the NMR receiving chain input SNR is 36.24 dB. The difference between this value and those from the two previous measurements is around 1.3 dB, which is a bit larger than our previous results (16% on the voltage scale). This error appears because now the expression of the noise figure (6.16) is somewhat more imprecise than in the case of expression (6.15) for the single-stage preamplifier, which will now be clarified. In the derivation of the expression (6.15) for the chain with a single-stage preamplifier, it was assumed that there is no signal reflection at the preamplifier output due to the next element in the chain being matched to Z_0 (Figure 7.2a). However, in the case of a two-stage preamplifier, the first stage amplifier output signal reaches the second stage amplifier input, which is not matched to Z_0, and there is a reflected wave coming back to the output of the first stage amplifier. This signal then attenuates and re-reflects again to reach the second stage amplifier input, after which the process repeats itself (Figure 7.2b). To take this into account one would have to measure both the amplitude and the phase of all four S parameters of both the amplifiers the two-stage amplifier cascade is comprised of and input them into expression (6.15). However, this would make the analysis much more complex and only slightly more precise. Therefore, for the sake of clarity, simplicity and to offer the NMR community an easy way to calculate the properties of the NMR receiving chain, the expression (6.16) will be kept as a good pragmatic result.

From the discussion of the results above it can clearly be seen that the derived expression for the NMR receiving chain noise figure describes an NMR setup well, and from it some important conclusions can now be drawn. First of all, when building an NMR setup, it is necessary to carefully choose the appropriate elements with respect to the existing ones. For example, when choosing the preamplifier focusing on the one with lowest noise figure alone might not be the best solution. It can be seen in Tables 7.2 and 7.3 that, although T77 has significantly lower noise figure than M290, the output SNR of the NMR receiving chain is

notably higher with the usage of M290 because its power gain is much higher than the gain of T77, and the impedance matching of M290 is much better done than the one of T77. This is why it is necessary to consider all three preamplifier values: its power gain, its noise figure and its impedance matching (or its input reflection coefficient), and select those with optimum values. Also, as it was previously mentioned, since the coaxial cable connecting the NMR coil and the duplexer are in front of the preamplifier, these two elements need to be of as high quality as possible.

The results of the two-stage amplification raises the question what type of an amplifier would give better output SNRs than the commercial unit M290. For this purpose, the expression (6.15) will be used to predict the receiving chain's output SNR for both measured samples in the case of using a hypothetical state-of-the-art NMR preamplifier [49] (abbreviated as SOA), which has a power gain and noise figure of 40 dB and 0.3 dB, respectively, and that is almost perfectly matched to Z_0 (its $|S_{11}|$ parameter equals -30 dB). The results of the prediction are shown in Table 7.4.

Table 7.4: Results of SNR_{in} prediction of NMR receiving chain using SOA

Compound	$SeCuO_3$	$Cs_2Cu_3SnF_{12}$
Frequency (MHz)	147.20	33.50
SNR_{in} (dB)	12.17	37.54
SNR_{out} using M290 (dB)	30.11	56.00
Predicted SNR_{out} using SOA (dB)	32.28	58.77
SNR_{out} enhancement (dB)	2.16	2.76
SNR_{out} enhancement (%)	65	89

Since M290 resulted in the greatest output SNR for the measurements of both samples, the SOA preamplifier was compared with this unit. So, for the same input SNR of ^{63}Cu in $SeCuO_3$, the receiving chain with the SOA preamplifier generates the SNR output 2.16 dB greater than the SNR of the receiving chain with M290. This corresponds to a 65% enhancement in linear scale with the SOA preamplifier, i.e. to reach equal output SNRs the SOA premplifer would in the existing configuration measure 1.65 times faster. This is a very significant decrease in measurement time. On the other hand, for ^{133}Cs measurements in $Cs_2Cu_3SnF_{12}$, this difference rises to 2.76 dB in logarithmic, or 89% in linear scale. Here, the measurement time is reduced almost two times, which is a drastic decrease. These two predictions prove that the properties of the preamplifier, along with those of the spectrometer, are indeed one of the most important in the NMR system, and that all the efforts to enhance the preamplifier's properties are justified.

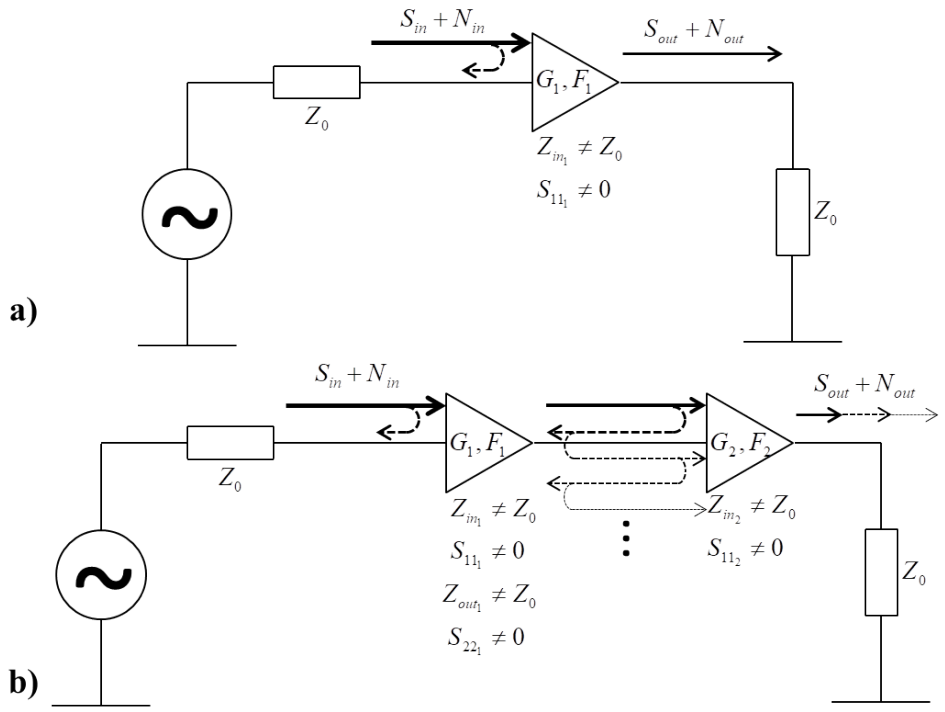

Figure 7.2: A noisy amplifier with an impedance mismatch at its input;
a) Single–stage preamplifier; b) Two–stage preamplifier

In order to better understand what is going on with the signal and its background noise when the signal propagates throughout the Rx chain, a graphical presentation of SNR value in dependence on the stage of the chain is shown in Figures 7.4 and 7.5, while signal and noise levels conversion throughout the chain is shown in Figure 7.6.

The first effect that can be seen is that SNR deteriorates as the signal propagates through the hardware part of the chain (from the input to the RF receiver) and that this deterioration can be tackled with the use of averaging. The effect of averaging is shown in the far right part of the charts (between the RF receiver and the output).

It can also be seen that the biggest deterioration occurs in the spectrometer, since its noise figure level is by far the highest in the chain (see Table 7.2). However, the slope of deterioration gets gentler as the power gain level of the preamplifier gets higher. This indicates that the ratio $\frac{F_5}{G_3}$ in the expression (6.15) is the factor that mostly determines the final value of the chain's noise figure. So, in order to achieve higher output SNR, this factor should be kept as low as possible. Furthermore, it can be seen in Figures 7.4b and 7.5b that SNR deteriorates less throughout almost entire chain when T77 is used because its noise figure level is lower than the one of M290. However, because its power gain level is notably lower than the one of M290, causing the $\frac{F_5}{G_3}$ ratio to be higher than in the case of M290, the final SNR at the output of the chain is lower than the case of M290. These two effects show that, in order to maximize SNR value at the output of the chain, one should use the preamplifier with both high power gain

and low noise figure levels. This is also why the case of two–stage preamplifier was analysed here: by the addition of the second stage to T77, its power gain level increased, causing the decrease of the $\frac{F_5}{G_3}$ ratio and, consequently, the increase of the output SNR. This can be seen in Figures 7.4a and 7.5a.

It is also worth mentioning that, because M290 and T77 have similar noise figure levels at lower frequencies (^{133}Cs measurements were done at the frequency of 33.5 MHz, which is significantly lower than the frequency of ^{63}Cu measurement: 147.2 MHz), the SNR level after preamplifier is not higher with the use of T77 in Figures 7.4a and 7.5a, as it is in Figures 7.4b and 7.5b. This is why, if one decides to buy a cryogenic preamplifier because of its low noise figure, it is important to make sure that its noise figure level really is low in the frequency band of the measurements to be done. Otherwise, there is no point in buying the cryogenic preamplifier because its performances would be similar or even worse than the ones of a room temperature preamplifier.

Finally, it can be seen that the input cable and the duplexer deteriorate the input SNR almost negligibly. This is because high–quality cable and low–loss duplexer were used in the measurements. However, if high–quality components were not used here, the SNR decrease would be much more visible. Figure 7.3 compares the loss of the standard coaxial cable in dB/m that was previously used in our NMR laboratory to the loss of the high–quality coaxial cable acquired during this study. It can be seen that just the cable replacement immediately improves noise figure for the value between 0.05 dB and 0.3 dB, depending on the operating frequency (the "ripples" in the transfer characteristics are caused by inherent small reflections, due to impedance mismatch, that always occur in practice). This is why it is important to also invest in good cables and duplexers, and not just preamplifiers and spectrometers, especially because cables and duplexers are a few orders cheaper than preamplifiers and spectrometers.

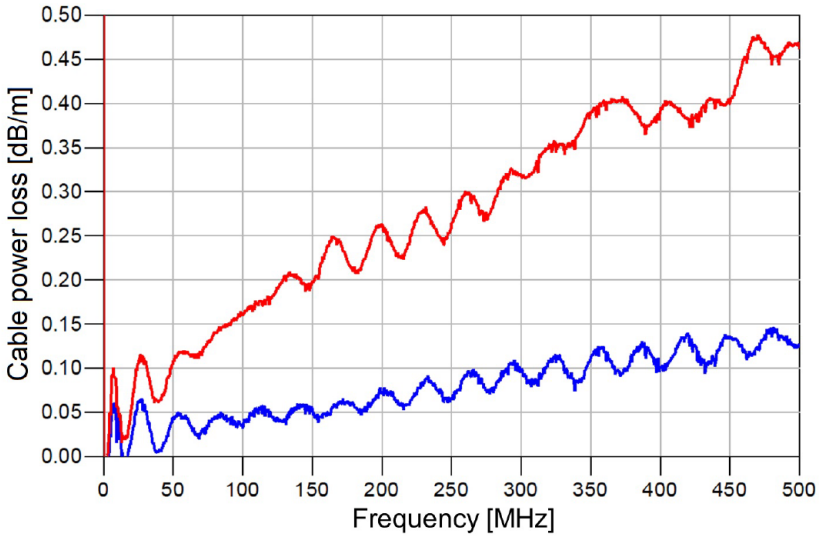

Figure 7.3: Losses per unit length in the case of a standard coaxial cable (red) and a high–quality coaxial cable produced by the Fujikura company (blue)

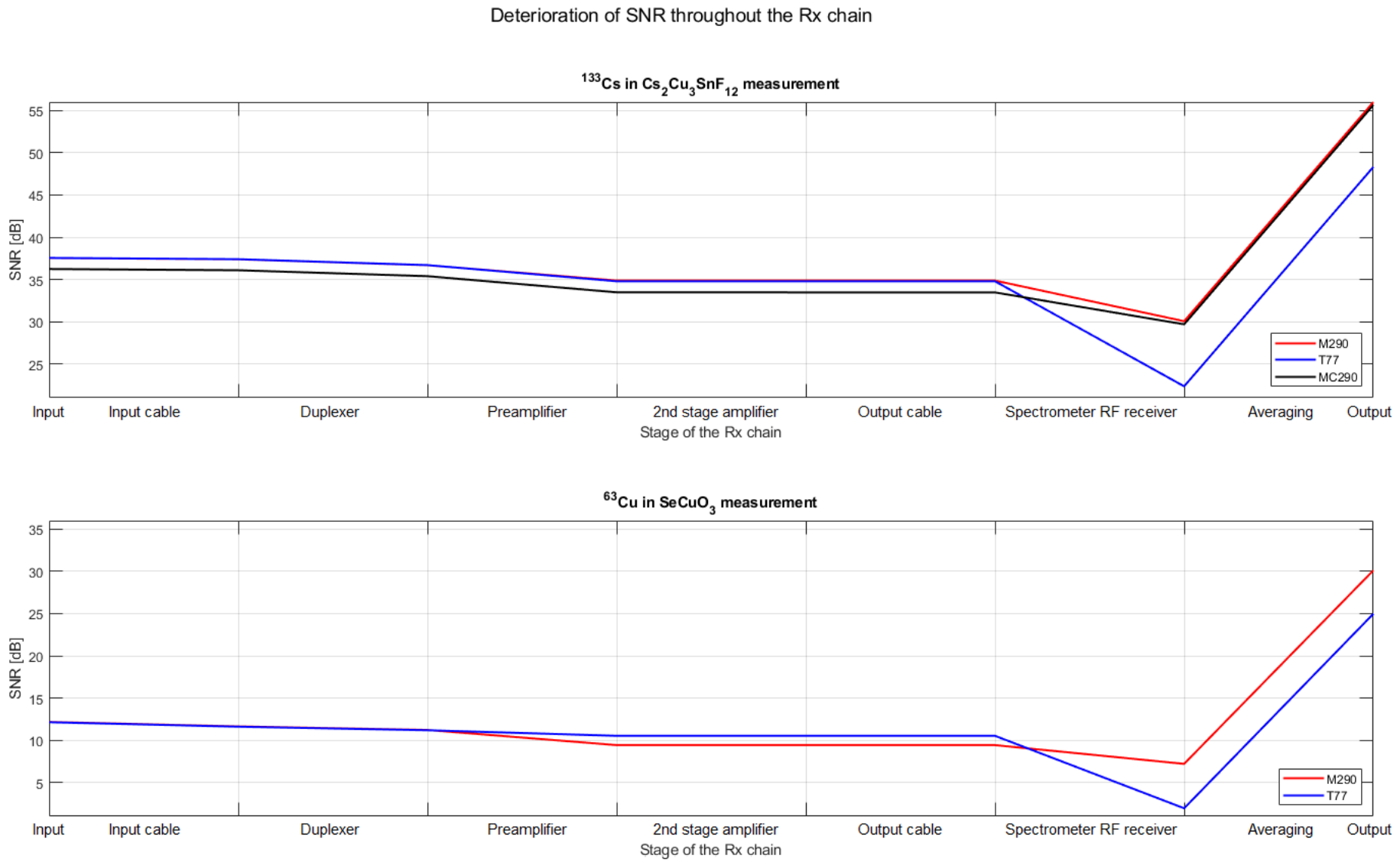

Figure 7.4: Deterioration of SNR through the NMR spectroscopy system Rx chain: a) ^{133}Cs measurement in $Cs_2Cu_3SnF_{12}$; b) ^{63}Cu measurement in $SeCuO_3$

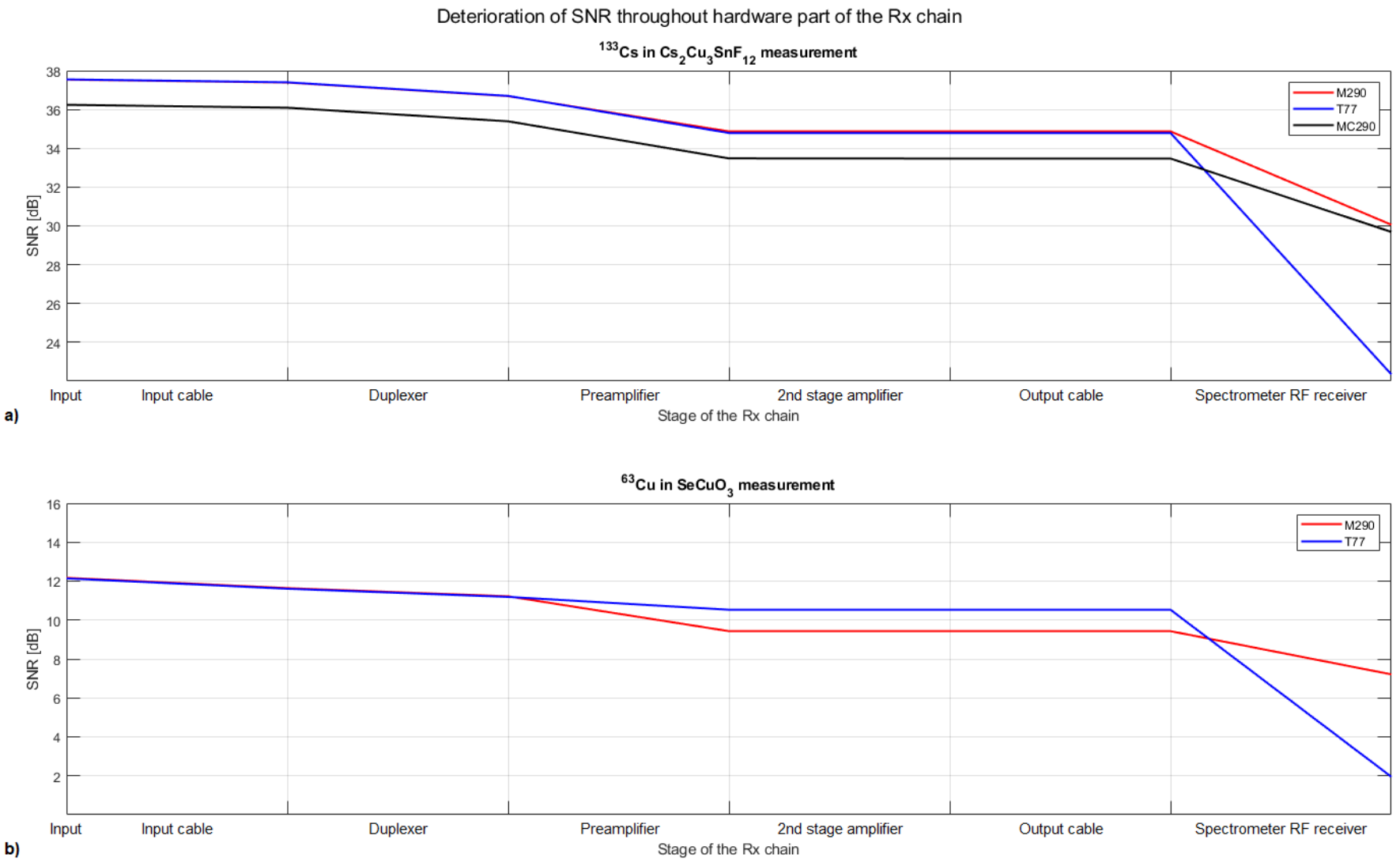

Figure 7.5: Deterioration of SNR through the hardware part of NMR spectroscopy system Rx chain – zoomed-in: a) ^{133}Cs measurement in $Cs_2Cu_3SnF_{12}$; b) ^{63}Cu measurement in $SeCuO_3$

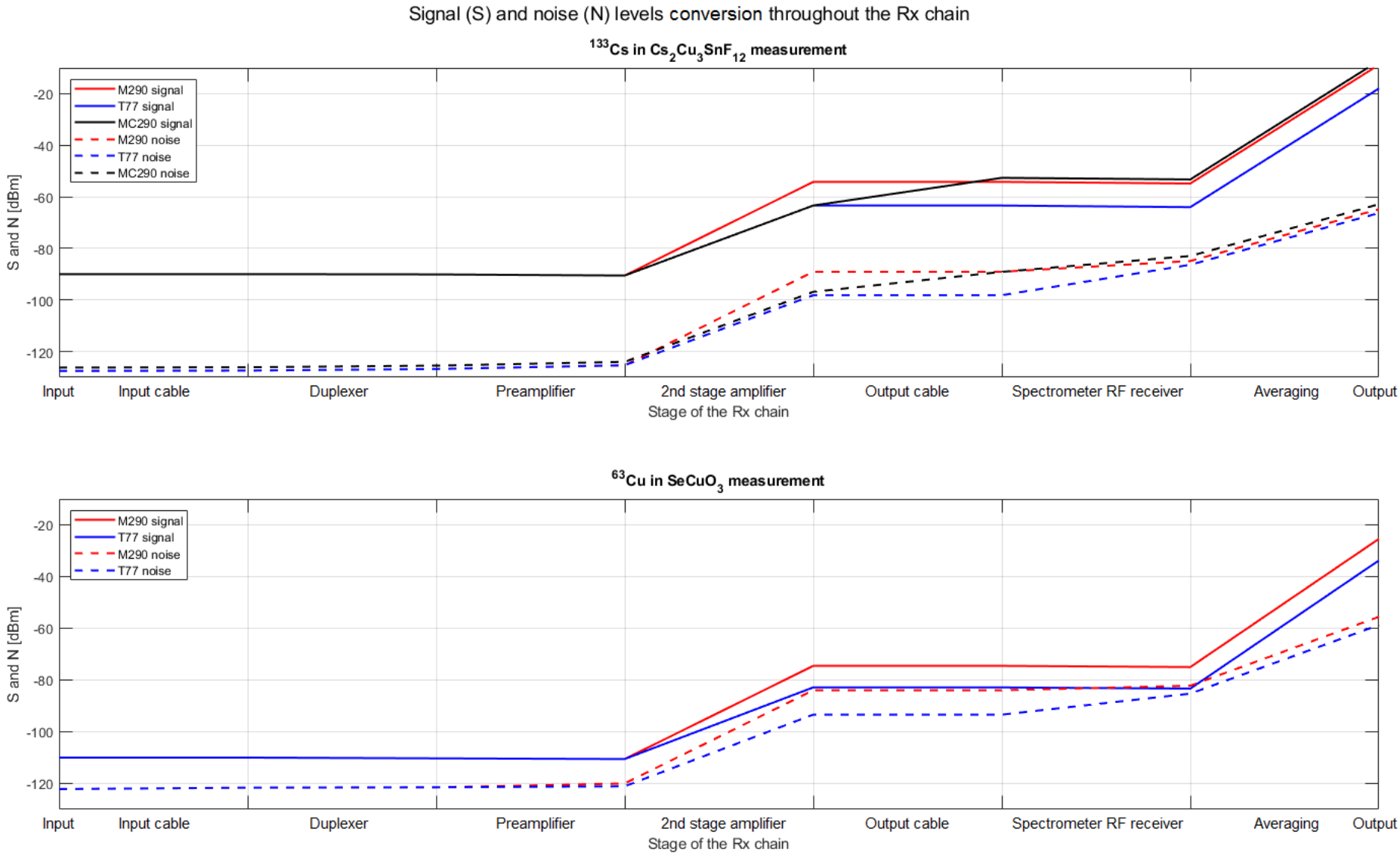

Figure 7.6: Conversion of signal and noise levels through the NMR spectroscopy system Rx chain: a) ^{133}Cs measurement in $Cs_2Cu_3SnF_{12}$; b) ^{63}Cu measurement in $SeCuO_3$

7.4 Summary

In order to summarize the contribution of the derived noise model of NMR spectroscopy Rx chain and to set the bottom line on its potential use, a good idea is to try the model out on the sample with very low level response signal, and hence, long measurement time. An example used here is the NMR measurement of the compound $Ce_3Pd_{20}Si_6$ [50]. In order to obtain the signal with its SNR of 24.08 dB at the spectrometer screen, using the hardware available in our NMR laboratory and M290 as the preamplifier, one needs to make 60000 acquisitions. Since the length of a single acquisition is equal to 53 ms, this means that the overall length of making 60000 acquisitions equals 3180 s, which is equal to 53 min. With the use of (6.15), the value of the input SNR is determined to be equal to –14.71 dB. Now, if one uses (6.15) again, but in the opposite direction, and imports the characteristics of the SOA preamplifier instead of the ones of the M290 preamplifier, the output SNR is determined to be equal to 27.12 dB. This means that, by the use of SOA instead of M290, one enhances output SNR of the NMR measurement for 3.03 dB. which equals 2.01 times greater output SNR on the linear scale. In other words, to obtain the output SNR with the use of the SOA preamplifier equal to the one with the use of M290 preamplifier, one would need to make 2.01 times less acquisitions, which is equal to 29839 acquisitions. This way, instead of 53 min, this NMR measurement could last only 26 min 21 s, which is less than a half of duration of the initial measurement with 60000 acquisitions!

This example clearly shows a couple of things. The first one, of course, is the use of the derived expression (6.15) "in action" – the process of its use in both ways is shown practically. The second thing is the enhancement of the NMR measurement results by the use of NMR preamplifier with high gain, low noise and extremely good impedance matching. This conclusion justifies all the efforts made to build as good NMR preamplifier as possible, and also invites to invest even more effort and resources in this analysis and development. Finally, now is a good moment to mention that, if the duration of a single acquisition could be shortened, than the overall duration of NMR measurements with multiple acquisitions would be shorter. This conclusion invites to also invest time, effort and resources in further development and enhancement of spectrometers, as the use of more precise and less noisy spectrometers would also result in the decrease of overall NMR measurement times.

The full description of the NMR measurement setup used in this example is available in Table 7.5 and the results of the analysis are available in Table 7.6.

Table 7.5: Electric parameters of the receiving chain elements used in the aforementioned example

Parameter	Symbol	value
Measurement frequency (MHz)	-	9.68
Coil and sample temperature (K)	T_{coil}	10
Input cable power loss (dB)	L_1	0.10
Duplexer power loss (dB)	L_2	0.43
M290 power gain (dB)	G_3	36.54
M290 noise figure (dB)	F_3	1.25
M290 reflection coefficient (dB)	S_{11_3}	-12.97
SOA power gain (dB)	G_3	40
SOA noise figure (dB)	F_3	0.30
SOA reflection coefficient (dB)	S_{11_3}	-30
Output cable power loss (dB)	L_4	0.62
Spectrometer noise figure (dB)	F_5	40
Number of measurements	n_{meas}	60000

Table 7.6: Results of the SNR output prediction of the NMR receiving chain using the SOA preamplifier

Measurement type	Value
Receiving chain input SNR (dB)	–14.71
Receiving chain output SNR using M290 (dB)	24.08
Predicted receiving chain output SNR using SOA preamplifier (dB)	27.12
Receiving chain output SNR enhancement (dB)	3.03
Receiving chain output SNR enhancement (lin.)	2.01

7.5 Improvement suggestions

In the end, it is necessary to make a couple of comments that describe how the NMR community can benefit from the derived expression, and also to point out the potential ways in which both hardware and software elements of the NMR setups could be developed.

The first and the most obvious benefit is the improvement of the NMR setups and shortening in the overall length of the NMR measurement time. The NMR measurements are mostly done by a "Trial and Error Method", where the user either changes the parameters of the spectrometer, the elements of the hardware part of the NMR spectroscopy system, or both, until the value of the output SNR of the NMR receiving chain (the SNR of the signal shown on the spectrometer screen), adopts the value satisfactory to the user. This approach can lead to numerous measurements of the same element, which can consume a lot of time for some samples. On the other hand, one can make only one measurement, use expressions (6.15) or (6.16) and (4.15), and to predict input SNR of the receiving chain. In the next step, the user can change some elements of the receiving chain only theoretically (in the model) and not physically, and then use the same expressions, but in the opposite order, to predict the value of the output SNR of the receiving chain. If the predicted value is satisfactory, the user can physically change the elements that were changed only theoretically, and then make the measurement. If not, the user changes another element in theory and tries again until the predicted value becomes satisfactory. This method can save a lot of measurement time in the case of a sample with low signal.

The second direct effect is a cheap and easy improvement that can be done to enhance noise properties of the receiving chain. If the cryostat and the spectrometer are distant from each other in the laboratory and it is necessary to use long cables to connect them, then the shortest and the least noisy cable (i.e. the cable with the lowest losses) needs to be placed at the beginning of the receiving chain (between the NMR probe and the duplexer), and the longest and the noisiest cable at the end of the chain (between the preamplifier and the spectrometer). This follows directly from expression (6.15), which shows that the noise properties of the elements placed in the chain after the preamplifier get more suppressed, while those of the elements before the preamplifier and the preamplifier itself do not. In fact, the noise generated in the first element of the chain (L_1) propagates along the receiving chain (the input cable is placed in front of the preamplifier). Significant noise reductions can be achieved if the least noisy cable is put at the beginning of the receiving chain and the noisiest cable at the end of it, rather than the other way around [51].

Due to similar reasons, the duplexer and the preamplifier are also critical elements of the receiving chain. Of all the hardware elements of the receiving chain, enhancements made on the noise properties of these two elements are going to affect the noise properties of the entire chain the most. To tackle the problem of the duplexer's noise properties, one can take two ap-

proaches. The first one is to directly modify its noise properties by, for example, cryogenically cooling the duplexer [20], just like it is already done with the preamplifier. The second one is to decrease the power loss of the duplexer, thus enhancing its noise properties. This can be achieved with the use of microwave substrates with a high relative permittivity, extremely low losses and an extremely conductive metallic layer [52], the use of ultra-fast and ultra-low-loss switching diodes [53, 54], the use of low-loss high-conductivity connectors [55] etc. When dealing with the noise properties of the preamplifier, on the other hand, one needs to take three conditions into consideration: the noise figure of the preamplifier needs to be as low as possible, its power gain as high as possible and the preamplifier needs to be matched to the characteristic impedance, Z_0. As it was already mentioned before, it is impossible to find a preamplifier that has all three conditions met perfectly, so a preamplifier with optimum properties at the corresponding frequencies of NMR measurements need to be found. Furthermore, if the preamplifier is comprised of two stages of amplifiers, it is necessary to pick their arrangement combination with the smallest noise measure value to accomplish better noise properties [39] (the concept and the idea of noise measure is described in the subsection 8.2). However, even the state-of-the-art duplexers and preamplifiers can not enhance overall noise properties of the NMR receiving chain if noise properties of the elements up to that point are poor. E.g. the tuning/matching network of the NMR coil and the coil itself are not always connected directly to the coaxial cable which connects them to the output of the NMR probe. In some cases, there is a non-insulated wire between the coil's tuning/matching network and the coaxial cable. This leads to much worse noise properties of the NMR response signal even before the signal leaves the NMR probe and enters the environment of the standard temperature, T_0. Here, noise properties of poor connection of the NMR coil to the rest of the network are the dominant noise properties of the entire NMR system and improving noise properties of the NMR receiving chain would not solve the problem.

The sole element in the NMR receiving chain that is the hardest and most expensive to change is, of course, the spectrometer. As Table 7.2 clearly shows, noise properties of the entire spectrometer are by far the worst of all the elements of the receiving chain. However, one more adjustment to the measurement setup that can be made is adding another preamplifier with its power gain as high as possible (and bigger by its value than the value of the spectrometer noise figure if possible) to decrease the influence of the noise properties of the spectrometer. If its gain is lower than the initial preamplifier, it is placed in the receiving chain as a second stage of amplification (i.e. behind the initial preamplifier). This is why the two-stage preamplifier is also analysed in this chapter. If there are no available single-stage preamplifiers with a power gain high enough, it is possible to compensate it by adding a second stage amplifier at the output of the preamplifier. Although this solves the problem, it needs to be done carefully so that the level of the output signal from the created two-stage preamplifier does not exceed the maximum input

level of the spectrometer. If this can be achieved, the noise properties of the receiving chain can be further enhanced this way.

The only non-hardware part of the NMR receiving chain which is directly taken into account in the derived expression for the noise figure of the receiving chain is the averaging of multiple measurements. Although this method is quite efficient, it can still be improved. If it is combined with different sorts of digital filtering, additional enhancement of the noise properties of the entire chain can be achieved [56]. It is also worth mentioning that the averaging of multiple measurements has its boundaries. The number of measurements can be increased only up to a point where the method reaches its saturation [57]. The saturation point is either dictated by the size of the instrument's memory (if all the measurement results are first saved in its memory, combined afterwards and then averaged) or by the maximum detectable signal level (if all the measurement results are combined live, during the measurement, and then averaged afterwards). In the former case, it is obviously impossible to average more measurements than it is possible to save in the instrument's memory. In the latter case, as signal level increases linearly with the increased number of combined measurements, the signal level gets clipped after it surpasses the instrument's maximum detectable signal level, causing the SNR to effectively decrease. This is why it is necessary to combine the hardware-based methods with digital filtering in order to shift the saturation point up to the higher number of measurements.

The last comment regarding the derived NMR receiving chain noise figure expression is the explanation of possible values of the chain's noise figure. While it is considered that the values of noise figure of a cascade can only be higher than 1 (i.e. 0 dB), this is only true if only hardware elements are being considered. Since the expression for the receiving chain contains the averaging of multiple measurements, which is a non-hardware part of the same chain, it is possible to achieve values of its noise figure lower than 1 (or 0 dB in logarithmic scale). As mentioned before, it is only "effective" noise figure that presumes that the system parameters did not change during the averaging.

Finally, the author also wants to point out his program, written in Python programming language [58], which calculates noise figure and predicts input and output SNRs of the NMR receiving chain using expressions (6.15), (6.16) and (4.15) after the user inputs the values of the receiving chain elements of his own NMR spectroscopy system. This program is available on GitHub [59] and Dropbox [60].

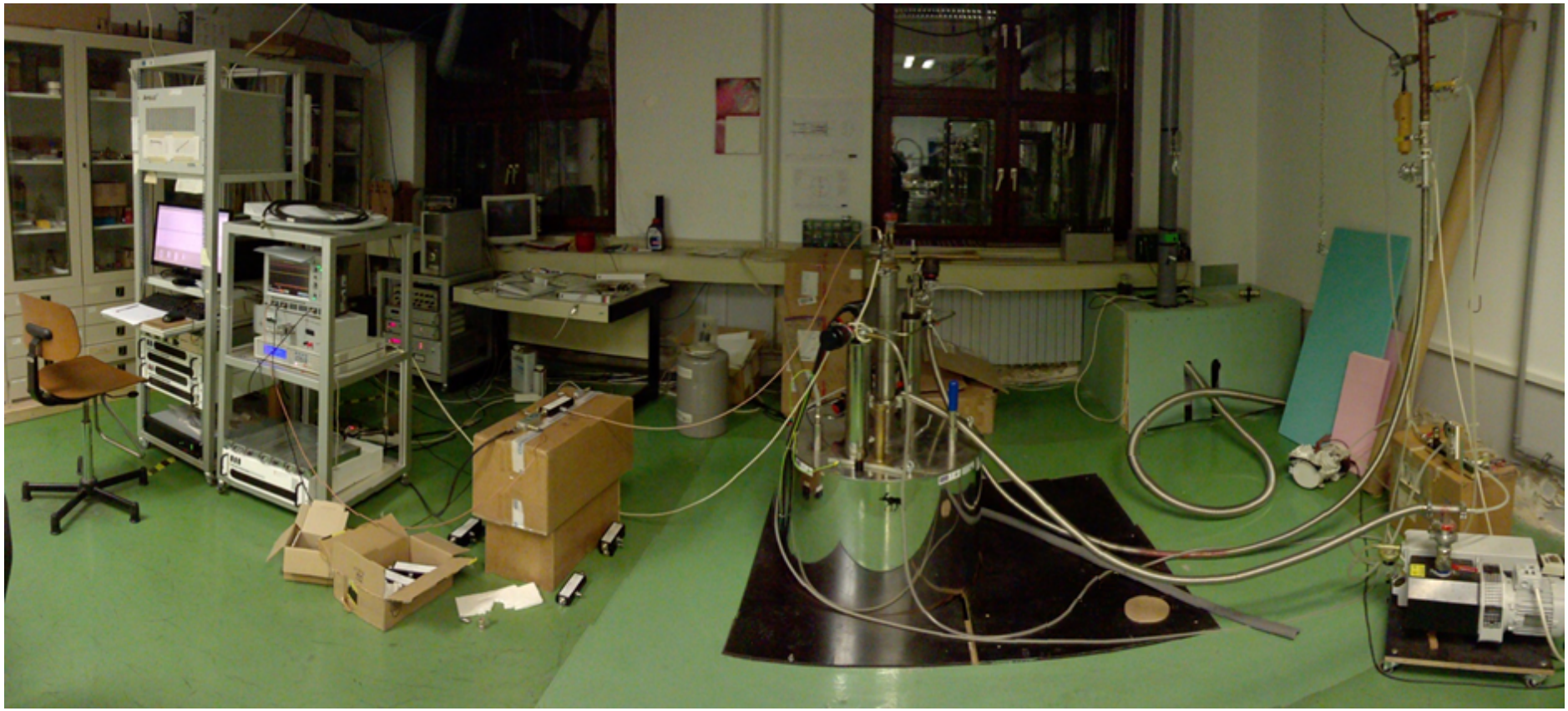

Figure 7.7: Measurement setup from the Laboratory for solid state NMR and high frequency measurement at the Department of Physics of Faculty of Science, University of Zagreb; from left to right: spectrometer and PC that controls it, temperature controller and digital oscilloscope, duplexer and preamplifier, NMR probe and cryostat, compressor (not directly a part of NMR spectroscopy Rx chain)

Chapter 8

Design and optimization of high–gain and low–noise NMR preamplifiers

In this chapter, the general process of optimization and design of microwave low–noise amplifiers is theoretically described. Furthermore, a practical example of optimization of commercially available cryogenic low–noise NMR preamplifier by the addition of a second stage power amplifier is given. Finally, a practical example of analysis, design and construction of a high–gain and low–noise NMR preamplifier is presented.

8.1 The process of optimization and design of microwave low–noise amplifiers

A standard approach to the design of an amplifier is to choose the active element – usually a transistor (or transistors if the amplifier is intended to be multi–stage), and use its parameters, given in its datasheet, to execute static and dynamic analysis of the amplifier to be made [61, 62]. However, this approach can be used only at lower frequencies (lower than the order of a ten MHz), where used electronic components are much smaller than the wavelengths (smaller than the order of a hundredth part) of the working frequencies, so all the components can be approximated as lumped components. This is not the case with working frequencies from the RF or microwave frequency bands, where the sizes of used electronic components are proportional to the wavelengths of working frequencies, and also where parasitic capacitances, inductances and resistances of all the components become so big that they cannot be neglected anymore. Fortunately, there is a way out. It is possible to characterize the entire amplifier circuit, with also taking parasitic values into consideration, by the matrix of the so–called *scattering* (S) *parameters* [63].

8.1.1 Scattering parameters

Scattering (S) parameters are one of the available types of paramaters that allow the user to characterize an electric circuit or just a single component as "the black box". The idea is to illuminate the circuit with electromagnetic radiation and then to observe the level of the radiation that reached certain points, called *ports*. When talking about standard amplifiers with one input and one output, the expression "port" is just a synonym for the amplifier's input and output terminals. So, in terms of S parameters, a standard amplifier with one input and one output can be called a *two–port network*. And because it is highly unlikely that the user will deal with an NMR preamplifier with more than two ports, two–port S parameters will be explained here, but it is necessary to bear in mind that it is possible to define S paramaters for any integer number of ports greater than zero. The block diagram of a two–port network described with S parameters is shown in Figure 8.1.

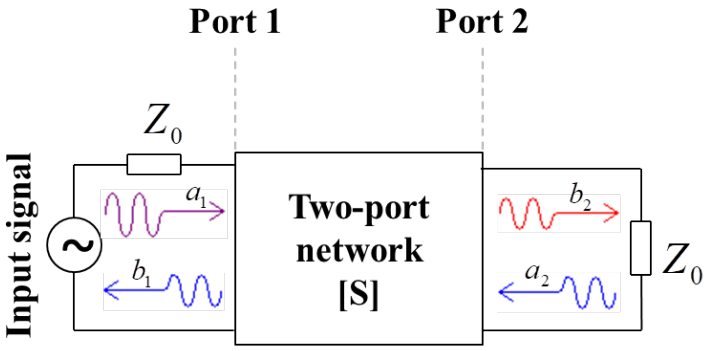

Figure 8.1: Two–port network described with S parameters

Signals a_1, b_1, a_2 and b_2, shown in Figure 8.1, are the waves whose unit of measure is equal to the square root of a watt ($\sqrt{\text{W}}$), so, although these signals are referred to as "power waves", their unit of measure is proportional to voltage. Here, a_1 stands for incident wave on Port 1, b_1 stands for reflected wave on Port 1, a_2 stands for incident wave on Port 2, or reflected wave from the load, while b_2 stands for reflected wave on Port 2, or transmitted wave from Port 1 [63]. These four waves are interconnected by the following two equations:

$$\begin{aligned} b_1 &= S_{11}a_1 + S_{12}a_2; \\ b_2 &= S_{21}a_1 + S_{22}a_2. \end{aligned} \tag{8.1}$$

These two equations can be reduced to a matrix form:

$$\begin{bmatrix} b_1 \\ b_2 \end{bmatrix} = \begin{bmatrix} S_{11} & S_{12} \\ S_{21} & S_{22} \end{bmatrix} \begin{bmatrix} a_1 \\ a_2 \end{bmatrix} \Rightarrow [b] = [S][a]. \tag{8.2}$$

Here, $[b]$ and $[a]$ matrices are comprised of the reflected and the transmitted waves at the inputs of each of the two ports, respectively. Furthermore, the $[S]$ matrix consists of all four S parameters of a two–port network:

$$[S] = \begin{bmatrix} S_{11} & S_{12} \\ S_{21} & S_{22} \end{bmatrix}. \tag{8.3}$$

Without further ado, here are the definitions of all four S parameters of a two–port network:

S_{11} parameter is defined as the ratio of the reflected wave, b_1, and the incident wave, a_1, at Port 1, respectively:

$$S_{11} = \left.\frac{b_1}{a_1}\right|_{a_2=0}. \tag{8.4}$$

Effectively, S_{11} parameter represents the refflection coefficient at the input of the two–port network, while there is no reflected wave a_2.

S_{21} parameter is defined as the ratio of the transmitted wave, b_2, and the incident wave, a_1, at Port 1, respectively:

$$S_{21} = \left.\frac{b_2}{a_1}\right|_{a_2=0}. \tag{8.5}$$

Effectively, S_{21} parameter represents the transmission coefficient from the input to the output of the two–port network.

S_{12} parameter, on the other hand, is defined as the ratio of the transmitted wave, b_1, and the incident wave, a_2, at Port 2, respectively:

$$S_{12} = \left.\frac{b_1}{a_2}\right|_{a_1=0}. \tag{8.6}$$

Effectively, S_{12} parameter represents the transmission coefficient from the output to the intput of the two–port network.

Finally, S_{22} parameter is defined as the ratio of the reflected wave, b_2, and the incident wave, a_2, at Port 2, respectively:

$$S_{22} = \left.\frac{b_2}{a_2}\right|_{a_1=0}. \tag{8.7}$$

Effectively, S_{22} parameter represents the refflection coefficient at the output of the two–port network.

As it was already mentioned in subsections 6.2.2 and 6.2.3, all four S parameters can be measured by a VNA, after which they can form the S matrix for the measured RF device.

Now that all the S parameters of a two–port network have been defined, it is possible to describe the process of design of RF and microwave low–noise amplifiers.

8.1.2 Design of low–noise microwave amplifiers: numerical approach

The block diagram of a microwave amplifier is shown in Figure 8.2. As it can be seen, a microwave amplifier, from the S parameters point of view, can be shown as a cascade of an input impedance matching network (with its gain equal to G_S), an active element – usually a transistor (with its gain G_0 and its S matrix), and an output impedance matching network (with its gain equal to G_L). Here, Γ_{in} and Γ_{out} stand for reflection coefficients at the input and the output of the active element, respectively, Γ_L stands for the reflection coefficient at the input of the output impedance matching network, while Γ_S stands for the reflection coefficient at the output of the input impedance matching network.

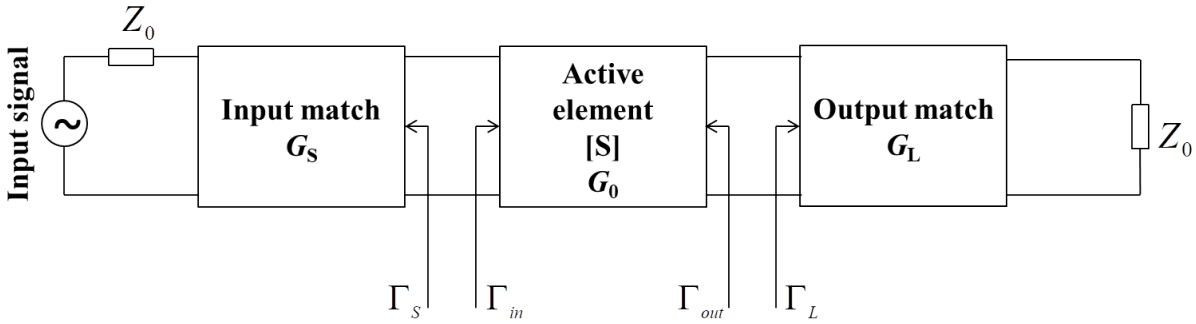

Figure 8.2: Block diagram of a microwave amplifier

Using the theory of microwave networks, it can be shown [64] that the reflection coefficients at the input and the output of the active element are given as:

$$\Gamma_{in} = S_{11} + \frac{S_{12}S_{21}\Gamma_L}{1 - S_{22}\Gamma_L}; \tag{8.8}$$

$$\Gamma_{out} = S_{22} + \frac{S_{12}S_{21}\Gamma_S}{1 - S_{11}\Gamma_S}. \tag{8.9}$$

In most of the NMR preamplifiers, the S_{12} parameter is shown to be small enough to be neglected. Such amplifiers form a special case of the *unilateral active element*, where effective gain levels of the input impedance matching network, the active element, and the output impedance matching network, respectively, can be expressed as [64]:

$$G_S = \frac{1 - |\Gamma_S|^2}{|1 - \Gamma_{in}\Gamma_S|^2}; \tag{8.10}$$

$$G_0 = |S_{21}|^2; \tag{8.11}$$

$$G_L = \frac{1 - |\Gamma_L|^2}{|1 - S_{22}\Gamma_L|^2}. \tag{8.12}$$

One of the most useful values for an amplifier is the *transducer gain*, which equals the ratio of the power delivered to the load and the power delivered by the source. In terms of gain coefficients, the transducer gain equals $G_T = G_S G_0 G_L$, but in terms of reflection coefficients and S parameters, it is given as [64]:

$$G_T = \frac{1-|\Gamma_S|^2}{|1-\Gamma_{in}\Gamma_S|^2}|S_{21}|^2\frac{1-|\Gamma_L|^2}{|1-S_{22}\Gamma_L|^2}. \tag{8.13}$$

Notice here that the maximum gain occurs when both input and output impedance matching networks provide conjugate matches: $\Gamma_S = S_{11}^*$ and $\Gamma_L = S_{22}^*$. So, with the use of expressions (8.8) to (8.13), one can design and optimize the gain of a microwave low–noise amplifier (LNA).

Furthermore, the LNA must operate in a stable configuration to ensure that it will not oscillate. Oscillations may occur if there is a negative real part of the impedance at the input or the output of the amplifier. This leads to $|\Gamma_{in}|$ and $|\Gamma_{out}|$ to be greater that the value of 1. Since these two are both dependent on Γ_L and Γ_S, stability can be achieved with proper impedance matching networks. There are two types of stability: *unconditional stability* and *conditional stability*. An unconditionally stable amplifier *always* has $|\Gamma_{in}|$ and $|\Gamma_{out}|$ lower than the value of 1, while a conditionally stable amplifier will have these two conditions fulfilled for only a certain range of passive source and load terminations. Also, if the amplifier is unilateral, it is sufficient that $|S_{11}|$ and $|S_{22}|$ have values lower than 1. All the aforementioned stability conditions are "squeezed" into two inequalities (known as the *Rollet condition* [35]) that need to be achieved in order to have unconditionally stable amplifier [64]:

$$|\Delta| = |S_{11}S_{22} - S_{12}S_{21}| < 1; \tag{8.14}$$

$$K = \frac{1-|S_{11}|^2-|S_{22}|^2+|\Delta|^2}{2|S_{12}S_{21}|} > 1. \tag{8.15}$$

Finally, one also needs to take into account noise properties of the amplifer for it to be low–noise. It is shown that minimum noise performance, F_{min}, occurs with a source termination with reflection coefficient Γ_{opt}. The noise figure of a two–port amplifier is given as:

$$F = F_{min} + \frac{4r_n|\Gamma_S - \Gamma_{opt}|^2}{(1-|\Gamma_S|^2)|1+\Gamma_{opt}|^2}, \tag{8.16}$$

where r_n stands for the equivalent noise resistance of the two–port amplifier, $r_n = \frac{R_n}{Z_0}$ [64]. Parameters r_n, F_{min} and Γ_{opt} are usually given in the datasheet of the active element, and if not, they can also be determined experimentally. Briefly, there is a minimum noise figure, F_{min}, possible for a device, which is achieved only when a particular reflection coefficient, Γ_{opt}, is presented to the input. So, the case where $\Gamma_S = \Gamma_{opt}$ leads to the minimum noise figure for the

amplifier built with this transistor. Furthermore, r_n is the normalized noise resistance, which expresses how fast the noise factor F increases from F_{min} as the source resistance Z_S departs from the optimal resistance Z_{opt}.

Usually, the design of an LNA consists of the trade–off between noise figure and gain while it also needs to operate at the required stability. Typically, a potentially unstable transistor is made unconditionally stable with the use of resistive loading or feedback at the expense of reduced power gain and degraded noise figure. But nowadays, the expressions (8.8) to (8.16) are built into most of modern microwave design CAD tools, so the user only needs to understand this technique physically, rather than having a detailed knowledge of the aforementioned equations.

8.1.3 Design of low–noise microwave amplifiers: graphical approach

Besides the numerical approach to the design of LNAs, one can approach the same problem graphically, using the so–called Smith chart, shown in Figure 8.3.

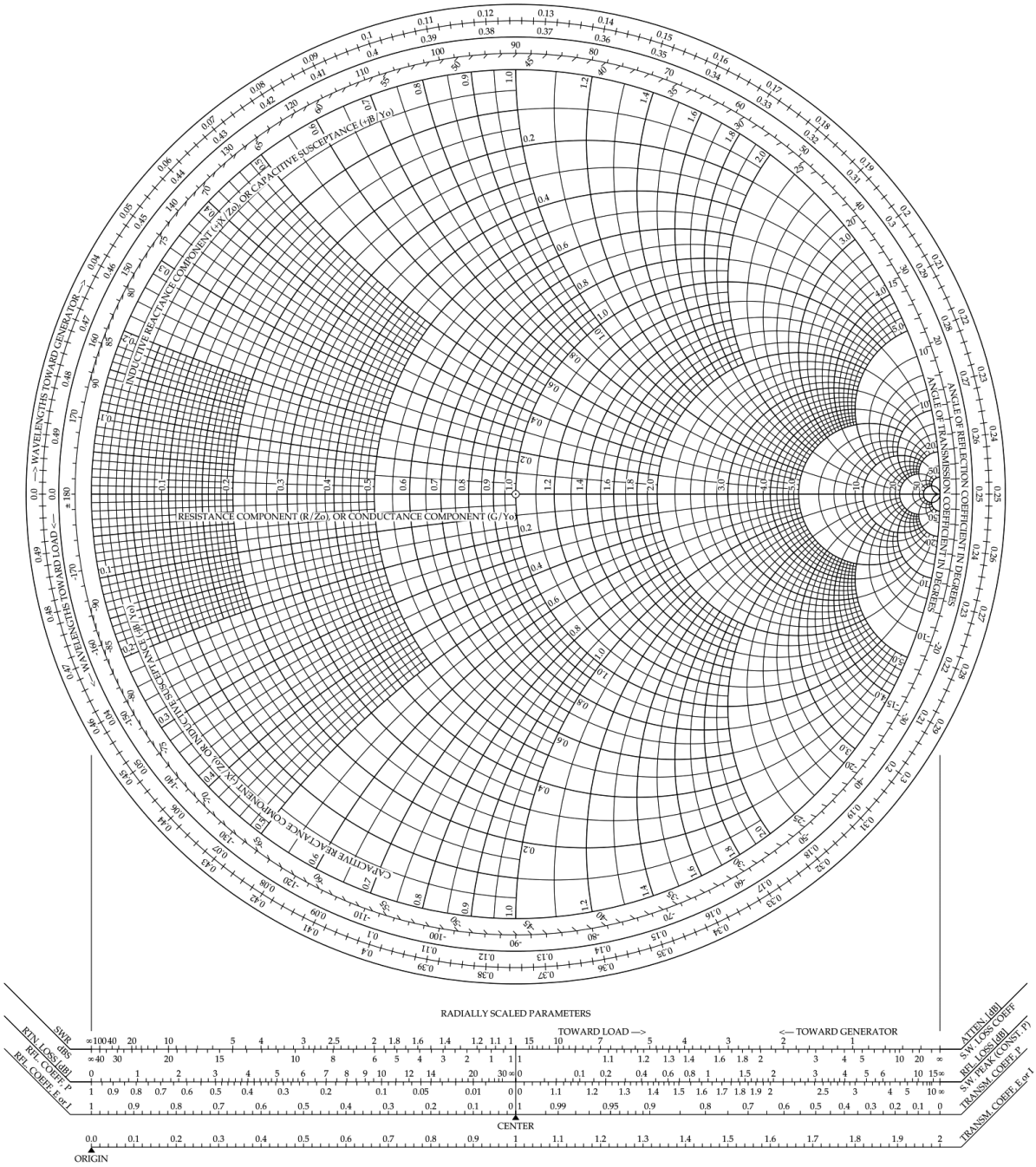

Figure 8.3: Smith chart [65]

Basically, this chart is a curvilinear impedance grid, superimposed on a polar plot of the voltage reflection coefficient, Γ. If one expresses the reflection coefficient in its polar form as $\Gamma = |\Gamma|e^{j\theta}$, then the magnitude $|\Gamma|$ represents the radius from the center of the chart ($|\Gamma| \leq 1$), while the angle θ ($-180^\circ \leq \theta \leq 180^\circ$) is measured counterclockwise from the right–hand side

of the horizontal diameter [35]. This means that any passively realizable ($|\Gamma| \leq 1$) reflection coefficient can be plotted as a unique point on the Smith chart. The reason why Smith chart is so powerful and has become so popular with RF and antenna engineers is because it can be used to convert reflection coefficients to normalized impedances (or admittances) and the other way around. The normalization constant is usually the characteristic impedance of the transmission line, Z_0. So, normalized impedance, z, can be expressed as $z = \frac{Z}{Z_0}$. If a lossless TL of characteristic impedance Z_0 is terminated with a load impedance Z_L, the reflection coefficient at the load can be written as [35]:

$$\Gamma = \frac{z_L - 1}{z_L + 1} e^{j\theta}, \tag{8.17}$$

where $z_L = \frac{Z_L}{Z_0}$ is the normalized load impedance. This expression can be solved for z_L [35]:

$$z_L = \frac{1 + |\Gamma| e^{j\theta}}{1 - |\Gamma| e^{j\theta}}. \tag{8.18}$$

This complex expression can be reduced to two real expressions by rewriting Γ and z_L in terms of their real and imaginary parts, $\Gamma = \Gamma_r + j\Gamma_i$ and $z_L = r_L + jx_L$ [35]:

$$r_L + jx_L = \frac{(1 + \Gamma_r) + j\Gamma_i}{(1 - \Gamma_r) - j\Gamma_i}. \tag{8.19}$$

After reduction of the expression (8.19) to real and imaginary part and after the rearrangement, one gets the expressions for resistance circles in the Γ_r plane and for reactance circle in the Γ_i plane, respectively [35]:

$$\left(\Gamma_r - \frac{r_L}{1 + r_L}\right)^2 + \Gamma_i^2 = \left(\frac{1}{1 + r_L}\right)^2; \tag{8.20}$$

$$(\Gamma_r - 1)^2 + \left(\Gamma_i - \frac{1}{x_L}\right)^2 = \left(\frac{1}{x_L}\right)^2. \tag{8.21}$$

As it can be seen in Figure 8.3, these two circles are orthogonal. Furthermore, the Smith chart is a more elegant and a less tedious alternative to a numerical calculation of problems that include transmission lines and matching circuits. Instead of the manipulation of fractions containing square roots of complex numbers, these problems can be reduced to the drawing of circles of constant standing wave ratio (SWR), and then travelling around their perimeters. The "travelling mileage" around the perimeter is determined by the length of the transmission line included in the problem being solved. A few problem solving examples with the use of a Smith chart can be seen in [66] and [67].

In order to use the Smith chart to design an LNA, the idea is to plot the so–called *constant–gain circles* and *constant–noise figure circles* on it, and then select an optimum trade–off point between them. Here, the expressions for both circles will be derived and an example of graphical LNA design will be given afterwards.

An assumption that is made is that the active element of the amplifier is unilateral. This is a legitimate assumption since for most transistors, $|S_{12}|$ really is small enough to be ignored. That being said, the effective gain levels of the input impedance matching network, G_S, and output impedance matching network, G_L, are given by (8.10) and (8.12) [35]:

$$G_S = \frac{1-|\Gamma_S|^2}{|1-\Gamma_{in}\Gamma_S|^2};$$

$$G_L = \frac{1-|\Gamma_L|^2}{|1-S_{22}\Gamma_L|^2}.$$

If impedance matching is conjugated both at the input and the output of the two–port network, G_S and G_L obtain their maximum values [35]:

$$G_{S_{max}} = \frac{1}{1-|S_{11}|^2}; \tag{8.22}$$

$$G_{L_{max}} = \frac{1}{1-|S_{22}|^2}. \tag{8.23}$$

Now it is possible to define normalized gain factors g_S and g_L [35]:

$$g_S = \frac{G_S}{G_{S_{max}}} = \frac{1-|\Gamma_S|^2}{|1-S_{11}\Gamma_S|^2}(1-|S_{11}^2|); \tag{8.24}$$

$$g_L = \frac{G_L}{G_{L_{max}}} = \frac{1-|\Gamma_L|^2}{|1-S_{22}\Gamma_L|^2}(1-|S_{22}^2|), \tag{8.25}$$

which are, obviously, both lesser than 1. For fixed values of g_S and g_L, expressions (8.24) and (8.25) represents circles in the Γ_S and Γ_L plane. After some manipulation over these two expressions, it is possible to determine the center of the circle, C_S, and its radius, R_S in the Γ_S plane [35]:

$$C_S = \frac{g_S S_{11}^*}{1-(1-g_S)|S_{11}|^2}; \tag{8.26}$$

$$R_S = \frac{\sqrt{1-g_S}(1-|S_{11}|^2)}{1-(1-g_S)|S_{11}|^2}, \tag{8.27}$$

as well as their equivalents in the Γ_L plane [35]:

$$C_S = \frac{g_L S_{22}^*}{1-(1-g_L)|S_{22}|^2}; \tag{8.28}$$

$$R_S = \frac{\sqrt{1-g_L}(1-|S_{22}|^2)}{1-(1-g_L)|S_{22}|^2}. \tag{8.29}$$

In the end, since these expressions are approximative because of the assumption that the active element is unilateral, it is possible to calculate the error in the transducer gain due to this assumption. It can be shown that the ratio $\frac{G_T}{G_{T_U}}$ is bounded by:

$$\frac{1}{(1+U)^2} < \frac{G_T}{G_{T_U}} < \frac{1}{(1-U)^2}, \tag{8.30}$$

where U represents the unilateral figure of merit [35]:

$$U = \frac{|S_{11}||S_{12}||S_{21}||S_{22}|}{(1-|S_{11}|^2)(1-|S_{22}|^2)}. \tag{8.31}$$

An error of a few tenths of dB or less usually justifies the unilateral assumption.

On the other hand, the derivation of the expressions of the center and the radius of the constant–noise figure circle starts with the expression for noise figure of a two–port network (8.16) [35]:

$$F = F_{min} + \frac{4r_n|\Gamma_S - \Gamma_{opt}|^2}{(1-|\Gamma_S|^2)|1+\Gamma_{opt}|^2}.$$

It can be shown that, for a fixed value of noise figure, F, this expression defines a circle in the Γ_S plane. But first, it is necessary to define the noise figure parameter, N [35]:

$$N = \frac{|\Gamma_S - \Gamma_{opt}|^2}{1-|\Gamma_S|^2} = \frac{F-F_{min}}{4r_n}|1+\Gamma_{opt}|^2, \tag{8.32}$$

which is a constant for a given noise figure and set of noise parameters. The expression (8.32) can be rewritten and manipulated to obtain the center of the constant–noise figure circle, C_F, and its radius, R_F, in the Γ_S plane [35]:

$$C_F = \frac{\Gamma_{opt}}{N+1}; \tag{8.33}$$

$$R_F = \frac{\sqrt{N(N+1-|\Gamma_{opt}|^2)}}{N+1}. \tag{8.34}$$

It can be seen from (8.33) and (8.34) that, by the variation of N, the LNA designer can basically see the effect of tuning in order to estimate the LNA's practical noise performance.

Now is the time to present the example of the use of the graphical approach to the design of LNAs [35]. Let us say that it is necessary to design the LNA having a 2.0 dB noise figure with the maximum gain that is compatible with this noise figure at 4 GHz, using a GaAs MESFET with the following S and noise parameters ($Z_0 = 50\Omega$): $S_{11} = 0.6\angle -60^\circ$, $S_{12} = 0.05\angle 26^\circ$, $S_{21} = 1.9\angle 81^\circ$, $S_{22} = 0.5\angle -60^\circ$, $F_{min} = 1.6$ dB, $\Gamma_{opt} = 0.62\angle 100^\circ$ and $R_N = 20\Omega$. For design purposes, it is assumed that the device is unilateral, so it is also necessary to calculate the maximum error in G_T resulting from this assumption.

The first thing needed to do is calculate Δ and K by the use of (8.14) and (8.15), respectively. Because $\Delta = 0.37$ and $K = 2.78$, the device is proved to be unconditionally stable, even without the approximation of a unilateral device.

The next step is to determine the unilateral figure of merit from (8.31), which in this case equals $U = 0.059$. From (8.30) the ratio $\frac{G_T}{G_{T_U}}$ is bounded as:

$$0.891 < \frac{G_T}{G_{T_U}} < 1.130.$$

In dB, this is equal to:

$$-0.50\text{dB} < \frac{G_T}{G_{T_U}} < 0.53\text{dB}.$$

Thus, an error less than about ± 0.5 dB in gain should be expected.

Now, with the use of (8.32), (8.33) and (8.34) one gets the values of the center and the radius of the 2 dB noise figure circle: $N = 0.0986$, $C_F = 0.56\angle 100^\circ$, $R_F = 0.24$. This noise figure circle in plotted in Figure 8.4a. Minimum noise figure ($F_{min} = 1.6$dB) occurs for $\Gamma_S = \Gamma_{opt} = 0.62\angle 100^\circ$.

The next step is to calculate data for several input section constant–gain circles. From (8.26) and (8.27) the results are:

G_S[dB]	g_S	C_S	R_S
1.0	0.805	$0.52\angle 60^\circ$	0.300
1.5	0.904	$0.56\angle 60^\circ$	0.205
1.7	0.946	$0.58\angle 60^\circ$	0.150

These circles are plotted in Figure 8.4a. It can be seen that the $G_S = 1.7$dB just intersects the $F = 2$dB noise figure circle, and that any higher gain will result in a worse noise figure. From the Smith chart, the optimum solution is $\Gamma_S = 0.53\angle 75^\circ$, yielding $G_S = 1.7$dB and $F = 2$dB.

For the output section it is chosen $\Gamma_L = S_{22}^* = 0.5\angle 60^\circ$ for a maximum G_L of 1.25 dB – calculated according to (8.23). Using (8.11), the transistor gain is equal to $3.61 = 5.58$dB, so

the overall transducer gain will be equal to:

$$G_{T_U} = G_S + G_0 + G_L = 8.53\text{dB}.$$

A complete AC circuit for the amplifier, using open–circuited shunt stubs in the matching sections, is shown in Figure 8.4b.

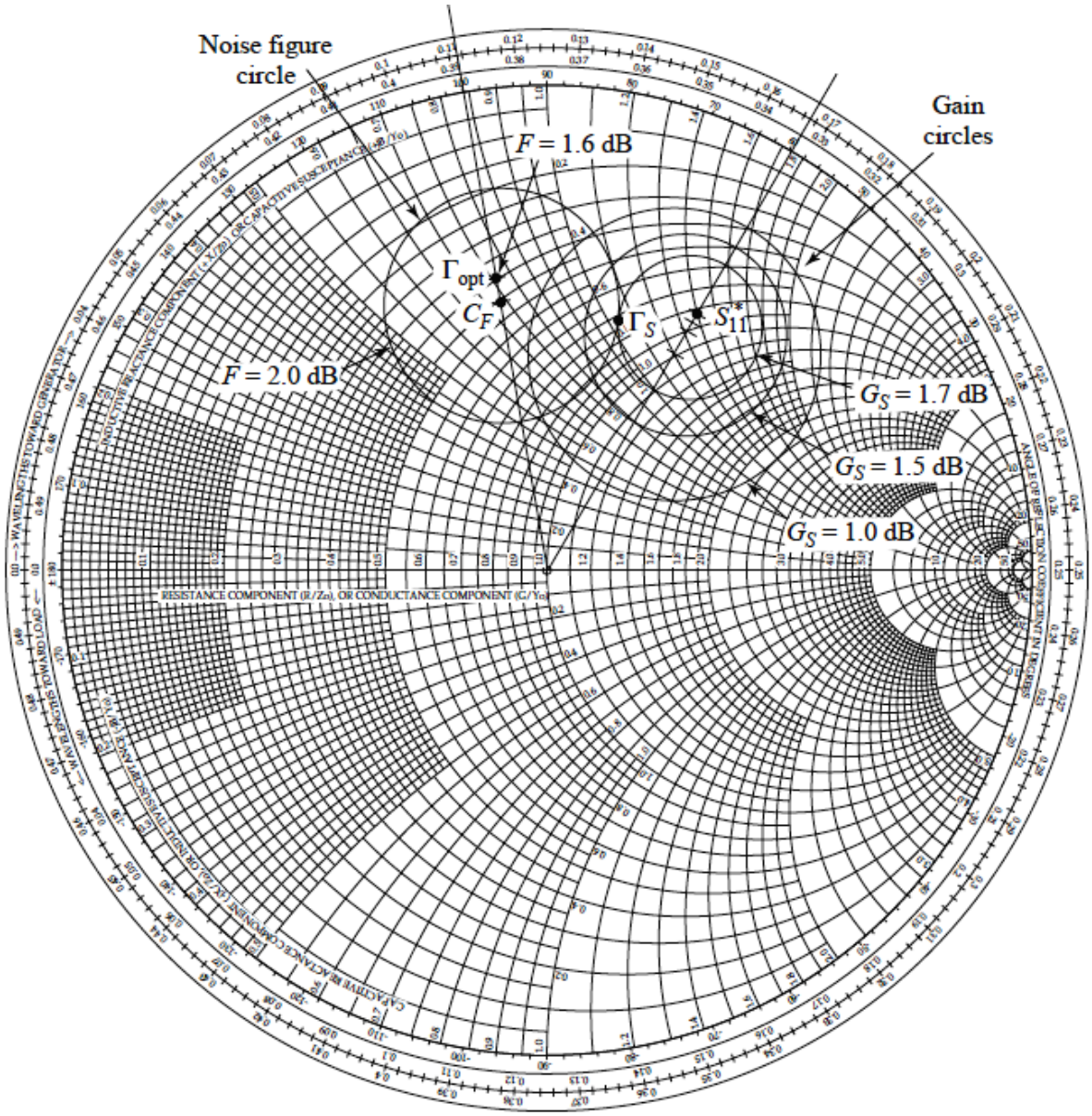

a)

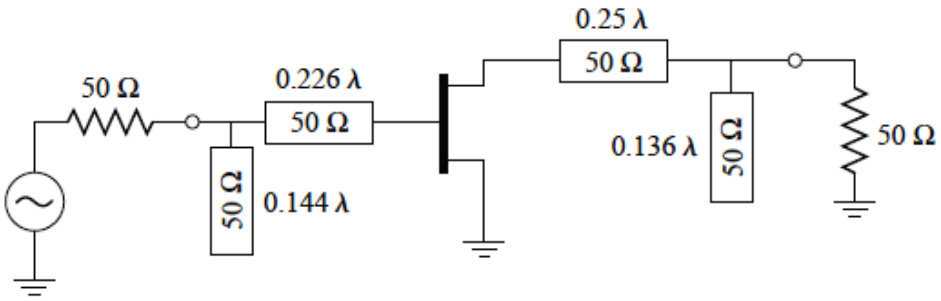

b)

Figure 8.4: LNA design example [35]: a) Constant–gain and constant–noise figure circles; b) RF circuit

However, it needs to be noticed that in both the examples, described in the last two subsections, the LNA's elements are chosen in such a way so that its wanted parameters (power gain level, noise figure level, impedance matching...) are achieved at a single point, ergo, for a single operating frequency. Therefore, these examples show how to design a *narrowband* LNA. If one wants to design and construct a *broadband* amplifier (as it will be shown to be the case in this thesis), a wanted frequency locus, and hence, multiple frequency points, need to be observed. Ideally, constant power gain and noise figure levels, as well as good impedance matching of the broadband LNA, would be achieved over the entire wanted frequency bandwidth. Unfortunately, the reality is usually far from ideal. It is possible to achieve some of the wanted parameters to be very close to the ideal case, but at the expense of achieving worse values of the rest of the parameters. For example [35]:

- It is possible to increase the LNA's operating frequency bandwidth with the use of the compensated matching networks, but at the expense of both input and output impedance matching.
- Good input and output impedance matching can be achieved with the use of the resistive matching networks, but at the expense of lower power gain level and higher noise figure level.
- Negative feedback can be used to both flatten the LNA's power gain curve and improve the impedance matching, both at the input and the output, but then the maximum power gain level drops, while the minimum noise figure level rises.
- By the use of two amplifiers having 90 degree couplers at their input and output (the so-called balanced amplifiers), it is possible to achieve good impedance matching on over an octave bandwidth, with the gain level being equal to the one of a single amplifier, but this design requires two transistors and twice the DC power.
- Several transistors cascaded along a transmission line (the so-called distributed amplifiers) can be used to achieve a flat power gain curve, good impedance matching and low noise figure level over a wide bandwidth. However, the circuit is large, and the power gain level is relatively low (compared to regular cascaded amplifiers).
- Using a differential amplifier (two amplifiers in a differential mode, with input signals of the opposite polarity) results with wider bandwidth and flatter power gain curve, but with a high noise figure level.

Obviously, it is necessary to prioritize some parameters of the LNA over the others in order to achieve its broadband operation. Therefore, after the right selection of the highest priority parameter is made, it is possible to choose some of the given examples in order to design and construct a broadband LNA.

8.2 Optimization of cryogenic NMR preamplifier with a second stage amplifier

In Chapter 6, noise model of the NMR Rx chain was derived and the value of its noise figure was described with the expression (6.15). From this expression, as well as in Figure 7.4 from Chapter 7, it can be seen that the elements closer to the beginning of the Rx chain affect the chain's noise properties more. This is why it is a good idea to acquire an NMR preamplifier with its noise figure level as low as possible. Because of this, cryogenic T77 preamplifier (THAMWAY N141-206AA(D)) was purchased in order to replace M290 (MITEQ AU-1114-SMA), as its noise figure is notably lower than the one of M290 on almost entire frequency bandwidth between 0 and 500 MHz. Noise figures of both preamplifiers can be seen in far right charts of Figure 8.8.

However, as the spectrometer's noise figure level was shown in Chapter 7 to be much higher than noise figure level of any other element in the Rx chain, this is the element that affects the overall Rx chain's noise figure the most, although it is the last element in the chain. Therefore, the preamplifier not only has to have noise figure level as low as possible, but it also needs to have its power gain as high as possible in order to soften the effect of the spectrometer on the overall noise figure of the Rx chain. As it was presented in Chapter 7, spectrometer's noise figure level was somewhere in between 33.5 dB and 38.5 dB for the obtained measurements. It can be seen in the middle charts of Figure 8.8 that the power gain levels ($|S_{21}|$ parameters) of M290 and T77 rest in between 33 and 36 dB, and 16 and 27 dB, respectively, in the frequency bandwidth between 0 and 500 MHz. Obviously, the power gain level of T77 is much lower both than the power gain level of M290, as well as the spectrometer's noise figure level. Because it cannot suppress spectrometer's noise characteristics as good as M290, T77 yields measurements of lower quality, although it has better noise characteristics than M290.

This is why the idea is to connect the second amplifier in a cascade along with T77. The function of the second amplifier, therefore, is to append the power gain level of T77 to the one of M290. The second amplifier chosen to be connected into cascade, along with T77, is MC290 (Mini-Circuits HELA -10D+). The absolute value of its S parameters and noise figure can be seen in the top part of Figure 8.9. The measurements of S parameters of all three amplifiers were made with the use of Rohde & Schwarz ZVL3 [68] VNA, while the related noise figures were measured with the use of Hewlett-Packard 8970B [69] noise figure meter.

Nevertheless, the arrangement in the cascade of these two amplifiers is important, as the characteristics of such created two–stage preamplifier are not the same in both cases. As it can be seen in the expression (4.17), which describes the noise figure of a cascade, the first element in a cascade affects the overall noise figure the most. So, although the power gain level of the cascade does not change with the change of the elements' arrangement, the overall noise figure

can differ notably for different arrangements.

For example, let us have two amplifiers: amplifier A, with its power gain level, G_A, equal to 30 dB and its noise figure level, F_A, equal to 0.5 dB; and amplifier B, with its power gain level, G_B, equal to 10 dB and its noise figure level, F_B, equal to 5 dB. The two possible arrangements, as well as the expressions for calculation of their noise figure levels and power gain levels, are shown in Figure 8.5, while their parameters and calculated noise figures and power gain levels are shown in Table 8.1.

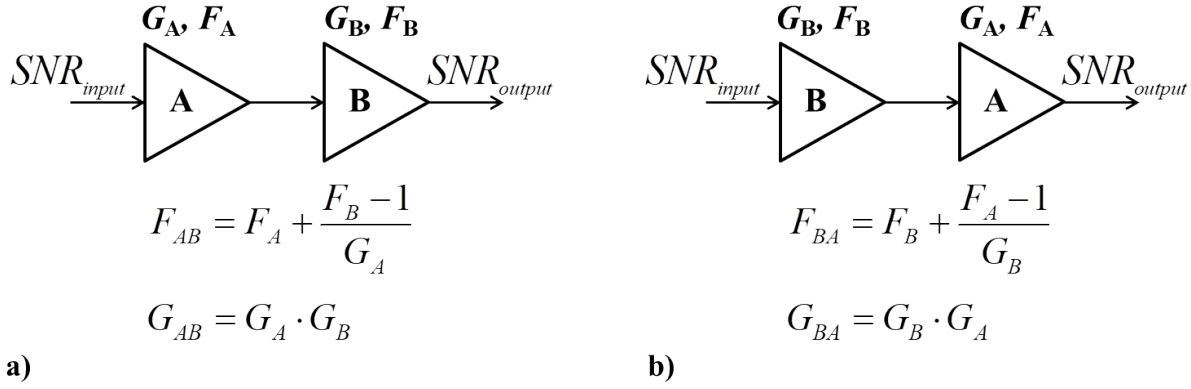

Figure 8.5: Two–stage amplifier: a) amplifier A as the first stage, amplifier B as the second stage; b) amplifier B as the first stage, amplifier A as the second stage

Table 8.1: Parameters of amplifiers A and B and calculated power gains and noise figures of the two possible cascade arrangements

Parameter	dB	lin.
G_A	30	1000
F_A	0.5	1.12
G_B	10	10
F_B	5	3.16
F_{AB}	0.5	1.12
G_{AB}	40	10000
F_{BA}	5.01	3.17
G_{BA}	40	10000

From Table 8.1 it can be seen that, just by switching places of the two amplifiers in the cascade, the power gain level stays the same, but the overall noise figure level can change for 4.51 dB, which is equal to 2.82 times in a linear scale! A quality factor that describes this

phenomenon is called noise measure, and it can be expressed as [39]:

$$M = \frac{F-1}{1-\frac{1}{G}}, \tag{8.35}$$

where M, F and G stand for noise measure, noise figure and power gain levels of the analysed cascade, respectively. The idea is to calculate noise measures for all possible arrangements of the elements in the cascade, and then pick the arrangement with the lowest noise measure value [39]. In the example described with Figure 8.5 and Table 8.1, noise measures M_{AB} and M_{BA} are equal to -9.21 dB and 3.37 dB in the logarithmic scale, or 0.12 and 2.17 in the linear scale, respectively. So, if one wants to achieve a two–stage NMR preamplifier with the lowest noise figure possible, the chosen cascade arrangement needs to be the one with the lowest noise measure. In the aforementoned example, that is the arrangement where the first stage is the amplifier A, while the second stage is the amplifier B. In fact, both possible combinations with the use of T77 and MC290 were tried out and the comparison of its measurements is shown in the lower part of Figure 8.9. Here, red curves represent the combination of MC290 as the first stage and T77 as the second stage, while blue curves represent the combination of T77 as the first stage and MC290 as the second stage. It can be seen that the power gain levels ($|S_{21}|$ parameters) are practically the same for both cases, but the overall noise figures differ for around 2.5 dB, which is equal to 1.78 times in the linear scale. Since power gain levels are equal, but the noise measure for the combination T77 + MC290 is 12.58 dB lower than for the case of the combination MC290 + T77, the former combination is chosen to be used as a two–stage NMR preamplifier (abbreviated as 2STA).

So, to sum up, with the cascade network comprised of the least noisy amplifier, T77, as the first stage, and MC290 as the second stage, a 2STA, whose power gain level is now comparable to the one of M290, but whose noise figure level is significantly lower than the one of M290, is created (absolute values of its S parameters and noise figure are shown as the blue curves in Figure 8.9). This preamplifier will now be compared to M290 and the frequency bandwidth, where the 2STA operates better than M290, will be determined.

The comparison of S parameters and noise figures of M290 (red curves) and 2STA (black curves) are shown in Figure 8.10. It can be seen that the 2STA has noise figure level lower than the one of M290 at almost entire frequency bandwidth between 0 and 500 MHz – the exception are frequencies lower than around 30 MHz. It can also be seen that its power gain level is greater than or equal to the one of M290 up to around one half of the frequency bandwidth between 0 and 500 MHz. This was expected, as upper operating frequency of MC290 is equal to 300 MHz, while M290 and T77 have upper operating frequencies equal to 500 MHz or higher. The output of the 2STA is also better isolated from the input, as its transmission parameter from the output to the input ($|S_{12}|$ parameter) is significantly lower than the one of M290. On the other

hand, both the input and the output of M290 are much better matched, which means that there will be less reflections in its vicinity. However, the 3 dB higher power gain level of the 2STA should compensate the impedance mismatch at its input and output. So, how to determine the frequency bandwidth in which the 2STA operates better than M290?

The idea is to first calculate corrected noise figures of both preamplifiers, as well as their corrected power gain levels, due to impedance mismatch at their inputs (according to subsection 6.2.3), and then calculate their ratios:

$$\Delta F_{corr.} = \frac{F_{corr.2STA}}{F_{corr.M290}} = \frac{1+\frac{F_{2STA}-1}{1-|S_{11_{2STA}}|^2}}{1+\frac{F_{M290}-1}{1-|S_{11_{M290}}|^2}}[\text{lin.}] = 10\log\left(\frac{1+\frac{F_{2STA}-1}{1-|S_{11_{2STA}}|^2}}{1+\frac{F_{M290}-1}{1-|S_{11_{M290}}|^2}}\right)[\text{dB}]; \tag{8.36}$$

$$\Delta G_{corr.} = \frac{G_{corr.2STA}}{G_{corr.M290}} = \frac{|S_{21_{2STA}}|^2(1-|S_{11_{2STA}}|^2)}{|S_{21_{M290}}|^2(1-|S_{11_{M290}}|^2)}[\text{lin.}] = 10\log\left(\frac{|S_{21_{2STA}}|^2(1-|S_{11_{2STA}}|^2)}{|S_{21_{M290}}|^2(1-|S_{11_{M290}}|^2)}\right)[\text{dB}]. \tag{8.37}$$

With the ratios (8.36) and (8.37) defined as such, the frequency bandwidth where 2STA operates better than M290, therefore, is the bandwidth where both $\Delta F_{corr.} < 1$ and $\Delta G_{corr.} > 1$ in the linear scale, or $\Delta F_{corr.} < 0$dB and $\Delta G_{corr.} > 0$dB in the logarithmic scale. These two ratios were obtained with the use of software suites MathWorks MATLAB [70] and Keysight Advanced Design System [71], and the results of the obtainment are shown in Figure 8.6.

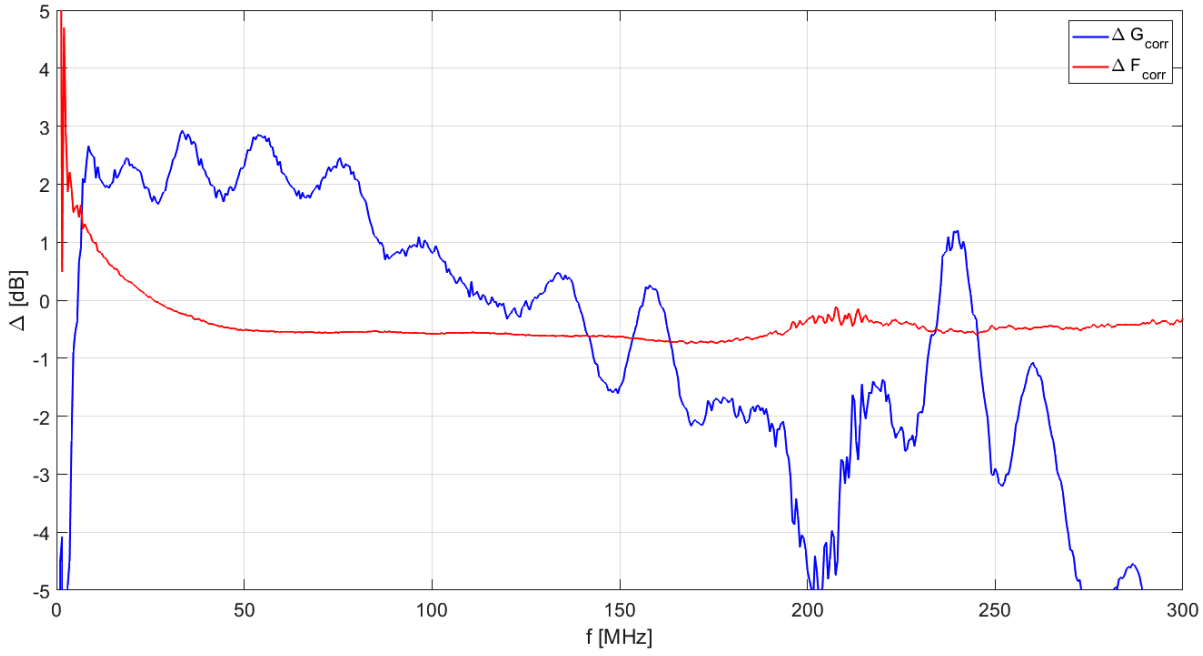

Figure 8.6: Enhanced performance area determination of the use of 2STA

From Figure 8.6 it can be seen that the condition $\Delta F_{corr.} < 0$dB is achieved in the frequency bandwidth $\langle 26\text{ MHz}, 300\text{ MHz}]$, while the condition $\Delta G_{corr.} > 0$dB is achieved in the frequency bandwidths $\langle 6\text{ MHz}, 114\text{ MHz}\rangle$, $\langle 127\text{ MHz}, 138\text{ MHz}\rangle$, $\langle 156\text{ MHz}, 160\text{ MHz}\rangle$ and $\langle 235\text{ MHz},$

243 MHz$\rangle$. So, the frequency bandwidth where both conditions are true are: $\langle 26\text{ MHz}, 114\text{ MHz}\rangle$, $\langle 127\text{ MHz}, 138\text{ MHz}\rangle$, $\langle 156\text{ MHz}, 160\text{ MHz}\rangle$ and $\langle 235\text{ MHz}, 243\text{ MHz}\rangle$. Roughly speaking, the enhanced performance area is achieved in the frequency bandwidth $\langle 26\text{ MHz}, 114\text{ MHz}\rangle$. This is an acceptable and actually a solid result as NMR measurements in the lower half of NMR measurement frequency bandwidth (which is equal to $\langle 0\text{ MHz}, 500\text{ MHz}]$) are the ones with the problem of low–level response signals from the samples under measurement

Furthermore, stability analysis of this amplifier, with the use of inequalities (8.14) and (8.15), has been performed, and the results can be seen in Figure 8.7.

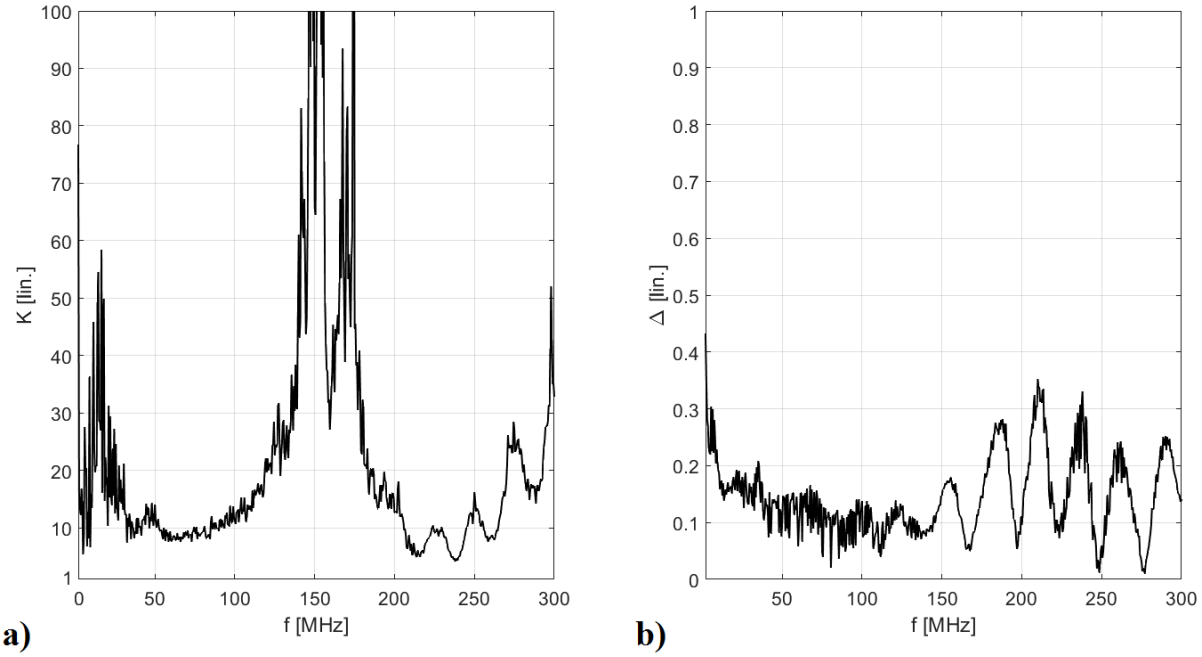

Figure 8.7: Stablity analysis of 2STA: a) Rollet condition (K); b) Auxiliary Rollet condition (Δ)

As it can be seen, both conditions ($K > 1$ and $\Delta < 1$) have been achieved, which proves the stable operation of 2STA. This concludes the analysis of the aforementioned amplifier.

Finally, it is necessary to mention that, although the frequency bandwidth of the enhanced performance area can be determined as described in this section, the level of overall enhanced performance of the entire NMR spectroscopy Rx chain cannot be determined without knowing the power gain, power loss, input reflection and noise figure levels of the rest of the elements in the chain. As the expression (6.16 shows), the overall enhancement performance area of the entire Rx chain depends on all the elements in the chain, so its level is different than the enhanced performance level of just the preamplifier.

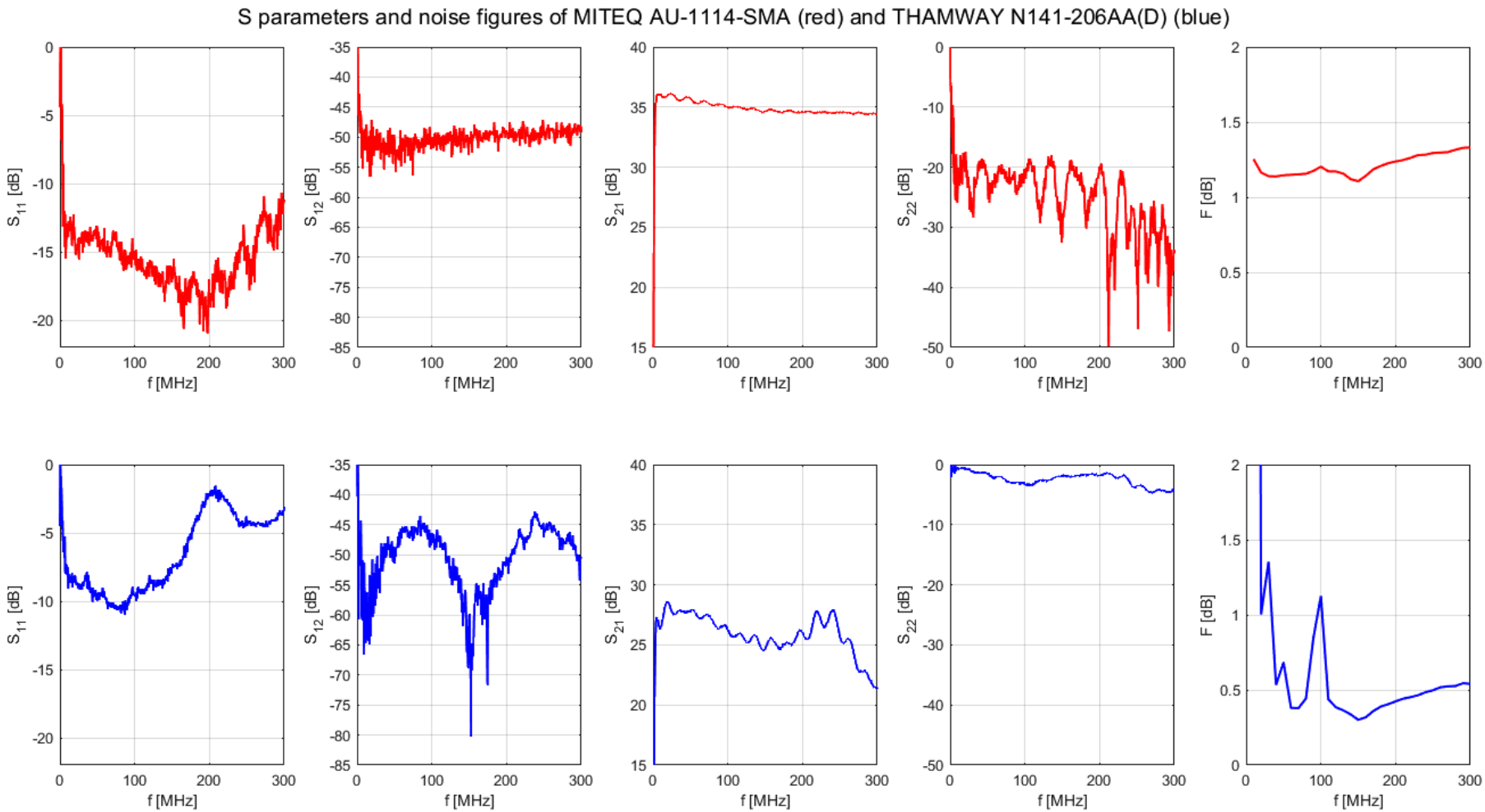

Figure 8.8: S parameters and noise figures of M290 (red) and T77 (blue)

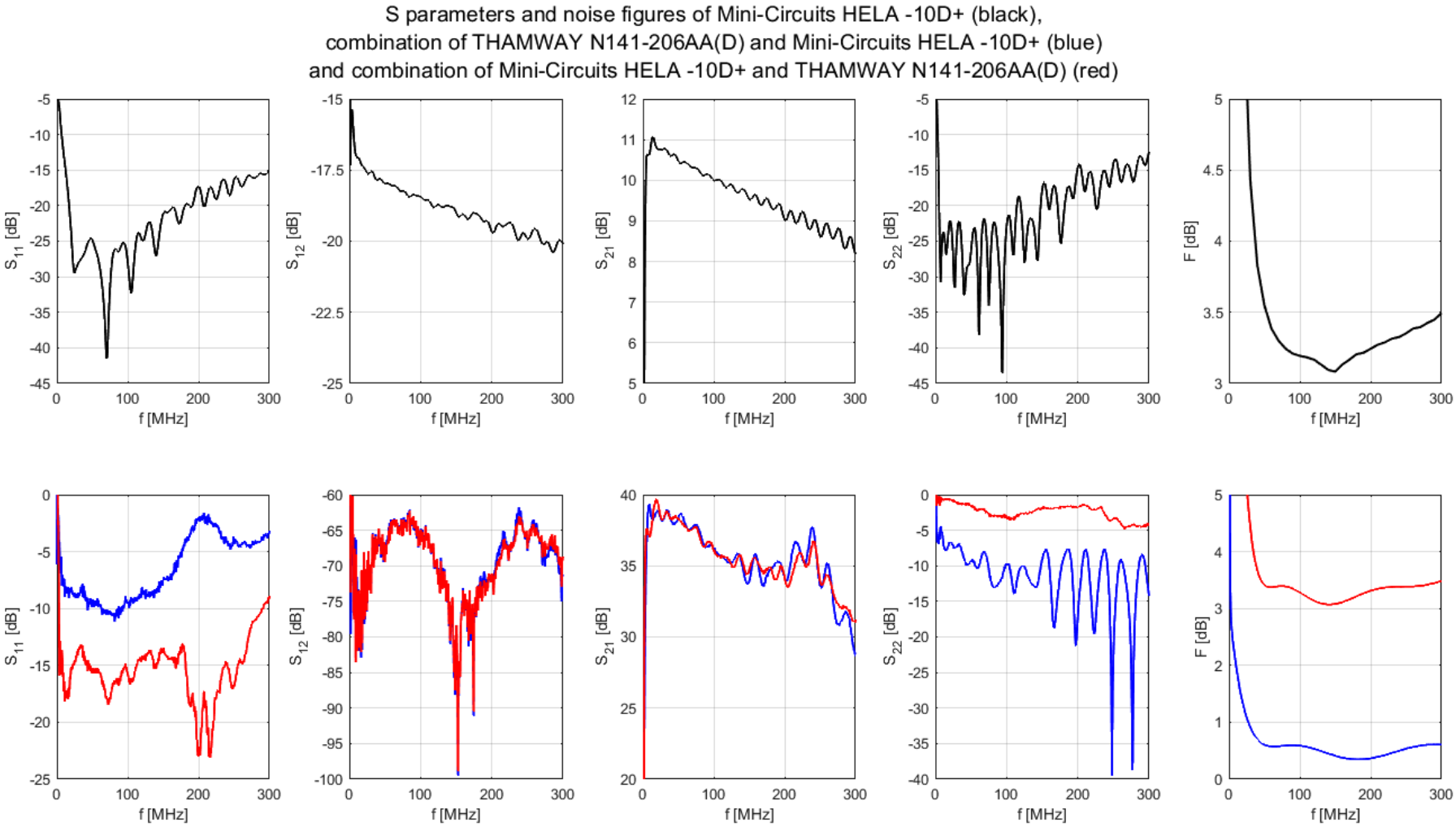

Figure 8.9: S parameters and noise figures of MC290 (black) and combinations of T77 + MC290 (blue) and MC290 + T77 (red)

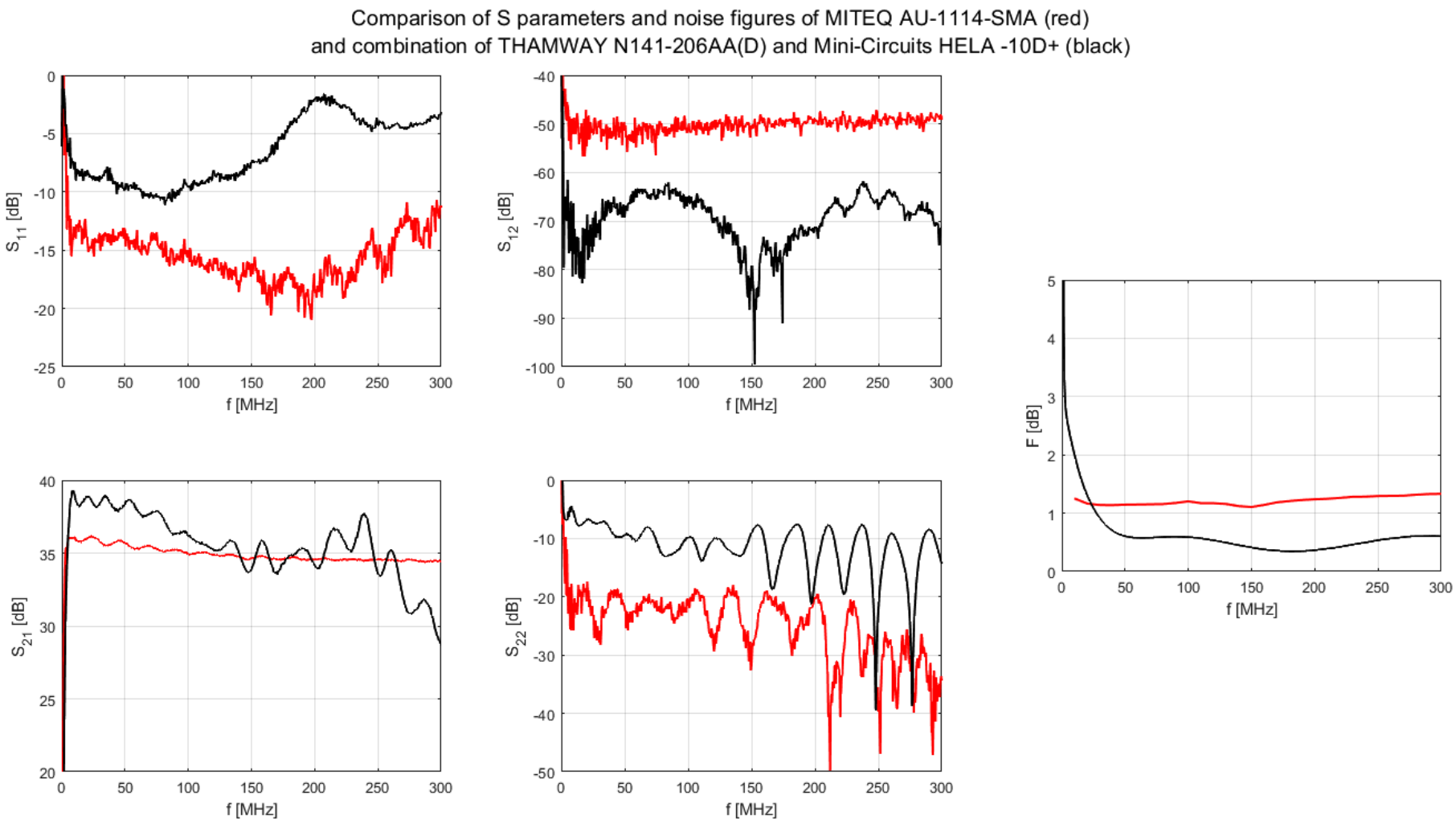

Figure 8.10: Comparison of S parameters and noise figures of M290 (red) and combination of T77 + MC290 (black)

8.3 Design and assembly of a high–gain and low–noise NMR preamplifier

In section 8.2, optimization process of the T77 cryogenic preamplifier by the addition of the MC290 second stage amplifier was described. It was shown that this way, it is possible to achieve enhanced performance in the frequency bandwidth between 26 MHz and 114 MHz. Although these results are more than satisfactory, frequencies below 26 MHz still cause problems as $1/f$ noise level becomes the dominant noise source. This occurs because its level becomes greater than the level of thermal noise. So the idea is to design and build a new NMR preamplifier, whose enhanced performance frequency bandwidth is situated below 26 MHz, by the use of the best available technology. Because T77 showed to have the lowest noise figure of all the available preamplifiers in our laboratory (see Table 7.2), the idea was to somehow analyse the technology used to build T77, and then make an attempt to design a new preamplifier with the guidance of the T77's example. So the first step was to perform X-ray scans of the T77 preamplifier in order to see what does it have "under the hood". X-ray scans of the preamplifier T77 are shown in Figure 8.11. They were performed at the Faculty of Mechanical Engineering and Naval Architecture of University of Zagreb, Croatia, in the Laboratory for Non-destructive Testing [72], under the guidance of professor Damir Markučič, PhD.

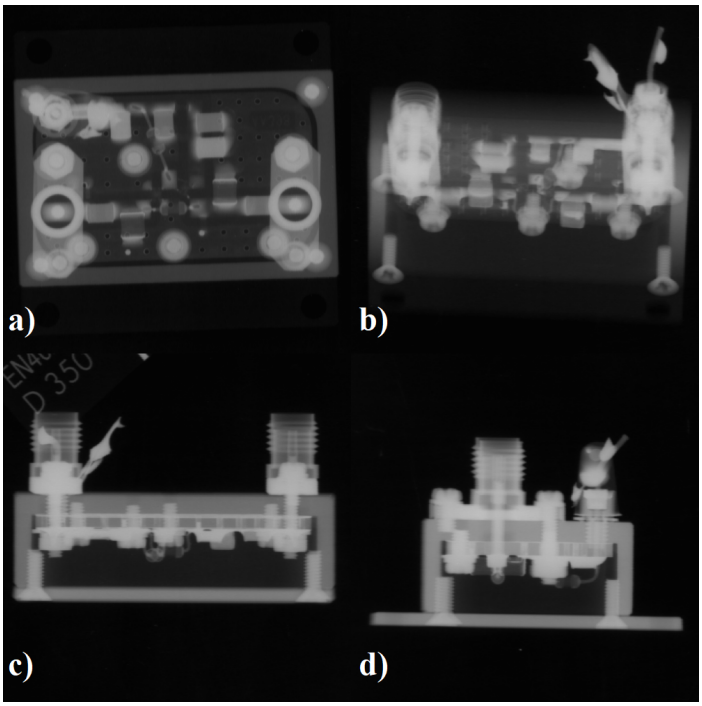

Figure 8.11: X-ray scan of T77: a) Top view; b) Long axis isometric view; c) Front view; d) Right side view

The analysis of obtained X-ray scans of T77 showed that it could potentially be a two–stage amplifier with basic transistor configurations (common emitter, common collector or common

base if BJTs are used, or common source, common drain or common gait if FETs are used). Furthermore, they showed potential positions of the active elements. However, as the scans also showed that it is possible to remove one side of the T77's enclosure without destroying the preamplifier, so that one could see its PCB by a naked eye, and not just by X-radiation, it was decided to do just that. Accordingly, the photo of T77 can be seen in Figure 8.12.

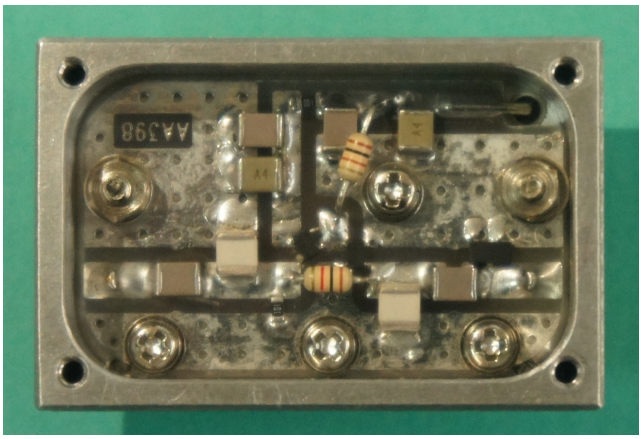

Figure 8.12: Photo of T77's PCB

In order to better see the package marking of the components on the PCB (since they are SMD components), microscopic photos of the T77 preamplifier were also obtained, and some of them can be seen in Figure 8.13. These photos were obtained at the Faculty of Electrical Engineering and Computing of University of Zagreb, Croatia, in the Applied Optics Laboratory [73], under the guidance of professors Dubravko Babić, PhD, and Zvonimir Šipuš, PhD.

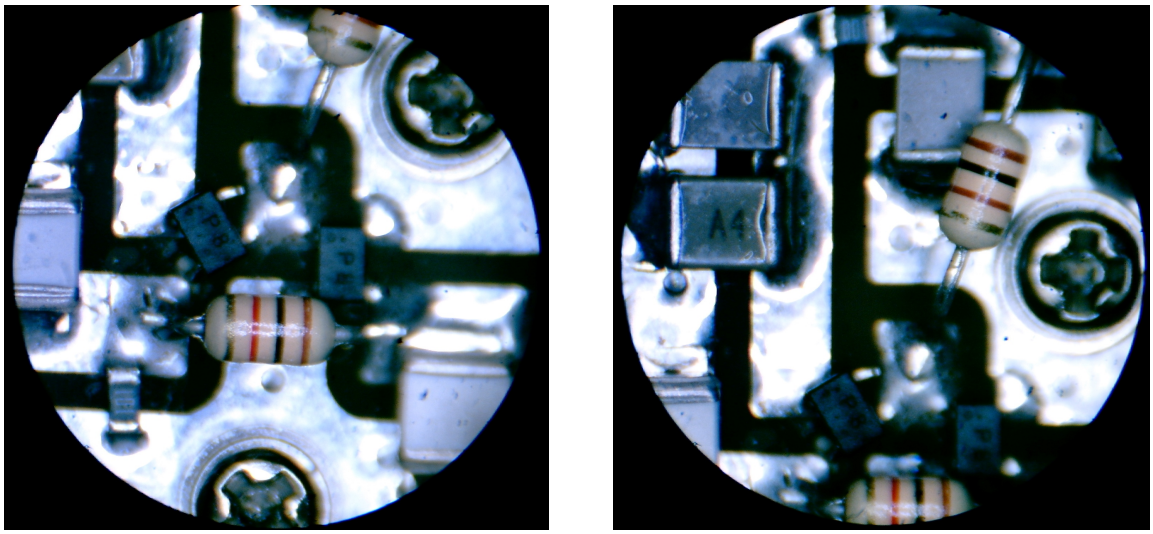

(a) (b)

Figure 8.13: Two microscopic photos of T77's active elements and their environment

According to all the taken photos of T77 (Figures 8.12 and 8.13), it is possible to derive the schematic of T77, which is shown in Figure 8.14.

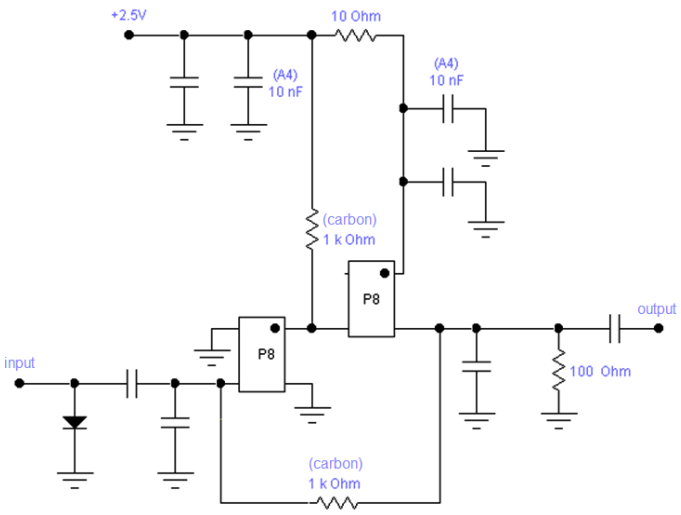

Figure 8.14: T77's schematic diagram (derived from Figures 8.12 and 8.13)

Of course, the biggest problem here is to determine the type of the active elements. At least, the package marking of both active elements are the same, so both the elements are the same type and model. In order to determine their type, it is necessary here to use the method of deduction.

First of all, one can see in Figure 8.14 that the inputs of both the active elements are not used as differential inputs, and none of the elements have a resistive voltage divider connected to its feedback. Therefore, these active elements cannot be operational amplifiers.

In order to determine the exact type of transistors, one needs to bear in mind that T77 has very low noise figure levels – even lower than 0.3 dB at certain frequencies (see Table 7.2 and Figure 8.8)! Therefore, an extensive research of databases of available transistors was done via websites of globally known electronic component distributors, such as Farnell [74] and Mouser Electronics [75], in order to find the right transistors with noise figure levels as low as 0.3 dB. Naturally, as BJTs are current controlled transistors, while FETs are voltage controlled transistors, the research has first shown that the BJTs in general are notably noisier than the FETs. Therefore, a further, and more precise, research of databases of available FET transistors was done in order to find FET transistors with appropriate noise figure levels. The research shown that the only type of FET transistors with such a low noise figure level is HEMT. So, the active elements that T77 is comprised of might be some kind of a HEMT.

After it was determined that the active elements inside T77 are HEMTs, another research of available HEMTs' databases via Farnell and Mouser Electronics was performed in order to determine model of transistors, whose characteristics (like its maximum gain, its maximum input signal levels, its statics and its power consumption) are close enough to the ones of the transistors inside T77. As it can be seen in Figure 8.13, the package marking on the transistors is "P8", and their packaging seems to be some kind of a SOT packaging – something like

SOT323 or SOT343. The aforementioned research clarified Broadcom ATF–34143 [76], or a similar model in the same family, as a potential transistor, since its packaging marking, as well as its SOT packaging, is similar to the one of the transistors inside T77. The comparison of the packaging of transistors inside T77 and ATF–34143 is shown in Figure 8.15. Furthermore, the drain current value of ATF–34143 showed to be of the same order of magnitude as the same current of the transistors inside T77, which means that this transistor model could be used to construct a low–noise NMR preamplifier.

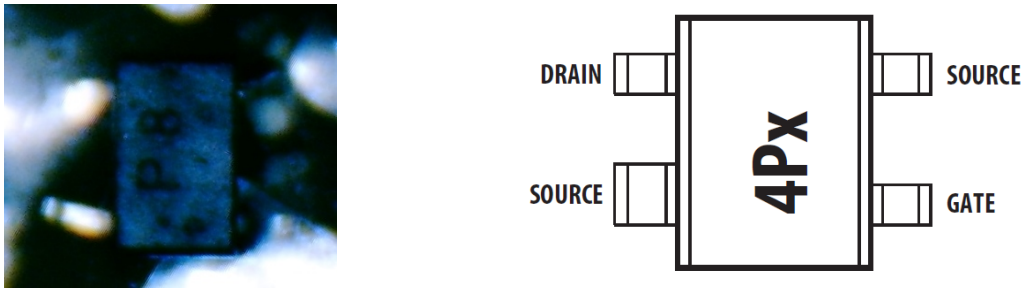

(a) Transistors inside T77 (b) ATF–34143

Figure 8.15: Transistors packaging comparison

Now that the type and the potential model of transistors inside T77 are known, the next step is to examine the schematic diagram of T77, shown in Figure 8.14. If the assumptions described here are true, then T77 is a two–stage preamplifier, where the second stage could be the common–drain amplifier (the so–called source follower), while the first stage could be the common–source amplifier. Here, the first stage is the one that is responsible for the amplification of the input signal, as the common–source topology offers the highest gain level of the three basic single–stage amplifier topologies. However, this topology offers output impedance much higher than Z_0, which causes high output reflection levels. This is why it is a good idea to insert the common–drain amplifier as the second stage amplifier, since this topology offers possible values of output impedance around the value of Z_0. The price paid is the decrease of overall gain level, as the second stage's topology offers gain levels lower than 1 (i. e. 0 dB). Another important thing to notice is the negative feedback, which is the 1 kΩ resistor connected between the output of the second stage and the input of the first stage. This feedback stabilizes the operation of the entire preamplifier, but the price paid is a slight decrease of overall gain level and a slight increase of overall noise figure level. Of the rest of the elements on the PCB, the resistors, except the one in the negative feedback, serve to define the operating point of the preamplifier, two capacitors connected in series to the input and the output of the preamplifier serve to isolate the preamplifier from DC signal coming from the power supply, while the rest of the capacitors are used as DC bias filters. The diode at the input of the preamplifier, connected to the ground, serves as the input power limiter in order to protect the preamplifier from input signals of too high level destroying it.

Furthermore, as it was shown in Table 3.1, that the HEMT–based technique is the best technique from the aspect of noise characteristics, to design and assemble a high–quality NMR preamplifier, the described schematic will serve as a foundation for a new design of NMR preamplifier, which should have notably higher power gain level than T77, while retaining noise figure level around the one of T77.

For the first step, in order to check if ATF–34143 transistors really are similar enough to the used transistors, a copy of T77 was constructed. The PCB of the constructed amplifier is shown in Figure 8.16.

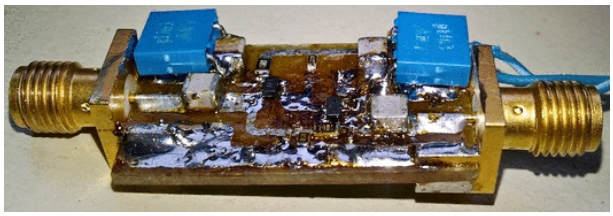

Figure 8.16: PCB of the constructed amplifier

Both original T77's gain (or S_{21} parameter) and phase, and the one of its "copy", were measured, and results comparison can be seen in Figure 8.17.

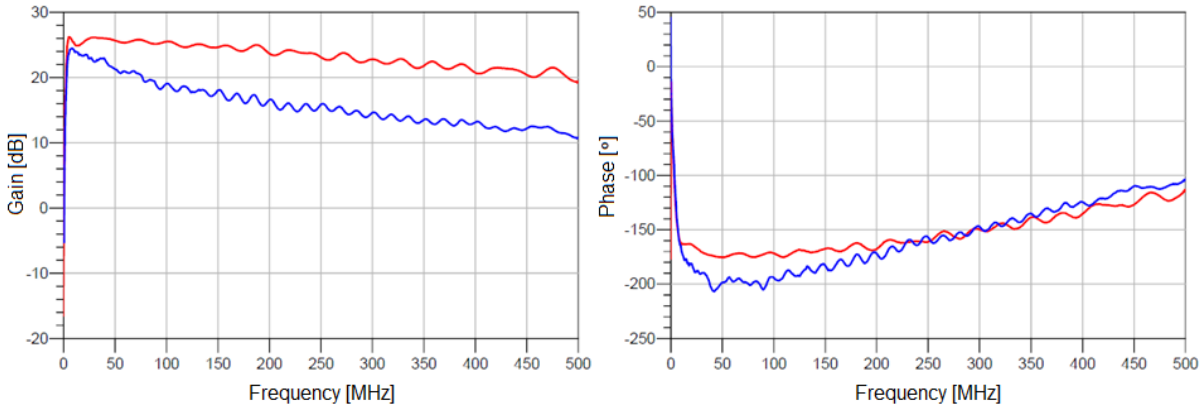

Figure 8.17: Comparison of gain levels and phases of original T77 (red) and its "copy" (blue)

It can be seen that maximum gain level of original T77 (red) is similar to the one of its "copy" (blue). There is, however, a difference in the roll–offs in transfer functions, as original T77's gain level declines for the value of 6 dB per the decade 50–500 MHz (red), while the gain level of the "copy" decays for the value of 16 dB per the same decade (blue). Because of this, it is obvious that the ATF–34143 transistors are not equal to the transistors used in T77, but since the power gain levels of both transistor types are almost identical at lower frequencies (which can be seen in Figure 8.17), it was decided that the ATF–34143 transistors are good enough to be used in the low–noise NMR preamplifier design, so the next stage of the design, which is the analysis, design and construction of the new–constructed amplifier, was immediately initiated.

But before the actual analysis, one more research has been performed. Although ATF–34143 transistor proved to be good enough for the new preamplifier, it was noticed that new, improved, transistors were made available in the same family of transistors. These transistors, such as ATF–54143 [77] and ATF–55143 [78] provided notably higher power gain level with noise figure of the same or even lower level than ATF–34143. In the end, ATF–55143 was chosen for the design of the new amplifier because, although its maximum power gain is slightly lower than the one of ATF–54143, it provides more stable operation of the device it is the main part of than ATF–54143, while their noise figure levels are almost identical. Finally, the next step is the analysis, design and construction of the new preamplifier.

The schematic diagram of the new–constructed NMR preamplifier is shown in Figure 8.33. The new–constructed preamplifier (NCP) is a two–stage amplifier, where its second stage is a regular common–drain amplifier (or source follower), while its first stage is a common–source amplifier with a noise compensating resistor (lower part of Figure 8.33). The power supply network (upper part of Figure 8.33) of NCP is done by a standard network with the use of a voltage regulator LM317 [79] as its main part. As the main objective for this amplifier is to achieve its gain (or its $|S_{21}|$ parameter) as high as possible, both stages were tuned in to their highest possible gains, while at the same time, the amplifier works in a stable operating regime. Also, because of the main objective, this amplifier has no feedback built in since the negative feedback lowers the overall gain down, while the positive feedback practically turns an amplifier into an oscillator, which is obviously an unwanted effect here.

To correctly explain the effect of the noise compensating resistor [26], one needs to examine both static (Figure 8.18) and dynamic analysis (Figure 8.19) of the first stage of the NCP – the common–source amplifier. If one derives an expression for the common–source's gate–to–source voltage, U_{GS}, without noise compensating resistor (Figure 8.18a), one gets the expression as follows:

$$U_{GS} = U_{DD} \frac{R_{G_2} R_{GS}}{R_{G_1} R_{G_2} + R_{G_1} R_{GS} + R_{G_2} R_{GS}}. \tag{8.38}$$

Furthermore, the expression for the same type of the amplifier, but with noise compensating resistor (Figure 8.18b), is expressed as:

$$U_{GS} = U_{DD} \frac{R_{GS}}{R_{comp} + R_{GS}} \frac{R_{G_2} R_{comp} + R_{G_2} R_{GS}}{R_{G_1} R_{G_2} + R_{G_1} R_{comp} + R_{G_1} R_{GS} + R_{G_2} R_{comp} + R_{G_2} R_{GS}}. \tag{8.39}$$

As FETs have input resistance, R_{GS}, much higher than the values of the resistors forming the transistors' operating points [61], (8.39) can be approximated to be equal to (8.38):

$$\begin{aligned} &\lim_{R_{GS} \to \infty} U_{DD} \frac{R_{G_2} R_{GS}}{R_{G_1} R_{G_2} + R_{G_1} R_{GS} + R_{G_2} R_{GS}} = U_{DD} \frac{R_{G_2}}{R_{G_1} + R_{G_2}} = \\ &= \lim_{R_{GS} \to \infty} U_{DD} \frac{R_{GS}}{R_{comp} + R_{GS}} \frac{R_{G_2} R_{comp} + R_{G_2} R_{GS}}{R_{G_1} R_{G_2} + R_{G_1} R_{comp} + R_{G_1} R_{GS} + R_{G_2} R_{comp} + R_{G_2} R_{GS}}. \end{aligned} \tag{8.40}$$

This means that the operating point values of the NCP's first stage practically remain unaltered with the addition of the noise compensating resistor and C_{G_2}, as it is shown in (8.40), since the change of U_{GS} value is negligible.

When one, on the other hand, performes dynamic analysis of the case without (Figure 8.19a) and with noise compensating resistor (Figure 8.19b), it can be seen that the capacitor C_{G_2} short–circuits resistors R_{G_1} and R_{G_2} to the ground, leaving only noise compensating resistor, R_{comp}, to affect the dynamics of this stage. Again, it is shown that the addition of R_{comp} and C_{G_2} does not change the U_{GS} voltage value, but there is one crucial thing that is changed here. As it is explained in Chapter 4, resistors are one of the main generators of thermal noise in every electronic circuit, and available thermal noise power generated by a single resistor can be expressed as described in (4.6):

$$N_t = kT\Delta f.$$

Furthermore, it can be shown that, since resistors are mutually non–correlated noise sources, their available thermal noise powers sum up [26]:

$$N_{t_{overall}} = N_{t_{R_1}} + N_{t_{R_2}} + \cdots + N_{t_{R_i}}. \tag{8.41}$$

Therefore, the overall available thermal noise power in the case without the noise compensating resistor (Figure 8.19a) is equal to:

$$N_{t_{woR_{comp}}} = N_{t_{R_{G_1}}} + N_{t_{R_{G_2}}} = kT\Delta f + kT\Delta f = 2kT\Delta f. \tag{8.42}$$

On the other hand, in the case with the noise compensating resistor (Figure 8.19b), if there would not have been the capacitor C_{G_2}, the overall available thermal noise power would here be equal to:

$$N_{t_{wR_{comp}}}|_{woC_{G_2}} = N_{t_{R_{G_1}}} + N_{t_{R_{G_2}}} + N_{t_{R_{comp}}} = kT\Delta f + kT\Delta f + kT\Delta f = 3kT\Delta f. \tag{8.43}$$

However, since the capacitor C_{G_2} is connected, it practically short–circuits resistors R_{G_1} and R_{G_2} to the ground, thus removing their generated thermal noise, leaving the overall available thermal noise power to be equal to:

$$N_{t_{wR_{comp}}}|_{wC_{G_2}} = N_{t_{R_{comp}}} = kT\Delta f. \tag{8.44}$$

To sum up, expressions (8.40), (8.42) and (8.44) show that the addition of the noise compensating resistor and the capacitor C_{G_2} does not change the operating point of the amplifier, while

decreasing the overall input thermal noise power to one half:

$$U_{GS_{woR_{comp}}} \approx U_{GS_{woR_{comp}}}; \quad \frac{N_{t_{woR_{comp}}}}{N_{t_{wR_{comp}}}} = 2. \tag{8.45}$$

This noise compensating method was used at the first stage of NCP only. As it was explained in section 4.4, the first stage of a system affects overall noise figure the most, and, if the power gain level of the first stage is high, the effects of the latter stages in the system are negligible. This is the case with NCP, as its first stage is set to have power gain level as high as possible. Therefore, the effect of the second stage on the overall noise level is negligible. Additionally, to show the effect of R_{comp} described in the last paragraphs, NCP's S parameters were simulated for both the cases when there is R_{comp} in its schematic, and when there is no R_{comp} in the schematic. The comparison results are shown in Figure 8.20.

It is also important to address the importance of the resistance value selection for the noise compensating resistor, R_{comp}. Namely, as this resistor creates a voltage divider with the parallel combination of R_{G_1} and R_{G_2} (see Figure 8.19b), it is necessary for the resistance value of R_{comp} to be much higher than the one of $R_{G_1}||R_{G_2}$ in order for the entire input signal to enter the transistor input and then get amplified and sent to the next stage of the NCP [26]:

$$R_{comp} \gg R_{G_1}||R_{G_2}. \tag{8.46}$$

As it can be seen in Figure 8.33, the parallel combination $R_{G_1}||R_{G_2}$ is equal to $R_{G_1}||R_{G_2} = 240\text{k}\Omega||10\text{k}\Omega = 9.6\text{k}\Omega$, which is less than one tenth of the resistance value of the noise compensating resistor, whose value is equal to 100kΩ. Clearly, the condition described in (8.46) is met here. On the other hand, R_{comp} needs to be kept a few orders of magnitude smaller than the transistors input resistance, R_{GS}, in order for the assumption, described with (8.40), to be true. Usually, FET's input resistances at lower frequencies go high up to an order of a few hundreds of MΩ, so the value of 100 kΩ for R_{GS} is clearly low enough for the aforementioned assumption to be fulfilled. Also, a good idea is to choose a low–noise resistor to be R_{comp} in order to additionally decrease input noise power level [26].

Of course, this method only decreases the input thermal noise levels. The input levels of the other noise types, such as $1/f$ noise, remain unaltered even after the use of this method. But as one of the main objectives in the design of the NCP is for the NCP to have the least noise figure possible, this method was still used in the new design, as it did fix the problem with at least one of the possible noise types, which is the thermal noise.

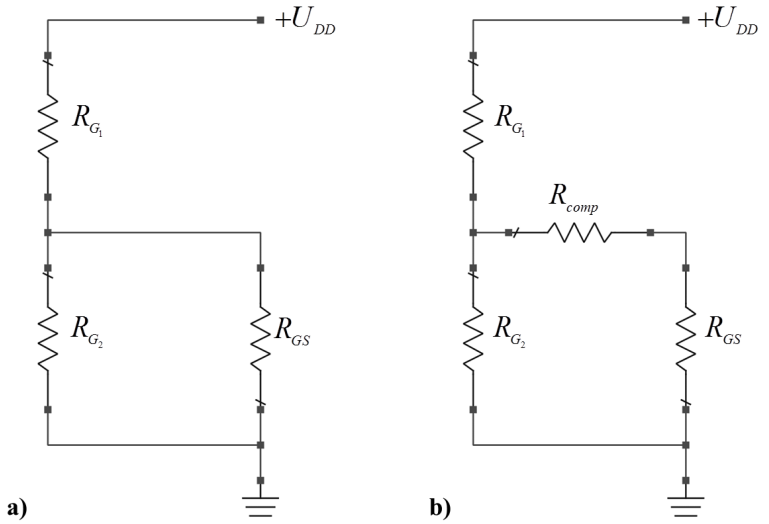

Figure 8.18: Static analysis of the NCP's first stage:
a) without noise compensating resistor; b) with noise compensating resistor

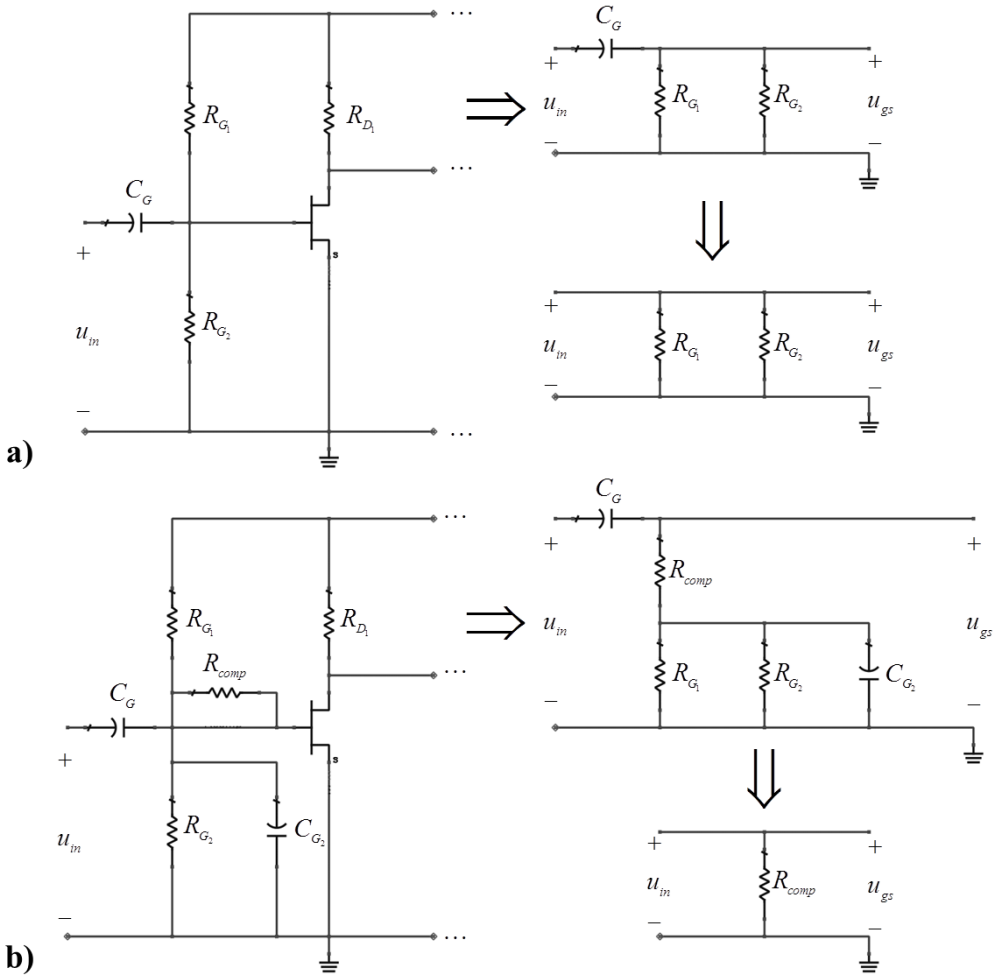

Figure 8.19: Dynamic analysis of the NCP's first stage:
a) without noise compensating resistor; b) with noise compensating resistor

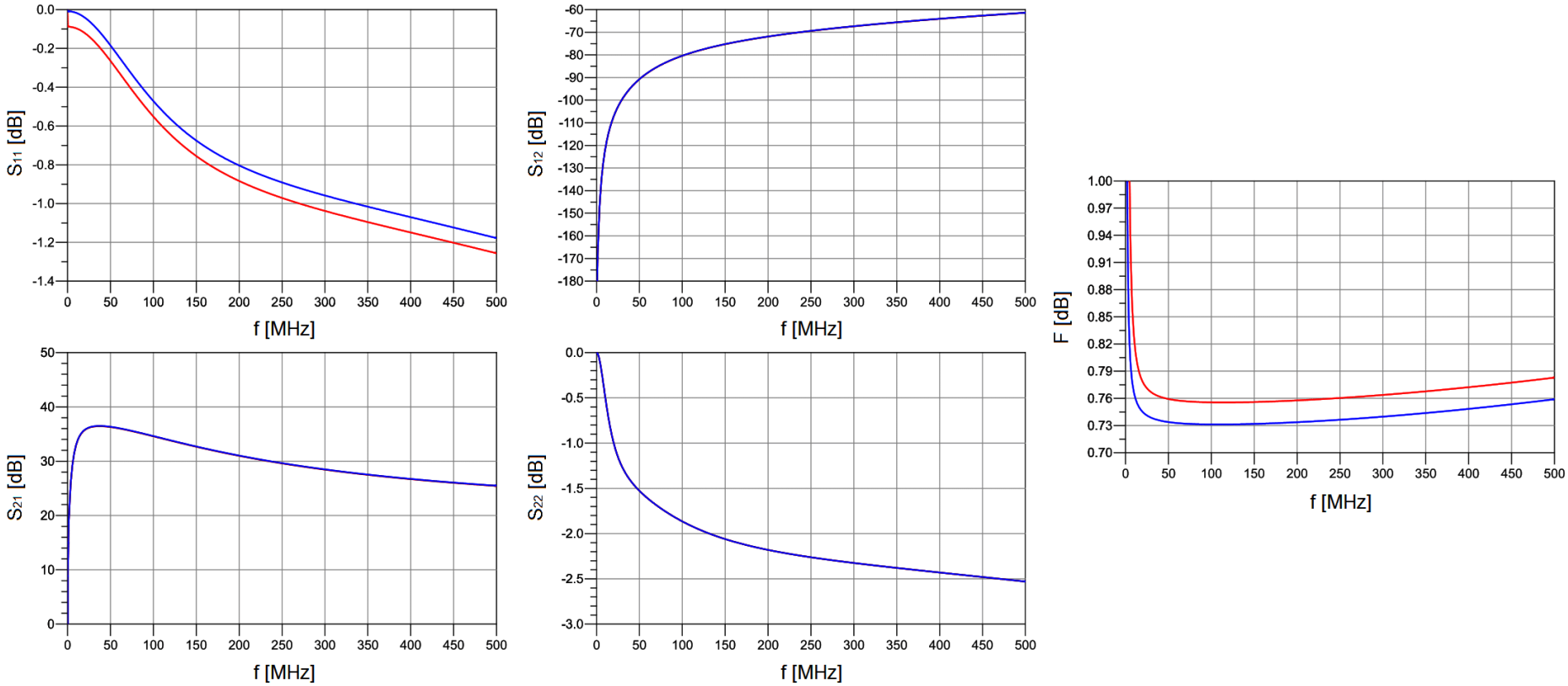

Figure 8.20: NCP's S parameters: red – without R_{comp}; blue – with R_{comp}

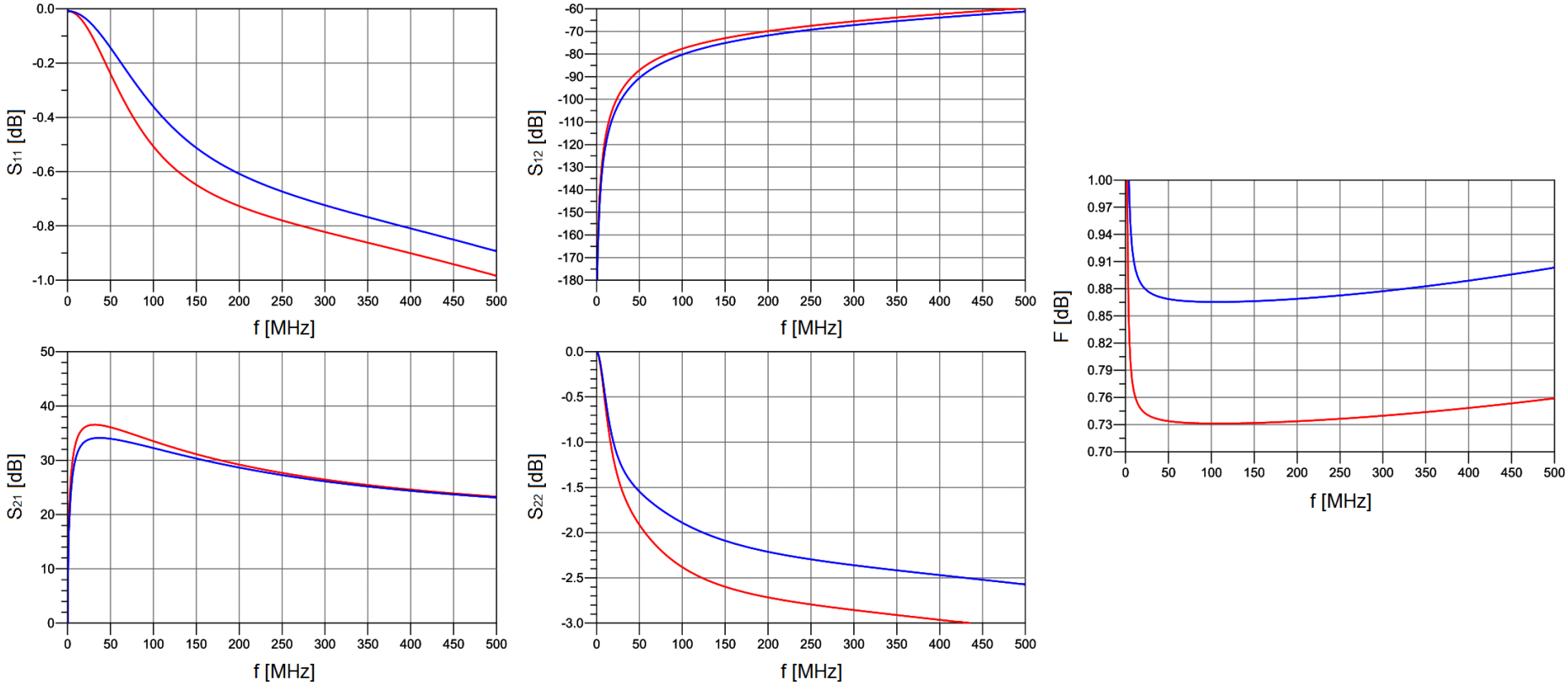

Figure 8.21: NCP's fine–tuning results: blue – initial state; red – fine-tuned state

The rest of the elements were chosen by performing static and dynamic analysis of the NCP so that it generates ultra high power gain and, hopefully, ultra low loss noise figure at low NMR frequencies (10–30 MHz). R_{G_1}, R_{G_2} and R_{D_1} were chosen so that the first stage of NCP generates power gain level of 40 dB for maximum input signal levels of 100 μVpp, with voltages U_{GS} and U_{DS} being equal to 0.4 V and 0.75 V, respectively. R_{G_3}, R_{G_4} and R_{S_2} were chosen so that the second stage of NCP generates power gain level of -0.5 dB for maximum input signal levels of 10 mVpp, with voltages U_{GS} and U_{DS} being equal to 0.5 V and 3 V, respectively.

It is important to mention here that these two operating points are different than the optimal operating point of ATF–55143 ($U_{DS} = 2.7$V, $U_{GS} = 0.47$V, $I_{DS} = 10$mA), quoted in its datasheet [78]. This is because the aforementioned operating point's operating frequency is equal to 2 GHz, as this type of transistors is primarily intended to be used in cellular, wireless data systems and other systems in the 450 MHz to 6 GHz frequency range. Therefore, the idea is to set the NCP's operating point in a way so that the U_{GS} voltage level is set as low as possible, causing the I_{DS} current level to be low. This way, $1/f$ noise levels in the resistors and shot noise levels in the transistors adopt lower values. Also, because of the lower I_{DS} value, the resistors get heated less, which leads to lower thermal noise levels generated by the resistors. Hence, the proposed schematic for NCP, shown in Figure 8.33, with elements' values determination described in the former paragraph, was simulated with the use of Keysight Advanced Design System [71], and all the NCP's elements were fine–tuned in order to achieve the lowest noise figure possible at low NMR frequencies (10–30 MHz), while in the same time allowing maximum input signal levels high enough for the expected input NMR response signals not to switch NCP's operation into saturation, or even destroy the amplifier. The fine–tuning results can be seen in Figure 8.21. Still, in the end, the chosen operating points of both transistors are not far from the optimal one, as the total current that the NCP "pulls out" from the supply equals 17 mA, which is quite close to 20 mA, the value of the current that the transistors would "consume" if their operating points would have had optimum values.

Now is the time to explain the selection of the resistance values for R_{G_1} and R_{G_2}. Although their ratio is only important for the first stage's operating point (as these two resistors form a voltage divider which sets the right potential of the transistor's gate), their resistance values need to be of a proper order of value. Namely, as FETs generally have very large input resistance (which is also true for the used ATF–55143 transistors), the resistance values of R_{G_1} and R_{G_2} need to be around the same order of magnitude of the transistor's input resistance value. This way, the reflections between these two resistors and the transistor's input become very low. Of course, as the input signal enters the amplifier from a 50–ohm system, the reflections between the amplifier's input and the two aforementioned resistors now become higher. However, as there is a notably smaller chance here of creation of a non–wanted positive feedback,

this scenario is more acceptable than the one with high reflections between the resistors and the transistor's input, as signal reflections don't get amplified this way, and there is no danger of the amplifier entering the unstable operating regime.

An additional thing a PCB designer needs to think about is the type selection of resistors to be put on the new PCB. It must not be forgotten that the NCP needs to be used in NMR spectroscopy, where the measured sample receives pulse excitation, and the measured signal is a pulse response signal (see Chapters 2 and 3). This means that the chosen resistors need to be able to withstand power levels of the NMR pulse response signals. On the other hand, as modern samples, measured with the use of NMR spectroscopy in the last few years, have very low–level response signals, the chosen resistors need to generate as little noise as possible, since any generated noise creates a problem for low–level measured NMR signals. Unfortunately, the type of resistors that withstands the highest–level pulses is not the one that generates the lowest noise power level. The comparison of pulse load capability of different resistor types can be seen in Figure 8.22a, while the comparison of generated noise of different resistor types can be seen in Figure 8.22b.

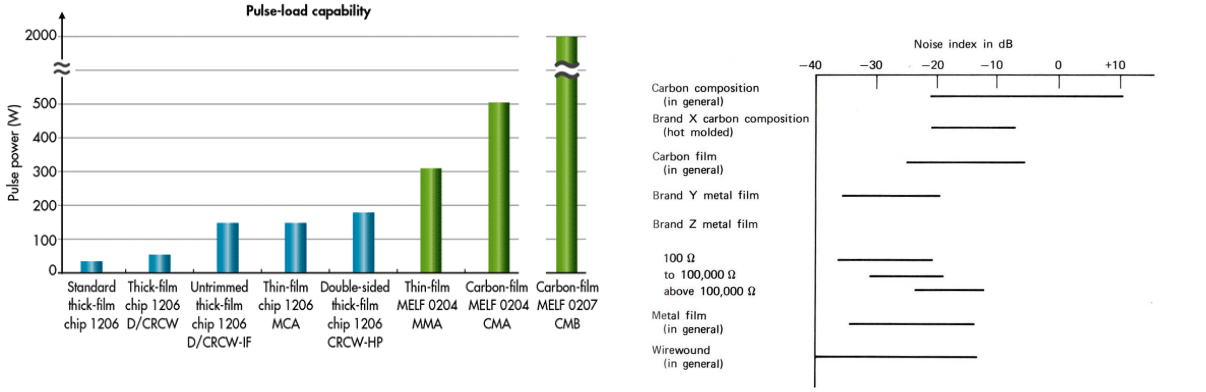

(a) Pulse load capacity of different resistor types [80]

(b) Generated noise of different resistor types [26]

Figure 8.22

This is why it is necessary to be able to predict the input signal power level in order to choose the right resistor type – the one that can withstand the predicted input signal power level, while at the same time it generates the lowest noise power level possible. Fortunately, as the power levels of the input NMR signals are lower than -50 dBm (which is equal to 10 nW), so all the resistor types can withstand such a low signal, thin metal film resistors were chosen to be put onto the NCP's PCB, as these resistors generate low noise levels.

As it was mentioned earlier, before the actual construction of the NCP, its simulations, with the use of Keysight Advanced Design System, were performed in order to tune in all the elements so that they achieve maximum gain with as low noise figure level as possible (Figure 8.21). Furthermore, stability analysis of simulated NCP, with the use of inequalities

(8.14) and (8.15), has been performed, and the results can be seen in Figure 8.23.

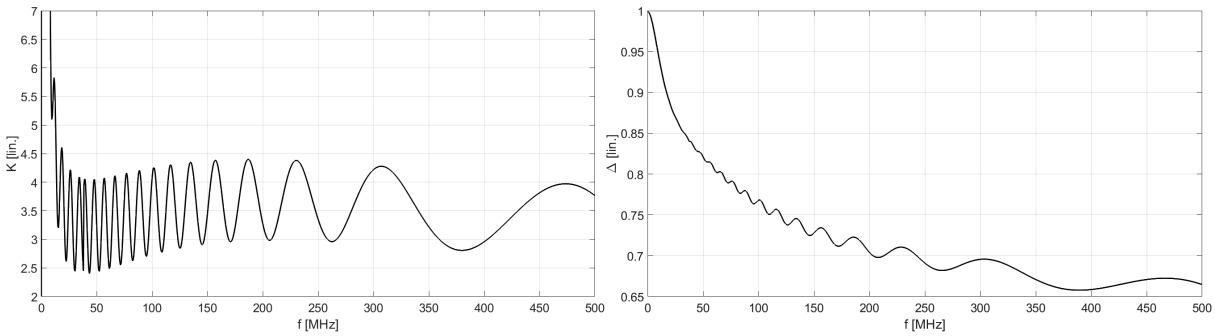

(a) Rollet condition (K)

(b) Auxiliary Rollet condition (Δ)

Figure 8.23: Stablity analysis of simulated NCP

As it can be seen, both conditions ($K > 1$ and $\Delta < 1$) have been achieved, which proves that NCP should have stable operation. Therefore, after the simulation results showed satisfactory results, the prototype of NCP has been designed and constructed and its measurement results have been compared to the simulation results. The results' comparison is shown in Figure 8.24a, simulated NCP's noise figure is shown in Figure 8.24b, while NCP's PCB layout and the prototype's PCB can be seen in Figures 8.31 and 8.30, respectively. The "ripples" in the measured S_{21} transfer characteristics are caused by a small reflection due to unavoidable small impedance mismatch, and relatively rugged VNA calibration (it was done without the through–open–short–match calibration kit; instead, the inputs of the cables connected to ports 1 and 2, when nothing is connected to them, were declared to be open, and by the de–embedding process of both ports in the S_{11} and S_{22} Smith charts, the calibration was done with the use of the VNA to "make" both cable inputs open in the entire observed frequency band – which is from 0 MHz to 500 MHz).

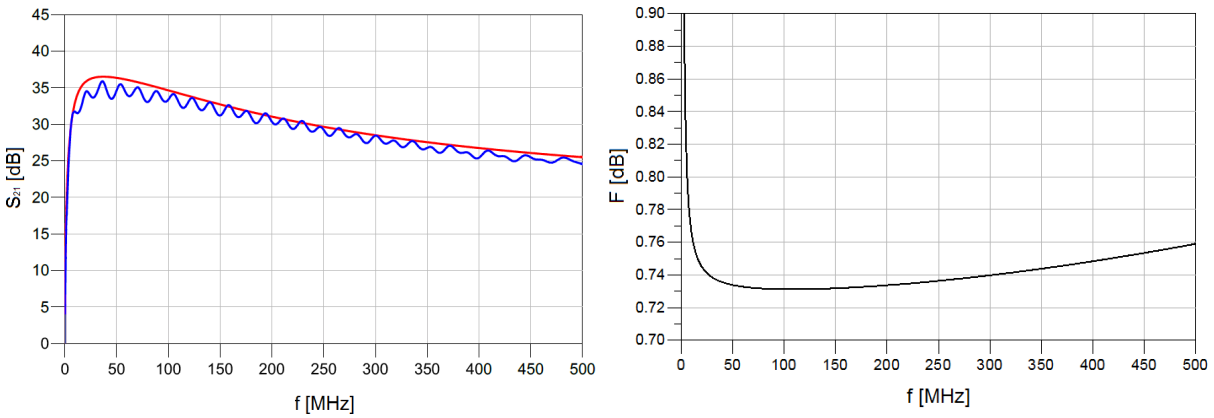

(a) Comparison of NCP's simulated (red) and measured S_{21} parameter results (blue)

(b) Simulated NCP's noise figure

Figure 8.24

The comparison of measured power gain levels of T77 and NCP can be seen in Figure 8.25a, while the comparison of measured T77's noise figure and simulated NCP's noise figure can be seen in Figure 8.25b.

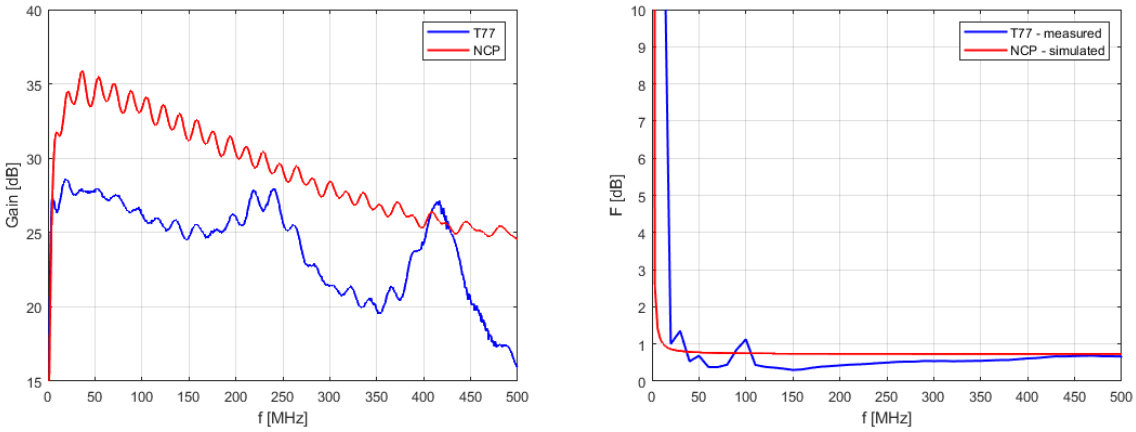

(a) Power gain comparison

(b) Noise figure comparison

Figure 8.25: Comparison of T77 vs NCP

As it was described at the end of section 8.2 of this chapter, in order to achieve enhanced results with NCP, compared to T77, both NCP's power gain level needs to be higher than the one of T77, and its noise figure level needs to be lower than the one of T77. It can be seen in Figure 8.25 that both conditions are achieved at low frequencies (around 30 MHz and below), which is exactly the targeted frequency bandwidth. Obviously, the enhancement of noise properties of NMR spectroscopy Rx chain can be achieved in the targeted frequency bandwidth with the use of NCP, so the next step is to develop the NCP's PCB and to solder all its elements on the PCB more precise than in the case of manual soldering. But first, it is necessary to measure the noise figure of the NCP's prototype. Indeed, the NCP's measured noise figure can be seen in Figure 8.26.

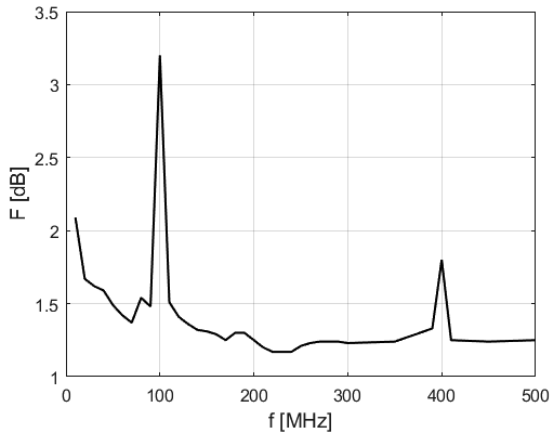

Figure 8.26: Measured noise figure of the NCP's prototype

An unexpected behaviour can be seen in Figure 8.26 around the frequencies of 100 MHz and 400 MHz. Such a behaviour arises suspicion of unwanted oscillations at the two frequencies. Therefore, the NCP was measured by a spectrum analyzer in order to check whether these effects really are caused by oscillations. The measurement results, obtained by the Anritsu Spectrum Master MS2721B spectrum analyzer [81], can be seen in Figure 8.27.

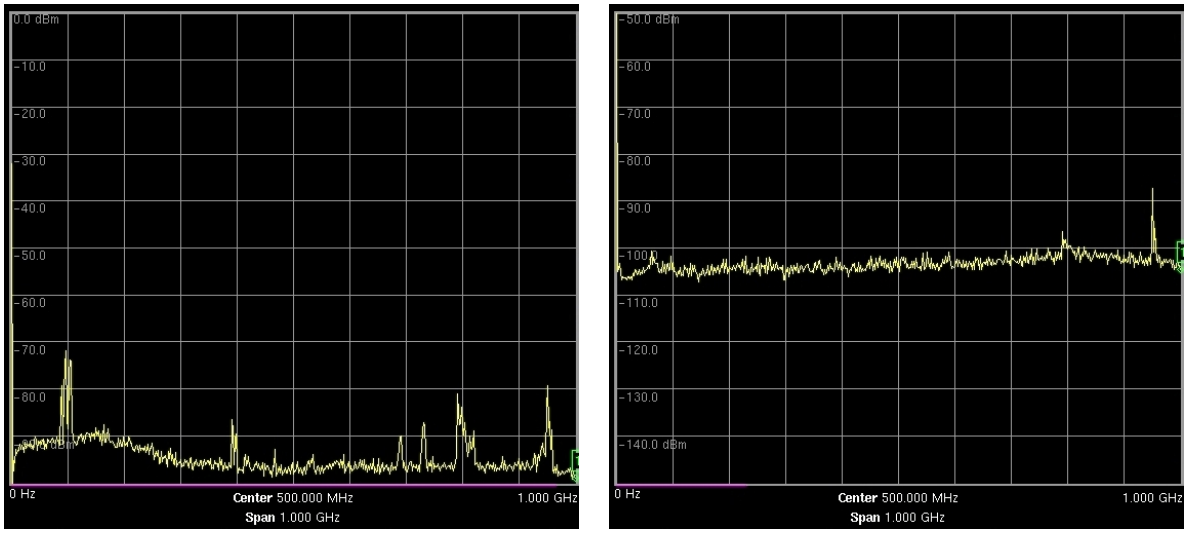

(a) (b)

Figure 8.27: Measured NCP's spectrum when NCP is turned: a) ON; b) OFF

Unfortunately, the same behaviour can be seen again at exactly 100 MHz and 400 MHz, as spectral components can be seen at these frequencies in Figure 8.27a. There are also some spectral components visible at 800 MHz and 950 MHz, even when the NCP is turned off. However, these components turned out to be nothing unusual, as the aforementioned frequency bands are occupied in Croatia by LTE and GSM mobile networks, respectively [82]. Furthermore, in order to verify that the spectral components at 100 MHz and 400 MHz are not caused by the external electromagnetic radiation, the NCP was put inside a metal enclosure, so that it is insulated from the influences of the external radiation. The enclosure (which can be seen in Figure 8.32) was grounded during the measurement, and the ground of NCP's PCB was connected to the enclosure via the SMA connectors, placed both at the input and at the output of NCP. Additionally, three coils, intended to serve as RF chokes, were inserted into the NCP's circuit. The NCP schematic with the inserted coils can be seen in Figure 8.34. Also, the NCP's power supply cables were replaced with a copper twisted pair cable, winded on the ferrite bead RF choke at its end closer to the NCP. After these modifications were applied to the NCP, the measurement shown in Figure 8.27 was repeated and the result of the repeated NCP's output spectrum measurement (which was obtained this time by the use of Anritsu MS2661C spectrum analyzer [83]) can be seen in Figure 8.29. Regrettably, the spectral components at 100 MHz and 400 MHz are present yet again, although the NCP is insulated from the external radiation in this case. Additionally, during this measurement, some higher harmonics emerged from noise be-

tween 500 MHz and 650 MHz. Therefore, it might be that the spectral components in question are either internal oscillations or interference components boosted by the reflection-amplifier-like process, caused by either a flaw in its design or a flaw in its construction. To the author's knowledge, there are three potential causes of these unwanted internally generated components. Firstly, although the simulations of the proposed NCP's schematic (shown in Figure 8.33) predicted its stable operation (which can be seen in Figure 8.23), one should bear in mind that all the electronic components' models in the simulation are ideal. In reality, every electronic component possesses a certain amount of parasitic resistance, inductance and capacitance, and its equivalent circuit becomes more complex as the operating frequency rises [84]. These parasitic values usually have a negative effect on both the characteristics, as well as the stability of the active circuit the electronic component is used in. Secondly, one can see in Figure 8.33 that the NCP's supply network is a basic supply network with a LM317 voltage regulator [79] at its core. As the operating frequency rises, there is a greater possibility for the output signal to be coupled to the input, with the supply network serving as a positive feedback [85]. Also, as the wavelengths of the electromagnetic waves become smaller with the rise of the operating frequency, there is a greater possibility for the supply cables to serve as antennas that inject unwanted external RF radiation into the circuit [86]. This is why the supply networks become more complex with the rise of the operating frequency – so that they would serve as a band-stop filter for the unwanted external radiation, as well as an isolation between the output and the input of the active circuit. Therefore, a basic supply network with a LM317 voltage regulator might not be good enough for the use with active RF circuitry. Thirdly, although enclosing the active circuit is mostly helpful for its stable operation, if it is not carried out properly, the vicinity of the active circuit's PCB to the enclosure's walls creates parasitic capacitance that can form an unwanted positive feedback from the output of the circuit to its input (Figure 8.28) [87]. Again, with the rise of the operating frequency, while the wavelengths consequently decrease, the grounding becomes more sensitive if it is poorly executed. Hence, the simplest enclosing and grounding process might not be enough for the use with active RF circuitry.

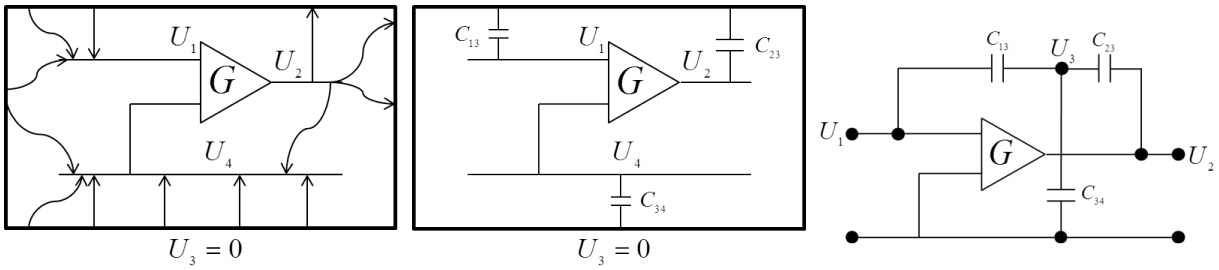

(a) Field lines in a circuit (b) Mutual capacitance diagram (c) Circuit representation

Figure 8.28: Going from field to circuit

However, in spite of these unwanted internally generated components, the NCP can still be used, even in its current state. If the operating frequency of the NMR measurement that is going to be executed is around 50 MHz or lower, the NCP can be used, as its spectrum is clear of all unwanted internally generated components in this frequency bandwidth.

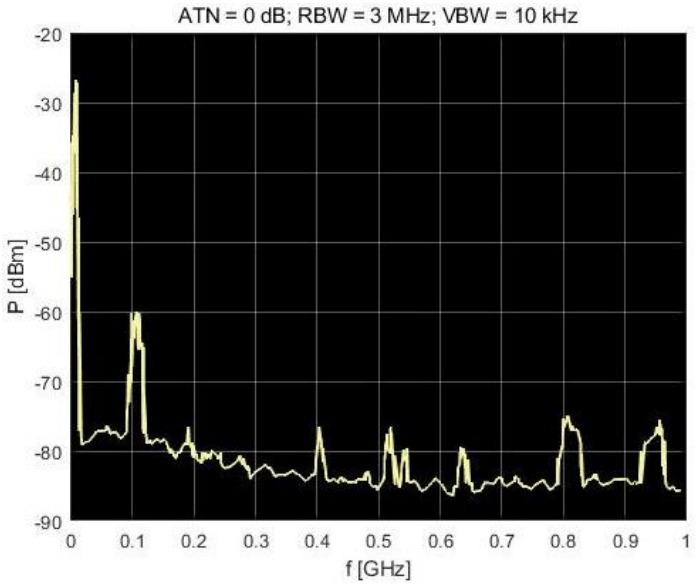

Figure 8.29: Repeated NCP's spectrum measurement
(Note: the -25 dBm spectral component at the lowest frequency is caused by the spectrum analyzer's local oscillator)

Undoubtedly, the three hypotheses, mentioned above, need to be investigated, while the NCP needs to be fixed and measured again until the cause of its unwanted internally generated components is found and removed. And only then, if the new measurements yield satisfactory results, the new PCB design, shown in Figure 8.35 (which is a modification of the original design shown in Figure 8.31, where both SMA connectors are moved apart from each other in order to reduce eventual crosstalk signals, while the rest of the PCB is left the same as in the original design), can be used and all the necessary electonic components can be soldered on it more precise than in the case of manual soldering. Furthermore, if the measurements show that the new design is satisfactory (both gain–wise and noise figure–wise), the idea is to split the supply network (lower part of Figure 8.35) and the amplifier network (upper part of Figure 8.35) to investigate the possibility of cooling the amplifier down with liquid nitrogen or liquid helium, thus decreasing the NCP's noise figure even lower. The PCB layout design of the split supply and gain networks can be seen in Figures 8.36 and 8.37, respectively.

Of course, in the end, the idea is to place the NCP into the NMR spectroscopy system's Rx chain and use it as an NMR preamplifier, with which use, the measurement times would be significantly shortened, compared to the measurement time needed with the use of NMR preamplifiers available in our lab right now. But these ideas will be performed and presented in the future research activities.

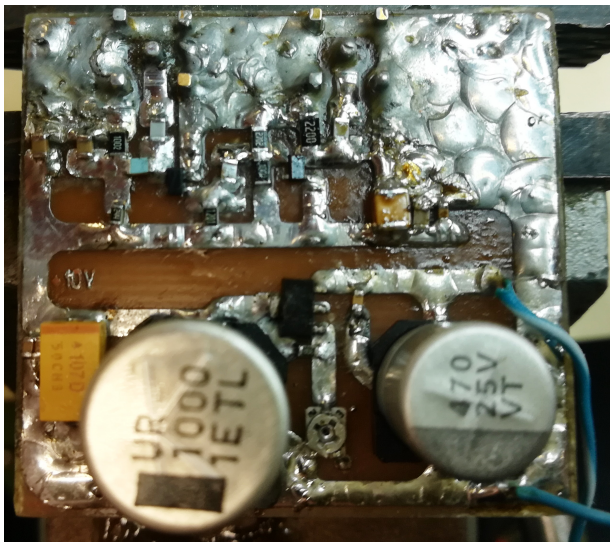

Figure 8.30: NCP's prototype – top view

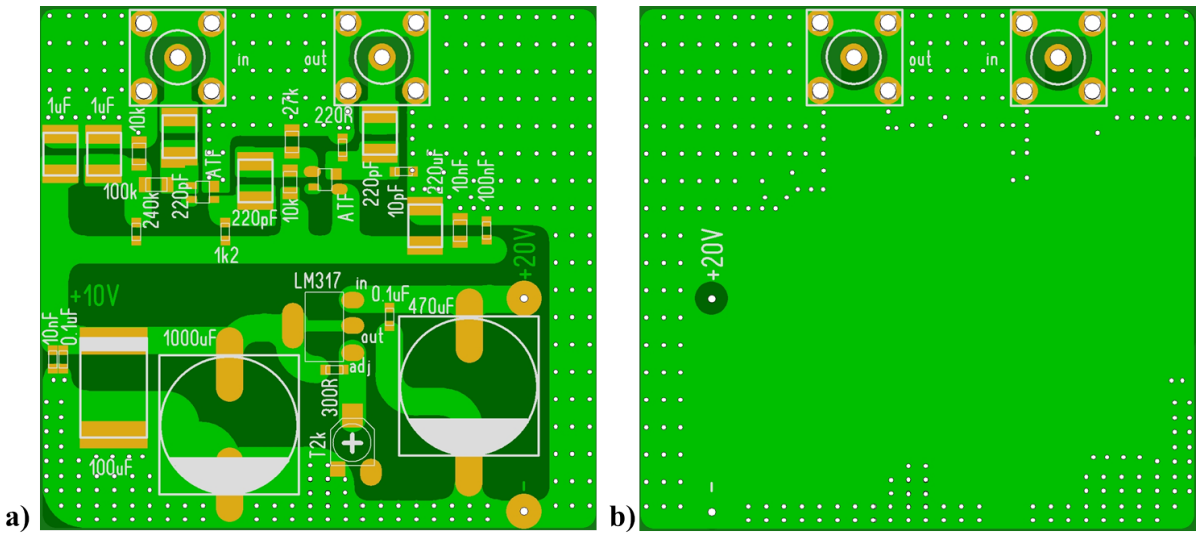

Figure 8.31: NCP's prototype layout design: a) top view; b) bottom view

Figure 8.32: NCP in a metal enclosure

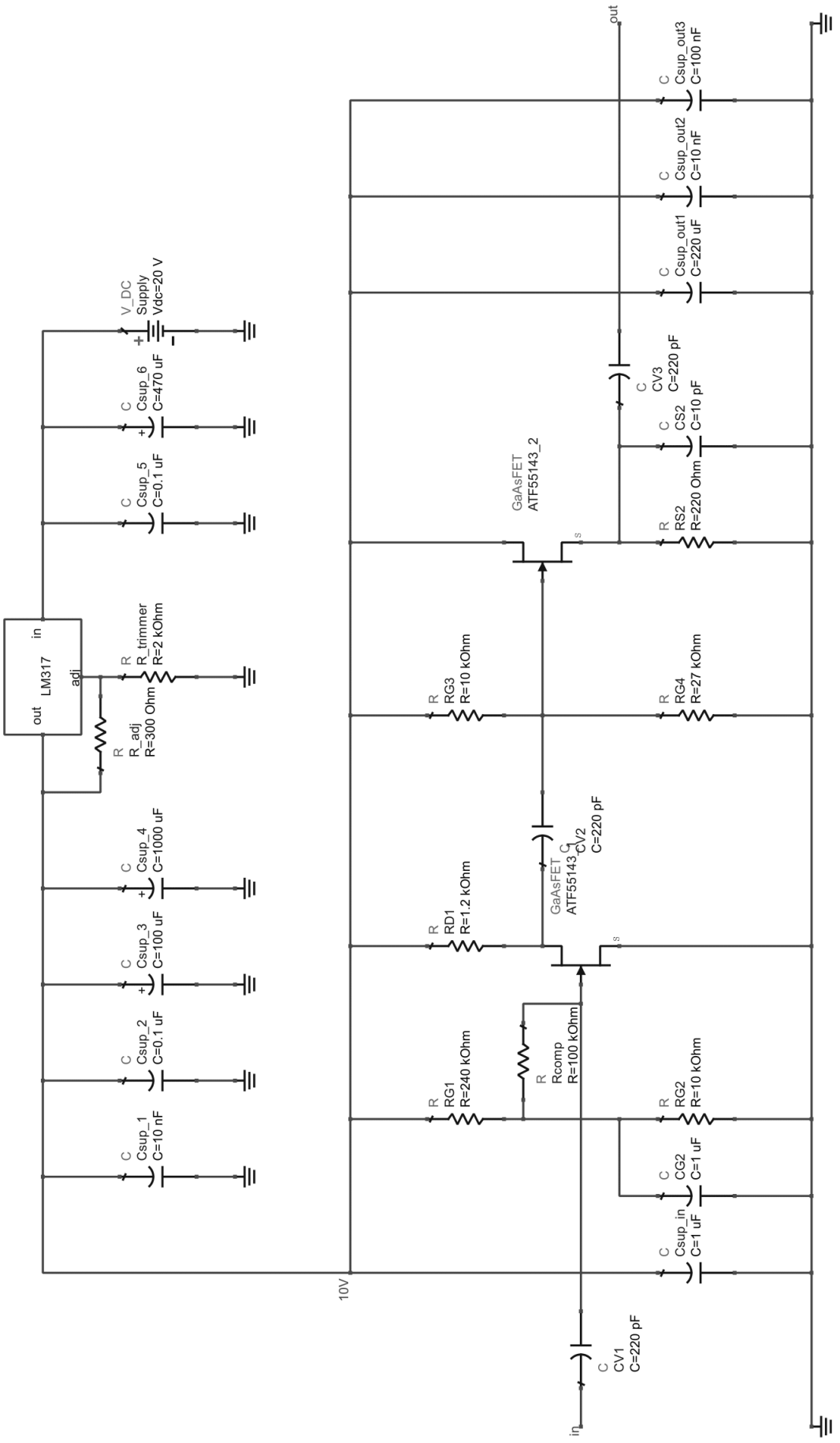

Figure 8.33: Schematic diagram of the new–constructed NMR preamplifier

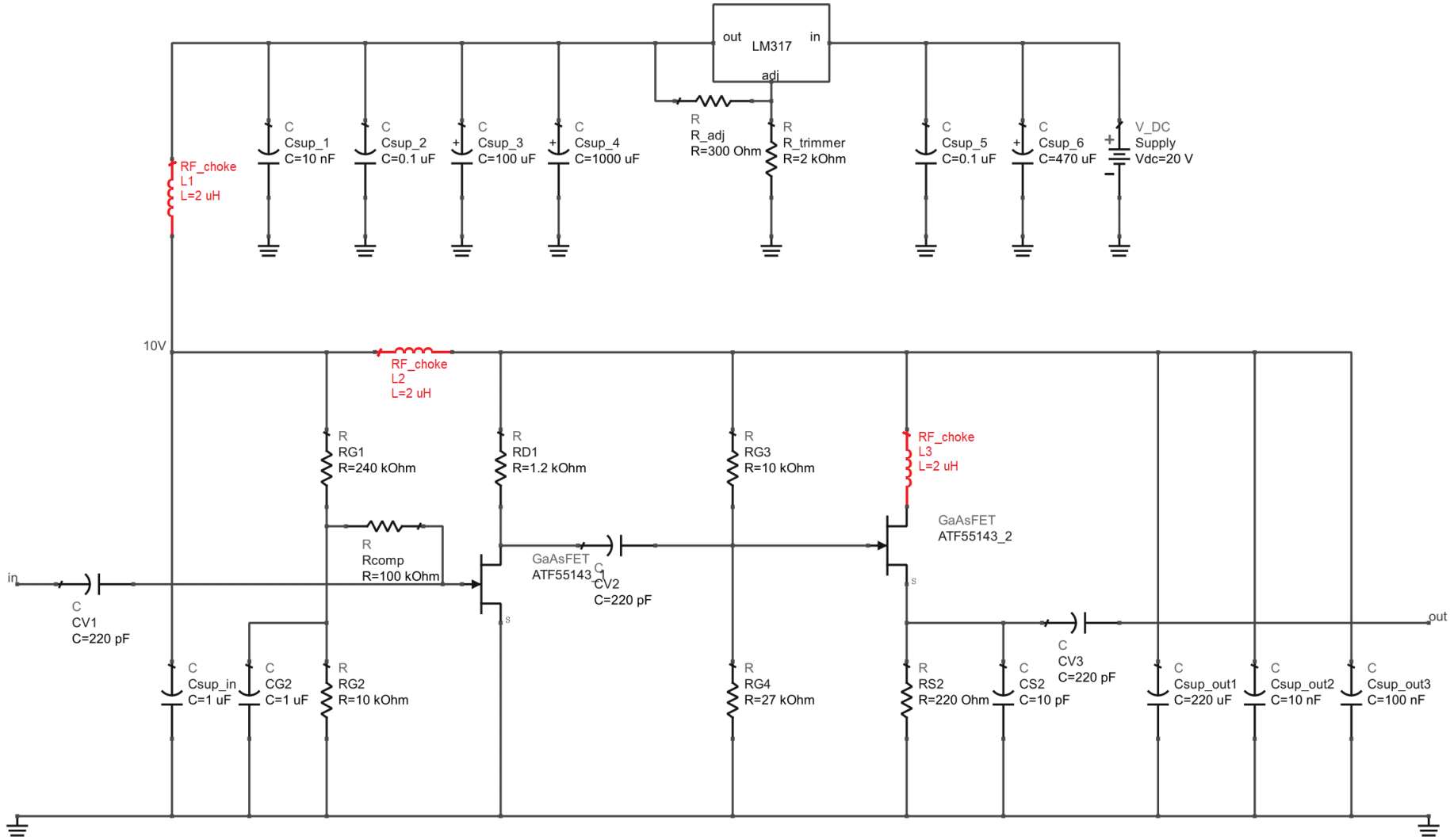

Figure 8.34: Schematic diagram of the new–constructed NMR preamplifier with RF chokes (red) inserted into the circuit

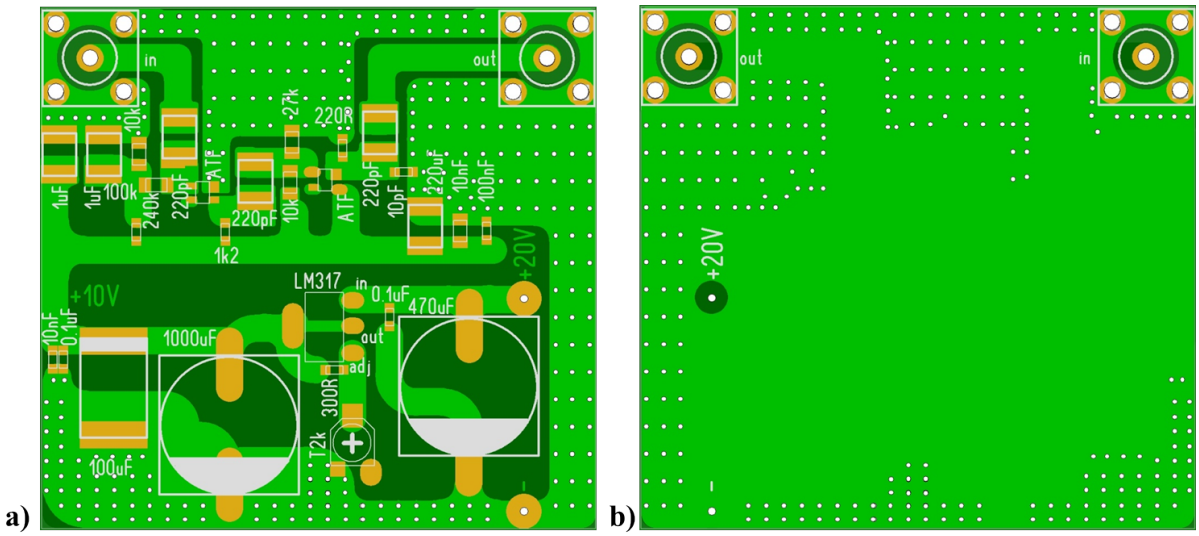

Figure 8.35: NCP's modified layout design: a) top view; b) bottom view

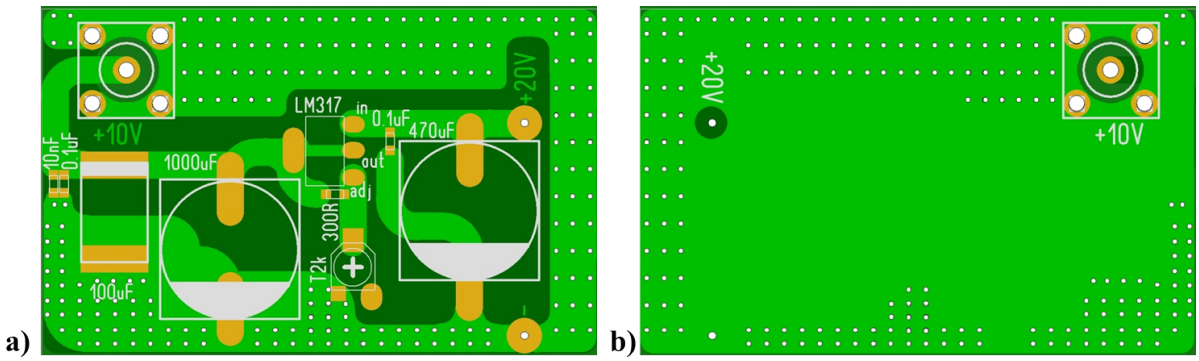

Figure 8.36: NCP's split supply network PCB layout design: a) top view; b) bottom view

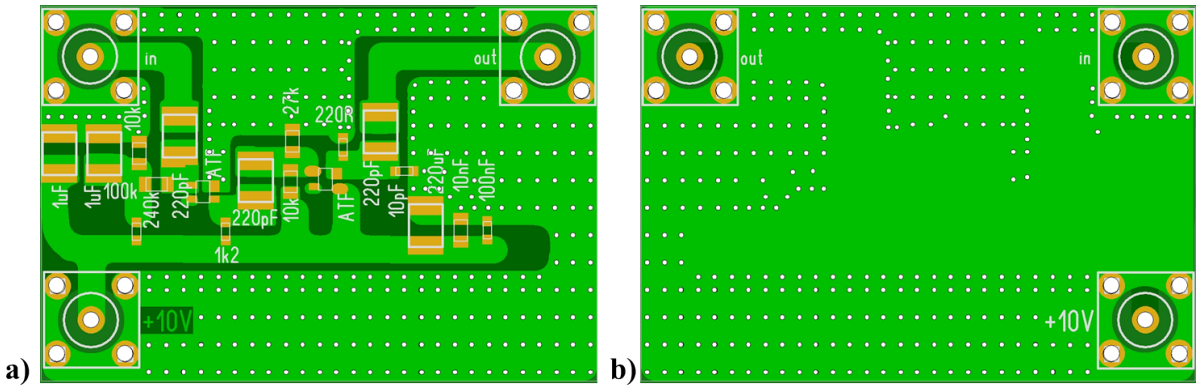

Figure 8.37: NCP's split gain network PCB layout design: a) top view; b) bottom view

All the PCB layouts (shown in Figures 8.31, 8.35, 8.36 and 8.37) were designed with the use of the Sprint Layout [88, 89] software package.

Conclusion

The biggest issue with modern NMR spectroscopy measurements, especially in condensed matter physics, is the trend of continuous decrease of magnitude of receiving signals. As response signal levels decrease, the background noise of the used NMR spectroscopy systems gradually becomes a bigger problem. The averaging of multiple measurements, which showed to be a mighty tool in any low–level signal measurements throughout the last thirty or so years, starts consuming exhausting amounts of time, as some modern NMR measurements can last up to ten hours. Some improvements, like the introduction of the cryogenic cooling process to the NMR spectroscopy systems – especially to the probes and, more recently, the preamplifiers – proved to be very efficient, but these improvements have been determined empirically, without the deeper understanding of their upper limit or the reason why and how these improvements work. The investigation, presented in this thesis, spawned a theoretical description of the most sensitive part of NMR spectroscopy systems from the aspect of noise, which is its receiving chain, and the correctness of this description has been confirmed both experimentally and numerically. Additionally, an electromagnetic model of the probe, which predicts SNR values at its output, has been derived and compared to the developed theoretical description of the NMR spectroscopy receiving chain. The comparison results proved the correctness of both developed models. Moreover, not only does the developed theoretical description evidently show the reasons why the empirically determined improvements work, but further possible improvements of NMR spectroscopy systems, from the aspect of noise, can also be seen very clearly. It has been shown that, with the appropriate selection of the crucial elements the NMR spectroscopy system is made of, it is possible to cut measurement times down to one half. It has also been shown that the possible improvements are far from their upper limit, so there is still a lot of relatively easily achievable improvements possible to implement into the NMR spectroscopy systems. Finally, two possible upgrades of NMR preamplifiers: one in terms of power gain level enhancement, with the addition of a second stage amplifier, and the other in terms of a new proposed scheme, PCB layout and proper electronic components selection for the NMR preamplifier, have been proposed in order to further improve noise properties of the NMR spectroscopy system receiving chain.

Appendix A

Receiving chain noise figure calculator

In this appendix, an entire program code of the created calculator for NMR spectroscopy receiving chain's noise figure will be given, as well as the figures used in it. This program is available in [59] and [60].

A.1 Program code

```
#Imported libraries
from math import log10, log2, ceil
import matplotlib.pyplot as plt
import matplotlib.image as mpimg
from sys import exit

#Constants
T0 = 290 #K

#Functions
def isfloat(value):
    '''Use to determine the possibility of converting chr
argument value to float'''
    try:
        float(value)
        return True
    except ValueError:
        return False

def capitalize_only(string):
    '''Use to only capitalize the first letter of the input
string without changing the rest of the letters'''
    str_1 = string[0]
    str_2 = string[1:]
    string = str_1.capitalize() + str_2
    return string

```

```
28 def model_select(selection_object):
29     '''Use for choosing one of two possible noise models'''
30     good_input = 0
31     while not good_input:
32         message = 'Choose ' + selection_object + ': '
33         model_no = input(message)
34         if model_no.isnumeric():
35             model_no = int(model_no)
36             if model_no == 1 or model_no == 2:
37                 good_input = 1
38             else:
39                 print('Input error! Try again.')
40         else:
41             print('Input error! Cannot convert input',
42                   'to integer! Try again.', sep=' ')
43     return model_no
44 
45 def init_selection():
46     '''Use for choosing the appropriate one of two possible
47 noise models and paths'''
48     #Showing both models
49     img = mpimg.imread('Models.png')
50     plt.imshow(img)
51     plt.axis('off')
52     mng = plt.get_current_fig_manager()
53     mng.full_screen_toggle()
54     plt.show()
55     #Choosing the model
56     model = model_select('model (1 or 2)')
57     #Showing both paths along with both models
58     if model == 1:
59         img = mpimg.imread('Model_1.png')
60     else:
61         img = mpimg.imread('Model_2.png')
62     plt.imshow(img)
63     plt.axis('off')
64     mng = plt.get_current_fig_manager()
65     mng.full_screen_toggle()
66     plt.show()
67     #Choosing the path
68     path = model_select('path (in-->out = 1; out-->in = 2)')
69     return model, path
70 
71 def dB_input(input_term, sign):
72     '''Use for input of the values expressed in decibels (dB)'''
73     if sign == '+':
74         good_input = 0
75         while not good_input:
76             message = 'Input ' + input_term + ' in dB: '
77             value = input(message)
78             if isfloat(value):
```

```
                value = float(value)
                if value >= 0:
                    good_input = 1
                else:
                    print('Input error! Try again.')
                    print('(', capitalize_only(input_term),
                          ' has to be greater than or equal to',
                          ' zero dB!)', sep='')
            else:
                print('Input error! Cannot convert input',
                      'to float! Try again.', sep=' ')
    elif sign == '-':
        good_input = 0
        while not good_input:
            message = 'Input ' + input_term + ' in dB: '
            value = input(message)
            if isfloat(value):
                value = float(value)
                if value < 0:
                    good_input = 1
                else:
                    print('Input error! Try again.')
                    print('(', capitalize_only(input_term),
                          ' has to be less than zero dB!)',
                          sep='')
            else:
                print('Input error! Cannot convert input',
                      'to float! Try again.', sep=' ')
    elif sign == 'both':
        good_input = 0
        while not good_input:
            message = 'Input ' + input_term + ' in dB: '
            value = input(message)
            if isfloat(value):
                value = float(value)
                good_input = 1
            else:
                print('Input error! Cannot convert input',
                      'to float! Try again.', sep=' ')
    else:
        print('Sign selection error! Fix that.')
        input('Press Enter to terminate the calculator...')
        exit()
    return value

def lin_pos_input(input_term):
    '''Use for input of the positive values in linear scale'''
    good_input = 0
    while not good_input:
        message = 'Input ' + input_term + ': '
        value = input(message)
```

```
130         if isfloat(value):
131             value = float(value)
132             if value > 0:
133                 good_input = 1
134             else:
135                 print('Input error! Try again.')
136                 print('(', capitalize_only(input_term),
137                       ' has to be greater than zero!)', sep='')
138         else:
139             print('Input error! Cannot convert input',
140                   'to float! Try again.', sep=' ')
141     return value
142 
143 def dB_2_lin(dB_value, ratio):
144     '''Use to transform dB values to linear scale'''
145     if ratio == 'power':
146         lin_value = 10 ** (dB_value/10)
147     elif ratio == 'voltage':
148         lin_value = 10 ** (dB_value/20)
149     else:
150         print('Ratio selection error! Fix that.')
151         input('Press Enter to terminate the calculator...')
152         exit()
153     return lin_value
154 
155 def lin_2_dB(lin_value, ratio):
156     '''Use to transform linear values to dB scale'''
157     if ratio == 'power':
158         dB_value = 10 * log10(lin_value)
159     elif ratio == 'voltage':
160         dB_value = 20 * log10(lin_value)
161     else:
162         print('Ratio selection error! Fix that.')
163         input('Press Enter to terminate the calculator...')
164         exit()
165     return dB_value
166 
167 def F11():
168     '''Model: 1; Path: in --> out'''
169     #Parameter input
170     print('\n~~~~~~~~~~~~~~~~~~~~~~~~~~~~~~~~Parameter input',
171           '~~~~~~~~~~~~~~~~~~~~~~~~~~~~~~~~', sep='')
172     SNRin = dB_2_lin(dB_input('input signal-to-noise ratio',
173                               'both'), 'power')
174     Tcoil = lin_pos_input('coil temperature in K')
175     L1 = dB_2_lin(dB_input('input cable loss', '+'), 'power')
176     L2 = dB_2_lin(dB_input('duplexer loss', '+'), 'power')
177     G3a = dB_2_lin(dB_input('pre-amplifier gain', '+'), 'power')
178     F3a = dB_2_lin(dB_input('pre-amplifier noise factor', '+'),
179                    'power')
180     S11_3a = dB_2_lin(dB_input('pre-amplifier S11 parameter',
```

```
                                    '-'), 'voltage')
    L4 = dB_2_lin(dB_input('output cable loss', '+'), 'power')
    F5 = dB_2_lin(
        dB_input('NMR spectrometer RF receiver noise factor',
                 '+'), 'power')
    n_meas = lin_pos_input('number of averaged measurements')
    #Calculation
    print('\n~~~~~~~~~~~~~~~~~~~~~~~~~~~~~~~Calculated values',
          '~~~~~~~~~~~~~~~~~~~~~~~~~~~~~~~', sep='')
    #Noise figure of hardware part of NMR spectroscopy Rx chain
    F_HW = 1 + ((2 * T0) / (Tcoil + T0)) * (L1 * L2 *
           (1 + (1 / (1 - (S11_3a ** 2))) * (F3a - 1 +
           ((L4 * F5 - 1) / G3a))) - 1)
    print('Noise figure of the hardware part of NMR',
          'spectroscopy Rx chain:\n{:.4f}'.format(F_HW),
          '(linear scale)',
          '= {:.4f} dB\n'.format(lin_2_dB(F_HW, 'power')))
    #Overall noise figure of NMR spectroscopy Rx chain
    F11 = F_HW / n_meas
    print('Overall noise figure of NMR spectroscopy system',
          'Rx chain:\n{:.4f} (linear scale) = {:.4f} dB\n'
          .format(F11, lin_2_dB(F11, 'power')))
    #Expected signal-to-noise ratio on the spectrometer screen
    SNRout = SNRin / F11
    print('Expected signal-to-noise ratio on the spectrometer',
          'screen:\n{:.4f}'.format(SNRout),
          '(linear scale; power ratio) =',
          '{:.4f} dB\n'.format(lin_2_dB(SNRout, 'power')))
    return

def F12():
    '''Model: 1; Path: out --> in'''
    #Parameter input
    print('\n~~~~~~~~~~~~~~~~~~~~~~~~~~~~~~~Parameter input',
          '~~~~~~~~~~~~~~~~~~~~~~~~~~~~~~~', sep='')
    str_1 = 'output signal-to-noise ratio\n'
    str_2 = '(shown on the spectrometer screen)'
    value = str_1 + str_2
    SNRout = dB_2_lin(dB_input(value, 'both'), 'power')
    n_meas = lin_pos_input('number of averaged measurements')
    F5 = dB_2_lin(
    dB_input('NMR spectrometer RF receiver noise factor',
                 '+'), 'power')
    L4 = dB_2_lin(dB_input('output cable loss', '+'), 'power')
    G3a = dB_2_lin(dB_input('pre-amplifier gain', '+'), 'power')
    F3a = dB_2_lin(dB_input('pre-amplifier noise factor', '+'),
                   'power')
    S11_3a = dB_2_lin(dB_input('pre-amplifier S11 parameter',
                               '-'), 'voltage')
    L2 = dB_2_lin(dB_input('duplexer loss', '+'), 'power')
    L1 = dB_2_lin(dB_input('input cable loss', '+'), 'power')
```

```
    Tcoil = lin_pos_input('coil temperature in K')
    #Calculation
    print('\n~~~~~~~~~~~~~~~~~~~~~~~~~~~~~~~~Calculated values',
          '~~~~~~~~~~~~~~~~~~~~~~~~~~~~~~~', sep='')
    #Noise figure of hardware part of NMR spectroscopy Rx chain
    F_HW = 1 + ((2 * T0) / (Tcoil + T0)) * (L1 * L2 *
           (1 + (1 / (1 - (S11_3a ** 2))) * (F3a - 1 +
           ((L4 * F5 - 1) / G3a))) - 1)
    print('Noise figure of the hardware part of',
          'NMR spectroscopy',
          'Rx chain:\n{:.4f} (linear scale) = {:.4f} dB\n'
          .format(F_HW, lin_2_dB(F_HW, 'power')))
    #Overall noise figure of NMR spectroscopy Rx chain
    F12 = F_HW / n_meas
    print('Overall noise figure of NMR spectroscopy',
          'system Rx chain:',
          '\n{:.4f} (linear scale) = {:.4f} dB\n'
          .format(F12, lin_2_dB(F12, 'power')))
    #Expected signal-to-noise ratio on the probe
    SNRin = SNRout * F12
    print('Expected signal-to-noise ratio on the probe:',
          '\n{:.4f} (linear scale; power ratio) = {:.4f} dB\n'
          .format(SNRin, lin_2_dB(SNRin, 'power')))
    return

def F21():
    '''Model: 2; Path: in --> out'''
    #Parameter input
    print('\n~~~~~~~~~~~~~~~~~~~~~~~~~~~~~~~~Parameter input',
          '~~~~~~~~~~~~~~~~~~~~~~~~~~~~~~~', sep='')
    SNRin = dB_2_lin(dB_input('input signal-to-noise ratio',
                              'both'), 'power')
    Tcoil = lin_pos_input('coil temperature in K')
    L1 = dB_2_lin(dB_input('input cable loss', '+'), 'power')
    L2 = dB_2_lin(dB_input('duplexer loss', '+'), 'power')
    G3a = dB_2_lin(dB_input('pre-amplifier gain', '+'), 'power')
    F3a = dB_2_lin(dB_input('pre-amplifier noise factor', '+'),
                   'power')
    S11_3a = dB_2_lin(dB_input('pre-amplifier S11 parameter',
                               '-'), 'voltage')
    G3b = dB_2_lin(dB_input('second stage amplifier gain', '+'),
                   'power')
    F3b = dB_2_lin(
        dB_input('second stage amplifier noise factor', '+'),
        'power')
    S11_3b = dB_2_lin(
        dB_input('second stage amplifier S11 parameter', '-'),
        'voltage')
    L4 = dB_2_lin(dB_input('output cable loss', '+'), 'power')
    F5 = dB_2_lin(
        dB_input('NMR spectrometer RF receiver noise factor',
```

```
283                             '+'), 'power')
284     n_meas = lin_pos_input('number of averaged measurements')
285     #Calculation
286     print('\n~~~~~~~~~~~~~~~~~~~~~~~~~~~~~~~Calculated values',
287           '~~~~~~~~~~~~~~~~~~~~~~~~~~~~~~~', sep='')
288     #Noise figure of hardware part of NMR spectroscopy Rx chain
289     F_HW = 1 + ((2 * T0) / (Tcoil + T0)) * (L1 * L2 *
290            (1 + (1 / (1 - (S11_3a ** 2))) * (F3a - 1 +
291            (1 / (G3a * (1 - (S11_3b ** 2)))) * (F3b - 1 +
292            ((L4 * F5 - 1) / G3b)))) - 1)
293     print('Noise figure of the hardware part of',
294           'NMR spectroscopy',
295           'Rx chain:\n{:.4f} (linear scale) = {:.4f} dB\n'
296           .format(F_HW, lin_2_dB(F_HW, 'power')))
297     #Overall noise figure of NMR spectroscopy Rx chain
298     F21 = F_HW / n_meas
299     print('Overall noise figure of NMR spectroscopy system',
300           'Rx chain:',
301           '\n{:.4f} (linear scale) = {:.4f} dB\n'
302           .format(F21, lin_2_dB(F21, 'power')))
303     #Expected signal-to-noise ratio on the spectrometer screen
304     SNRout = SNRin / F21
305     print('Expected signal-to-noise ratio on the spectrometer',
306           'screen:',
307           '\n{:.4f} (linear scale; power ratio) = {:.4f} dB\n'
308           .format(SNRout, lin_2_dB(SNRout, 'power')))
309     return
310
311 def F22():
312     '''Model: 2; Path: out --> in'''
313     #Parameter input
314     print('\n~~~~~~~~~~~~~~~~~~~~~~~~~~~~~~~Parameter input',
315           '~~~~~~~~~~~~~~~~~~~~~~~~~~~~~~~', sep='')
316     str_1 = 'output signal-to-noise ratio\n'
317     str_2 = '(shown on the spectrometer screen)'
318     value = str_1 + str_2
319     SNRout = dB_2_lin(dB_input(value, 'both'), 'power')
320     n_meas = lin_pos_input('number of averaged measurements')
321     F5 = dB_2_lin(
322         dB_input('NMR spectrometer RF receiver noise factor',
323                  '+'), 'power')
324     L4 = dB_2_lin(dB_input('output cable loss', '+'), 'power')
325     G3b = dB_2_lin(dB_input('second stage amplifier gain', '+'),
326                    'power')
327     F3b = dB_2_lin(
328         dB_input('second stage amplifier noise factor', '+'),
329         'power')
330     S11_3b = dB_2_lin(
331         dB_input('second stage amplifier S11 parameter', '-'),
332                      'voltage')
333     G3a = dB_2_lin(dB_input('pre-amplifier gain', '+'), 'power')
```

```
334     F3a = dB_2_lin(dB_input('pre-amplifier noise factor', '+'),
335                    'power')
336     S11_3a = dB_2_lin(dB_input('pre-amplifier S11 parameter',
337                                '-'), 'voltage')
338     L2 = dB_2_lin(dB_input('duplexer loss', '+'), 'power')
339     L1 = dB_2_lin(dB_input('input cable loss', '+'), 'power')
340     Tcoil = lin_pos_input('coil temperature in K')
341     #Calculation
342     print('\n~~~~~~~~~~~~~~~~~~~~~~~~~~~~~~Calculated values',
343           '~~~~~~~~~~~~~~~~~~~~~~~~~~~~~~', sep='')
344     #Noise figure of hardware part of NMR spectroscopy Rx chain
345     F_HW = 1 + ((2 * T0) / (Tcoil + T0)) * (L1 * L2 *
346            (1 + (1 / (1 - (S11_3a ** 2))) * (F3a - 1 +
347            (1 / (G3a * (1 - (S11_3b ** 2)))) * (F3b - 1 +
348            ((L4 * F5 - 1) / G3b)))) - 1)
349     print('Noise figure of the hardware part of',
350           'NMR spectroscopy',
351           'Rx chain:\n{:.4f} (linear scale) = {:.4f} dB\n'
352           .format(F_HW, lin_2_dB(F_HW, 'power')))
353     #Overall noise figure of NMR spectroscopy Rx chain
354     F22 = F_HW / n_meas
355     print('Overall noise figure of NMR spectroscopy system',
356           'Rx chain:',
357           '\n{:.4f} (linear scale) = {:.4f} dB\n'
358           .format(F22, lin_2_dB(F22, 'power')))
359     #Expected signal-to-noise ratio on the probe
360     SNRin = SNRout * F22
361     print('Expected signal-to-noise ratio on the probe:',
362           '\n{:.4f} (linear scale; power ratio) = {:.4f} dB\n'
363           .format(SNRin, lin_2_dB(SNRin, 'power')))
364     return
365
366 def formula_determinator(model, path):
367     '''Use for choosing the appropriate noise model of NMR
368 spectroscopy Rx chain'''
369     if model == 1:
370         if path == 1:
371             F11()
372         else:
373             F12()
374     else:
375         if path == 1:
376             F21()
377         else:
378             F22()
379
380 #Main program written as a function
381 def main():
382     '''NMR spectroscopy system Rx chain
383 noise figure calculator'''
384     print('~~~~~~~~~~~~',
```

```
385             'NMR Spectroscopy System Rx Chain',
386             ' Noise Figure Calculator',
387             '~~~~~~~~~~~~', sep='')
388     print()
389     #Noise model and path selection
390     model, path = init_selection()
391     #Calculation
392     F = formula_determinator(model, path)
393     input('For calculator termination press Enter...') #so that
394     #the program doesn't close immediately after execution
395     #when run via cmd
396     return
397 
398 #Main program execution
399 main()
```

A.2 Used figures

The three figures used in the created program are shown on the next three pages of this thesis in landscape orientation.

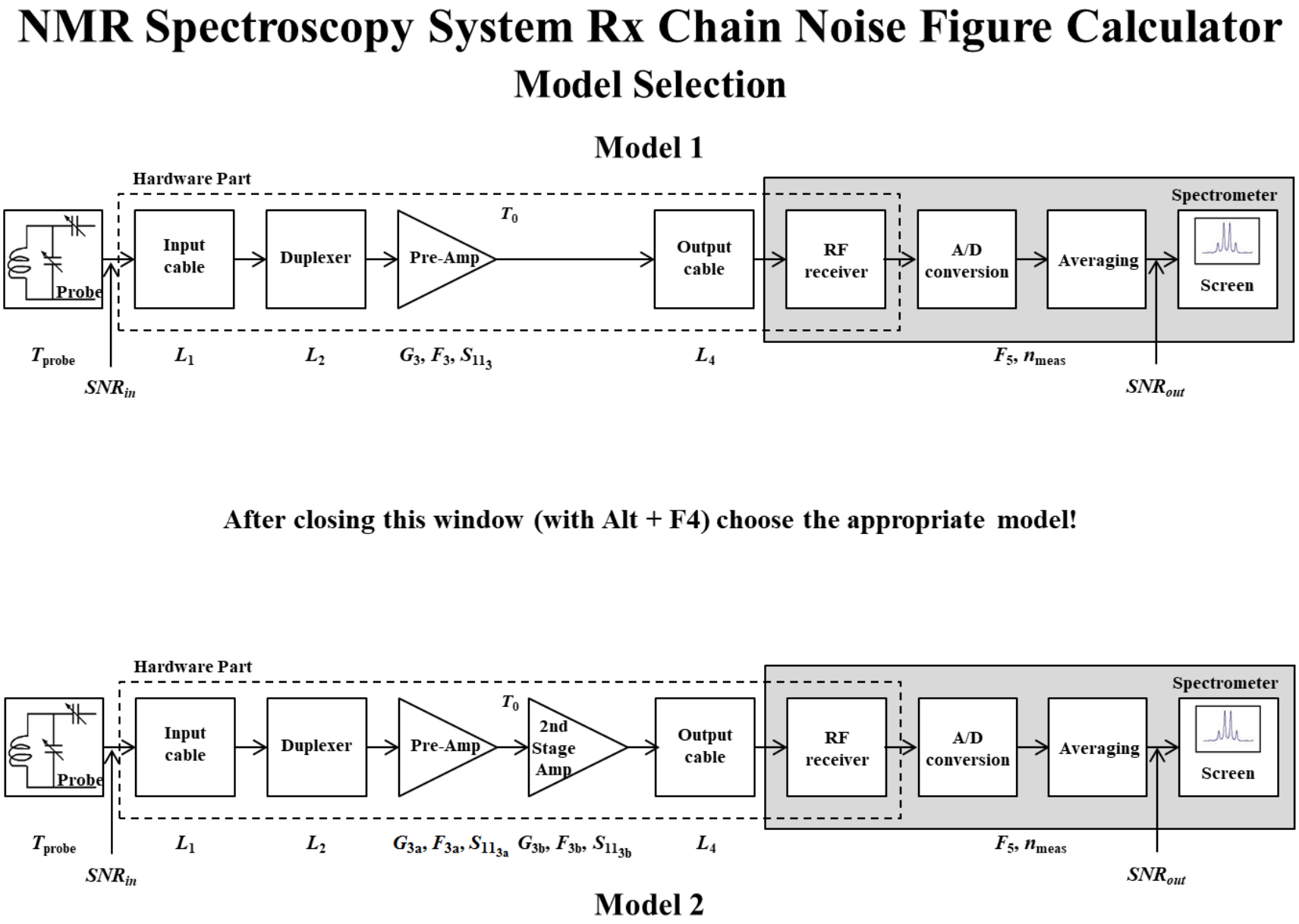

Figure A.1: NMR spectroscopy receiving chain model selector; this is the figure that pops up after the initiation of the program

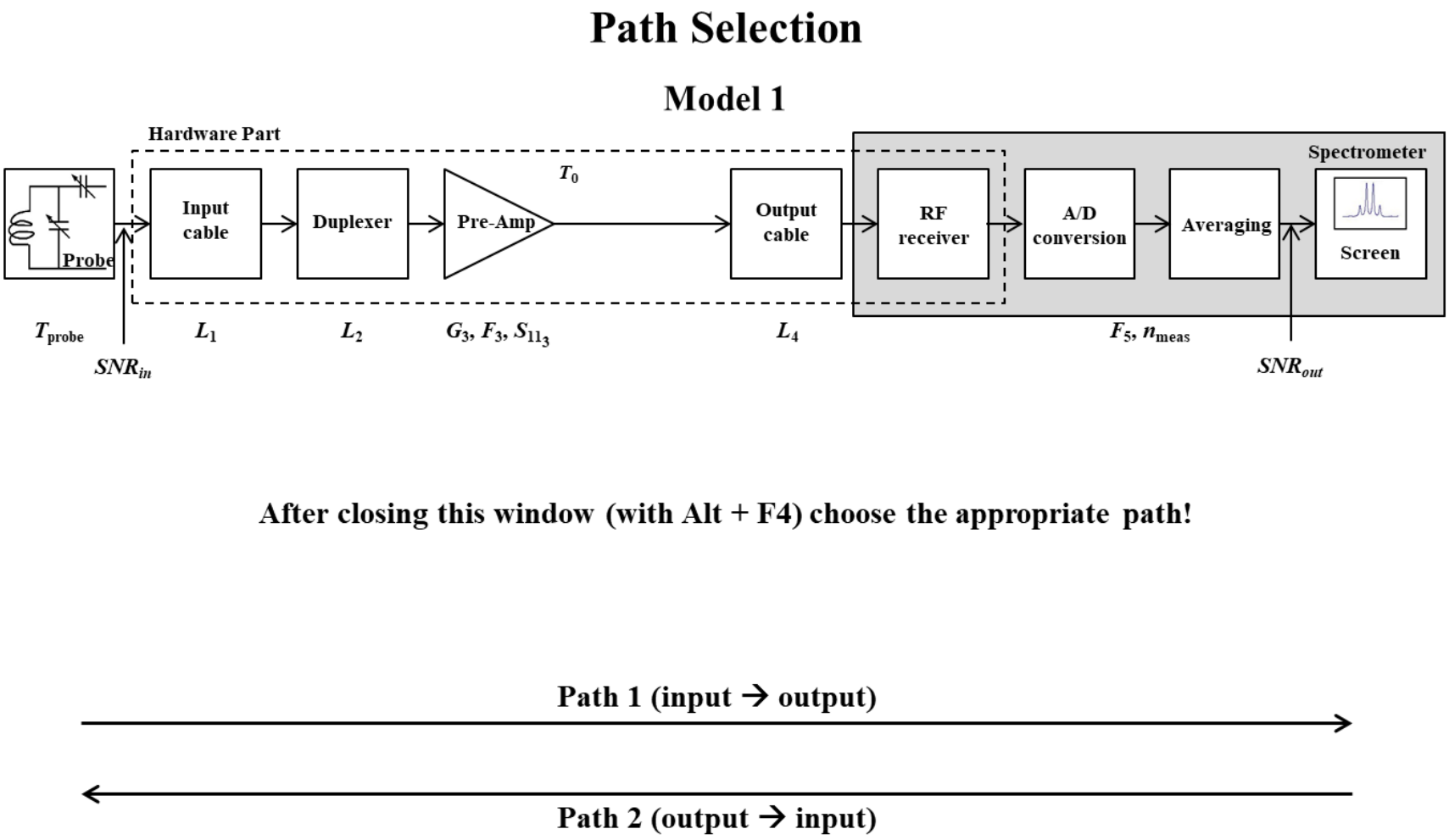

Figure A.2: NMR spectroscopy receiving chain Model 1 path selection; this is the figure that pops up after the selection of Model 1

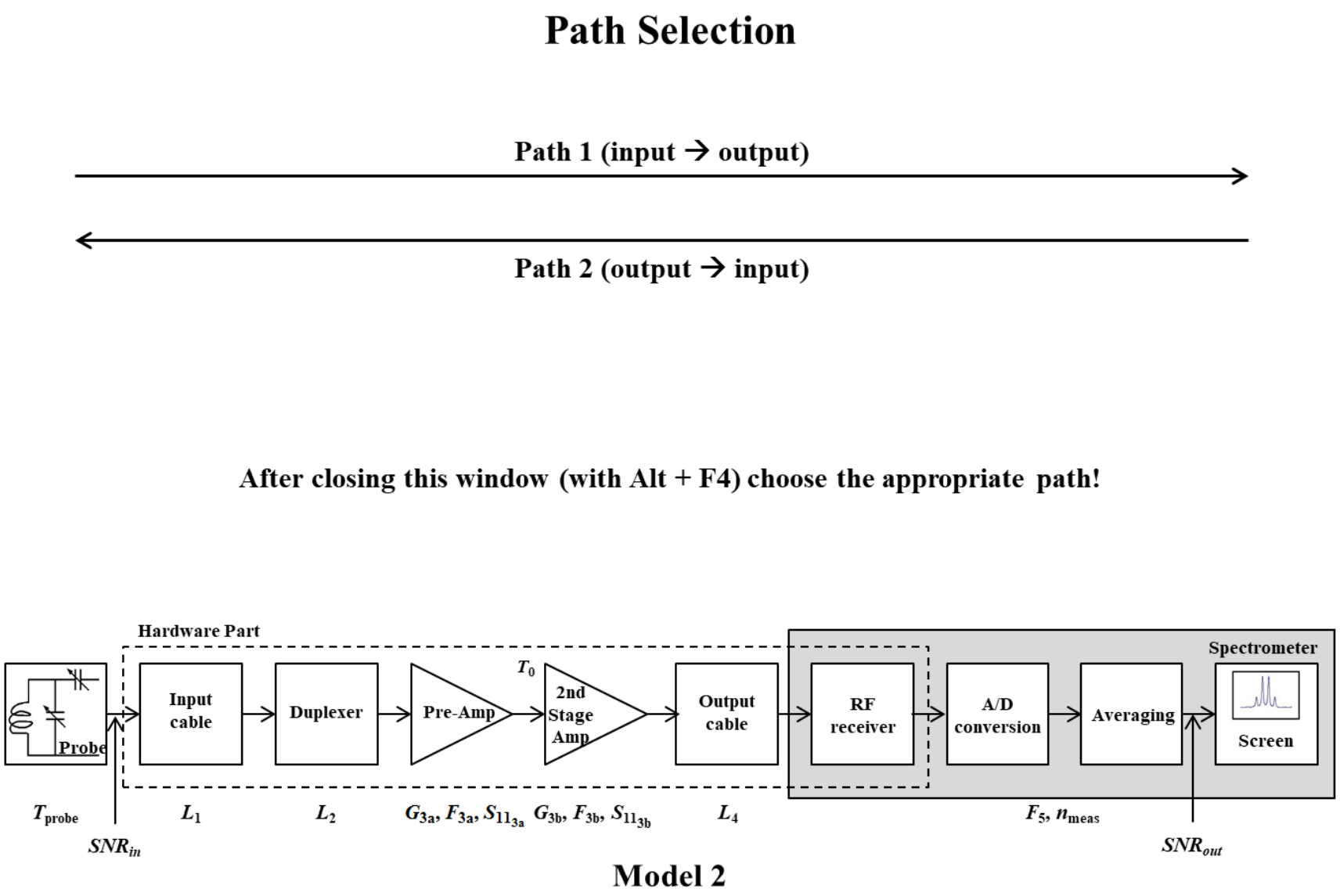

Figure A.3: NMR spectroscopy receiving chain Model 2 path selection; this is the figure that pops up after the selection of Model 2

Bibliography

[1] Levitt, M. H., Spin Dynamics: Basics of Nuclear Magnetic Resonance, 2nd ed. Chichester, UK: John Wiley & Sons, Ltd, 2008.

[2] Abragam, A., The principles of nuclear magnetism. Oxford, UK: Oxford University Press, 1978.

[3] Slichter, C. P., Principles of Magnetic Resonance, 3rd ed. Berlin, Germany: Springer-Verlag, 1990.

[4] Marshall, A. G., Verdun, F. R., Fourier Transforms in NMR, Optical, and Mass Spectrometry: A User's Handbook. Amsterdam, Netherlands: Elsevier Science Publishers B.V., 1990.

[5] Rahman, A., Choudhary, M., Wahab, A., Solving Problems with NMR Spectroscopy, 2nd ed. San Diego, USA: Elsevier Academic Press, 2016.

[6] Smith, J. A. S., "Nuclear quadrupole resonance spectroscopy: General principles", Journal of Chemical Education, Vol. 48, No. 1, January 1971, pp. 39.

[7] Fukushima, E., Roeder, S. B. W., Experimental Pulse NMR: A Nuts and Bolts Approach. Reading, Massachusetts, USA: Addison-Wesley Publishing Company, Inc., 1981.

[8] Clark, W. G., Hanson, M. E., Lefloch, F., Ségransan, P., "Magnetic resonance spectral reconstruction using frequency-shifted and summed Fourier transform processing", Review of Scientific Instruments, Vol. 66, No. 3, March 1995, pp. 2453 - 2464.

[9] Freitas, J. C. C., Scopel, W. L., Paz, W. S., Bernardes, L. V., Cunha-Filho, F. E., Speglich, C., Araújo-Moreira, F. M., Pelc, D., Cvitanić, T., Požek, M., "Determination of the hyperfine magnetic field in magnetic carbon-based materials: DFT calculations and NMR experiments", Scientific Reports, Vol. 5, No. 14761, October 2015.

[10] Blinder, R., Dupont, M., Mukhopadhyay, S., Grbić, M. S., Laflorencie, N., Capponi, S., Mayaffre, H., Berthier, C., Paduan-Filho, A., Horvatić, M., "Nuclear magnetic resonance

study of the magnetic-field-induced ordered phase in the $NiCl_2{-}4SC(NH_2)_2$ compound", Physical Review B, Vol. 95, No. 020404(R), January 2017.

[11] Pelc, D., Grafe, H.-J., Gu, G. D., Požek, M., "Cu nuclear magnetic resonance study of charge and spin stripe order in $La_{1.875}Ba_{0.125}CuO_4$", Physical Review B, Vol. 95, No. 054508, February 2017.

[12] Cvitanić, T., Šurija, V., Prša, K., Zaharko, O., Kupčić, I., Babkevich, P., Frontzek, M., Požek, M., Berger, H., Magrez, A., Rønnow, H. M., Grbić, M. S., Živković, I., "Singlet state formation and its impact on the magnetic structure in the tetramer system $SeCuO_3$", Physical Review B, Vol. 98, No. 054409, August 2018.

[13] Dale, B. M., Brown, M. A., Semelka, R. C., MRI: Basic Principles and Applications, 5th ed. Chichester, UK: Wiley Blackwell, 2015.

[14] Berger, D., "Infrared spectroscopy and Fourier transforms", Bluffton University, CEM 222 Organic Chemistry II Lecture, January 2011, available: https://www.bluffton.edu/homepages/facstaff/bergerd/classes/CEM222/Handouts/IR.pdf

[15] Kleckner, I. R., Foster, M. P., "An introduction to NMR-based approaches for measuring protein dynamics", Biochimica et Biophysica Acta (BBA) - Proteins and Proteomics, Vol. 1814, No. 8, August 2011, pp. 942 - 968.

[16] Zheng, X., Wang, Z. G., Huang, Y. C., "Implementation of a two-stage digital AGC for spectrum analyzer", in 2011 International Conference on Applied Superconductivity and Electromagnetic Devices, December 2011, pp. 37 - 40.

[17] Traficante, D. D., "Time averaging. Does the noise really average toward zero?", Concepts in Magnetic Resonance, Vol. 3, No. 2, April 1991, pp. 83 - 87.

[18] McLachlan, L. A., "Lumped circuit duplexer for a pulsed NMR spectrometer", Journal of Magnetic Resonance, Vol. 39, No. 1, April 1980, pp. 11 - 15.

[19] Cofrancesco, P., Moiraghi, G., Mustarelli, P., Villa, M., "A new NMR duplexer made with quadrature couplers", Measurement Science and Technology, Vol. 2, No. 2, 1991, pp. 147 - 149.

[20] Mizuno, T., Takegoshi, K., "Development of a cryogenic duplexer for solid-state nuclear magnetic resonance", Review of Scientific Instruments, Vol. 80, No. 12, December 2009, pp. 124702.

[21] Purcell, E. M., Electricity and Magnetism (Berkeley Physics Course - Volume 2), 1st ed. San Francisco, USA: McGraw-Hill Book Company, 1965.

[22] Stutzman, W. L., Thiele, G. A., Antenna Theory and Design, 3rd ed. New York, USA: John Wiley & Sons, Inc., 2013.

[23] Saitoh, K., Yamamoto, H., Kawasaki, K., Fukuda, Y., Tanaka, H., Okada, M., Kitaguchi, H., "Development of cryogenic probe system for high-sensitive NMR spectroscopy", Journal of Physics: Conference Series, Vol. 97, No. 1, 2008, pp. 012141.

[24] Gafner, A., "Construction of NMR equipment to be used in the Physical Properties Measurement System (PPMS, Quantum Design)", Master's thesis, University of Zürich, Zürich, Switzerland, July 2006.

[25] "Choosing a Low-Noise Amplifier", Maxim Integrated, Application Note 3642, November 2005, available: https://www.maximintegrated.com/en/app-notes/index.mvp/id/3642

[26] Motchenbacher, C. D., Connelly, J. A., Low-Noise Electronic System Design. Toronto, Canada: John Wiley & Sons, Inc., 1993.

[27] Carter, B., Mancini, R., Op Amps for Everyone, 3rd ed. Burlington, USA: Newnes, 2009.

[28] Lain, R., Allen, B. A., Yang, C. C., Shaw, L., Brunone, D., Tan, K. L., Streit, D. C., Liu, P. H., Bautista, J. J., Ortiz, G. G., "Cryogenic noise performance of InGaAs/InAlAs/InP HEMTs", in LEOS 1992 Summer Topical Meeting Digest on Broadband Analog and Digital Optoelectronics, Optical Multiple Access Networks, Integrated Optoelectronics, and Smart Pixels, April 1992, pp. 507-510.

[29] Guitton, G., "Design Methodologies for multi-mode and multi-standard Low-Noise Amplifiers", Doctoral thesis, University of Bordeaux, Bordeaux, France, December 2017.

[30] Johnson, J. B., "Thermal Agitation of Electricity in Conductors", Physical Review, Vol. 32, No. 1, July 1928, pp. 97 - 109.

[31] Nyquist, H., "Thermal Agitation of Electric Charge in Conductors", Physical Review, Vol. 32, No. 1, July 1928, pp. 110 - 113.

[32] "Noise Analysis in Operational Amplifier Circuits", Texas Instruments, Application Report, 2007, available: http://www.ti.com/lit/an/slva043b/slva043b.pdf

[33] Alexander, C. K., Sadiku, M. N. O., Fundamentals of Electric Circuits, 3rd ed. USA: McGraw-Hill Companies, 2006.

[34] Hoult, D. I., Richards, R. E., "The Signal–to–Noise Ratio of the Nuclear Magnetic Resonance Experiment", Journal of Magnetic Resonance, Vol. 24, No. 1, October 1976, pp. 71 - 85.

[35] Pozar, D. M., Microwave Engineering, 4th ed. USA: John Wiley & Sons, Inc., 2011.

[36] Richards, M. G., Andrews, A. R., Lusher, C. P., Schratter, J., "Cryogenic GaAs FET amplifiers and their use in NMR detection", Review of Scientific Instruments, Vol. 57, No. 3, October 1986, pp. 404 - 409.

[37] Styles, P., Soffe, N., Scott, C., Crag, D., Row, F., White, D., White, P., "A high–resolution NMR probe in which the coil and preamplifier are cooled with liquid helium", Journal of Magnetic Resonance, Vol. 60, No. 3, December 1984, pp. 397 - 404.

[38] Hiebel, M., Fundamentals of Vector Network Analysis, 6th ed. Germany: Rohde & Schwarz, 2014.

[39] "Fundamentals of RF and Microwave Noise Figure Measurements", Keysight Technologies, Application Note, 2017, available: http://literature.cdn.keysight.com/litweb/pdf/5952-8255E.pdf

[40] W. B. Davenport, J., Root, W. L., An Introduction to the Theory of Random Signals and Noise. New York, USA: McGraw–Hill Book Company, Inc., 1958.

[41] Robinson, F. N. H., Noise and fluctuations in electronic devices and circuits. Oxford, UK: Clarendon Press, 1974.

[42] "Noise Figure: Overview of Noise Measurement Methods", Tektronix, White Paper, 2014, available: https://download.tek.com/document/37W-30477-0%20Noise%20Figure%20WP.pdf

[43] Kester, W., (ed.), Data Conversion Handbook. Burlington, Massachusetts, USA: Newnes, 2005.

[44] Cvitanić, T., Lukas, M., Grbić, M. S., "Two-axis goniometer for single-crystal nuclear magnetic resonance measurements", https://arxiv.org/abs/1810.09108.

[45] "Tecmag Redstone Spectrometer", http://www.tecmag.com/redstone/.

[46] "MITEQ AU-1114", https://nardamiteq.com/docs/1114-1606276-L0910.PDF.

[47] "THAMWAY N141-206AA", http://www.thamway.co.jp/english/product07-08_e.html.

[48] "Mini-Circuits HELA -10D+ ", https://www.minicircuits.com/WebStore/dashboard.html?model=HELA-10%2B.

[49] "Liquid nitrogen cooled broadband preamplifier", http://www.cc.kochi-u.ac.jp/~kitag/ln2amp/index.html.

[50] Custers, J., Lorenzer, K.-A., Müller, M., Prokofiev, A., Sidorenko, A., Winkler, H., Strydom, A. M., Shimura, Y., Sakakibara, T., Yu, R., Si, Q., Paschen, S., "Destruction of the Kondo effect in the cubic heavy-fermion compound $Ce_3Pd_{20}Si_6$", Nature Materials, Vol. 11, January 2012, pp. 189 - 194.

[51] Kolar, P., Hrabar, S., Grbić, M. S., "Towards optimal noise properties of NMR antenna–receiver chain", in 2017 11th European Conference on Antennas and Propagation (EuCAP), May 2017, pp. 1054 - 1056.

[52] Bialkowski, M. E., Ibrahim, S. Z., Abbosh, A. M., "Wideband performance of 3 dB microstrip-slot coupler using different substrates", Microwave and Optical Technology Letters, Vol. 53, No. 7, April 2011, pp. 1618 - 1624.

[53] Seeber, D. A., Hoftiezer, J. H., Pennington, C. H., "Positive-intrinsic-negative diode-based duplexer for microcoil nuclear magnetic resonance", Review of Scientific Instruments, Vol. 71, No. 7, June 2000, pp. 2908 - 2913.

[54] Brorsson, C., "PIN diode drive circuits optimized for fast switching", Master's thesis, Chalmers University of Technology, Göteborg, Sweden, 2011.

[55] Perregrini, L., "Microwave connectors", University of Pavia, Course on Microwave Measurements Lecture, September 2014, available: http://microwave.unipv.it/pages/microwave_measurements/appunti/01b_MM_connectors.pdf

[56] Moskau, D., "Application of real time digital filters in NMR spectroscopy", Concepts in Magnetic Resonance, Vol. 15, No. 2, December 2002, pp. 164 - 176.

[57] Giovannetti, G., Hartwig, V., Viti, V., Gaeta, G., Francesconi, R., Landini, L., Benassi, A., "Application of undersampling technique for the design of an NMR signals digital receiver", Concepts in Magnetic Resonance Part B: Magnetic Resonance Engineering, Vol. 29B, No. 3, July 2006, pp. 107 - 114.

[58] "Python programming language", https://www.python.org/.

[59] "NMR Spectroscopy Rx Chain Noise Figure Calculator - GitHub", https://github.com/5ARK/NMR_F_Calc.

[60] "NMR Spectroscopy Rx Chain Noise Figure Calculator - Dropbox", https://www.dropbox.com/s/ah3fl94zxshya7q/NMR_Rx_NF_Calculator.rar?dl=0.

[61] Sedra, A. S., Smith, K. C., Microelectronic Circuits, 6th ed. Oxford, UK: Oxford University Press, 2010.

[62] Jaeger, R. C., Blalock, T. N., Microelectronic circuit design, 5th ed. New York, USA: McGraw–Hill Education, 2016.

[63] Grebennikov, A., RF and Microwave Power Amplifier Design, 2nd ed. New York, USA: McGraw–Hill Education, 2015.

[64] Chen, W.-K., (ed.), The Electrical Engineering Handbook. Burlington, USA: Elsevier Academic Press, 2004.

[65] "Smith Chart", https://www.acs.psu.edu/drussell/Demos/SWR/SmithChart.pdf.

[66] "Antenna Theory: The Smith Chart", http://www.antenna-theory.com/tutorial/smith/chart.php.

[67] "Impedance Matching and the Smith Chart Tutorial", Maxim Integrated, Tutorial 742, July 2002, available: https://www.maximintegrated.com/en/design/technical-documents/tutorials/7/742.html

[68] "Rohde & Schwarz ZVL3 Vector Network Analyzer", https://www.rohde-schwarz.com/us/product/zvl3-productstartpage_63493-9015.html.

[69] "Hewlett-Packard 8970B noise figure meter", http://www.dudleylab.com/HP%208970B%20Noise%20Figure%20Meter.pdf.

[70] "MathWorks MATLAB", https://www.mathworks.com/products/matlab.html.

[71] "Keysight Advanced Design System", https://www.keysight.com/en/pc-1297113/advanced-design-system-ads?cc=HR&lc=eng.

[72] "Laboratory for Non-Destructive Testing", https://www.fsb.unizg.hr/ndt/.

[73] "Applied Optics Laboratory", https://aolab.fer.hr/aolab.

[74] "Farnell", https://www.farnell.com/.

[75] "Mouser Electronics", https://www.mouser.com/.

[76] "Broadcom ATF–34143", https://www.broadcom.com/products/wireless/transistors/fet/atf-34143.

[77] "Broadcom ATF–54143", https://www.everythingrf.com/products/rf-transistors/broadcom/659-950-atf-54143.

[78] "Broadcom ATF–55143", https://www.everythingrf.com/products/rf-transistors/broadcom/659-950-atf-55143.

[79] “Texas Instruments LM317”, http://www.ti.com/product/LM317#.

[80] Elsen, A., “Carbon-Film MELF: Pulse-Load Champion”, https://www.electronicdesign.com/power/carbon-film-melf-pulse-load-champion.

[81] “Anritsu Spectrum Master MS2721B spectrum analyzer”, https://www.anritsu.com/en-us/test-measurement/products/ms2721b.

[82] “HAKOM – Croatian Regulatory Authority for Network Industries”, https://www.hakom.hr/default.aspx?id=7.

[83] “Anritsu MS2661C spectrum analyzer”, https://www.anritsu.com/en-us/test-measurement/products/ms2661c.

[84] Gustrau, F., RF and Microwave Engineering: Fundamentals of Wireless Communications. Chichester, UK: John Wiley & Sons, Ltd, 2012.

[85] Havill, R. L., Walton, A. K., Elements of Electronics for Physical Scientists, 2nd ed. Houndmills, UK: Macmillan Publishers Ltd, 1985.

[86] Terrell, D. L., Keenan, R. K., Digital Design for Interference Specifications: A Practical Handbook for EMI Suppression, 2nd ed. Boston, USA: Newnes, 1999.

[87] Morrison, R., Grounding and Shielding Techniques, 4th ed. New York, USA: John Wiley & Sons, Inc., 1998.

[88] “Sprint Layout”, https://www.electronic-software-shop.com/lng/en/electronic-software/sprint-layout-60.html.

[89] “Sprint Layout – The Ultimate Tutorial And Experience”, https://www.wellpcb.com/pcb/sprint-layout.html.

Biography

Petar Kolar was born on January 20th, 1992 in Koprivnica, Croatia. He finished elementary school in Ferdinandovac in 2006, and graduated from high school in Đurđevac in 2010. That same year, he enrolled into university education at the Faculty of electrical engineering and computing, University of Zagreb, Croatia, where he finished both his undergraduate and graduate study in 2013 and 2015, respectively. He specialized in the field of Wireless Technologies in both of his studies under the supervision of professor Silvio Hrabar, Ph.D. After graduating, he began a postgraduate doctoral study in the field of electrical engineering at his parent faculty and under the same supervision. In 2016, he started working as a research and teaching assistant at The Experimental Physics Division of the Department of Physics at the Faculty of Science, University of Zagreb, Croatia, on the "Unity through knowledge Fund" project, entitled "Quantum Critical Matter in Strongly Correlated Electronic Systems (Quantum CorES)", under the supervision of assistant professor Mihael Srđan Grbić, Ph.D. Besides in his scientific work, he was also engaged in teaching college level courses "Computers in Education", "Laboratory in Fundamentals in Electronics" and "Electronics Lab" at the Department of Physics of the Faculty of Science, University of Zagreb, Croatia. Since September 2019, he is employed as a senior software developer at Ericsson Nikola Tesla d.d. in Zagreb, Croatia. He is an author of one international journal paper and three conference papers. He also participated in two conference papers as a co-author.

Publications

Journal papers

1. Kolar, P., Grbić, M. S., Hrabar, S., “Sensitivity Enhancement of NMR Spectroscopy Receiving Chain Used in Condensed Matter Physics”, Sensors, Vol. 19, Issue 14, July 2019, pp. 3064.

Conference papers

1. Hrabar, S., Kolar, P., Perić, A., “Broadband negative-capacitor-based enhanced transmission through subwavelength aperture”, in 2014 USNC-URSI Radio Science Meeting (Joint with AP-S Symposium), July 2014, pp. 150
2. Hrabar, S., Kolar, P., Krois, I., Lončar, J., “Broadband non-Foster-based Tunneling in radiofrequency regime”, in 2015 9th International Congress on Advanced Electromagnetic Materials in Microwaves and Optics (METAMATERIALS), September 2015, pp. 415-417
3. Kolar, P., Hrabar, S., Grbić, M. S., “Towards optimal noise properties of NMR antenna-receiver chain”, in 2017 11th European Conference on Antennas and Propagation (EUCAP), March 2017, pp. 1054-1056
4. Kolar, P., Hrabar, S., Grbić, M. S., “What Actually Limits the Sensitivity of NMR Antenna–Receiver Chain?”, in 2017 IEEE AP-S Symposium on Antennas and Propagation and USNC-URSI Radio Science Meeting, July 2017, pp. TU-UB.2P.4
5. Kolar, P., Hrabar, S., Grbić, M. S., “Optimalna šumna svojstva prijemnog lanca NMR sustava”, in 2017 10. znanstveni sastanak Hrvatskog fizikalnog društva, October 2017, pp. 54

Životopis

Petar Kolar rođen je 20. siječnja 1992. godine u Koprivnici. Osnovnu školu završio je 2006. godine u Ferdinandovcu, a srednju školu 2010. godine u Đurđevcu. Iste godine upisao je Fakultet elektrotehnike i računarstva Sveučilišta u Zagrebu, gdje je 2013. godine završio preddiplomski, a 2015. diplomski studij, oboje na smjeru Radiokomunikacijske tehnologije pod vodstvom prof.dr.sc. Silvija Hrabara. Po završetku diplomskog studija upisao je poslijediplomski doktorski studij elektrotehnike na matičnome fakultetu pod vodstvom istog mentora, a 2016. godine zaposlio se kao asistent na Zavodu za eksperimentalnu fiziku Fizičkog odsjeka Prirodoslovno-matematičkog fakulteta Sveučilišta u Zagrebu, na projektu Fonda „Jedinstvo uz pomoć znanja“, s nazivom „Quantum Critical Matter in Strongly Correlated Electronic Systems (Quantum CorES)“, pod vodstvom doc.dr.sc. Mihaela Srđana Grbića. Osim u istraživačkom radu, također je sudjelovao i u nastavnim aktivnostima na kolegijima „Uporaba računala u nastavi“, „Praktikum iz osnova elektronike“ i „Praktikum iz elektronike“ na Fizičkom odsjeku Prirodoslovno-matematičkog fakulteta Sveučilišta u Zagrebu. Od rujna 2019. godine zaposlen je kao inženjer specijalist za razvoj softvera u Ericsson Nikola Tesla d.d. u Zagrebu. Autor je jednog rada u međunarodnom časopisu iz SCIE baze i tri konferencijska članka, a na dva konferencijska članka participirao je kao koautor.